UNIVERSITÉ DE NICE-SOPHIA ANTIPOLIS

ÉCOLE DOCTORALE STIC
SCIENCES ET TECHNOLOGIES DE L'INFORMATION ET DE LA COMMUNICATION

THÈSE

pour obtenir le titre de

Docteur en Sciences
de l'Université de Nice-Sophia Antipolis

Mention: Automatique, Traitement du Signal et des Images

Présentée par

Minh Duc HUA

Contributions au contrôle automatique de véhicules aériens

Thèse préparée dans le projet AROBAS, INRIA Sophia Antipolis

Dirigée par

Pascal MORIN, Chargé de Recherche, INRIA
Tarek HAMEL, Professeur, UNSA et I3S-CNRS

Soutenue publiquement le 01 Décembre 2009 devant le jury composé de :

Président :	Yves ROUCHALEAU, Professeur, CMA, MINES ParisTech
Rapporteurs :	Lorenzo MARCONI, Professeur, Université de Bologne
	Nicolas PETIT, Professeur, Directeur du CAS, MINES ParisTech
Examinateurs :	Claude SAMSON, Directeur de Recherche, INRIA
	Patrick FABIANI, Docteur, Directeur du DCSD, ONERA CERT
	Carlos Jorge SILVESTRE, Professeur, IST
Invité :	Daniel TROUCHET, Ingénieur, Bertin Technologies

HUA Minh Duc

CONTRIBUTIONS TO

THE AUTOMATIC CONTROL OF AERIAL VEHICLES

Abstract

The control of underactuated vehicles has received increasing interests in relation with various robotic applications. This thesis focuses more specifically on the general problem of automatic control of aerial vehicles, and in particular of Vertical Take-Off and Landing vehicles. The contributions of this work is twofold. Firstly, this work sets the foundations of a general control approach for a large family of thrust-propelled underactuated vehicles in order to stabilize reference trajectories either in thrust direction, velocity, or position. The basic modeling assumption is that the vehicle is propelled via a thrust force along a single body-fixed direction and that it has full torque actuation for attitude control. Motivated by robustness issues, a novel nonlinear integrator technique is proposed allowing to compensate for modeling errors and perform robustly against external perturbations. Secondly, we propose two novel attitude estimation algorithms, based on measurements provided by a GPS and an IMU embarked on the vehicle. The proposed methods make use of the measurement of the linear velocity to estimate the vehicle's acceleration, and improve significantly the precision of the estimated attitude, especially in the case of important accelerations.

Keywords: Feedback control, Attitude estimation, Underactuated vehicles, VTOL UAV, System modeling, Robustness, Nonlinear anti-windup integrator.

Résumé

Le contrôle automatique de véhicules sous-actionnés suscite depuis de nombreuses années un grand intérêt pour des applications diverses et variées. Cette thèse est consacrée au problème général du contrôle automatique de véhicules aériens, en particulier des véhicules à décollage et atterrissage vertical. Ce travail présente deux contributions théoriques. La première contribution concerne le développement d'une approche de commande générique pour une large classe de véhicules sous-actionnés. Cette approche exploite la structure d'actionnement commune à la plupart de véhicules conçus par l'homme, à savoir une seule commande en poussée dans une direction privilégiée du véhicule et un actionnement complet de la dynamique de rotation. La méthode de synthèse est conçue de façon incrémentale afin de traiter différents modes opérationnels: stabilisation de la direction de poussée, de la vitesse, ou de la position du véhicule. Une nouvelle technique d'intégrateur non-linéaire est proposée afin de garantir un comportement robuste vis-à-vis de perturbations extérieures ou d'erreurs de modèle. La seconde contribution concerne deux nouvelles méthodes d'estimation d'attitude du véhicule à partir de mesures fournies par une centrale inertielle et de mesures GPS. Les solutions proposées utilisent la mesure de vitesse linéaire pour estimer l'accélération du véhicule, et améliorent significativement la précision de l'attitude estimée, notamment en cas d'accélérations importantes du système.

Mos-clés: Commande par retour d'état, Estimation d'attitude, Véhicule sous-actionné, Véhicule à décollage et atterrissage vertical, Modélisation, Robustesse, Intégrateur anti-windup nonlinéaire.

This thesis is

dedicated to my maternal grandfather PHAN Huu Nghien,
my parents HUA Ton Hieu and PHAN Thi Hong Van,
and my sister HUA Bao Khanh;

and in memory of my maternal grandmother NGUYEN Thi Sau
and my parental grandfather HUA Thieu Mong.

About the Author

HUA Minh Duc was born on January 17th, 1982 in Nghe An province, Vietnam. But most of his childhood was spent in Quy Nhon city, Binh Dinh province. He was student of Hồ Chí Minh City University of Technology from 1999 to 2002 before studying at Ecole Polytechnique in France. In 2006, he received an Engineer degree of Ecole Polytechnique, an Engineer degree of ENSTA-ParisTech, and a M.S. degree in Automatics and Signal Processing of Paris-Sud 11 University. He expects to receive a Ph.D. degree in Automatics and Signal Processing of University of Nice Sophia Antipolis in December 2009. His research interests include nonlinear control and estimation with applications in Aerial Robotics.

Acknowledgements

First and foremost, I deeply indebted to my parents and my whole family for everything I am and everything I have achieved. I am grateful for their unrelenting love and unconditional support.

In the journey of life, I met three Masters. No one is similar to each other, but they are all strong. Their supreme knowledge, skills, and intuition have always been the constant source of admiration and inspiration for me, and I hope to become as strong as them some day. I would like to express my deepest gratitude and appreciation to my Masters: Claude Samson, Pascal Morin, and Tarek Hamel. An important part of my "path of life" has been carved with their advices and guidance, and the debts I owe to them are limitless.

I would like to acknowledge all the members of my Ph.D. Jury for evaluating the present work. In particular, I am grateful to Prof. Lorenzo Marconi and Prof. Nicolas Petit for reviewing this manuscript and for their constructive criticism. My special thanks go to Prof. Yves Rouchaleau for chairing the Jury. I am also thankful to Dr. Patrick Fabiani and Prof. Carlos Jorge Silvestre for examining the present work.

I am grateful to the UAV team of Bertin Technologies Company for the collaboration within the SCUAV project. Thank to them I learnt many things about tailsitter UAVs. My special thanks go to the team leader Daniel Trouchet for his kindness and constant availability.

I am thankful to Prof. Robert Mahony for the valuable discussion on the topic of attitude estimation that I benefited to achieve part of the present work.

I owe my sincere gratitude to the past and current members of AROBAS, a robotics team of INRIA Sophia Antipolis-Méditérannée, and also of its antecedent team ICARE for providing a stimulating atmosphere for the exchange and discussion of ideas during my Ph.D. there. My special respect and appreciation go to the team leader Patrick Rives. Some fellows students and friends in the team I would like to acknowledge for making my life in INRIA more pleasant and exiting include Hicham Hadj-Abdelkader, Melaine Gautier, Tiago Ferreira Gonçalves, Cyril Joly, Gabriela Gallegos, Adan Salazar, Maxime Meilland, Alexandre Chapoulie, Vincent Brandou, Stefan May, Ezio Malis, Geraldo Silveira, Andrew Comport, Benoit Vertut, Christopher Mei, Omar Tahri, Mauro Maya, Wladyslaw Magiera, Rémi Desouche, Glauco Scandaroli, Daniele Pucci. I am specially honored to count Pedro Machado Manhães de Castro and Doan Viet Dung among my best friends in INRIA.

I would like to thank INRIA Sophia Antipolis-Méditérannée, I3S-CNRS, and University of Nice Sophia Antipolis for providing me with the means and support to carry out this work.

Contents

List of Figures

List of Tables

Mathematical notation and properties

Some mathematical notations are introduced in this thesis.

- $\{i_1, i_2\}$: canonical basis of $\mathbb{R}^2$.

- $\{e_1, e_2, e_3\}$: canonical basis of $\mathbb{R}^3$.

- I_n: $n \times n$ identity matrix.

- $|.|$: Euclidean norm in $\mathbb{R}^n$.

- $\langle ., . \rangle$: inner product.

- $\times$: cross product.

- $\top$: transpose operator.

- $S(\cdot)$: 3×3 skew-symmetric matrix associated with the cross product $\times$, *i.e.* $S(u)v = u \times v$, $\forall u, v \in \mathbb{R}^3$.

- $\forall H \in \mathbb{R}^{3 \times 3}$, $\mathbf{tr}(H)$ is the trace of H, $\mathbf{det}(H)$ the determinant of H, and $\mathbf{P_a}(H)$ the anti-symmetric part of H, *i.e.* $\mathbf{P_a}(H) = (H - H^\top)/2$.

- $|| \cdot ||$: Frobenius norm in $\mathbb{R}^{3 \times 3}$, *i.e.* $\forall H \in \mathbb{R}^{3 \times 3}$, $||H|| = \sqrt{\mathbf{tr}(H^\top H)}$.

- A function $\eta : [t_o, +\infty) \longrightarrow \mathbb{R}^p$ is u.b. (for *ultimately bounded*) by a constant c, if there exists a time t_1 such that $|\eta(t)| \leq c$, $\forall t \geq t_1$. An output $y = h(x, t) \in \mathbb{R}^p$ is u.u.b. (for *uniformly ultimately bounded*) by a constant c along the solutions to a differential equation $\dot{x} = f(x, t)$ if, $\forall (x_o, t_o)$, $y(.) = h(x(., x_o, t_o), .)$ is u.b. by c, where $x(\tau, x_o, t_o)$ denotes the solution at time τ with initial condition x_o at $t = t_o$.

Some mathematical properties are also recalled.

- $\forall x, y \in \mathbb{R}^3$, $\mathbf{tr}(xy^\top) = x^\top y$, $S(x \times y) = yx^\top - xy^\top$.

- $\forall A, B \in \mathbb{R}^{3 \times 3}$, $\mathbf{tr}(A) = \mathbf{tr}(A^\top)$, $\frac{d}{dt}(\mathbf{tr}(A)) = \mathbf{tr}(\dot{A})$, $\mathbf{tr}(AB) = \mathbf{tr}(BA)$, and $\mathbf{tr}(AB) \leq (||A||^2 + ||B||^2)/2$.

- $\forall x \in \mathbb{R}^3$ and for all symmetric matrix $H \in \mathbb{R}^{3 \times 3}$, $\mathbf{tr}(HS(x)) = 0$.

Acronyms

AHRS	Attitude and Heading Reference System
ANR	Agence Nationale de la Recherche
AROBAS	Advanced ROBotics and Autonomous Systems
AUV	Autonomous Underwater Vehicle
AVATAR	Autonomous Vehicle Aerial Tracking And Reconnaissance
AWBT	Anti-Windup Bumpless Transfer
CoM	Center of Mass
DGPS	Differential Global Positioning System
EKF	Extended Kalman Filter
ESOQ	Estimator of the Optimal Quaternion
FOAM	Fast Optimal Attitude Matrix
FOG	Fiber Optic Gyroscope
GPS	Global Positioning System
IMU	Inertial Measurement Unit
INS	Inertial Navigation System
KF	Kalman Filter
LQG	Linear-Quadratic-Gaussian
LQR	Linear-Quadratic-Regulator
MEMS	Micro Electro-Mechanical System
MIMO	Multi-Input-Multi-Output
NOTAR	NO Tail Rotor
PID	Proportional Integral Derivative
PVTOL	Planar Vertical Take-Off and Landing
QUEST	QUaternion ESTimator
REQUET	Recursive QUaternion ESTimator
RLG	Ring Laser Gyroscope
RPM	Round Per Minute
RWVTOL	Rotary-Wing Vertical Take-Off and Landing
SCUAV	Sensory Control of Unmanned Aerial Vehicles
SISO	Single-Input-Single-Output
SRSK	Short Range Station Keeping
STLC	Small Time Locally Controllable
SVD	Singular Value Decomposition
UAV	Unmanned Aerial Vehicle
VTOL	Vertical Take-Off and Landing

Prologue

Underactuated vehicles are abundant in real life and appear in a broad range of applications including Robotics, Aerospace Systems, Marine Systems, Mobile Systems, Locomotive Systems, *etc.*. They are characterized by the fact that they have more degrees of freedom than actuator(s), so that the control design of these vehicles is often challenging. The present thesis focuses more specifically on the family of *thrust-propelled* underactuated vehicles and in particular Rotary-Wing Vertical Take-Off and Landing (RWVTOL) vehicles, as exemplified by helicopters, quadrotor helicopters, and tailsitters. The last decades have witnessed an increasing interest in the construction and control design of Unmanned Aerial Vehicles (UAVs), especially RWVTOL UAVs. One can mention the examples of the HoverEye (Pflimlin, 2006), the iSTAR (Lipera et al., 2001), the GTSpy (Johnson and Turbe, 2005), the University of Bologna's ducted fan tailsitter (Naldi et al., 2008), the SLADe (Peddle et al., 2009), the X4-flyer (Hamel et al., 2002), the Vigilant (Fabiani et al., 2007), the Goliath (Vissière et al., 2008), the GTMax (Johnson and Kannan, 2005), and the AVATAR (Saripalli et al., 2002). Thanks to versatile flight capabilities, these vehicles have found numerous (military and civil) applications such as surveillance, inspection, cartography, cinematography, searching, and rescuing, *etc.*. Since the last decades, advances in technologies have been crucial for the development of UAVs. For instance, the autonomy of aerial robots have been significantly improved thanks to advances in engines, batteries, materials, and electronics. The appearance of the Global Positioning Systems (GPS) and especially its availability for civil applications since 1995 have revolutionized the aerospace Guidance, Navigation, and Control in general, and the development of UAVs in particular. The fast development in sensors, embarked electronic systems, and wireless communication devices have directly impacted on the development of navigation system for UAVs. Last but not least, the availability of compact, light-weight, and powerful computers enables the implementation of expensive computational algorithms (*e.g.* vision-based algorithms) for real-time applications. Nowadays, it is possible to embark on small UAVs all elements necessary for autonomous navigation.

The development of aerial robotic vehicles encompasses several challenges including mechanical and geometrical conceptions, system modeling, state[1] reconstruction, and control design. These issues are further amplified for small and/or light aerial vehicles due to a combination of factors. Firstly, the complexity of aerodynamic effects impedes to obtain a precise dynamic model valid in a large operating domain, which can be used for control design purposes. Then, these vehicles are often subjected to rapidly changing perturbations whose magnitude can be commensurable with the available actuation power. Due to aerodynamic perturbations, the attitude of RWVTOL UAVs can vary rapidly in large proportions, making the problems of state estimation and control design more challeng-

---

1. The state is the set of position, attitude, linear and angular velocities.

ing. Finally, the limited payload often poses important restrictions on the choice of sensors, which may induce significant measurement/estimation errors of the vehicle's state. This negatively impacts on the control performance. The present thesis is principally dedicated to two aspects: *i) control design for stabilization of reference trajectories*, and *ii) attitude estimation*.

▷ **Control design for stabilization of reference trajectories.**

Due to an important number of uncertainties and unmodeled dynamics associated with aerial robotic vehicles, robustness issues are particularly important for control design. This is even more critical for small-size RWVTOL UAVs. Since the last decades, robust control design for these vehicles has been a challenging research topic for the automatic community. In the context of linear control theory, robust control techniques like H_2, H_∞, LQR, LQG have been applied to these vehicles. However, several shortcomings limit their applications. First of all, linear control designs are based on a linear approximation of the system's dynamics, which is only valid in a local domain. Then, they make use of a minimal parametrization of the attitude (like Euler angles), which artificially introduces control singularities. Finally, determining a linear approximation of the system's dynamics requires the precise knowledge of aerodynamic effects along the considered reference trajectory. Since the angles of attack of RWVTOL vehicles can vary a lot as a function of the reference trajectory, the process of identifying aerodynamic effects in a large domain of flight can be both difficult and costly. Therefore, recent studies have been devoted to nonlinear control design techniques for RWVTOL UAVs, allowing to partially overcome shortcomings of linear control approaches. Nevertheless, nonlinear control design techniques addressing robustness issues, like *e.g.* (Mahony and Hamel, 2004), (Pflimlin et al., 2006), (Isidori et al., 2003), (Marconi and Naldi, 2007), are not numerous. The present thesis is a contribution to robust control design and analysis of these vehicles. In this work nonlinear control laws, with (quasi) global stability and convergence results, are conceived for incrementally complex objectives (ranging from joystick-augmented-control of the vehicle's orientation to autonomous trajectory tracking), with the support of rigorous Lyapunov-based stability analyses. We have also developed a novel anti-windup nonlinear integrator allowing to effectively compensate for imprecise knowledge of the external forces acting on the vehicle.

▷ **Attitude estimation.**

A precise knowledge of the vehicle's state improves the performance and robustness of feedback control laws. Although a well-designed feedback control is expected to grant robustness with respect to uncertainties, the larger the uncertainties the higher the risk of system destabilization. Among the state, the attitude information is involved in all the proposed feedback control laws, and it is particularly difficult to obtain at high frequency especially for small-size RWVTOL UAVs. This is essentially due to *i)* the possibly fast variation of attitude due to wind-induced perturbations, and *ii)* the restriction on the choice of sensors due to the vehicle's size and limited payload, and equally economic reasons. In this document we focus on the problem of attitude estimation based on measurements of an Inertial Measurement Unit (IMU) and the velocity measurement provided by a GPS. Difficulties are typically related to the fact that a three-axis accelerometer does not directly measure the gravity direction during accelerated motions. Most works on the topic make use of the restrictive assumption that the vehicle's acceleration is negligible compared to the gravitational acceleration in order to approximate the accelerometer

measurement with the measurement of the gravity (see, *e.g.*, (Mahony et al., 2008)). A recent study (Martin and Salaun, 2008) allowing to loosen this assumption has motivated our study. In this thesis we propose two solutions to the robust and effective attitude observer design and analysis.

This work has been carried out during my Ph.D. within AROBAS [2], a robotics research team of INRIA [3]. I was also attached to the laboratory I3S (UNSA–CRNS) [4]. My research was supported by the *Conseil Régional Provence-Alpes-Côte d'Azur* and the French *Agence Nationale de la Recherche (ANR)* in the scope of the national ANR project SCUAV (Sensory Control of Unmanned Aerial Vehicles). The present document is organized in three chapters.

- **Chapter 1 – Overview on Rotary-Wing Vertical Take-Off and Landing vehicles.** This chapter is devoted to a general introduction to the family of RWV-TOL vehicles. Several mechanical configurations are recalled showing how force and torque controls are generated and, subsequently, how these vehicles achieve flight. Some sensor technologies allowing them to localize themselves are also reviewed. Then, the general equations of motion of these vehicles along with some examples are presented. Finally, existing control techniques in the literature for these vehicles are discussed.

- **Chapter 2 – Control design of thrust-propelled underactuated vehicles.** A novel nonlinear robust control approach is developed for a class of thrust-propelled underactuated vehicles evolving in the 3D-space, or on the 2D-plane. The control design is incrementally conceived for several control objectives: *i)* stabilization of reference thrust direction, *ii)* stabilization of reference linear velocities, *iii)* stabilization of reference position trajectories, *iv)* combined stabilization of reference horizontal linear velocities and reference altitude. The constraint of unilaterality of the thrust direction and environmental dissipative effects are also taken into account in the control design process and the associated analyses. The performance and robustness of the proposed control laws are illustrated through simulations based on some models of ducted fan tailsitters and single rotor helicopters.

- **Chapter 3 – Attitude estimation.** This chapter starts with a survey on attitude estimation approaches proposed in the literature and a review of some attitude parametrizations. Then, two attitude estimation algorithms based on GPS and IMU measurements are proposed. Finally, simulations are carried out to illustrate the compared performance and robustness between our solutions and some solutions proposed in the literature.

Most of the results reported in this thesis have been published (or are about to be published) in research papers (Hua et al., 2007), (Hua et al., 2008), (Hua et al., 2009a), (Hua et al., 2009b), (Hua et al., 2009c), (Hua, 2009), (Hua, 2010). Part of Chapter 2 appeared in (Hua et al., 2007), (Hua et al., 2008), (Hua et al., 2009a), (Hua et al., 2009b), (Hua et al., 2009c). Part of Chapter 3 can be found in (Hua, 2009), (Hua, 2010).

---

2. Research team in *"Advanced ROBotics and Autonomous Systems"* – https://www-sop.inria.fr/arobas/

3. The French *National Institute for Research in Computer Science and Control* – http://www.inria.fr/

4. The French *Laboratoire d'Informatique, Signaux et Système de Sophia Antipolis* – http://www.i3s.unice.fr/I3S/

Chapter 1

Overview on Rotary-Wing Vertical Take-Off and Landing vehicles

1.1 Introduction

Flying was no longer science fiction when the Montgolfière brothers made the first trip in a free-flying balloon in 1783 and the Wright brothers made the first flight by means of a vehicle heavier than air in 1903 [1]. The profound understanding of the nature of lift and the invention of powerful engines since the last century have greatly impacted on the conceptions of various flying machines. Nevertheless, Man has never ceased to envy the birds although he can now fly faster, farther, higher, and longer than them with the help of his inventions. To achieve what Man has achieved up to date many sacrifices have been made [2], but the journey will still be long until he can compete with birds in terms of energy efficiency and robustness. Today, several families of flying machines exist: fixed-wing aircrafts, rotary-wing aircrafts, flapping-wing aircrafts, and many others. Flapping-wing aircrafts are still in the state of research [3], but the first two families including airplanes and helicopters are now abundant in real life. Unlike fixed-wing aircrafts which use forward flight speed and their fixed-wings to generate lift, rotary-wing aircrafts use rotating wings (*i.e.* a rotor with blades spinning about a shaft) to provide lift and thus do not need runways to take-off or land. They belong to the family of *Vertical Take-Off and Landing* (VTOL) vehicles which are not only able to vertically take-off and land, but also hover motionless in the air and cruise. In fact, "the idea of a vehicle that could lift itself vertically from the ground and hover motionless in the air was probably born at the same time that Man first dreamed of flying" [4]. Thanks to their versatile flight capabilities, rotary-wing aircrafts have found tremendous interests in military and civil (manned or unmanned) applications, despite the fact that designing, constructing, and controlling rotary-wing aircrafts require vastly and maturely scientific, engineering, and technological knowledge. For instance, various aerodynamic and mechanical problems must be understood and overcome; engines with high power-to-ratios, high-strength and low-weight materials for the rotor and airframe must be developed; *etc.*. Besides, helicopter pilots know how hard it is to fly a helicopter especially in hover control mode. Today, fully autonomous reduced

---

1. That the airplane was first invented by the Wright brothers or Santos-Dumont is still a debate.
2. Lilienthal's last word: "Sacrifices must be made." after his glider seriously crashed in 1896.
3. Indeed, the nature still has many things for us to learn.
4. Statement of Sikorsky, one of pioneers of aviation in both helicopters and fixed-wing aircrafts.

scale helicopters as well as other autonomous aerial vehicles, where computers replace human pilots, exist as a consequence of technological advances on electronic embarked systems and sensors, advances in automatic control and artificial intelligence, *etc.*. These autonomous vehicles, often called *Unmanned Aerial Vehicles* (UAV), or aerial drones, or aerial robots in the literature, have been increasingly developed in the last decades.

In what follows we present some existing categories of Rotary-Wing VTOL vehicles and recall some of their flying characteristics. Then, some sensor technologies allowing an aerial robot to know its state and to localize itself with respect to its surrounding environment are reviewed. Finally, surveys on the modeling and control of these vehicles are provided. Note that some related surveys can be found in (Pflimlin, 2006), (Naldi, 2008), (Guenard, 2007), (Vilchis, 2001), (Martini, 2008).

1.2   Rotary-Wing VTOL (RWVTOL) vehicles

Several categories of RWVTOL vehicles have been designed since the last century as exemplified by helicopters, tilt-rotors, tailsitters, *etc.*. In general, a RWVTOL vehicle has one (or several) main rotor(s) to generate lift (*i.e.* thrust force) in one privileged direction allowing to counterbalance its weight and also aerodynamic perturbations induced by wind gusts. But generating lift is not everything. The vehicle must be designed to deal with other aerodynamic and mechanical problems, among which the following issues are crucial:

1. How to regulate the thrust force?

2. How to generate moments (*i.e.* torques) to control the vehicle's orientation (*i.e.* attitude)?

3. How to counter parasite torques generated by drag forces acting on the main rotor(s)?

It is now well understood that the lift force generated by a rotor with blades rotating about a shaft is a function of the blades' angles of attack (*i.e.* pitch angles) and the rotor's rotational velocity (*i.e. Rounds Per Minute* (RPM)) (see *e.g.* (Prouty, 2002)). Therefore, a RWVTOL vehicle, according to its design, can possess one or two controls of lift. For instance, quadrotor helicopters and ducted fan tailsitters only possess an RPM control. On the contrary, besides the RPM control, conventional single rotor helicopters can also regulate lift force magnitude by changing the blades' pitch angles. This is done via the collective pitch control of the so-called *swashplate* mechanism (see Fig. 1.2). For some helicopters, the RPM is maintained at a specific value and lift force is regulated only via the collective pitch. As for the second issue, the torque actuation allowing to control the vehicle's attitude is typically obtained via the cyclic pitch control of the swashplate (*e.g.* helicopters), secondary propellers (*e.g.* quadrotor helicopters), rudders or flaps (*e.g.* tailsitters), *etc.*. Finally, part of the third issue can be solved by generating an antitorque opposed to the parasite rotor torque. Many solutions for antitorque control have been proposed. For instance, the use of a smaller rotor mounted vertically on the vehicle's tail was proposed by Sikorsky, and the use of two or more horizontal rotors turning in opposite directions was proposed by Ponton d'Amecourt. Other solutions will be discussed hereafter.

1.2.1 Helicopters

Among the family of RWVTOL vehicles, helicopters [5] have the longest history. Even in the last decades, there have been many studies to understand and overcome several difficult technical problems associated with helicopter flights, particularly in relation to aerodynamic limitations imposed by the main rotor (see *e.g.* (Hirschberg, 2000) and the references therein). Today, helicopters are safe, versatile, reliable, and the most widely used VTOL aircrafts. Besides, reduced scale helicopters (*i.e.* miniature helicopters) have recently become powerful platforms for numerous robotic applications. In what follows several helicopter configurations will be presented.

1.2.1.1 Helicopters with a single main rotor

The most important parts of a helicopter are: *i)* the main rotor(s) (the key element of flight), and *ii)* the antitorque system (allowing to annihilate parasite rotor torque which intends to cause the helicopter to turn in the opposite direction of the main rotor, and allowing to monitor the yaw motion of the helicopter).

▷ **Main rotor**

The main rotor consists of a mast, hub, rotor blades, and a swashplate. The hub is located at the top of the mast and is the attachment point for the rotor blades. The main rotor rotation generates lift through aerodynamic lift forces acting on the blades. Three basic classifications of the main rotor are fully articulated rotor, rigid rotor (*i.e.* hingeless rotor), and semirigid rotor (*i.e.* teetering rotor) according to how the rotor blades are attached and move relative to the main rotor hub.

- **Fully articulated:** The blades are allowed to flap, feather, and lead or lag independently of each other (see Fig. 1.1). The horizontal hinge, called the flapping hinge, allows the blade to move up and down. This movement allows to compensate for dissymmetry of lift. The vertical hinge allows the blade to move back and forth. This movement allows to compensate for the acceleration and deceleration caused by Coriolis effect. Each blade can also be feathered, *i.e.* rotated around its spanwise axis. Feathering the blade induces the change of its pitch angle. By changing the blades' pitch angles the thrust magnitude and direction can be controlled.

- **Rigid:** The blades, hub, and mast are rigid with respect to each other. The rigid rotor system is mechanically simpler than the fully articulated rotor system. There are no vertical or horizontal hinges so that the blades cannot flap or drag, but they can be feathered. By flexing, the blades themselves partially compensate for the forces which required rugged hinges in the previous configuration.

- **Semirigid:** A semirigid rotor system allows for flapping and feathering. This system is normally composed of two blades rigidly attached to the rotor hub. The hub is then attached to the rotor mast by a teetering hinge and is free to tilt with respect to the main rotor shaft. This allows the blades to flap together. As one blade flaps down, the other flaps up. Feathering is accomplished by the feathering hinge, which

---

5. The word "helicopter" originates from the Greek *helix/helik* = "spiral" and *pteron* = "wing".

changes the pitch angle of the blade. Since there is no vertical hinge, drag forces are partially absorbed through blade bending.
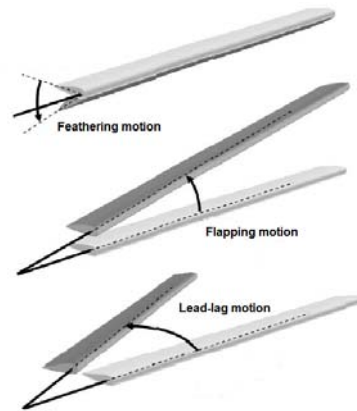
Figure 1.1: Blade articulations (source (Pflimlin, 2006)).
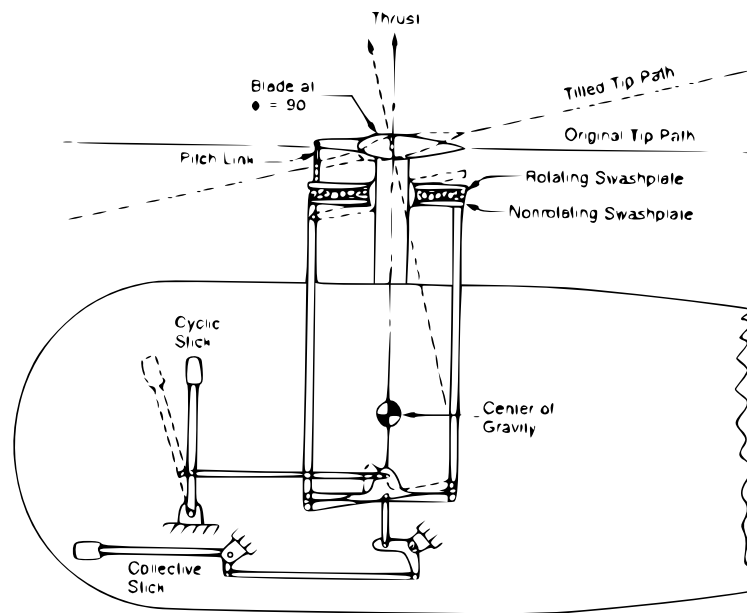
Figure 1.2: Schematic of Swashplate Control System (source (Prouty, 2002)).

The last and very important part of the main rotor is the swashplate mechanism. It allows a pilot (or autopilot) to control the blades' pitch angles resulting in the change of lift magnitude, via the *collective pitch* control, and also to change the orientation of the main rotor disk in order to modify the thrust direction, via the *cyclic pitch* control. Fig. 1.2 shows a schematic of this system.

▷ **Antitorque configurations**

The most classical, and also most used, antitorque design is an auxiliary rotor mounted vertically on the tail of the vehicle (see Fig. 1.3). The tail should be long so that a small tail rotor can generate a torque large enough to counter the main rotor torque. The thrust

of the antitorque system can be regulated to maintain directional control whenever the main rotor torque changes, or to control the yaw motion of the helicopter.

Figure 1.3: Helicopter with conventional tail rotor (source *wikipedia*).

An alternative architecture to the antitorque conventional tail rotor is the ducted fan configuration (often called fenestron or FANTAIL, and originally conceived by Sud Aviation in the 1960's) (see Fig. 1.4). This design not only provides more protection for the tail rotor (and people on the ground) but also improves aerodynamic efficiency and significantly reduces external noise and vibration. The disadvantages of this configuration compared to the conventional tail rotor are its higher weight and higher energy consumption.

Figure 1.4: Fenestron and FANTAIL helicopter.

Another antitorque configuration is the NO TAil Rotor (NOTAR) antitorque system conceived by McDonnell Douglas Helicopter Systems in the beginning of the 1980's (see Fig. 1.5). This system is based on the Coanda effect. It uses a fan inside the tailboom to create a high volume of low-pressure air, which exits through two slots and generates a boundary layer of airflow along the tailboom utilizing the Coanda effect. The boundary layer changes the direction of airflow around the tailboom, creating a thrust opposite the motion imparted to the fuselage by the main rotor torque effect. The yaw control is achieved through a vented, rotating drum at the end of the tailboom. Benefits of the

NOTAR system include increased safety and greatly reduced external noise.
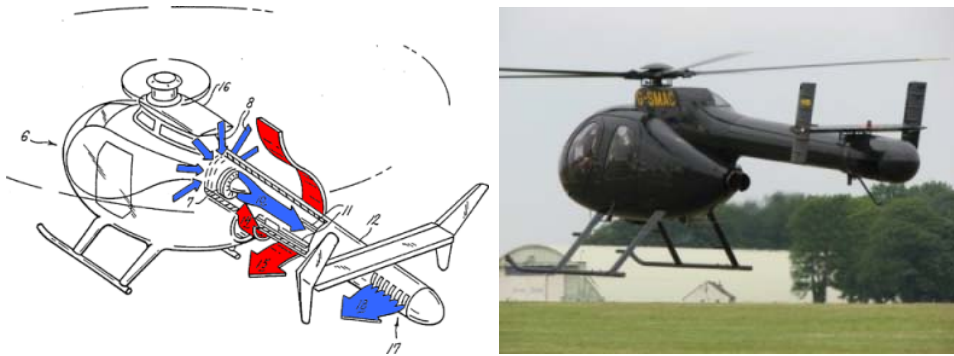
Figure 1.5: NO Tail Rotor helicopter and NOTAR MD500 (source *wikipedia*).

1.2.1.2 Helicopters with counter-rotating rotors

Counter-rotating rotor helicopters constitute another important family of helicopters. Several configurations can be found such as coaxial rotor helicopters, tandem rotor helicopters, intermeshing rotor helicopters, and quadrotor helicopters, *etc.*. For these vehicles, a separate antitorque system (like *e.g.* a tail rotor) is not required because the rotor systems rotate in opposite directions and thereby neutralize or eliminate each other's torque. Compared to single rotor helicopters, a principal disadvantage of most of counter-rotating rotor helicopters, like coaxial rotor helicopters, tandem rotor helicopters, and intermeshing rotor helicopters, is the increased mechanical complexity which, in an elementary engineering sense, is more prone to failure. However, the great advantage of these vehicles is the full participation of the available engine power to lift and thrust.

▷ **Coaxial rotor helicopters**

Figure 1.6: Coaxial rotor helicopters Kamov Ka-26 and Ka-50.

This configuration have been developed since the late 1950's by the Russian Kamov helicopter design bureau (see Fig. 1.6). Coaxial rotor configuration consists of a pair of rotors mounted in a mast one above the other, and turning in opposite directions about the same axis of rotation. Compared to conventional helicopters, coaxial rotor helicopters are normally more compact thanks to the absence of the tail rotor, and thus less sensitive to wind gusts. Flying controls act on the coaxial rotors with cyclic pitch, and collective

pitch controls similarly to a single rotor helicopter. The yaw control is achieved through differential collective pitch. An *automatic mixer box* ensures that the rotors' total lift remains constant during yaw manoeuvres by increasing the blades' pitch angles of one rotor while decreasing the blades' pitch angles of another rotor.

▷ **Tandem rotor helicopters**
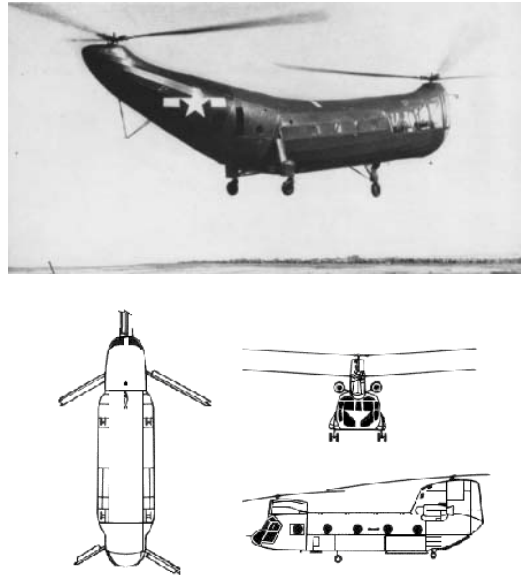
Figure 1.7: Tandem rotor helicopters Piasecki HRP Rescuer and Boeing CH-47 Chinook.

The first tandem rotor helicopter was designed by Piasecki and built by Piasecki Helicopter in 1945 (see Fig. 1.7). Especially used on large cargo helicopters, the tandem rotor configuration has two large horizontal rotors (*i.e.* front and aft rotors) mounted on each end of the fuselage and turning in opposite directions. The two rotors are synchronized by a transmission mechanism ensuring that they do not hit each other even during an engine failure. Each rotor operates similarly to the main rotor of a single rotor helicopter, except for the direction of rotation of the aft rotor and the method of keeping directional control. The tandem rotor design achieves yaw control by applying opposite left and right cyclic pitch to each rotor. To achieve pitch, opposite collective pitch is applied to each rotor, allowing to decrease the lift at one end and increase lift at the opposite end and thereby tilt the helicopter forward or backward. Alike coaxial rotor helicopters, because there is no antitorque rotor full engine power can be applied to lift. However, disadvantages of tandem rotor helicopters are a complex transmission and more drag due to its large shape.

▷ **Intermeshing rotor helicopters**

The first concept of this family was developed in Germany by Flettner in 1938. Nowadays, this concept is used and further developed by Kaman Aircraft Corporation (see Fig. 1.8). Intermeshing rotor helicopters are highly stable and have powerful lift capabilities. Intermeshing rotor configuration consists of a set of two rotors turning at the same speed and in opposite directions, with each rotor mast is mounted on the helicopter with a slight angle to the other. The two rotors are synchronized by a transmission mechanism

ensuring that the blades intermesh without colliding. To achieve translational or lateral or vertical flight, a same cyclic pitch or collective pitch control is applied to both rotors, similarly to a single rotor helicopter. In turn, the yaw control is achieved by applying asymmetric control on the flapping hinge of the two rotors.
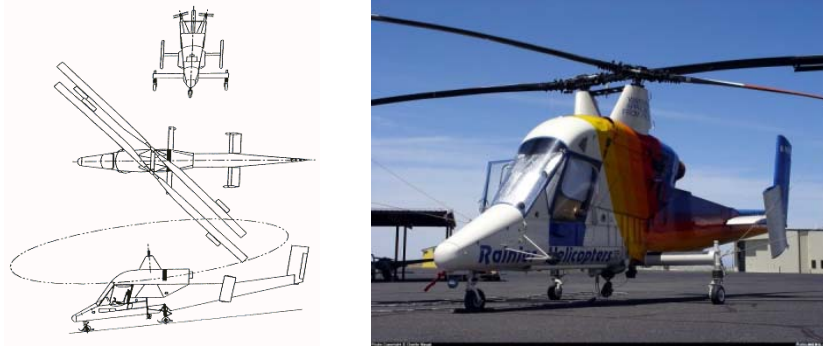
Figure 1.8: Intermeshing rotor helicopter Kaman K-MAX.

▷ **Quadrotor helicopters**
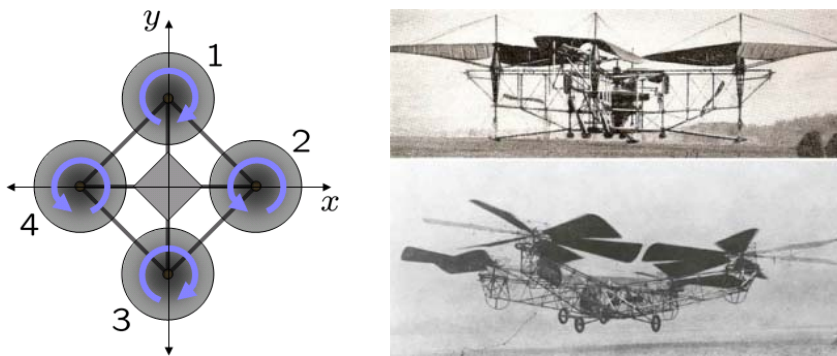
Figure 1.9: De Bothezat quadrotor helicopter.

Quadrotor helicopters were developed during the early days of the helicopter history, as exemplified by the Breguet's gigantic quadrotor (1907), the De Bothezat quadrotor (1921) (see Fig. 1.9), the Oemichen (1922), but rapidly fell into disuse due to their impracticality compared to other helicopters. However, this configuration has recently received increasing interests in the robotics field because many robotic applications such as surveillance, inspection, cartography, *etc.* do not require the vehicle to carry heavy load or to have a large size (see Fig. 1.10). Many studies on aerodynamics, modeling, and control design have been carried out recently for reduced scale quadrotor helicopters (*e.g.* (Hamel et al., 2002), (Guenard, 2007), (Pounds et al., 2002), (Pounds et al., 2006), (Defara et al., 2006), (Tayebi and McGilvray, 2006), (Bristeau et al., 2009), (Huang et al., 2009)). Quadrotor helicopters are mechanically less complex than other helicopters due to the absence of the swashplate and transmission mechanisms. A quadrotor helicopter is lifted and propelled by four rotors, with two of them turning in the opposite directions of the others to neutralize the yaw torque. Unlike conventional helicopters for which lift can be regulated via the rotor speed and the collective pitch, the lift of quadrotor helicopters is solely controlled via the rotor speed. Pitch, roll, and yaw are achieved by solely controlling the differential

speed of the four rotors. More precisely, the differential lift of the rotors generate pitch and roll torques, while the yaw control is achieved by the differential rotor torques induced by drag forces acting on the four rotors. Mathematical details will be given in Section 1.4.3.

Figure 1.10: Reduced scale quadrotor helicopters developed by Australian National University, by the Centre d'Energie Atomique of France, and by Draganfly Innovations Inc.

1.2.2   Tailsitters
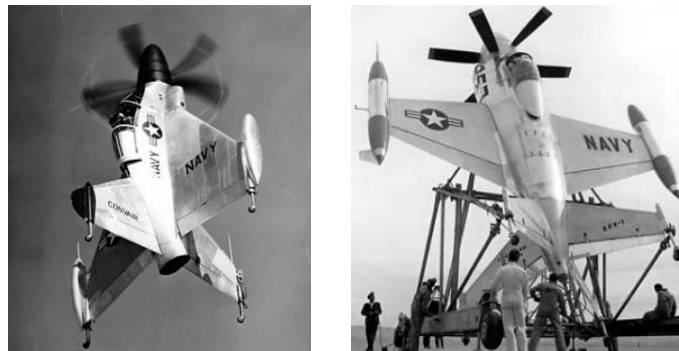
Figure 1.11: Tailsitters Convair XFY-1 Pogo and Convair XFV-1.

A tailsitter is a category of VTOL aircraft that launches and lands on its tail. Some concepts, as exemplified by the Convair XFY-1 Pogo, the Convair XFV-1 (see Fig. 1.11), are part of the aviation history, but they are now nearly forgotten. However, alike quadrotor helicopters, this family has received recently increasing interests in the robotics field for both military and civil applications. Several reduced scale prototypes have been developed during the last decade, among which ducted fan tailsitters are the most studied (*e.g.* (Lipera et al., 2001), (Fleming et al., 2003), (Fleming et al., 2004), (Graf et al., 2005), (Ko et al., 2007), (Pflimlin, 2006), (Pflimlin et al., 2007a), (Zhao and Bil, 2008), (Naldi, 2008)). A ducted fan tailsitter comprises at least the two following parts: *i)* a single rotor or a pair of coaxial counter-rotating rotors located inside a duct to generate lift, and *ii)* active tail fins (*i.e.* flaps or rudders) located below the rotor system to achieve full controllability of the vehicle's orientation. In the counter-rotating rotor configuration like the Allied Aerospace iSTAR (Lipera et al., 2001), the Bertin Technologies HoverEye (Pflimlin et al., 2006), the Honeywell, the Goldeneye (see Fig. 1.12), a separate antitorque system is not required. On the contrary, in the single rotor configuration two separate layers of flaps located below the rotor system are designed, like the ducted fan tailsitter of the University of Bologna (see Fig. 1.13) (Marconi and Naldi, 2006), where one layer of flaps is used to compensate for the rotor torque and to control the yaw motion, and the second layer is used to control the vehicle's pitch and roll.

Figure 1.12: Ducted fan tailsitters: iSTAR, HoverEye, Honeywell, Goldeneye.
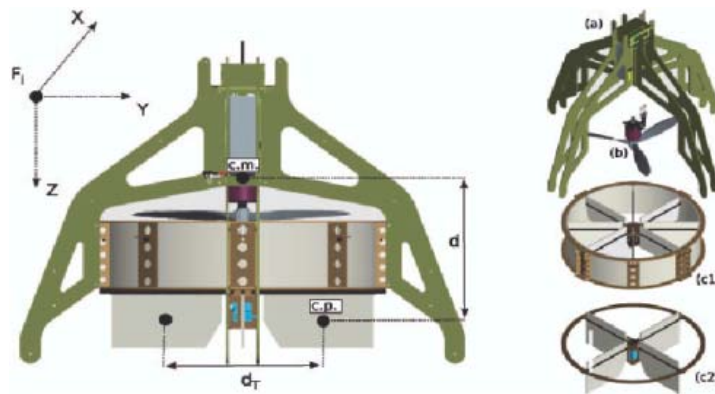
Figure 1.13: The University of Bologna's ducted fan tailsitter (source (Naldi, 2008)).

1.3　Sensor technologies

Families of VTOL vehicles have been presented. In a general manner, the control of their motion relies on the production of: *i)* a thrust force along a body-fixed direction whose intensity is controlled via the velocity and/or the angles of attack of rotating blades, and *ii)* a full torque actuation to control the vehicle's attitude and to monitor the thrust direction. When a person pilots a helicopter or any VTOL vehicle, he must estimate the vehicle's state (*i.e.* position, velocity, attitude), or at least part of it, in order to decide on control actions. Similarly, automatic control requires sensors that provide information on the vehicle's state and surrounding environment (*e.g.* distance to obstacles, wind direction and magnitude, external forces acting on the vehicle, *etc.*). In fact, the required information for control design may depend on the application and the control design technique itself. It can be measured or estimated from data provided by sensors embarked on the vehicle. For instance, the vehicle's vertical linear velocity can be measured by an embarked GPS, but it can also be estimated using the information of the vehicle's altitude (and vertical acceleration). Besides, the vehicle's acceleration may not be measured directly but it can be calculated via accelerometer measurements and the knowledge about the vehicle's attitude. This short discussion points out that signal processing also plays a role in the problem of state estimation and that several solutions are often available to obtain the required information. In what follows we briefly review some sensors that can be used for UAV applications.

▷ **Global Positioning System (GPS)**

The GPS is a satellite-based navigation system developed by the U.S. Department of Defense in the early 1970s. Initially, it was developed as a military system to fulfill U.S. military needs, and it has been available to civilians since 1995. The GPS consists, normally, of a constellation of 24 operational satellites which are placed such that at any location on the Globe one can observe simultaneously from four to eight satellites. Theoretically, measurements from three satellites are necessary to determine the location of the coordinates (*i.e.* longitude, latitude, altitude) of the receiver by simply applying the well-known concept of resection (see *e.g.* (Grewal et al., 2001), (El-Rabbany, 2002), (Tsui, 2005)). In practice, the accuracy obtained with this method should be 10 to $30\,m$. The so-called differential method (*i.e.* DGPS), which employs two receivers simultaneously tracking the same GPS satellites, can be used to further improve the GPS positioning accuracy. In this case a positioning accuracy level of the order of a subcentimeter to a few meters can be obtained. The GPS can also be used to determine the vehicle's linear velocity. The most widely used method, based on estimating the Doppler frequency of the received GPS signal, provides an accuracy level of the order of a few centimeters per second. The GPS may also be used to determine the attitude of a rigid body by equipping the body with a minimum of three GPS receivers (or a special receiver) connected to three antennas (more details will be provided in Chapter 3). It is worth noting that the GPS only provides measurements at low frequency and that time-delay can be significant.

▷ **Accelerometers**

Conceptually, an accelerometer behaves as a damped mass on a spring. When the accelerometer experiences an external force, the mass is displaced until the external force is balanced by the spring force. The displacement is translated into acceleration. A three-axis accelerometer embarked on a vehicle provides the measurement, in the vehicle's body frame, of the so-called *"specific acceleration"* or *"non-gravitational acceleration"* representing the sum of all non-gravitational forces applied to the vehicle divided by its mass. More precisely, it measures the term $R\left(\mathbf{a} - \mathbf{g}\right)$, where $\mathbf{a}$ is the vector of coordinates of the vehicle's acceleration and $\mathbf{g}$ is the vector of coordinates of the gravitational acceleration, both expressed in the inertial frame, and R is the rotation matrix which carries the inertial frame into the vehicle's body frame. Modern accelerometers are often small Micro Electro-Mechanical Systems (MEMS), and are indeed the simplest MEMS devices possible. These sensors are low-cost, small, light-weight, and widely used in aerial robotic applications. Accelerometers have found several applications:

- If accelerometers are highly reliable, they can be used to estimate the vehicle's linear velocity and position by means of integration and double integration respectively. This technique is typically used in Inertial Navigation Systems (INS) for short-term or medium-term applications (see e.g. (McClure, 1960)). But the estimation error diverges over time. In this case accelerometers can be combined with exteroceptive sensors like GPS for a more reliable estimation.

- In the case of weak acceleration (*i.e.* $|\mathbf{a}| \ll |\mathbf{g}|$), accelerometers can be used as inclinometers to measure the gravity direction. In this situation they can be fused with gyroscopes (and magnetometers) for attitude estimation (see e.g. (Hamel and Mahony, 2006)).

- Accelerometers can also be used to measure external forces acting on the vehicle which can be used as a feedforward term for control design purposes (see Section 2.5).

▷ **Gyroscopes**

A gyroscope detects mechanical rotation and provides the measurement of the angular velocity about its axis. A three-axis gyroscope strapped on a vehicle can measure the three components of the angular velocity of a frame attached to the vehicle relative to an inertial frame. Fiber optic gyroscopes (FOG) and ring laser gyroscopes (RLG), which make use of the interference of light (*i.e.* the Sagnac effect) to detect mechanical rotation, are highly accurate and insensitive to ambient conditions, and to the vibration and acceleration of the platform. However, their high price, large size, and important weight limit their utilization in small-scale aerial robotic applications. On the contrary, MEMS gyroscopes are less reliable than FOG and RLG, but the low price, light weight, and reasonable accuracy have made them widely popular. The principle of Inertial Navigation uses gyroscopes to measure the vehicle's angular velocity and to obtain the vehicle's heading or attitude by integrating the rigid body kinematic equation of rotation (see e.g. (McClure, 1960)). But the heading or attitude estimation error can diverge rapidly due to sensors' drift and noise. Therefore, gyroscopes are often combined with directional sensors (*e.g.* magnetometers, inclinometers, gyrocompass, *etc.*) to overcome this issue.

▷ **Inertial Measurement Unit (IMU)**

The term IMU is widely used to refer to a system containing a three-axis accelerometer and a three-axis gyroscope. Some IMU also contain a three-axis magnetometer and/or a GPS for the improved accuracy of attitude and position estimation. Two principle types of IMU to be distinguished are gimballed gyrostabilized IMU and strapdown IMU (see e.g. (Radix, 1993)).

- **Gimballed gyrostabilized IMU:** Its sensors are placed on a gimballed gyrostabilized platform which uses gyroscope measurements to control two motors of the gimballed platform, allowing to maintain the platform at the initial orientation. The vehicle's attitude is measured directly. The vehicle's position can be obtained by double integrating the acceleration measurements in the IMU frame. An important disadvantage of this type of IMU is that it uses many expensive precision mechanical parts. Their large size and high weight limit also their utilization in UAV applications.

- **Strapdown IMU:** Its sensors are strapped to the vehicle. Therefore, the accelerometer and gyroscope measurements are reported in the vehicle's body frame. The vehicle's attitude can be deduced by integrating the rigid body kinematic equation of rotation using the gyroscope measurements. The vehicle's position can be obtained by means of double integration of the vehicle's acceleration, deduced from the accelerometer measurements and the calculated attitude. Although the performance of strapdown IMUs cannot match gimballed gyrostabilized IMUs, the possibility of miniaturization make them widely used in UAV applications.

▷ **Magnetometers**

A magnetometer provides measurements of the intensity and/or direction of a magnetic

field. In particular, they can be used to measure the direction of the Earth's magnetic field (*i.e.* the geomagnetic field). However, the major inconvenience of these sensors is the influence of magnetic perturbations (due to, *e.g.*, magnetic objects in the environment or the parasite magnetic field generated by electric motors and ferrous metal on the vehicle) to their measurements. In addition, Hall effect magnetometers, which are widely used, are very sensitive to temperature change, and their measurement offsets vary also with the ambient temperature. Another application of magnetometers concerns the use of magnetic disturbances to improve IMU-based position estimation (Vissière et al., 2007).

▷ **Gyrocompasses**

A gyrocompass is a compass that finds true north by using an electrically powered fast-spinning wheel and friction forces in order to exploit the rotation of the Earth. Gyrocompasses have two main advantages over magnetic compasses: *i)* they find true north, *i.e.* the direction of Earth's rotational axis, as opposed to magnetic north, and *ii)* they are far less sensitive to external magnetic fields. However, their high price and important weight limit their utilization in small-scale aerial robotic applications.

▷ **Pitot tubes**

A pitot tube is a pressure measurement instrument for the measurement of the fluid flow velocity. It can be used to determine the airspeed of an aircraft, *i.e.* the speed of an aircraft relative to the air. The basic pitot tube consists of a tube pointing directly into the fluid flow. The measured pressure is the stagnation pressure of the fluid, also known as the total pressure. According to Bernoulli's principle, one has $p_t = p_s + \rho V^2/2$, where V is the fluid velocity, p_t is stagnation or total pressure, p_s is static pressure, and ρ is fluid density. Then, the fluid velocity can be directly deduced from this relation. Being widely used in airplane applications, pitot tubes are in turn rarely used in VTOL UAVs. This is essentially due to the fact that control design for a VTOL vehicle is often based on its linear velocity rather than the airspeed as in the case of airplanes.

▷ **Barometric altimeters**

A barometric altimeter measures the atmospheric pressure at its level and converts the pressure measurement to an indication of altitude above sea level. As the air pressure decreases at altitudes above sea level, the actual reading of the instrument is dependent upon its location. The standard pressure-altitude relationship (up to $11000\,m$) is given by $h = (1 - (P/P_{sl})^{0.19026})\, 288.15/0.0065\,(m)$, with P the measured pressure and P_{sl} the sea level pressure (both measured in pascals). The altitude measurement is strongly related to environmental situations, and, subsequently, it can be rather erroneous due to, *e.g.*, wind gusts. Therefore, these sensors, especially MEMS types, are preferred for indoor applications of UAVs (rather than outdoor applications).

▷ **Telemeters**

This family of sensors provides the measurement of the distance to a remote target. They can be mounted on a rotating platform to reconstruct the scene on a horizontal plane. They are classified by the nature of the transmitting signal (*e.g.* ultrasound, laser, radio wave) and also by the method to deduce the distance. Basically, a signal is propagated from the telemeter's transmitter to the target and returns to its receiver by

reflection. Then, the distance is deduced from the actual measurements. For instance, laser telemeters can use either *"time of flight"* or *"interferometry"* methods for distance measurements.

- In *time of flight* method, the time delay $T = 2L/c$ (with c the signal speed) for the reflection to return is measured and the distance follows as $L = cT/2$.

- In *interferometry* method, a coherent laser beam is used in the propagation to the target. The returned field is detected and compared with a reference field on a photodetector to deduce the differential phase measurement which itself allows the calculation of the distance to the nearest obstacle in the beam direction.

Radar telemeters or sonar telemeters measure the distance to an object based on the *time of flight* method. They transmit a short pulse of radio signal or ultrasonic signal and measure the time it takes for the reflection to return. Radar telemeters can also measure a relative velocity between the sensors and obstacles using the Doppler effect. Laser and radar telemeters are suitable for obstacle avoidance in UAV applications because they have wide operating ranges. On the contrary, sonar telemeters are rarely used for such a mission due to their limited ranges. In turn, they are often used for automatic landing of VTOL vehicles.

▷ **Cameras**

Cameras can be mounted on UAVs to provide visual information on the surrounding environment. Cameras are probably the most versatile sensors, but they have also many shortcomings including the sensitivity to light of the visual information and the expensive computation of image processing. Classically, cameras are used to estimate the vehicle's pose (*i.e.* position and orientation) relative to observed target. For UAV applications, this information can be used, instead of the GPS measurements, for tracking control design. There exist basically two strategies to derive the vehicle's pose from the visual information.

- The first strategy consists in using two (or more) cameras and the mapping of visual data obtained by each camera. For instance, stereo camera (*i.e.* a pair of cameras) operates similarly to human eyes for pose estimation (see e.g. (Trucco and Verri, 1998), (Ma et al., 2004)). Note that the accuracy of the estimated pose is proportional to the baseline length (*i.e.* the distance between two cameras). Limited accuracy of the estimated pose is thus to be expected for small-size UAVs.

- The second strategy combines a camera with other information (like, *e.g.*, the measurements provided by other sensors or a priori knowledge on the visual target). For instance, a camera can be combined with GPS and IMU for an improved estimation of the vehicle's state by means of filtering process.

Another application concerns the bio-inspired approach which uses a single camera to calculate the optical flow (see e.g. (Trucco and Verri, 1998) for the theory and (Ruffier et al., 2009) for numerous citations). This can be used for obstacle avoidance, altitude stabilization, or landing in UAV applications (see e.g. (Ruffier and Franceschini, 2004), (Herisse et al., 2009) and the references therein).

1.4   Modeling of RWVTOL vehicles

Classically, RWVTOL vehicles are modeled as rigid bodies and their equations of motion are derived from the application of Newton's and Euler's theorems of mechanics. Flapping dynamics of the propellers are also modeled in the literature (Prouty, 2002), (Bristeau et al., 2009), (Huang et al., 2009), (Pounds et al., 2010). However, for simplicity they are not considered in the present section. Consider a vehicle moving in a 3D-space and subjected to a force vector $F_{\mathcal{B}} \in \mathbb{R}^3$ and a torque vector $\Gamma_{\mathcal{B}} \in \mathbb{R}^3$, applied at its center of mass (CoM) and expressed in the vehicle's body frame. Then, the vehicle's equations of motion, expressed in the body frame, are given by (see *e.g.* (Murray et al., 1994))

$$\begin{bmatrix} mI_3 & 0 \\ 0 & J \end{bmatrix} \begin{bmatrix} \dot{v} \\ \dot{\omega} \end{bmatrix} + \begin{bmatrix} \omega \times mv \\ \omega \times J\omega \end{bmatrix} = \begin{bmatrix} F_{\mathcal{B}} \\ \Gamma_{\mathcal{B}} \end{bmatrix}, \tag{1.1}$$

where $v \triangleq [v_1, v_2, v_3]^\top \in \mathbb{R}^3$ is the vehicle's linear velocity vector expressed in the body frame, $\omega \triangleq [\omega_1, \omega_2, \omega_3]^\top \in \mathbb{R}^3$ is the body angular velocity vector, $m \in \mathbb{R}$ specifies its mass, $J \in \mathbb{R}^3$ is its inertia matrix. Denote $x \in \mathbb{R}^3$ as the position of the vehicle's CoM expressed in the inertial frame, and R the rotation matrix of the body frame relative to the inertial frame. Using $\dot{x} = Rv$ and [6] $\dot{R} = RS(\omega)$ the vehicle's equations of motion can be rewritten as

$$\begin{bmatrix} \dot{x} \\ m\dot{v} \\ \dot{R} \\ J\dot{\omega} \end{bmatrix} = \begin{bmatrix} Rv \\ -mS(\omega)v + F_{\mathcal{B}} \\ RS(\omega) \\ -S(\omega)J\omega + \Gamma_{\mathcal{B}} \end{bmatrix}, \tag{1.2}$$

In what follows models of RWVTOL vehicles, found in the literature, will be reviewed.

1.4.1   Single rotor helicopter model

A number of helicopter models can be found in the literature (see *e.g.* (Prouty, 2002), (Mettler, 2002), (Koo and Sastry, 1998), (Mahony et al., 1999), (Marconi and Naldi, 2008), (Vilchis, 2001), (Martini, 2008)). Here, we choose a helicopter model which may be seen as a combination of the models reported in (Koo and Sastry, 1998), (Mahony et al., 1999), and (Marconi and Naldi, 2008). More precisely, the model of forces and torques created by the helicopter's force/torque generation mechanism is given in (Koo and Sastry, 1998), and the model of the aerodynamic forces and torques induced by the interaction of the fuselage, the vertical fin, and the horizontal stabilizer with the relative wind are reported in (Marconi and Naldi, 2008). According to these works, the force and torque vectors $F_{\mathcal{B}}, \Gamma_{\mathcal{B}}$ can be modeled as

$$\begin{cases} F_{\mathcal{B}} = \begin{bmatrix} X_M \\ Y_M + Y_T \\ Z_M \end{bmatrix} + R^\top mge_3 + F_{ae}^{\mathcal{B}} \\ \Gamma_{\mathcal{B}} = \begin{bmatrix} R_M \\ M_M + M_T \\ N_M \end{bmatrix} + \begin{bmatrix} -Y_M h_M + Z_M y_M - Y_T h_T \\ -Z_M l_M + X_M h_M \\ -X_M y_M + Y_M l_M + Y_T l_T \end{bmatrix} + \Gamma_{ae}^{\mathcal{B}} \end{cases} \tag{1.3}$$

with $[l_M, y_M, h_M]^\top$ and $[l_T, y_T, h_T]^\top$ the coordinates of the center of the main and tail

---

6. $S(\cdot)$ is the 3×3 skew-symmetric matrix associated with the cross product $\times$, *i.e.* $S(u)v = u \times v$, $\forall u, v \in \mathbb{R}^3$.
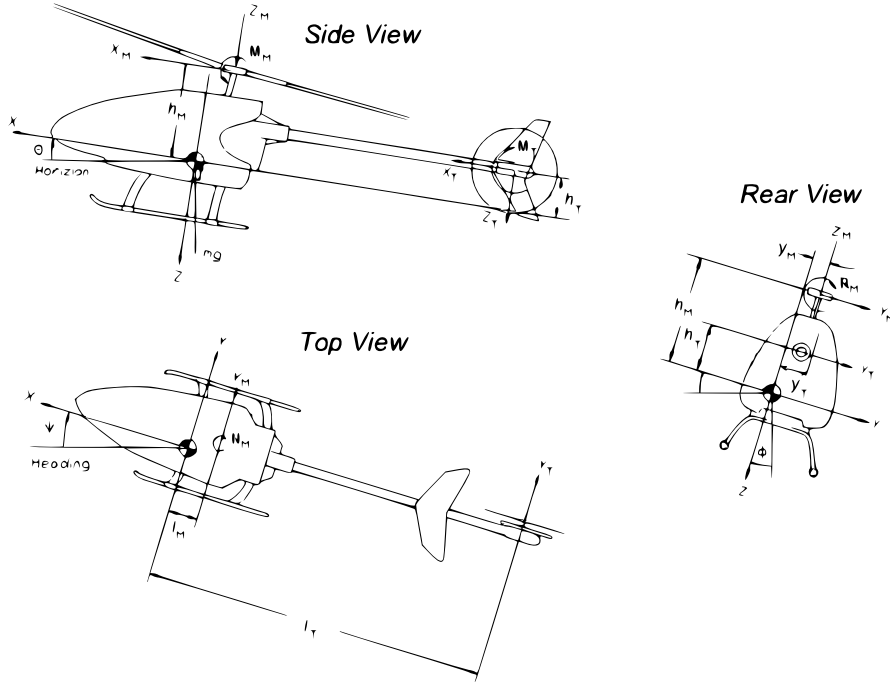
Figure 1.14: Diagram of a helicopter (source (Koo and Sastry, 1998)).

rotor disks, expressed in the body frame (see Fig. 1.14), g the magnitude of the gravity acceleration, and $e_3 \triangleq [0, 0, 1]^\top$. Note that the configuration illustrated in Fig. 1.14 corresponds to $l_M < 0$, $y_M > 0$, $h_M < 0$, $l_T < 0$, $y_T > 0$, $h_T < 0$. The forces and torques generated by the main and tail rotors, involved in (1.3), are modeled as [7]

$$
\begin{aligned}
X_M &= \frac{-T_M \sin a \cos b}{\sqrt{1 - \sin^2 a \sin^2 b}}, & R_M &= \frac{\partial R_M}{\partial b} b - \frac{Q_M \sin a \cos b}{\sqrt{1 - \sin^2 a \sin^2 b}}, \\
Y_M &= \frac{T_M \sin b \cos a}{\sqrt{1 - \sin^2 a \sin^2 b}}, & \text{and} \quad M_M &= \frac{\partial M_M}{\partial a} a + \frac{Q_M \sin b \cos a}{\sqrt{1 - \sin^2 a \sin^2 b}}, \\
Z_M &= \frac{-T_M \cos a \cos b}{\sqrt{1 - \sin^2 a \sin^2 b}}, & N_M &= \frac{-Q_M \cos a \cos b}{\sqrt{1 - \sin^2 a \sin^2 b}}, \\
Y_T &= -T_T, & M_T &= -Q_T,
\end{aligned}
$$

where T_M, T_T are, respectively, the main rotor thrust and the tail rotor thrust; a, b ($\ll 1$) are, respectively, the longitudinal and lateral tilts of the path plane of the main rotor about the shaft; $\partial R_M / \partial b$, $\partial M_M / \partial a$ are the so-called *rolling moment stiffness* and *pitching moment stiffness*, representing the flapping dynamics of the main rotor; Q_M and Q_T are, respectively, the total main rotor and tail rotor parasite torques. Let us recall that:

- The thrust force T_M (resp. T_T) and the torque Q_M (resp. Q_T) can be modeled as functions of the angular velocity and angle of attack of the main rotor (resp. the tail rotor). See (Koo and Sastry, 1998) and (Marconi and Naldi, 2008) for two different modelings of Q_M and Q_T. For instance, in (Koo and Sastry, 1998) they are modeled

---

7. Some errors in (Koo and Sastry, 1998) have been rectified in (Mahony et al., 1999).

as $Q_i = C_i^Q T_i^{1.5} + D_i^Q$, for $i = M, T$, with C_i^Q, D_i^Q some parametric constants depending on the characteristics of the blades.

- The terms $\partial R_M / \partial b$ and $\partial M_M / \partial a$ are modeled as constant parameters in (Koo and Sastry, 1998) and (Marconi and Naldi, 2008). However, this modeling is only meaningful if the angular velocity of the main rotor varies in a "small" neighborhood of the nominal value (*i.e.* the value for which, with a nominal collective pitch, the intensity of the main rotor thrust is equal to the vehicle's weight). In (Prouty, 2002), as a consequence of Coriolis effect acting on the rotating blades, $\partial R_M / \partial b$ and $\partial M_M / \partial a$ are modeled as functions proportional to the square of the angular velocity of the main rotor.

The aerodynamic force and torque vectors $F_{ae}^{\mathcal{B}}$, $\Gamma_{ae}^{\mathcal{B}} \in \mathbb{R}^3$ are modeled as (see (Marconi and Naldi, 2008), (Naldi, 2008) for more details)

$$F_{ae}^{\mathcal{B}} = \begin{bmatrix} -k_1^f v_{e,1} V_\infty \\ -k_2^f v_{e,2} V_\infty - k_2^a v_{vf}^2 \\ -k_3^f (v_{e,3} + V_{induced}) V_\infty - k_3^a v_{hs}^2 \end{bmatrix}, \quad \Gamma_{ae}^{\mathcal{B}} = \begin{bmatrix} k_2^a h_T v_{vf}^2 - k_3^a y_T v_{hs}^2 \\ k_3^a l_T v_{hs}^2 \\ -k_2^a l_T v_{vf}^2 \end{bmatrix}, \quad (1.4)$$

where k_1^f, k_2^f, k_3^f, k_2^a, k_3^a are aerodynamic drag coefficients; $v_{vf} \triangleq v_2 + l_T \omega_3$; $v_{hs} \triangleq v_3 - l_T \omega_2$; the air velocity induced by the main rotor $V_{induced}$ is given by $V_{induced} \triangleq \sqrt{2T_M/(\rho A_{disk})}$ with ρ the air density, A_{disk} the main rotor disk area; the relative-wind velocity v_e, expressed in the body frame, is given by $v_e \triangleq R^\top (\dot{x} - \dot{x}_f)$, with $\dot{x}_f$ the wind velocity vector expressed in the inertial frame; and $V_\infty \triangleq \sqrt{v_{e,1}^2 + v_{e,2}^2 + (v_{e,3} + V_{induced})^2}$. Throughout this dissertation, the analytic expressions of $F_{ae}^{\mathcal{B}}$ and $\Gamma_{ae}^{\mathcal{B}}$, here introduced, are only used for simulation purposes.

Now let us review approximations often made in the literature for control design purposes. Firstly, by considering the vector $[T_M, b, a, T_T]^\top$ as the available control inputs, and by using the approximations $\sin a \approx a$, $\sin b \approx b$, $\cos a \approx 1$, $\cos b \approx 1$ (since $a, b \ll 1$), and equally Eq. (1.3), one obtains

$$\begin{cases} F_{\mathcal{B}} \approx -T_M e_3 + F_\varepsilon + R^\top mg e_3 + F_{ae}^{\mathcal{B}} \\ \Gamma_{\mathcal{B}} \approx A(T_M) \begin{bmatrix} b \\ a \\ T_T \end{bmatrix} + B(T_M) + \Gamma_{ae}^{\mathcal{B}} \end{cases} \quad (1.5)$$

with

$$A(T_M) \triangleq \begin{bmatrix} -T_M h_M + \frac{\partial R_M}{\partial b} & -Q_M & h_T \\ Q_M & -T_M h_M + \frac{\partial M_M}{\partial a} & 0 \\ T_M l_M & T_M y_M & -l_T \end{bmatrix}, \quad B(T_M) \triangleq \begin{bmatrix} -T_M y_M \\ T_M l_M - Q_T \\ -Q_M \end{bmatrix},$$

and

$$F_\varepsilon \triangleq \begin{bmatrix} -T_M a \\ T_M b - T_T \\ 0 \end{bmatrix}.$$

The force vector F_ε, which is the so-called *"small body forces"* in the literature, represents the couplings between forces and moments produced by the vehicle actuators. This term is often neglected in the control model for the sake of control design.

Further approximations can be made when $\partial R_M/\partial b$, $\partial M_M/\partial a$, Q_M, and Q_T are negligible against $T_M h_M$, so that by considering $T \in \mathbb{R}$ and $\Gamma \in \mathbb{R}^3$ as control inputs, with

$$\Gamma = \begin{bmatrix} -h_M & 0 & h_T \\ 0 & -h_M & 0 \\ l_M & y_M & -l_T \end{bmatrix} \begin{bmatrix} bT \\ aT \\ T_T \end{bmatrix}, \quad T = T_M, \tag{1.6}$$

one obtains $F_\varepsilon \approx \Sigma_R \Gamma$, $B(T_M) \approx T\Sigma_T$, and

$$\begin{cases} F_\mathcal{B} \approx -Te_3 + \Sigma_R \Gamma + R^\top mge_3 + F_{ae}^\mathcal{B} \\ \Gamma_\mathcal{B} \approx \Gamma + T\Sigma_T + \Gamma_{ae}^\mathcal{B} \end{cases} \tag{1.7}$$

with

$$\Sigma_T \triangleq \begin{bmatrix} -y_M \\ l_M \\ 0 \end{bmatrix}, \Sigma_R \triangleq \begin{bmatrix} 0 & \varepsilon_1 & 0 \\ \varepsilon_2 & \varepsilon_3 & \varepsilon_4 \\ 0 & 0 & 0 \end{bmatrix}$$

$$\varepsilon_1 \triangleq \frac{1}{h_M}, \; \varepsilon_2 \triangleq \frac{l_M - l_T}{h_M l_T - h_T l_M}, \; \varepsilon_3 \triangleq \frac{y_M(h_M - h_T)}{h_M(h_M l_T - h_T l_M)}, \; \varepsilon_4 \triangleq \frac{h_M - h_T}{h_M l_T - h_T l_M}. \tag{1.8}$$

Note that Σ_T and Σ_R are constant. Such approximations allow to express the couplings between the force and torque control inputs, *i.e.* T, Γ, in an affine manner. Note that $y_M \ll 1$ for most of helicopter designs, so that ε_3 can be neglected. In particular, if $h_M = h_T$ then $\Sigma_R = -1/h_M S(e_3)$.

1.4.2 Ducted fan tailsitter model
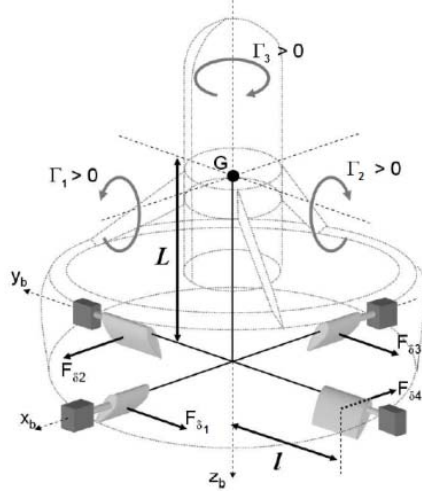
Figure 1.15: Diagram of a ducted fan tailsitter (source (Pflimlin, 2006)).

Some models of ducted fan tailsitters have been proposed recently (see *e.g.* (Pflimlin et al., 2007a), (Pflimlin, 2006), (Naldi, 2008)). In this subsection we briefly present a model of a class of ducted fan tailsitters with counter-rotating rotors whose shapes correspond to the one depicted in Fig. 1.15. These vehicles are symmetric about the z-axis and their inertia matrix has a particular diagonal form $J = \mathbf{diag}(J_1, J_1, J_3)$. The model of the

forces and torques generated by the force/torque generation mechanism can be found in (Pflimlin et al., 2007a), (Pflimlin, 2006). Aerodynamic effects are modeled in (Hua, 2006) and (Hua et al., 2008) for the HoverEye ducted fan tailsitter based on wind-tunnel measurements reported in (Pflimlin, 2006). More precisely, one has (see (Pflimlin, 2006))

$$
\begin{cases}
F_{\mathcal{B}} = -Te_3 + \begin{bmatrix} F_{\delta_2} + F_{\delta_4} \\ F_{\delta_1} + F_{\delta_3} \\ 0 \end{bmatrix} + R^\top mge_3 + F_{ae}^{\mathcal{B}} \\
\Gamma_{\mathcal{B}} = \Gamma + \Gamma_{ae}^{\mathcal{B}}
\end{cases}
\tag{1.9}
$$

where $T \in \mathbb{R}$ and $\Gamma \in \mathbb{R}^3$ are, respectively, the thrust force and torque control inputs; F_{δ_i} ($i = 1, 2, 3, 4$) are aerodynamic lift forces created by the system of flaps located below the rotor system. They apply respectively at the points $A_1 = [l, 0, L]^\top$, $A_2 = [0, l, L]^\top$, $A_3 = [-l, 0, L]^\top$, $A_4 = [0, -l, L]^\top$, with coordinates expressed in the body frame (see Fig. 1.15). The model of aerodynamic force and torque vectors $F_{ae}^{\mathcal{B}}$ and $\Gamma_{ae}^{\mathcal{B}}$ is given in (Hua, 2006) as follows

$$
\begin{aligned}
F_{ae}^{\mathcal{B}} &= \begin{bmatrix} -k_1^e \sqrt{v_{e,1}^2 + v_{e,2}^2}\, v_{e,1} - k_2^e |v_e| v_{e,1} \\ -k_1^e \sqrt{v_{e,1}^2 + v_{e,2}^2}\, v_{e,2} - k_2^e |v_e| v_{e,2} \\ -k_3^e (v_{e,1}^2 + v_{e,2}^2) - k_4^e |v_{e,3}| v_{e,3} \end{bmatrix} - k_5^e \sqrt{T} v_e\,, \\
\Gamma_{ae}^{\mathcal{B}} &= \varepsilon_{ae} \begin{bmatrix} k_1^e \sqrt{v_{e,1}^2 + v_{e,2}^2}\, v_{e,2} + k_2^e |v_e| v_{e,2} \\ -k_1^e \sqrt{v_{e,1}^2 + v_{e,2}^2}\, v_{e,1} - k_2^e |v_e| v_{e,1} \\ 0 \end{bmatrix} - \varepsilon_m k_5^e \sqrt{T} S(e_3) v_e\,,
\end{aligned}
\tag{1.10}
$$

where k_i^e ($i = 1, .., 5$) are aerodynamic coefficients, ε_{ae}, ε_m are aerodynamic level arms, and the relative-wind velocity v_e expressed in the body frame is given by $v_e \triangleq R^\top(\dot{x} - \dot{x}_f)$, with $\dot{x}_f$ the wind velocity vector expressed in the inertial frame. The first term in the expression of $F_{ae}^{\mathcal{B}}$ in (1.10) corresponds to the sum of aerodynamic drag and lift forces acting on the duct, whereas the second term corresponds to the momentum drag resulting from the airflow circulated through the ducted structure, and from a direct application of the momentum theory (see (Pflimlin et al., 2007a), (Pflimlin, 2006) for more details). Throughout this dissertation, the analytic expressions of $F_{ae}^{\mathcal{B}}$ and $\Gamma_{ae}^{\mathcal{B}}$, here introduced, are only used for simulation purposes.

The forces F_{δ_i} ($i = 1, 2, 3, 4$) are modeled as functions of the deflection angles of the flaps δ_i and the thrust force T as $F_{\delta_i} = k_\delta T \delta_i$, with k_δ an aerodynamic parameter. They are also related to the torque control input Γ by the relationship (see (Pflimlin, 2006))

$$
\Gamma = PF_\delta,
$$

with

$$
P \triangleq \begin{bmatrix} -L & 0 & -L & 0 \\ 0 & L & 0 & L \\ l & -l & -l & l \end{bmatrix}, \quad F_\delta \triangleq [F_{\delta_1}, F_{\delta_2}, F_{\delta_3}, F_{\delta_4}]^\top.
$$

In (Pflimlin, 2006), using that $PP^\top$ is full rank ($PP^\top = \mathbf{diag}(2L^2, 2L^2, 4l^2)$) and that $\Gamma = PF_\delta$, a formula to convert Γ into the elementary force control F_δ is proposed as

$$
F_\delta = P^\top (PP^\top)^{-1} \Gamma.
$$

As a consequence, relationships in (1.9) can be rewritten as

$$
\begin{cases}
F_{\mathcal{B}} = -Te_3 + \Sigma_R \Gamma + R^\top mge_3 + F_{ae}^{\mathcal{B}} \\
\Gamma_{\mathcal{B}} = \Gamma + \Gamma_{ae}^{\mathcal{B}}
\end{cases}
\tag{1.11}
$$

with

$$
\Sigma_R \triangleq -\frac{1}{L}S(e_3).
\tag{1.12}
$$

The term $\Sigma_R \Gamma$ is the *"small body forces"* representing the couplings between moments and forces produced by actuators. These couplings are physically justified by the fact that the moment control inputs are intermediately monitored via aerodynamic lift forces acting on the system of flaps. Alike the case of helicopters, they are often neglected for the sake of control design when the translation dynamics is involved (*e.g.* for velocity or position stabilization).

In (Pflimlin, 2006), a solution to eliminate the torque control Γ in the translational dynamics is proposed. It consists in considering a specific control point, located on the z-axis and above the vehicle's CoM. More precisely, by setting

$$
\begin{cases}
x_D \triangleq x + dRe_3 \\
v_D \triangleq v - dS(e_3)\omega, \quad \text{with} \quad d \triangleq -\dfrac{J_1}{mL}, \\
\overline{T} \triangleq T + md|\omega|^2
\end{cases}
$$

and using System (1.2) with $F_{\mathcal{B}}$ and $\Gamma_{\mathcal{B}}$ given in (1.11), one obtains the following equations of motion of the new control point

$$
\begin{bmatrix}
\dot{x}_D \\
m\dot{v}_D \\
\dot{R} \\
J\dot{\omega}
\end{bmatrix}
=
\begin{bmatrix}
Rv_D \\
-mS(\omega)v_D - \overline{T}e_3 + R^\top mge_3 + F_{ae}^{\mathcal{B}} + \frac{1}{L}S(e_3)\Gamma_{ae}^{\mathcal{B}} + \Delta_r \\
RS(\omega) \\
-S(\omega)J\omega + \Gamma + \Gamma_{ae}^{\mathcal{B}}
\end{bmatrix},
\tag{1.13}
$$

with $[\overline{T}, \Gamma]^T$ the new control inputs, and [8]

$$
\Delta_r = -\frac{\omega_3}{L}\left(J_3\omega_1 e_1 + J_3\omega_2 e_2 + J_1\omega_3 e_3\right).
\tag{1.14}
$$

The term Δ_r is called *"perturbation term"* in (Pflimlin, 2006). If the yaw angular velocity is regulated near zero, this term can be neglected.

1.4.3   Quadrotor helicopter model

Unlike single rotor helicopters and ducted fan tailsitters where *small body forces* $\Sigma_R \Gamma$ appear in the translational dynamics, for quadrotor helicopters these forces are basically absent. To be more precise, let us recall the model of a quadrotor helicopter in free, still air proposed in (Hamel et al., 2002). The four rotors position offsets from the vehicle's CoM are characterized by the points $A_1 = [d, 0, h]^\top$, $A_2 = [0, d, h]^\top$, $A_3 = [-d, 0, h]^\top$, $A_4 = [0, -d, h]^\top$, with coordinates expressed in the body frame (see Fig. 1.16). The thrust

---

8. $\{e_1, e_2, e_3\}$ denote the canonical base of $\mathbb{R}^3$.
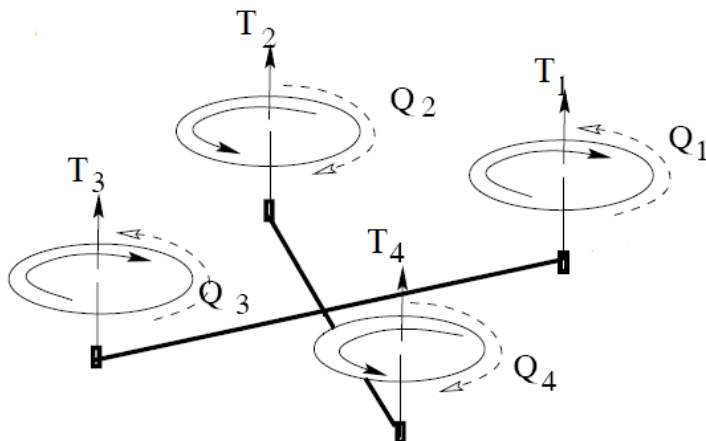
Figure 1.16: Diagram of a quadrotor helicopter (source (Hamel et al., 2002)).

force T_i and the antitorque Q_i (due to rotor drag) generated by the rotor i ($i = 1, .., 4$) can be modeled as

$$T_i = -b\varpi_i^2 e_3 \,,$$
$$Q_i = \kappa \varpi_i^2 \,,$$

where ϖ_i is the angular velocity of the rotor i about its axis, and $b > 0$ and $\kappa > 0$ are aerodynamic parameters. By denoting $T \in \mathbb{R}$ and $\Gamma \in \mathbb{R}^3$ the thrust force and torque control inputs applied to the vehicle, one deduces that

$$\begin{bmatrix} T \\ \Gamma \end{bmatrix} = \begin{bmatrix} -b & -b & -b & -b \\ 0 & db & 0 & -db \\ db & 0 & -db & 0 \\ \kappa & -\kappa & \kappa & -\kappa \end{bmatrix} \begin{bmatrix} \varpi_1^2 \\ \varpi_2^2 \\ \varpi_3^2 \\ \varpi_4^2 \end{bmatrix} = A \begin{bmatrix} \varpi_1^2 \\ \varpi_2^2 \\ \varpi_3^2 \\ \varpi_4^2 \end{bmatrix} \,.$$

One can verify that the matrix $A \in \mathbb{R}^{4\times 4}$ defined above is invertible for $d, b, \kappa > 0$. Then, the vehicle's equations of motion in free, still air are given by

$$\begin{bmatrix} \dot{x} \\ m\dot{v} \\ \dot{R} \\ J\dot{\omega} \end{bmatrix} = \begin{bmatrix} Rv \\ -mS(\omega)v - Te_3 + R^\top mge_3 \\ RS(\omega) \\ -S(\omega)J\omega + \Gamma + \Gamma_g \end{bmatrix} \,, \tag{1.15}$$

where Γ_g is the gyroscopic torque vector given by

$$\Gamma_g = -\sum_{i=1,..,4} I_r \varpi_i S(\omega) e_3 \,,$$

and I_r is the moment of inertia of a rotor about its axis.

1.4.4   General model

In view of the three above modeling examples we note that, with a good approximation, the equations of motion of a RWVTOL vehicle are given by

$$
\begin{bmatrix} \dot{x} \\ m\dot{v} \\ \dot{R} \\ J\dot{\omega} \end{bmatrix} = \begin{bmatrix} Rv \\ -mS(\omega)v - Te_3 + \Sigma_R\Gamma + R^\top mge_3 + F_{ae}^{\mathcal{B}} \\ RS(\omega) \\ -S(\omega)J\omega + \Gamma + T\Sigma_T + \Gamma_{ae}^{\mathcal{B}} \end{bmatrix},
\tag{1.16}
$$

with $T \in \mathbb{R}$ and $\Gamma \in \mathbb{R}^3$ the thrust force and torque control inputs; $F_{ae}^{\mathcal{B}} \in \mathbb{R}^3$ and $\Gamma_{ae}^{\mathcal{B}} \in \mathbb{R}^3$ the sum of all aerodynamic forces and torques acting on the vehicle, expressed in the body frame; $\Sigma_R \in \mathbb{R}^{3\times3}$ and $\Sigma_T \in \mathbb{R}^3$ constant matrices, representing the coupling between forces and torques created by the force/torque generation mechanism.

   The influence of the translational dynamics on the rotational dynamics appears through the term $T\Sigma_T$. In the case of single rotor helicopter, this term is physically justified by the fact that the thrust force vector does not apply at the vehicle's CoM exactly. However, this term is not bothering because, for most RWVTOL vehicles, it is rather "small", thus, it can be compensated via full torque actuation. On the other hand, the influence of the rotational dynamics on the translational dynamics is more involved. Generally, Σ_R is different from the null matrix, except the case of quadrotor helicopters. For instance, Σ_R is given by Eq. (1.12) for ducted fan tailsitters, and by Eq. (1.8) for single rotor helicopters. It is not null either for tandem helicopters (see *e.g.* (Dzul et al., 2002) for details). However, as long as small body forces $\Sigma_R\Gamma$ remain small, and the control law is adequately designed, these forces are not problematic. In turn, the issue of robustness with respect to aerodynamic perturbations, *i.e.* the terms $F_{ae}^{\mathcal{B}}$ and $\Gamma_{ae}^{\mathcal{B}}$, is more important. In practice, it is extremely difficult to obtain a well-tuned model of these aerodynamic effects which can be used for control design purposes. Unpredictable wind gusts resulting in unpredictable aerodynamic effects complicate this robustness issue even more. In the next section, more details clarifying these control difficulties will be provided, along with associated solutions proposed in the literature.

1.5   Survey on the control of RWVTOL vehicles

RWVTOL vehicles have long attracted the automatic community due to a number of challenges associated with these systems. Control difficulties are directly related to the fact that these vehicles are underactuated and strongly nonlinear, that their envelop of flight can be very large, and that they are usually subjected to uncertainties and unmodeled dynamics, *etc.*. Control design methods for these vehicles have been investigated in both contexts of linear and nonlinear control systems. In what follows a panorama of these methods is sketched.

1.5.1   Linear control using linear approximations

In the context of linear control theory, the control design for helicopters and other RWVTOL vehicles is based on linear approximations along trim trajectories[9]. Commonly, the

---

   9. Trajectories for which $\dot{v} = 0$, $\dot{\omega} = 0$.

direct application of linear approximations leads to the use of Euler angles $\{\phi, \theta, \psi\}$ for attitude parametrization, allowing for the decoupling of the linearized system into four Single-Input-Single-Output (SISO) systems associated with the regulation of a single variable (longitudinal position or velocity, lateral position or velocity, yaw, and altitude) (see *e.g.* (Prouty, 2002), (Pflimlin et al., 2007a), (Peddle et al., 2009), *etc.*). To be more precise, let us recall an example case reported in (Pflimlin et al., 2007a) for the hovering control mode of a symmetric ducted fan tailsitter in the absence of wind gusts. The system under consideration takes the form of System (1.2) with $F_{\mathcal{B}}$ and $\Gamma_{\mathcal{B}}$ given by (1.11) (see Section 1.4.2). By assuming that the vehicle's translational and rotational velocities are relatively small (*i.e.* near hover flight), all aerodynamic drag and lift forces, which are proportional to the square of the vehicle's velocities, can be neglected. In turn, the momentum drag (a particularity of ducted fan tailsitters) can be approximated by $-Qv$, with $Q \triangleq k_5^e \sqrt{mg}$. Therefore, one obtains

$$\begin{cases} F_{\mathcal{B}} \approx -(T - mg)e_3 - \dfrac{1}{L}S(e_3)\Gamma - Qv \\ \Gamma_{\mathcal{B}} \approx \Gamma - \varepsilon_m Q S(e_3)v \end{cases}$$

Denoting $v_{\mathcal{I}} \triangleq \dot{x}$ and using Euler angles for attitude parametrization, in first-order approximations the system is equivalent to the four following SISO linear systems:

- The longitudinal channel

$$\begin{bmatrix} \dot{x}_1 \\ \dot{v}_{\mathcal{I},1} \\ \dot{\theta} \\ \dot{\omega}_2 \end{bmatrix} = \begin{bmatrix} 0 & 1 & 0 & 0 \\ 0 & -Qm^{-1} & -g & 0 \\ 0 & 0 & 0 & 1 \\ 0 & -\varepsilon_m Q J_1^{-1} & 0 & 0 \end{bmatrix} \begin{bmatrix} x_1 \\ v_{\mathcal{I},1} \\ \theta \\ \omega_2 \end{bmatrix} + \begin{bmatrix} 0 \\ (mL)^{-1} \\ 0 \\ J_1^{-1} \end{bmatrix} \Gamma_2 \, ;$$

- The lateral channel

$$\begin{bmatrix} \dot{x}_2 \\ \dot{v}_{\mathcal{I},2} \\ \dot{\phi} \\ \dot{\omega}_1 \end{bmatrix} = \begin{bmatrix} 0 & 1 & 0 & 0 \\ 0 & -Qm^{-1} & g & 0 \\ 0 & 0 & 0 & 1 \\ 0 & \varepsilon_m Q J_1^{-1} & 0 & 0 \end{bmatrix} \begin{bmatrix} x_2 \\ v_{\mathcal{I},2} \\ \phi \\ \omega_1 \end{bmatrix} + \begin{bmatrix} 0 \\ -(mL)^{-1} \\ 0 \\ J_1^{-1} \end{bmatrix} \Gamma_1 \, ;$$

- The altitude channel

$$\begin{bmatrix} \dot{x}_3 \\ \dot{v}_{\mathcal{I},3} \end{bmatrix} = \begin{bmatrix} 0 & 1 \\ -Qm^{-1} & 0 \end{bmatrix} \begin{bmatrix} x_3 \\ v_{\mathcal{I},3} \end{bmatrix} + \begin{bmatrix} 0 \\ -m^{-1} \end{bmatrix} (T - mg) \, ;$$

- The yaw channel

$$\begin{bmatrix} \dot{\psi} \\ \dot{\omega}_3 \end{bmatrix} = \begin{bmatrix} 0 & 1 \\ 0 & 0 \end{bmatrix} \begin{bmatrix} \psi \\ \omega_3 \end{bmatrix} + \begin{bmatrix} 0 \\ J_3^{-1} \end{bmatrix} \Gamma_3 .$$

From here, all kinds of linear control design techniques can be applied to each channel.

Linear control methods have been applied (with more or less success) to many RWVTOL vehicles. For instance, Proportional Integral Derivative (PID) control laws were designed for hover control and slow translational motion control for RWVTOL vehicles such as the iSTAR (Lipera et al., 2001), SLADe (Peddle et al., 2009), HoverEye (Pflimlin et al., 2007a) ducted fan tailsitters, or a quadrotor helicopter (Castillo et al., 2005), *etc.*. Besides, optimal control techniques have been widely applied to these systems. Let us review some examples:

- Linear-Quadratic-Regulator (LQR) controllers (Kwakernaak and Sivan, 1972) were proposed, *e.g.*, for the Short Range Station Keeping (SRSK) task of an assault helicopter (Rynaski, 1966), for the stabilization of the lateral position and roll angle of a quadrotor helicopter (Castillo et al., 2005), for the altitude stabilization of the Caltech ducted fan in forward flight (Teel et al., 1997), for velocity control of a tailsitter (Stone, 2004), *etc.*.

- The Linear-Quadratic-Gaussian (LQG) control technique (Stein and Athans, 1987), which can be simply viewed as a combination of a Kalman filter with a LQR, has been investigated for helicopter control (see *e.g.* (Bendotti and Morris, 1995), (Mammar, 1992), (Benallegue et al., 2006), and the references therein).

- The H_2 and H_∞ control techniques (see *e.g.* (Zames, 1981), (Francis and Zames, 1984), (Doyle et al., 1989)) have also been widely used (see *e.g.* (Mammar and Duc, 1992), (Takahashi, 1993), (Civita et al., 2003), (Luo et al., 2003), (Prempain and Postlethwaite, 2005), and the references therein). In (Bendotti and Morris, 1995), (Mammar, 1992) the authors recorded through simulation and experimental results that H_∞ controllers (defined by the authors) provided better performance and robustness than LQG controllers (also defined by the authors).

Other control design studies can also be found in the literature in the context of linear optimal control for RWVTOL vehicles. Basically, all optimal control methods first express the control problem as a mathematical optimization problem (*e.g.* a quadratic cost function, a H_2 or H_∞ norm of a transfer matrix, *etc.*) and then find the controller to solve this. They may provide good robustness and performance. But this strongly relies on the level of exactitude of the model for control design.

The principle weakness of linear control techniques for RWVTOL vehicles lies in the fact that the control design is based on a linear approximation. Theoretically, the stability of the controlled system is only guaranteed in a limited basin of attraction. A popular remedy for this issue is the gain-scheduling technique (Shamma, 1988), (Shamma and Athans, 1992). In the context of helicopter control, some gain-scheduling controllers have been proposed (see *e.g.* (Kadmiry and Driankov, 2004), and the references therein, *etc.*). Basically, this technique consists of two steps. Firstly, local linear controllers, based on linearized models about several trim configurations, are designed to cover a large operating domain. Then, a global controller is obtained by interpolating, *i.e.* "scheduling", the gains of the local controllers. Gain scheduling may be able to incorporate mature linear control methodologies into nonlinear control design. However, despite its wide-spread use, this technique is merely an engineering practice or a heuristic approach. For instance, the robustness, performance, and stability properties of the global gain scheduled controller are not explicitly addressed in the control design process, and therefore only extensive simulations and experiments allow to evaluate these properties.

Limitations of linear control techniques applied to strongly nonlinear systems like RWVTOL vehicles are well understood. Beside the limitation of the local stability and convergence results, other shortcomings require also close attention:

- The linearization requires a good knowledge of the equilibrium trajectory. Note that determining an equilibrium trajectory necessitates a precise model of aerodynamic effects. Since the attitude of RWVTOL vehicles can vary in large proportions as a

function of the reference trajectory, the process of identifying aerodynamics effects in a large operating domain can be both difficult and costly. Besides, unpredictable wind gusts and model uncertainties further complicate the problem of equilibrium determination.

- Due to aerodynamic perturbations, the system under consideration often operates far from the desired trajectory. In this case the linearization is no longer significant of the real dynamics of the vehicle.

- The linearization requires a minimal parametrization (*e.g.* Euler angles parametrization) of the rotation matrix, an element of the group SO(3). This leads to singularities in the representation which artificially limit the stability domain of the controllers.

- Linear controllers based on linear approximations do not make use of the symmetry properties (*i.e.* for a rigid body the cinematic system is invariant under the group SE(3)). Therefore, instead of simplifying the control design they often make it more complicated.

Nonlinear control design techniques allow to bypass most of these shortcomings.

1.5.2 Nonlinear control

In a common sense, a nonlinear control law is expected to grant better performance and robustness than a linear control law because it can compensate for nonlinear dynamic effects. Several nonlinear control design techniques have been proposed in the literature for RWVTOL vehicles. Nevertheless, none is completely satisfying.

Let us first discuss the *input-output exact linearization* technique (*i.e.* state space exact linearization, or exact linearization by state feedback) (Isidori, 1995). For MIMO systems, this differential geometry-based technique consists in seeking a set of output variables and new control inputs allowing to transform the original system into a linear controllable system whose state and control inputs only depend on the chosen output variables and their time-derivatives (and the original control inputs and their time-derivatives). It is, indeed, one of the most widely used nonlinear techniques for aircraft control. However, the application of this technique is not completely trivial for helicopters. A naive control law, derived from this technique, can result in very bad performance. This issue has been carefully studied in (Koo and Sastry, 1998)[10], or in a more detailed version (Koo et al., 2001). These studies are based on a nonlinear model[11] of a tail-rotor helicopter whose equations of motion have the form of System (1.2). The terms $F_\mathcal{B}$ and $\Gamma_\mathcal{B}$, involved in this model, are similar to the ones given in Eq. (1.3) but without aerodynamic force and torque models (*i.e.* $F_{ae}^\mathcal{B} = 0$, $\Gamma_{ae}^\mathcal{B} = 0$). Additionally, the simplified dynamics of the actuators of T_M, T_T, a, b (defined in Section 1.4.1) are considered. Finally, the Euler angles $\{\phi, \theta, \psi\}$ are used for attitude parametrization. Now let us review some key elements of this study.

---

10. (Koo and Sastry, 1998) can be viewed as one of the first studies on the exact linearization by state feedback technique for a helicopter model. However, the proof, based on the differential geometry and Jakubczyk-Respondek's theorem, is only sketched. Note that omitted computational complexities are mainly due to the use of Euler angles for the attitude parametrization.

11. Parts of this model are given in Section 1.4.1.

- The authors proved that the input-output exact linearization technique is unable to linearize the considered system. This is essentially due to the *small body forces*, *i.e.* the term $\Sigma_R\Gamma$ in Eq. (1.16). Furthermore, the authors showed that for some choices of outputs this technique, by partially linearizing the system (*i.e.* transforming it into a normal form), results in unstable zero dynamics or marginally stable zero dynamics [12]. More precisely, when $\{x, \psi\}$ are chosen as outputs, the zero dynamics is marginally stable; and when $\{\phi, \theta, \psi, x_3\}$ are chosen as outputs the zero dynamics is unstable. Such a system is called *non-minimum phase* in the literature.

- By neglecting the small body forces [13] in the control model, the authors showed that the *approximated system* becomes feedback linearizable by choosing the vehicle's position and heading as outputs [14] (and, subsequently, differentially flat). It was also shown, from a Lyapunov-based analysis, that the control law derived from the state-feedback linearized system based on the approximated system ensures bounded tracking errors for the "true" system. This solution is called *approximate feedback linearization approach* in the literature. It is only meaningful if the small body forces are "small" so that the tracking errors are "acceptable". Helicopter designs normally ensure this.

However, this approximate feedback linearization approach has several drawbacks:

- The use of Euler angles for attitude parametrization may lead to the classical issue of singularities when performing some manoeuvres, such as loops, barrel rolls, *etc.*.

- This technique makes use of a dynamic extension of the thrust force T with the help of a triple integrator to overcome the problem of underactuation in the translational dynamics, and, subsequently, the third-order time-derivative of the thrust force is used as a control input, instead of the "true" control variable $\dot{T}$ [15]. The variables T, $\dot{T}$ and $\ddot{T}$ are considered as the system's state variables and are involved in the feedback control law. This can be problematic because they are not always available to measurements. In practice, it is also difficult to estimate these variables because the

---

12. See *e.g.* (Isidori, 1995) for the definition of zero dynamics.

13. Note that the aerodynamic effects $F_{ae}^{\mathcal{B}}$, $\Gamma_{ae}^{\mathcal{B}}$ are already neglected in the considered model.

14. As defined in (Hauser et al., 1992), this helicopter model is said to be *slightly non-minimum phase* in the sense that the true system is non-minimum phase but the approximated system is minimum phase.

15. Now to simplify the explanation how the dynamic extension of the thrust force T are used by this technique, let us consider the System (1.16) without the terms $\Sigma_R\Gamma$, $T\Sigma_T$, $F_{ae}^{\mathcal{B}}$, $\Gamma_{ae}^{\mathcal{B}}$, and with T and Γ considered as the "true" control variables. One easily deduces that

$$
\begin{cases}
\dot{X}_1 = \dfrac{1}{m}X_2 \\
\dot{X}_2 = X_3 \\
\dot{X}_3 = X_4 \\
\dot{X}_4 = U
\end{cases}
$$

with $X = (X_1, X_2, X_3, X_4) \triangleq (x, m\dot{x}, -TRe_3 + mge_3, -R\delta)$, $\delta \triangleq (T\omega_2, -T\omega_1, \dot{T})^T$,

$$
U \triangleq -R\left(\ddot{T}e_3 - TS(e_3)J^{-1}\Gamma - 2\dot{T}S(e_3)\omega + TS(\omega)^2 e_3 + TS(e_3)J^{-1}S(\omega)J\omega\right).
$$

Therefore, if $\ddot{T}$ is used as a control variable and if $T \neq 0$, the application $(\ddot{T}, \Gamma) \longrightarrow U$ is surjective. This allows to consider U as the new control variable.

associated estimators require the position measurement which can only be obtained in low frequency.

- The proposed approach does not contain any compensation part (*e.g.* an integral action) allowing to cope with parametric uncertainties and unmodeled dynamics, including the small body forces ignored in the control design and aerodynamic perturbations induced by wind gusts (*i.e.* the terms $F_{ae}^{\mathcal{B}}$ and $\Gamma_{ae}^{\mathcal{B}}$).

- To take into account aerodynamic effects in the control design, this technique requires an analytic expression of these effects which is usually difficult to obtain.

These aforementioned drawbacks may impede the application of the input-output exact linearization technique to RWVTOL UAVs. However, the idea of designing a control law based on an approximated model obtained by neglecting the *small body forces* in (Koo and Sastry, 1998), has continuously inspired other nonlinear (or linear) control design techniques (see *e.g.* (Mahony et al., 1999), (Mahony and Hamel, 2004), (Mahony and Hamel, 2001), (Frazzoli et al., 2000), (Marconi and Naldi, 2006), *etc.*) for helicopters and other VTOL vehicles, like *e.g.* ducted fan tailsitters[16]. This idea itself was, in fact, inspired by a previous work for a planar vertical takeoff and landing (PVTOL) aircraft model (Hauser et al., 1992).

For ducted fan tailsitters, small body forces can be neglected in the approximated model for control design purposes, like in (Marconi and Naldi, 2006). Besides, another solution for eliminating small body forces, *i.e.* the torque control inputs, in the translational dynamics of a symmetric tailsitter consists in considering a specific control point rather than the vehicle's CoM (Pflimlin et al., 2004), (Pflimlin et al., 2006), (Pflimlin et al., 2007b), (Pflimlin, 2006)[Ch.4]. This solution has been presented in Section 1.4.2. However, the vehicle's rotational velocity undesirably appears in the so-called *"perturbation term"*, *i.e.* the term Δ_r defined by Eq. (1.14), in the translational dynamics of the new control point. It also complicates the control design. Thus, an assumption that the yaw angular velocity ω_3 is very small can be made, so that this term can be neglected in the velocity or position stabilization control design. This necessitates a control strategy allowing to maintain ω_3 always at small values, while independently ensuring other control objectives, like *e.g.* position trajectory tracking. For instance, in (Pflimlin et al., 2006) such a control strategy is proposed for a symmetric ducted fan tailsitter. It makes use of *i)* Γ_3, the third component of the torque control vector Γ, to stabilize ω_3 about zero, and of *ii)* the thrust force T, and the first and second components of Γ (*i.e.* Γ_1, Γ_2) to stabilize the position of the control point about a reference fixed value.

When small body forces do not appear in the translational dynamics, the (approximated) control model possesses a cascade structure well suited for a classical decoupled control architecture between inner and outer loops, where *i)* the inner control loop uses torque control inputs to stabilize the vehicle's attitude R (or the thrust direction Re_3) to a desired value which is generated by the outer loop, and *ii)* the outer control loop uses the thrust control and the vehicle's attitude R (or the thrust direction Re_3) as (intermediary) control variables to stabilize the vehicle's velocity and/or position (and eventually the yaw angle if the Euler angles parametrization is involved). The key element of the control design consists in ensuring the stability of the overall loop by means

---

16. Note that ducted fan tailsitters are also non-minimum phase, although to our knowledge no proof is available in the literature in this respect. In Appendix A an analysis for this issue is provided.

of, *e.g.*, a backstepping procedure or a high gain controller. The design of the inner and outer controllers normally leads to an overall loop characterized by a time-scale separation between a fast dynamics of the inner attitude loop and a slow dynamics of the outer translational loop. Many Lyapunov-based control design techniques following this direction have been proposed recently like backstepping control design techniques [17] (Mahony et al., 1999), (Mahony and Hamel, 2004), (Mahony and Hamel, 2001), (Pflimlin et al., 2004), (Pflimlin et al., 2007b), (Pflimlin, 2006)[Ch.4], (Frazzoli et al., 2000), (Frazzoli, 2001)[Ch.5], (Olfati-Saber, 2002)[Ch.5], (Hamel et al., 2002), hierarchical and backstepping mixed control technique (Pflimlin et al., 2006), and nested saturations (Isidori et al., 2003), (Marconi and Naldi, 2007), (Marconi and Naldi, 2008), (Naldi, 2008). To avoid the problem of singularities associated with the Euler angles attitude parametrization, the control design can be done directly on the Lie group SO(3) (see *e.g.* (Mahony and Hamel, 2001), (Pflimlin et al., 2004), (Pflimlin et al., 2006), (Pflimlin et al., 2007b), (Frazzoli et al., 2000), *etc.*), or by means of the quaternion attitude parametrization (Isidori et al., 2003). Finally, let us note that using the thrust direction Re_3 as an intermediary control input for the outer loop seems to be more natural than using the attitude R, because the choice of attitude parametrization can be avoided, and the position control and the yaw motion control can be decoupled (see *e.g.* (Pflimlin et al., 2004), (Pflimlin et al., 2006)).

Some of the backstepping control design techniques among those mentioned above are discussed next:

- In (Mahony and Hamel, 2004), a backstepping control law is designed for the position tracking of a helicopter, based on an approximated model where small body forces and aerodynamic effects are neglected. Then, a Lyapunov-based analysis on the original model which contains the small body forces is provided. It shows that the position and heading tracking errors are ultimately bounded by "small" values. However, uncertainties like aerodynamic perturbations are not taken into account in the control design process.

- The backstepping technique is rather convenient to cope with uncertainties when designing a tracking control law. For instance, during takeoff and landing manoeuvres of a helicopter ground effects may generate aerodynamic uncertainties related to the thrust control. In (Mahony and Hamel, 2001) the authors proposed an adaptive controller to deal with these parametric uncertainties (supposed to be constant) by means of a backstepping control design. In other studies (Pflimlin et al., 2004), (Pflimlin et al., 2007b), (Pflimlin, 2006)[Ch.4], the controllers, derived from a similar backstepping technique, deal with the fixed-point stabilization of a ducted fan tailsitter in wind gusts, under the assumption that aerodynamic forces and moments are constant (or slowly time-varying). Of course these adaptive approaches are only meaningful if the dynamics of the estimated parameters are slower than the dynamics of the closed-loop system.

- Let us note that, alike the input-output exact linearization technique (Koo and Sastry, 1998), in a general manner backstepping control design techniques for VTOL vehicles make use of a dynamic extension of the thrust force T with the help of a double integrator. The second-order time-derivative of T is used as a control input

---

17. Backstepping procedure was initially proposed in 1990 by Kokotovic (Khalil, 2002). It provides a generic procedure to progressively construct a Lyapunov function.

(instead of T), whereas T and $\dot{T}$ are used as the system's state variables. However, the fact that T and $\dot{T}$ are not always available to measurements in practice represents a shortcoming of these techniques. A remedy for this issue has been proposed in (Pflimlin et al., 2006) (also for the position stabilization of a ducted fan tailsitter in wind gusts). This solution is actually a mix of the backstepping technique and the so-called hierarchical control. Basically, two backstepping design procedures are applied independently to the inner and the outer loops, then the stability of the overall loop is derived from the singular perturbation theory. This handy technique is promising for practical implementations compared to other backstepping controllers, because it does not require the measurements of T and $\dot{T}$ in the control design. However, the approach presents some shortcomings. For instance, in the outer translational loop the vector TRe_3 is used as an intermediary control vector input to monitor the translational dynamics. It is defined as the PID controller

$$(TRe_3)_r = mge_3 + k_1\widetilde{x} + k_2\int\widetilde{x} + k_3\dot{\widetilde{x}},$$

with k_1, k_2, k_3 positive constants, and $\widetilde{x}$ the position tracking error. Then, for the inner attitude loop the desired thrust direction to be stabilized is defined as

$$(Re_3)_r = \frac{(TRe_3)_r}{|(TRe_3)_r|}.$$

Note that $(Re_3)_r$ is not well-defined if $(TRe_3)_r = 0$. This can be problematic even when $\widetilde{x}$ and $\dot{\widetilde{x}}$ remain close to zero because the integral term in the control law is not bounded and is free to vary arbitrarily. From here one would like to limit the contribution of terms dependent upon $\widetilde{x}$, $\int\widetilde{x}$, and $\dot{\widetilde{x}}$ in $(TRe_3)_r$ in order to ensure that $(TRe_3)_r$ does not evolve near zero. Saturation or nested saturation techniques may be viewed as perspectives for this issue. Note that the term $k_2\int\widetilde{x}$ is introduced to compensate for unknown aerodynamic forces. Thus, an inadequate saturation of this term may limit the domain of attraction with respect to the magnitude of these forces.

Another important route for robust control design for RWVTOL vehicles in the presence of uncertainties is the nested saturation techniques (Teel, 1992), (Marconi and Isidori, 2000). In this category let us first mention (Isidori et al., 2003) which can be viewed as an extension of a previous result obtained for a PVTOL aircraft model (Marconi et al., 2002). In this study the authors addressed the problem of autonomous vertical landing for a helicopter on an oscillating platform (supposed to be a superposition of a finite number of sinusoidal signals of unknown frequency, amplitude, and phase), while stabilizing the lateral and horizontal position and maintaining a constant attitude. Similar control laws can be found in (Marconi and Naldi, 2007), (Marconi and Naldi, 2008), (Naldi, 2008) which consist in solving the tracking problem of a known position trajectory for helicopters and/or ducted fan tailsitters. Now, for more details on the proposed approach let us discuss the study (Marconi and Naldi, 2007). For instance, if we neglect the engine dynamics, the system in question may take the form of System (1.16) without the terms $\Sigma_R\Gamma$, $T\Sigma_T$, $F_{ae}^{\mathcal{B}}$, and $\Gamma_{ae}^{\mathcal{B}}$. The proposed control approach consists in decoupling the altitude control from the lateral and longitudinal control. It makes use of Euler angles for the

attitude parametrization. The inner-outer loop architecture control is applied to the lateral and longitudinal control. Nested saturations are designed for the altitude control and for the outer loop of the lateral and longitudinal control. A mix of small and high gains is imposed to ensure practical stability. Note that uncertainties assumed to be parametric (including the vehicle's mass, its inertia matrix, and the aerodynamic coefficients related to thrust and torque control inputs) are compensated by means of integrators. Principle advantages of this nested saturation approach include the boundedness of the control inputs and robustness with respect to parametric uncertainties. However, robustness towards unmodeled aerodynamic forces and moments (like, *e.g.*, lift, drag, momentum drag forces and moments, *etc.*) is not addressed in either the control design or the associated stability analysis, though we are aware that the presence of compensation integrators may provide levels of robustness with respect to aerodynamic perturbations.

Besides those mentioned and discussed previously, other techniques like model-based predictive control (Jadbabaie et al., 1999), (Kim et al., 2002), (Bertrand et al., 2007), sliding mode control (Bouabdallah and Siegwart, 2005), (Xu and Ozguner, 2008), (Lee et al., 2009) neural-network-based adaptive control (Johnson and Kannan, 2005), image based visual servoing control (Hamel and Mahony, 2002), (Le-Bras et al., 2006), (Le-Bras et al., 2007), (Guenard et al., 2008), (Bourquardez, 2008), *etc.* have also contributed to the global panorama. Finally, nonlinear control design techniques, addressing robustness issues, have also been applied to other types of underactuated vehicles like, *e.g.*, blimps (Moutinho and Azinheira, 2005), (Azinheira and Moutinho, 2008), Autonomous Underwater Vehicles (AUVs) (Leonard and Graver, 2001), (Refsnes et al., 2006), (Antonelli, 2006), *etc..*

1.5.3   Summary

Many (linear or nonlinear) control techniques have been applied to the control of RWVTOL vehicles. Through this control survey we have reviewed some control difficulties associated with the mechanics and aerodynamics of RWVTOL vehicles:

- These vehicles are normally strongly nonlinear systems. Their envelop of flight can vary in a very large operating domain like, *e.g.*, when a helicopter makes a loop or when a ducted fan tailsitter changes from hover to high speed forward flight.

- These vehicles are underactuated. Generally, only four control inputs are available to monitor six degrees of freedom.

- Small and/or light VTOL vehicles are very sensitive to wind gusts, and a precise model of aerodynamic forces and moments valid in a large operating domain is usually not available for control design.

- Parametric uncertainties of these vehicles are often present and impact on the performance and robustness of controllers.

- The *small body forces* representing the couplings between forces and moments further complicate the control design and the associated analyses.

In the following chapter we present a novel control design method for thrust-propelled underactuated vehicles which addresses some of these robustness issues.

Chapter 2

Control design of thrust-propelled underactuated vehicles

2.1 Introduction

Our original motivation is dedicated to the control design of a class of ducted fan tailsitters. However, a closer look at the equations of motion of different kinds of vehicles brings evidence that the development of a general control for a larger class of vehicles is technically relevant. What do airplanes, helicopters and other VTOL vehicles, blimps, rockets, hydroplanes, ships and submarines have in common? These vehicles form a class often designated as *thrust-propelled* or *thrust-vectored* underactuated vehicles in the literature. They are basically composed of a main body immersed in a fluid medium (air or water) or in an empty space, and are commonly controlled via *i)* a propulsive thrust force directed along a body-fixed privileged axis, and *ii)* a torque vector with one, two or three complementary independent components in charge of modifying the body's orientation, and thereby the thrust direction. These vehicles are underactuated in the sense that, apart from the direction associated with the thrust force, the other possible direction(s) of displacement, or *degree(s) of freedom*, is (are) not directly actuated. Interestingly, the aforementioned structural similitude has seldom been exploited to develop a general control framework for these vehicles. Various reasons can be proposed. For instance, there exist important differences between an airplane (Etkin and Reid, 1996), (Abzug and Larrabee, 2002) and a ship (Fossen, 1994). The first vehicle evolves in air and 3D-space, whereas the other is (partly) immersed in water and essentially moves on a 2D-plane; the ambient fluid is not the same and it produces either aerodynamic or hydrodynamic reaction forces with different properties and magnitude; gravity is not compensated by buoyancy in the case of an airplane, but lift-force effects are more systematic and preponderant; added-mass effects mostly concern ships, submarines, and blimps; *etc.*. Another probable reason is historical: aerospace and naval engineering communities involved in the control of these vehicles have not addressed common issues (the design of autopilots, for instance) in a coordinated manner, nor at the same time, nor with the same constraints (physical, economical, *etc.*), nor even with the same approaches. In this chapter we attempt to set the foundations of a general control approach for this large family of thrust-propelled underactuated vehicles. In the sequel, *the "2D-plane case"* refers to a vehicle moving on a 2D-plane with two control inputs (*i.e.* one thrust control and one torque control) whereas *the "3D-space case"* corresponds to the general case of a vehicle moving in a 3D-space

with four control inputs (*i.e.* one thrust control and three torque controls).

In this chapter the control design of this family of thrust-propelled underactuated vehicles is investigated for several control modes typically associated with different levels of motion autonomy. Particular attention is paid to the following problems: *i)* stabilization of (desired) reference thrust direction, *ii)* stabilization of reference linear velocities, *iii)* stabilization of reference position-trajectories, and *iv)* (only for the 3D-space case) combined stabilization of reference horizontal linear velocities and reference altitude. The first, second, and fourth control problems relate typically to manual joystick-augmented-control situations, whereas the third one is associated with fully autonomous motion applications. At first glance, the proposed control approach is reminiscent of methods described in (Frazzoli et al., 2002), (Pflimlin et al., 2007b), (Sepulchre et al., 1997) for the stabilization of hovering VTOL vehicles, based on the idea of: *i)* using the thrust force and the vehicle's attitude (or the thrust direction) as control variables to stabilize the vehicle's velocity and/or position, and *ii)* applying a classical backstepping procedure or a high-gain controller to determine torque-inputs capable of stabilizing the desired attitude (or the thrust direction). Here instead of the attitude or the thrust direction we use its angular velocity as intermediary control input. This alleviates several difficulties associated with control inputs which belong to a compact manifold and enter the system's equation in a non-affine manner. It also allows to cast linear velocity and position control problems as natural extensions of the basic thrust direction control one.

An important motivation of the control design is related to robustness issues, which can be critical for the systems under consideration, as explained in the previous chapter. Robustness issues are particularly important for light and/or small vehicles, like blimps or reduced scale VTOL vehicles. Therefore, robust control strategies ensuring (quasi) global stability, are of great need. The present thesis is a contribution in this respect. Besides, dealing with unmodeled dynamics is not less important. It is well-known from control theory that integral correction constitutes an effective means to compensate for modeling, measurement, and/or estimation static errors (biases). However, it is also well-known that this type of correction may generate instability and windup problems. Many control design techniques addressing these problems have been proposed during the last decades, like linear Anti-Windup Bumpless Transfer (AWBT) schemes (see (Kothare et al., 1994) and the references therein), or nonlinear nested saturations approaches (Teel, 1992), (Marconi and Isidori, 2000). AWBT schemes can efficiently reduce windup effects, but their global stability is difficult to guarantee. Nested saturation approaches yield bounded correction terms, thus reduce effectively the risk of saturation of the actuators which could jeopardize the stability of the controlled system. However, this does not prevent the integral terms involved in the correction function to grow arbitrarily large, leading to slow desaturation and sluggish dynamics. The nonlinear integrator bounding technique incorporated with the control design that we propose in this chapter deals with these problems. Finally, the way energy dissipation produced by motion reaction forces is exploited for the control design and the stability analyses constitutes to our knowledge a novel interpretation which justifies the use of simple models and supports observations made by other authors (Refsnes et al., 2006).

In this chapter we first focus our study on developing a control strategy for the 3D-space case. Then, we show how this control approach can be directly modified for the 2D-plane case by just considering this case as a degenerate situation of the 3D-space case. This chapter is organized as follows. Some notation is given in Section 2.2. The

system modeling is given in Section 2.3. In Section 2.4 control laws are proposed for the 3D-space case for several control objectives, under the assumption that external forces are known. We discuss in Section 2.5 different ways to estimate these forces, and propose an observer based on a coarse model. Simulation results for the 3D-space case are described in Section 2.6 to illustrate the concepts. Then, the control design for the 2D-plane case is given in Section 2.7. To avoid that mathematical technicalities mask the simplicity of some ideas, all proofs are reported in Section 2.8.

2.2   Notation

We focus on vehicles moving in the the 3D-space case which can be modeled as rigid bodies immersed in a fluid. The following notation is introduced (see Fig. 2.1):

- G is the vehicle's center of mass, $m \in \mathbb{R}$ its mass, and $J \in \mathbb{R}^{3 \times 3}$ its inertia matrix.

- $\mathcal{I} = \{O; \vec{\imath}_o, \vec{\jmath}_o, \vec{k}_o\}$ is a fixed (inertial or Galilean) frame with respect to which the vehicle's absolute pose is measured. This frame is chosen as the NED frame (North-East-Down) with $\vec{\imath}_o$ pointing to the North, $\vec{\jmath}_o$ pointing to the East, and $\vec{k}_o$ pointing to the center of the earth.

- $\mathcal{B} = \{G; \vec{\imath}, \vec{\jmath}, \vec{k}\}$ is a frame attached to the body. The vector $\vec{k}$ is parallel to the thrust force axis. This leaves two possible and opposite directions for this vector. The direction here chosen ($\vec{k}$ pointing downward nominally) is consistent with the convention used for VTOL vehicles.
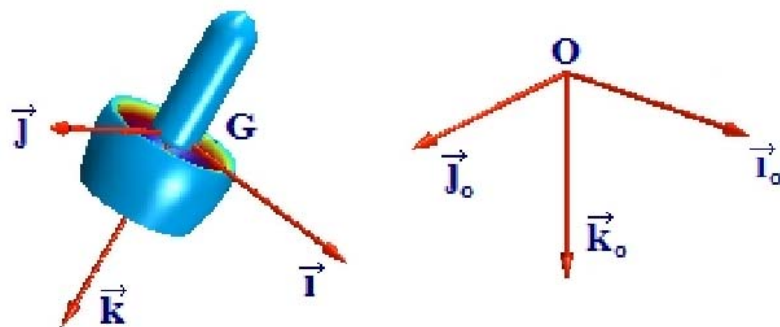
Figure 2.1: Inertial frame $\mathcal{I}$ and body frame $\mathcal{B}$ (the 3D-space case).

- The vector of coordinates of G in the basis of the fixed frame $\mathcal{I}$ is denoted as $x = (x_1, x_2, x_3)^\top$. Therefore, $\overrightarrow{OG} = x_1 \vec{\imath}_o + x_2 \vec{\jmath}_o + x_3 \vec{k}_o$, a relation that we also write in a more concise way as $\overrightarrow{OG} = (\vec{\imath}_o, \vec{\jmath}_o, \vec{k}_o)x$.

- The orientation of the body frame $\mathcal{B}$ with respect to the inertial frame $\mathcal{I}$ is represented by the rotation matrix R. The column vectors of R correspond to the vectors of coordinates of $\vec{\imath}, \vec{\jmath}, \vec{k}$ expressed in the basis of $\mathcal{I}$.

- The vector of coordinates associated with the linear velocity of G with respect to $\mathcal{I}$ is denoted as $\dot{x} = (\dot{x}_1, \dot{x}_2, \dot{x}_3)^\top$ when expressed in the basis of $\mathcal{I}$, and as $v = (v_1, v_2, v_3)^\top$ when expressed in the basis of $\mathcal{B}$, i.e. $\overrightarrow{v} = \frac{d}{dt}\overrightarrow{OG} = (\overrightarrow{\imath}_o, \overrightarrow{\jmath}_o, \overrightarrow{k}_o)\dot{x} = (\overrightarrow{\imath}, \overrightarrow{\jmath}, \overrightarrow{k})v$.

- The angular velocity vector of the body frame $\mathcal{B}$ relative to the fixed frame $\mathcal{I}$, expressed in $\mathcal{B}$, is denoted as $\omega = (\omega_1, \omega_2, \omega_3)^\top$.

- The notation with the subscript "$_r$" is used to denote reference trajectories. For example, $\overrightarrow{v}_r$ denotes a reference velocity vector associated with the vehicle's velocity vector $\overrightarrow{v}$. We assume that the reference trajectories are defined on $\mathbb{R}_+ = [0, +\infty)$.

- The ambient fluid velocity with respect to $\mathcal{I}$ is denoted as $\overrightarrow{v}_f = (\overrightarrow{\imath}_o, \overrightarrow{\jmath}_o, \overrightarrow{k}_o)\dot{x}_f$ $= (\overrightarrow{\imath}, \overrightarrow{\jmath}, \overrightarrow{k})v_f$. The *"apparent velocity"* of the body $\overrightarrow{v}_a$ is the difference between the velocity of G and the ambient fluid velocity, i.e. $\overrightarrow{v}_a = \overrightarrow{v} - \overrightarrow{v}_f$. One has also $\overrightarrow{v}_a = (\overrightarrow{\imath}_o, \overrightarrow{\jmath}_o, \overrightarrow{k}_o)\dot{x}_a = (\overrightarrow{\imath}, \overrightarrow{\jmath}, \overrightarrow{k})v_a$, with $\dot{x}_a = \dot{x} - \dot{x}_f$ and $v_a = v - v_f$.

2.3   System modeling

System modeling of a vehicle is a fundamental process to determine basic equations of motion on which any control design method is bound to rely. The initial stage of this modeling process generally involves modeling external forces and torques acting on the vehicle, so that the vehicle's equations of motion can be derived from the fundamental theorems of mechanics. A profound understanding about environmental effects and a fine model of these effects are crucial for a designer to optimize the vehicle's geometrical and mechanical characteristics suited for desired intrinsic properties of stability and manoeuvrability. They are also necessary for simulations purposes in order to evaluate the performance and robustness properties of a controller. However, modeling various components of environmental effects is generally difficult, time-consuming and costly. Furthermore, the knowledge of a precise and well-tuned model for control design may not be as critically important as for simulation. Two classical reasons are that:

i) a well-designed feedback control is expected to grant robustness –in the sense of performance insensitivity– with respect to model inaccuracies,

ii) using on-line measurements or estimations of these external efforts based on a coarse model in the control can be preferable to using a sophisticated but nonetheless imperfect model of these efforts.

Inspired by this insight, a crude model of external efforts under some simplifying assumptions will be introduced for the sake of the control design and associated analyses.

2.3.1   Equations of motion

The considered family of underactuated vehicles is modeled as rigid bodies immersed in a fluid. We assume that the thrust $\overrightarrow{T} = -T\overrightarrow{k}$ applies at a point that lies on, or close to, the axis $\{G; \overrightarrow{k}\}$ so that it does not create an important torque at G. Furthermore, for concerns of generality and genericity we assume also that the vehicle under consideration possesses a torque vector control inputs $\Gamma \in \mathbb{R}^3$ with three independent components, and

the couplings between forces and moments induced by the torque generation mechanism can be neglected. All external forces acting on the vehicle (gravity and buoyancy forces, added-mass forces, and dissipative aerodynamic or hydrodynamic reaction forces) are summed up in a vector $\overrightarrow{F}_e$, so that the total resultant force applied to the vehicle is $\overrightarrow{F} = \overrightarrow{T} + \overrightarrow{F}_e$. In the absence of motion reaction forces exerted by the ambient fluid on the vehicle, only gravity, eventually counteracted by buoyancy forces of roughly constant magnitude, is present in $\overrightarrow{F}_e$. This force can then be modeled as a constant vector parallel to the $\{0; \overrightarrow{k}_o\}$ axis associated with the fixed frame $\mathcal{I}$. However, due to aerodynamic or hydrodynamic reaction forces, this vector generally depends on the apparent body velocity and acceleration (via added-mass effects), *i.e.* on $(\dot{x}_a, \ddot{x}_a, \omega, \dot{\omega})$ as well as on the vehicle's orientation R. It may also depend on the vehicle's position when the characteristics of the ambient fluid are not the same everywhere. For simplicity, this latter dependence will not be considered here. Moreover, whereas the dependence on accelerations is roughly linear, it is known that the intensities of motion reaction forces vary like the square of $|\dot{x}_a|$. Therefore, the intensity and direction of $\overrightarrow{F}_e$ can vary considerably as soon as the vehicle's velocity is modified significantly, or due to important modifications of the ambient environment (waves, wind, *etc.*).

Using System (1.16) and neglecting the coupling between the forces and torques produced by the vehicles actuators (*i.e.* neglecting $\Sigma_R \Gamma$ and $T \Sigma_T$ in System (1.16)) one obtains

$$\begin{cases} \Sigma_1^{3d} : \begin{bmatrix} \dot{x} \\ m\dot{v} \\ \dot{R} \end{bmatrix} = \begin{bmatrix} Rv \\ -mS(\omega)v - Te_3 + R^\top F_e(\dot{x}, \ddot{x}, R, \omega, \dot{\omega}, t) \\ RS(\omega) \end{bmatrix} \\ \Sigma_2^{3d} : \quad J\dot{\omega} \quad = \quad -S(\omega)J\omega + \Gamma + \Gamma_e(\dot{x}, \ddot{x}, R, \omega, \dot{\omega}, t) \end{cases} \tag{2.1}$$

with $F_e \in \mathbb{R}^3$ the vector of coordinates of $\overrightarrow{F}_e$ expressed in the inertial frame $\mathcal{I}$ and $\Gamma_e \in \mathbb{R}^3$ the external torque vector. Note that $F_e = mge_3 + RF_{ae}^{\mathcal{B}}$ and $\Gamma_e = \Gamma_{ae}^{\mathcal{B}}$. As a consequence, the vehicle's translational dynamics expressed in the inertial frame $\mathcal{I}$ is given by

$$m\ddot{x} = -TRe_3 + F_e(\dot{x}, \ddot{x}, R, \omega, \dot{\omega}, t), \tag{2.2}$$

2.3.2   Assumptions

For the concerns of generality of the control design, modeling assumptions concerning the environmental forces (drag, lift, gravity, etc) will be introduced next to simplify the control design and associated analyses.

Assumption 1 *F_e depends only on the vehicle's linear velocity $\dot{x}$ and the independent time variable t. Moreover, it is continuously differentiable with respect to these variables, and the functions $t \longmapsto F_e(\dot{x}, t)$, $t \longmapsto \dfrac{\partial F_e}{\partial \dot{x}}(\dot{x}, t)$, and $t \longmapsto \dfrac{\partial F_e}{\partial t}(\dot{x}, t)$ are bounded on $\mathbb{R}_+$, uniformly with respect to $\dot{x}$ in compact sets.*

The non-dependence of $\overrightarrow{F}_e$ on the vehicle's attitude is physically justified when the aerodynamic (and/or hydrodynamic) forces do not depend on the vehicle's orientation, a property which depends essentially on the vehicle's shape. This assumption is clearly

violated in the case of airplanes (see *e.g.* airplanes (Abzug and Larrabee, 2002)) which are subjected to lift forces whose intensities are very sensitive to angles of attack, but it better holds in the case of most wingless VTOL vehicles (see *e.g.* (Frazzoli et al., 2002), (Hamel et al., 2002), (Lipera et al., 2001), (Marconi et al., 2002)). As for the non-dependence upon the angular velocity ω, Assumption 1 is better justified when *i)* the external forces apply at points close to the vehicle's center of mass, *ii)* motion reaction forces resulting from the vehicle's rotation can be neglected when compared to those produced by translational motion. Finally, the non-dependence on the acceleration variables $\ddot{x}$ and $\dot{\omega}$ is justified when added-mass effects can be neglected. These effects can be ignored when the density of the body is much more important than that of the ambient fluid. The example of a dense spherical body whose center coincides with its center of mass can be used to concretize a physical situation for which Assumption 1 holds with a good approximation.

Assumption 2 *There exist two real numbers $c_1 \geq 0, c_2 > 0$ such that*

$$|F_e(\dot{x}, t)| \leq c_1 + c_2|\dot{x}|^2 , \quad \forall(\dot{x}, t). \tag{2.3}$$

Assumption 3 *There exist two real numbers $c_3 \geq 0, c_4 > 0$ such that*

$$\dot{x}^\top F_e(\dot{x}, t) \leq c_3|\dot{x}| - c_4|\dot{x}|^3 , \quad \forall(\dot{x}, t). \tag{2.4}$$

Assumption 2 indicates that the intensity of $\overrightarrow{F}_e$ cannot grow faster than the square of the intensity of the vehicle's velocity vector. This is consistent with common models of aerodynamic and hydrodynamic drag and lift forces (see *e.g.* (Fossen, 1994, Ch.2,3), (Stevens and Lewis, 1992, Ch.2)). The constant c_1 allows to take into account the force of gravity, when it is active, and the action of perturbation forces produced by wind or sea-current. Assumption 3 follows from Assumption 2 and the "dissipativity", or "passivity", property of drag and lift forces. In particular, it indicates that for "large" velocities, the negative work of these forces increases like the cube of the body's apparent velocity, and thus becomes predominant when all other forces remain bounded. This property plays a crucial role for the effective online estimation of $\overrightarrow{F}_e$ and, subsequently, the design of the control laws endowed with good stabilization properties in a large operational domain.

Finally, the following assumption allows us to avoid non-essential complications in the analyses. However, it is not restrictive from application points of view.

Assumption 4 *The reference velocity $\dot{x}_r$ is bounded in norm on $\mathbb{R}_+$ by a constant $\overline{\mathbf{v}}_{\mathbf{r}}$, and its first and second order derivatives $\dfrac{d}{dt}\dot{x}_r$ and $\dfrac{d^2}{dt^2}\dot{x}_r$ are well-defined and bounded on this set.*

2.3.3 Model for control design

System (2.1) shows that the dynamical subsystem Σ_2^{3d} is fully-actuated. Exponential convergence of the angular velocity ω to any bounded desired reference value is theoretically possible, especially when the external forces apply at points close to the center of mass G, so that $|\Gamma_e|$ is negligible. In this case one may view ω as an intermediary control input. In practice, this corresponds to the classical decoupled control architecture between inner and outer loops. The inner control loop provides high gain stabilization of the vehicle's

angular velocity based on direct measurement of the angular velocity from an IMU. The outer control loop uses pose measurement along with estimation or measurement of the linear velocity as sensor inputs, and the angular velocity set point and thrust intensity as control inputs. For many applications, the time-scale separation between the two loops is sufficient to ensure that the interaction terms can be ignored in the control design. Therefore, in the sequel we consider T and ω as the control inputs, and we focus on the control of the subsystem Σ_1^{3d}.

Using Assumption 1, the subsystem Σ_1^{3d} of System (2.1) can be simplified as follows

$$
\begin{cases}
\dot{x} &= Rv \\
\dot{v} &= -S(\omega)v - ue_3 + R^\top \gamma_e(\dot{x}, t) \\
\dot{R} &= RS(\omega)
\end{cases}
\tag{2.5}
$$

with $\gamma_e(\dot{x}, t) \triangleq F_e(\dot{x}, t)/m$ called the *"apparent acceleration"*, and $u \triangleq T/m$ and ω used hereafter as the control inputs. Note that Assumptions 1–3 are still satisfied when F_e is replaced by γ_e and each c_i is replaced by c_i/m.

The knowledge of F_e, *i.e.* γ_e, is very important for the control design. It can be measured but it can also be estimated. In Section 2.5, we will propose an estimation of this force based on a high gain observer and the measurements of the vehicle's linear velocity, attitude, and also the thrust force intensity. Throughout the next section, we assume that F_e and its time-derivatives are known with "reasonably" good accuracy. We assume also that m is constant so as to facilitate the control design, knowing that this assumption is violated in the case of rockets or any kind of vehicles using combustible energy.

2.4   Control design

In this section a Lyapunov-based control approach is developed for the following control objectives:

1) stabilization of the vehicle's thrust direction;

2) stabilization of the vehicle's linear velocity;

3) stabilization of the vehicle's position;

4) combined stabilization of the vehicle's horizontal linear velocity and altitude;

5) extension of these objectives by taking the constraint of unilaterality of the thrust direction into account.

In what follows basic controllers are proposed under some simplifying assumptions, allowing to facilitate the presentation. Then, they will be robustified to comply with more realistic assumptions. Let us remark that the angular velocity ω_3 about the thrust axis is not involved in the realization of the aforementioned control objectives, so that this degree of freedom can be used for complementary objectives and defined case-by-case, depending on the considered vehicle and application. *A priori*, there are infinitely many possibilities at this level, starting with the simplest choice $\omega_3 = 0$. In (Pflimlin, 2006) (pages 105–108) this variable is determined in order to take advantage of lift forces associated with an asymmetric VTOL vehicle. In the sequel, to simplify the control design and the associated analyses we assume that ω_3 is well-defined and bounded on $\mathbb{R}_+$.

2.4.1 Basics of the control design

In what follows some basic control laws are presented.

2.4.1.1 Thrust direction control

The objective is to stabilize the vehicle's thrust direction $\overrightarrow{k}$ about a desired thrust direction $\overrightarrow{\gamma}$. In practice this desired direction may be specified by a manual joystick. Let $\gamma \in \mathbb{R}^3$ denote the normalized vector ($|\gamma| = 1$) of coordinates of $\overrightarrow{\gamma}$, expressed in the inertial frame $\mathcal{I}$. Then, the control objective is equivalent to stabilizing $R^\top \gamma$ about e_3. Define

$$\overline{\gamma} \triangleq R^\top \gamma, \tag{2.6}$$

and let $\widetilde{\theta} \in (-\pi; \pi]$ denote the angle between the two unit vectors e_3 and $\overline{\gamma}$, so that $\cos \widetilde{\theta} = \overline{\gamma}_3$, the third component of $\overline{\gamma}$. The control objective is also equivalent to the asymptotic stabilization of $\widetilde{\theta} = 0$. The control result is stated next.

Proposition 1 *Let k denote a positive constant, and apply the control law*

$$\begin{cases} \omega_1 = -\dfrac{k\overline{\gamma}_2}{(1 + \overline{\gamma}_3)^2} - \gamma^\top S(Re_1)\dot{\gamma} \\[3mm] \omega_2 = \dfrac{k\overline{\gamma}_1}{(1 + \overline{\gamma}_3)^2} - \gamma^\top S(Re_2)\dot{\gamma} \end{cases} \tag{2.7}$$

to the system $\dot{R} = RS(\omega)$. Then the equilibrium point $\widetilde{\theta} = 0$ of the controlled system is exponentially stable with domain of attraction equal to $(-\pi, \pi)$.

The proof, based on the candidate Lyapunov function $V \triangleq 1 - \overline{\gamma}_3$, is given in Section 2.8.3. It essentially relies on the following technical lemma (which is also used to establish the forthcoming control results).

Lemma 1 *Let $\overline{\gamma} \triangleq R^\top \gamma$, with $\gamma \in \mathbb{R}^3$ a non-zero time-dependent vector and $R \in SO(3)$ satisfying $\dot{R} = RS(\omega)$. Let $\overline{\gamma}_{1,2}$ denote the vector $(\overline{\gamma}_1, \overline{\gamma}_2)^\top$. Then,*

$$\frac{d}{dt}\left(\frac{\overline{\gamma}}{|\gamma|}\right) = \frac{1}{|\gamma|}S\left(\overline{\gamma}\right)\left(\omega - \frac{1}{|\gamma|^2}R^\top S(\gamma)\dot{\gamma}\right),$$

$$\frac{d}{dt}\left(1 - \frac{\overline{\gamma}_3}{|\gamma|}\right) = \frac{1}{|\gamma|}\overline{\gamma}_{1,2}^\top\left(\begin{bmatrix} -\omega_2 \\ \omega_1 \end{bmatrix} + \frac{1}{|\gamma|^2}\begin{bmatrix} -\gamma^\top S(Re_2)\dot{\gamma} \\ \gamma^\top S(Re_1)\dot{\gamma} \end{bmatrix}\right).$$

The proof is given in Section 2.8.2. In view of this lemma, one remarks that the variation of $V \triangleq 1 - \overline{\gamma}_3/|\gamma|$ is independent of the yaw angular velocity ω_3. That explains why ω_3 is not involved in the realization of this control objective (and also other control objectives presented in the sequel).

Remark 1 *The control law (2.7) (like those presented next) makes use of the feedforward term $\dot{\gamma}$, which is not always available in practice. Simulations with the VTOL model and numerical data of Section 2.6 have shown that good performance (in the sense of "small" ultimate tracking errors) is also obtained when $\dot{\gamma}$ in (2.7) is set equal to zero and its actual value is not too large. This can be justified rigorously using the Lyapunov function $V = 1 - \overline{\gamma}_3$.*

Remark 2 *To simplify the stability statement, the equilibrium set and domain of attraction have been expressed in term of the variable $\widetilde{\theta}$. However, Proposition 1 can be stated without referring to $\widetilde{\theta}$, by defining the equilibrium set as $\{R^* \in SO(3)\,|\,R^* e_3 = \gamma\}$ and the associated domain of attraction as $\{R \in SO(3)\,|\,\langle Re_3, \gamma(0)\rangle \neq -1\}$.*

In what follows we show how this controller can be extended to other control problems.

2.4.1.2   Velocity control

Let $\dot{x}_r$ denote the reference velocity expressed in the inertial frame $\mathcal{I}$, $\ddot{x}_r$ its time-derivative, and $\widetilde{v} \triangleq R^\top(\dot{x} - \dot{x}_r)$ the velocity error expressed in the body frame $\mathcal{B}$. The problem of asymptotic stabilization of the linear velocity error $\dot{x} - \dot{x}_r$ to zero is clearly equivalent to the asymptotic stabilization of $\widetilde{v}$ to zero.

Using System (2.5) one obtains the following error model

$$\dot{\widetilde{x}} = R\widetilde{v} \tag{2.8a}$$

$$\dot{\widetilde{v}} = -S(\omega)\widetilde{v} - ue_3 + R^\top(\gamma_e(\dot{x},t) - \ddot{x}_r(t)) \tag{2.8b}$$

$$\dot{R} = RS(\omega) \tag{2.8c}$$

with either $\widetilde{x} \triangleq \int_0^t (\dot{x}(s) - \dot{x}_r(s))\,ds$, the integral of the velocity error, or $\widetilde{x} \triangleq x - x_r$, the position tracking error when a reference trajectory x_r is specified.

Now instead of defining γ as a reference unit vector like previously, we define

$$\gamma(\dot{x},t) \triangleq \gamma_e(\dot{x},t) - \ddot{x}_r(t). \tag{2.9}$$

Eq. (2.8b) indicates that $\widetilde{v} \equiv 0$ implies that

$$-ue_3 + R^\top\gamma(\dot{x},t) \equiv 0. \tag{2.10}$$

As long as $\gamma(\dot{x},t)$ is different from zero, one can define a locally unique thrust direction solution to Eq. (2.10). However, this solution cannot be prolonged by continuity at $\gamma = 0$. As a matter of fact, one can verify that this singularity corresponds to the case when the linearization of System (2.8b)–(2.8c) at any equilibrium point $(\widetilde{v}, R) = (0, R^*)$ is not controllable. More precisely,

Lemma 2 *(See (Morin and Samson, 2006)) Consider System (2.8) with u and ω as control inputs. Suppose that $\gamma(t) = 0\ \forall t \in \mathbb{R}_+$. Then, $\forall R^* \in SO(3)$*

1) the point $(\widetilde{x}, \widetilde{v}, R) = (0, 0, R^*)$ is an equilibrium;

2) the system is Small Time Locally Controllable (STLC) but the associated linearized system is not;

3) there does not exist any time-invariant $\mathcal{C}^1$ feedback control law that asymptotically stabilize the system at the equilibrium point $(\widetilde{x}, \widetilde{v}, R) = (0, 0, R^*)$.

Very specific (and still prospective) nonlinear control techniques are required to address stabilization issues in this case (Morin and Samson, 2006). However, this critical case is not the subject of this thesis. Beyond technical difficulties associated with this case (which could be addressed in future studies), the main reason is that the vanishing of γ does not correspond to a generic situation for a large class of thrust-propelled underactuated vehicles (those for which $\gamma_e(\dot{x}_r(t), t)$ is nominally different from zero). We thus essentially discard this issue here by making the following assumption.

Assumption 5 *There exists a constant $\delta > 0$ such that $|\gamma(\dot{x}, t)| \geq \delta$, $\forall(\dot{x}, t)$.*

Although this assumption is restrictive, it simplifies the exposition of a basic and generic control design. In Section 2.4.2, however, we will weaken this assumption and propose an *ad-hoc* adaptation of the control design in order to ensure the well-posedness of the controller's expression and maintain a minimal control of the vehicle when $|\gamma|$ gets close to zero. When both Assumption 5 and relation (2.10) hold, using Eq. (2.6) one deduces that $\overline{\gamma} = \pm|\gamma|e_3$. Let $\widetilde{\theta} \in (-\pi; \pi]$ denote the angle between the two unit vectors e_3 and $\overline{\gamma}/|\gamma|$, so that $\cos\widetilde{\theta} = \overline{\gamma}_3/|\gamma|$. The control objective implies that either $\widetilde{\theta} = 0$ (*i.e.* $\overline{\gamma} = |\gamma|e_3$) or $\widetilde{\theta} = \pi$ (*i.e.* $\overline{\gamma} = -|\gamma|e_3$) must be asymptotically stabilized. The choice between these two equilibria is often made via simple physical considerations such as minimizing the energy consumption in relation to actuator's efficiency and vehicle's shape, or by taking into account the unilaterality of the thrust direction as in the case of most VTOL vehicles. Without loss of generality, we henceforth assume that the choice has been made to stabilize $\widetilde{\theta} = 0$. Based on the above notation the second control result is stated next.

Proposition 2 *Let k_1, k_2, k_3 denote some positive constants, and apply the control law*

$$\begin{cases} u = \overline{\gamma}_3 + |\gamma|k_1\widetilde{v}_3 \\[2mm] \omega_1 = -|\gamma|k_2\widetilde{v}_2 - \dfrac{k_3|\gamma|\overline{\gamma}_2}{(|\gamma| + \overline{\gamma}_3)^2} - \dfrac{1}{|\gamma|^2}\gamma^\top S(Re_1)\dot{\gamma} \\[3mm] \omega_2 = |\gamma|k_2\widetilde{v}_1 + \dfrac{k_3|\gamma|\overline{\gamma}_1}{(|\gamma| + \overline{\gamma}_3)^2} - \dfrac{1}{|\gamma|^2}\gamma^\top S(Re_2)\dot{\gamma} \end{cases} \tag{2.11}$$

to System (2.8) with γ defined by Eq. (2.9). Suppose that Assumptions 1, 4, and 5 are satisfied. Then, for System (2.8b)–(2.8c), the equilibrium point $(\widetilde{v}, \widetilde{\theta}) = (0, 0)$ of the controlled system is asymptotically stable with domain of attraction equal to $\mathbb{R}^3 \times (-\pi, \pi)$.

The proof of this proposition is given in Section 2.8.4. It is based on the use of the candidate Lyapunov function

$$V \triangleq \frac{1}{2}|\widetilde{v}|^2 + \frac{1}{k_2}\left(1 - \frac{\overline{\gamma}_3}{|\gamma|}\right) = \frac{1}{2}|\widetilde{v}|^2 + \frac{1}{k_2}(1 - \cos\widetilde{\theta}),$$

whose time-derivative is negative semi-definite along any solution of the controlled system.

The control law (2.11) makes use of terms inversely proportional to $(|\gamma|+\overline{\gamma}_3)^2$. They are introduced to maximize the domain of stability of the equilibrium point $(\widetilde{v}, \widetilde{\theta}) = (0, 0)$ of the controlled system and also to ensure that u converges to $|\gamma|$, a positive value. However, this control expression is not well-posed at points (in a set) corresponding to $\widetilde{\theta} = \pi$ (*i.e.* $\overline{\gamma} = -|\gamma|e_3$) even when Assumption 5 is satisfied. In fact, one can modify this control expression, so that it is well-defined everywhere (supposing that Assumption 5 is satisfied) by multiplying the term $1/(|\gamma| + \overline{\gamma}_3)^2$ by $\mu(|\gamma| + \overline{\gamma}_3)$ where μ is a non-negative function of the class $\mathcal{C}^1$ such that

$$\lim_{s \to 0} \frac{\mu(s)}{s^2} < +\infty.$$

Further details on this robustification process will be provided in Section 2.4.2.

2.4.1.3   Velocity control with integral term

For the stability and convergence analysis of the control law (2.11), it is implicitly assumed that $\gamma(\dot{x}, t) = \gamma_e(\dot{x}, t) - \ddot{x}_r(t)$ is perfectly known. In practice, however, due in particular to the difficulty of obtaining precise measures or estimates of F_e the apparent acceleration γ_e is not known exactly, nor is γ therefore. Note that an estimation error of the vehicle's mass induces also an error in γ_e. It is well-known from the theory of linear control systems that integral correction terms can compensate for additive perturbations which, in the present case, may take the form of a constant bias in the measurement (or estimation) of γ_e. We show hereafter that the control (2.11) can be modified in order to still ensure the convergence of $\dot{x} - \dot{x}_r$ to zero when such a bias is present. To this purpose let us introduce the following integral term

$$I_v(t) \triangleq \int_0^t \left(\dot{x}(s) - \dot{x}_r(s) \right) ds + I_0, \tag{2.12}$$

with I_0 an arbitrary constant vector. Also, let h denote a smooth bounded positive function defined on $[0, +\infty)$ such that, for some positive constants η, β,

$$\forall s \in \mathbb{R}, \quad |h(s^2)s| < \eta, \tag{2.13}$$

$$\forall s \in \mathbb{R}, \quad 0 < \frac{\partial}{\partial s}(h(s^2)s) < \beta. \tag{2.14}$$

An example of h is $h(s) = \eta/\sqrt{1+s}$, with η a positive constant. Let $\widehat{\gamma}_e$ denote the measure (or estimate) of γ_e and define now γ as follows (in replacement of relation (2.9))

$$\gamma \triangleq \widehat{\gamma}_e - \ddot{x}_r + h(|I_v|^2)I_v. \tag{2.15}$$

From here the third control result is stated next.

Proposition 3 *Apply the control law (2.11) to System (2.8) with γ defined by Eq. (2.15). Suppose that*

 i) Assumptions 1, 4, and 5, with γ given by Eq. (2.15), are satisfied;

 ii) the measurement (or estimation) error $c \triangleq \gamma_e - \widehat{\gamma}_e$ is constant;

iii) $\displaystyle\lim_{s \to +\infty} h(s^2)s > |c|.$

Then, for System (2.8b)–(2.8c) complemented with the equation $\dot{I}_v = R\widetilde{v}$, there exists a constant vector $I_v^* \in \mathbb{R}^3$ such that the equilibrium point $(I_v, \widetilde{v}, \widetilde{\theta}) = (I_v^*, 0, 0)$ of the controlled system is asymptotically stable, with domain of attraction equal to $\mathbb{R}^3 \times \mathbb{R}^3 \times (-\pi, \pi)$.

The proof, similar to the proof of Proposition 2, is given in Section 2.8.5. We now briefly comment on the role of the function h and its properties. Property (2.13) of h is introduced in order to limit, via relation (2.15), the influence of the integral I_v in the control action. However, Assumption *iii)* of Proposition 3 also points out that the upper-bound η associated with the choice of this function should not be too small in order to compensate for a large estimation error c. On the other hand, in view of Eq. (2.15) a small value for η may reduce the risk of $|\gamma|$ evolving close to zero. This policy leads, for instance, to choose $\eta < g$ in the case when γ_e is essentially equal to the gravity acceleration, and the estimation error c and $\ddot{x}_r$ are small compared to this acceleration. These considerations illustrate that a trade-off must be found, depending on the considered application.

2.4.1.4   Position control

Now the control objective is the combined stabilization of the velocity error $\widetilde{v}$ (or $\dot{x} - \dot{x}_r$) and the position error $\widetilde{x} = x - x_r$ to zero. A first solution to this problem is provided by the control proposed in Proposition 3 since, by setting $I_0 = x(0) - x_r(0)$ in Eq. (2.12), one has $I_v = \widetilde{x}$. Now, alike the velocity stabilization case, it can be useful (and even necessary) in practice to complement the control action with a position integral correction term. A possibility consists in using a term proportional to the output z of a classical integrator of $\widetilde{x}$ (i.e. $\dot{z} = \widetilde{x}$) in the control expression. However, this solution presents several drawbacks. For example, the integral correction term may grow very large and this may in turn cause large overshoots of the position tracking error. To avoid this problem, and also cope with actuator limitations, one must saturate the integral term. This can be done in many ways, some better than others. For instance, it is important to prevent the so-called desaturation (or windup) problem from occurring in order to not overly increase the system's time response. The solution that we propose is based on a nonlinear dynamical extension yielding a type of bounded nonlinear integrator. More precisely, we denote z the solution to the following differential equation driven by $\widetilde{x}$

$$\ddot{z} = -2k_z\dot{z} - k_z^2(z - \mathrm{sat}_\Delta(z)) + k_z h_z(|\widetilde{x}|^2)\widetilde{x},$$
$$(k_z > 0,\ z(0) = 0,\ \dot{z}(0) = 0),$$
$$\tag{2.16}$$

where h_z denotes a smooth bounded positive function satisfying Properties (2.13), (2.14) for some positive constants η_z, β_z, and sat_Δ is a continuous "saturation function" characterized by the following properties, with Δ a positive number associated with this function,

P1. sat_Δ is right-differentiable along any smooth curve and its derivative is bounded;

P2. $\forall x \in \mathbb{R}^3$, if $|x| \le \Delta$, $\mathrm{sat}_\Delta(x) = x$;

P3. $\exists \overline{\Delta} > 0$ such that $\forall x \in \mathbb{R}^3$, $|\mathrm{sat}_\Delta(x)| \le \overline{\Delta}$;

P4. $\forall(c, x) \in \mathbb{R}^3 \times \mathbb{R}^3$ such that $|c| \le \Delta$, $|\mathrm{sat}_\Delta(x + c) - c| \le |x|$.

A possible choice (for which $\Delta = \overline{\Delta}$) is the classical saturation function (see Lemma 8 in Section 2.8.14 for the proof)

$$\mathrm{sat}_\Delta(x) \triangleq x \min\left(1, \frac{\Delta}{|x|}\right), \quad (\Delta > 0). \tag{2.17}$$

It is verified from Eq. (2.16) that ultimate uniform upper-bounds of $|z|$, $|\dot{z}|$, and $|\ddot{z}|$ are $\overline{\Delta} + \eta_z/k_z$, $2(k_z\overline{\Delta} + \eta_z)$, and $6k_z(k_z\overline{\Delta} + \eta_z)$ respectively (see Lemma 9 in Section 2.8.14 for the proof).

Define

$$y \triangleq \widetilde{x} + z \,, \tag{2.18}$$

$$\overline{v} \triangleq \widetilde{v} + R^\top \dot{z} \,, \tag{2.19}$$

$$\gamma \triangleq \widehat{\gamma}_e - \ddot{x}_r + h(|y|^2)y + \ddot{z} \,, \tag{2.20}$$

where $\widehat{\gamma}_e$ denotes the measurement (or estimation) of γ_e, and h is a smooth bounded positive function satisfying Properties (2.13), (2.14) [1] for some constants η, $\beta > 0$. From here the position control is stated next.

Proposition 4 *Let k_1, k_2, k_3 denote some positive constants. Apply the following control law*

$$\begin{cases} u \;=\; \overline{\gamma}_3 + |\gamma| k_1 \overline{v}_3 \\[2mm] \omega_1 \;=\; -|\gamma| k_2 \overline{v}_2 - \dfrac{k_3 |\gamma| \overline{\gamma}_2}{(|\gamma| + \overline{\gamma}_3)^2} - \dfrac{1}{|\gamma|^2} \gamma^\top S(Re_1)\dot{\gamma} \\[3mm] \omega_2 \;=\; |\gamma| k_2 \overline{v}_1 + \dfrac{k_3 |\gamma| \overline{\gamma}_1}{(|\gamma| + \overline{\gamma}_3)^2} - \dfrac{1}{|\gamma|^2} \gamma^\top S(Re_2)\dot{\gamma} \end{cases} \tag{2.21}$$

to System (2.8) with $\overline{v}$, γ, and y (which intervenes in the definition of γ) defined by Eqs. (2.19), (2.20), and (2.18) respectively. Suppose that

i) Assumptions 1, 4, and 5, with γ given by Eq. (2.20), are satisfied;

ii) the measurement (or estimation) error $c \triangleq \gamma_e - \widehat{\gamma}_e$ is constant;

iii) $\lim\limits_{s\to+\infty} h(s^2)s > |c|$;

iv) $\Delta > |z^*|$, where z^* denote the unique solution to the equation $h(|z^*|^2)z^* = c$.

Then, for System (2.8) complemented with System (2.16), the equilibrium point $(z, \dot{z}, \widetilde{x}, \widetilde{v}, \widetilde{\theta}) = (z^*, 0, 0, 0, 0)$ of the controlled system is asymptotically stable, with domain of attraction equal to $\mathbb{R}^3 \times \mathbb{R}^3 \times \mathbb{R}^3 \times \mathbb{R}^3 \times (-\pi, \pi)$.

The proof is given in Section 2.8.6. The role of the function h has been commented upon previously. For position stabilization, we further remark that the property (2.13) of h bounds the contribution of the position error $\widetilde{x}$ in γ defined by Eq. (2.20), and thus also in the control inputs defined by Eq. (2.21). This limits the influence of large initial position errors on the control inputs intensity and reduces the risk of saturating the actuators. Note that the choice of h is still a matter of compromise. Let us comment on the role of the coefficient k_z. Eq. (2.16) points out that k_z influences the rate of desaturation of z which can be observed, for instance, when $|z|$ is initially larger than Δ and $\widetilde{x} = 0$. The larger k_z, the faster the desaturation and the smaller the influence of this integral action on the system's time response. On the other hand, since upper-bounds of $|\ddot{z}|$ and $|\gamma|$ are proportional to k_z, a "small" value of k_z tends to limit the risk of saturating the actuators. A large value of k_z also increases the range interval of $|\gamma|$ and, subsequently, the risk of getting $|\gamma|$ close to zero (a value for which the control is no longer defined). The tuning of k_z is thus again a matter of compromise to be solved case-by-case depending on the considered application.

---

1. Note that h can be different from h_z.

2.4.1.5   Combination of horizontal velocity and altitude control

Position control, the most advanced control mode, necessitates the measurements of the vehicle's full state. However, the measurement of the vehicle's position is not always available due to associated sensor problems. For instance, the GPS signal is not reliable in bad weather conditions or in urban zones and can be lost in indoor environments. This is one of many reasons for which, in practice, a horizontal velocity control mode complemented with altitude control (*i.e.* $\dot{x}_{1,2}$ and x_3) can be of interest[2]. This control objective can be interpreted as the combined stabilization of the velocity error $\widetilde{v}$ (or $\widetilde{\dot{x}} \triangleq \dot{x} - \dot{x}_r$) and the altitude error $\widetilde{x}_3 \triangleq x_3 - x_{r,3}$ to zero. To this purpose the control laws proposed in Propositions 3 and 4 can be combined.

Let us introduce the following integral terms

$$I_{v,i}(t) \triangleq \int_0^t (\dot{x}_i(s) - \dot{x}_{r,i}(s))\,ds + I_{0,i}, \ \ (i = 1, 2), \tag{2.22}$$

with $I_{0,1}$ and $I_{0,2}$ arbitrary constant numbers. The nonlinear integrator bounding technique proposed previously (*i.e.* System (2.16)) is also recalled. Denote $z \in \mathbb{R}$ the solution to the following differential equation driven by $\widetilde{x}_3$

$$\ddot{z} = -2k_z\dot{z} - k_z^2(z - \mathrm{sat}_\Delta(z)) + k_z h_z(\widetilde{x}_3^2)\widetilde{x}_3,$$
$$(k_z > 0, \ z(0) = 0, \ \dot{z}(0) = 0), \tag{2.23}$$

where h_z denotes a smooth bounded positive function satisfying (2.13)–(2.14) for some positive constants η_z, β_z, and sat_Δ is a continuous saturation function satisfying properties *P1, P2, P3, P4* given in Section 2.4.1.4.

Define

$$y \triangleq I_{v,1}e_1 + I_{v,2}e_2 + (\widetilde{x}_3 + z)e_3\,, \tag{2.24}$$

$$\overline{v} \triangleq \widetilde{v} + \dot{z}R^\top e_3\,, \tag{2.25}$$

$$\gamma \triangleq \widehat{\gamma}_e - \ddot{x}_r + h(|y|^2)y + \ddot{z}e_3\,, \tag{2.26}$$

where $\widehat{\gamma}_e$ denotes the measurement (or estimation) of γ_e, and h is a smooth bounded positive function satisfying Properties (2.13) and (2.14) for some positive constants η, β. From here the control result is stated next.

Proposition 5 *Apply the control law (2.21) to System (2.8) with $\overline{v}, \gamma, y$ defined by Eqs. (2.25), (2.26), and (2.24) respectively. Suppose that*

  i) Assumptions 1, 4, and 5, with γ given by Eq. (2.26), are satisfied;

  ii) the measurement (or estimation) error $c \triangleq \gamma_e - \widehat{\gamma}_e$ is constant;

  iii) $\lim_{s \to +\infty} h(s^2)s > |c|;$

  iv) $\Delta > z_3^*$ *with z_3^* the third component of $z^* \in \mathbb{R}^3$, the unique solution to the equation* $h(|z^*|^2)z^* = c.$

---

2. A pitot-tube can be used for velocity measurement and a barometer can be used for altitude measurement.

Then, for System (2.8b)–(2.8c) *complemented with System* (2.23) *and the equation*

$$\left(\dot{I}_{v,1}, \dot{I}_{v,2}, \dot{\tilde{x}}_3\right)^{\top} = R\widetilde{v},$$

the equilibrium point $\left((I_{v,1}, I_{v,2}, z)^{\top}, \dot{z}, \widetilde{x}_3, \widetilde{v}, \widetilde{\theta}\right) = (z^*, 0, 0, 0, 0)$ *of the controlled system is asymptotically stable, with domain of attraction equal to* $\mathbb{R}^3 \times \mathbb{R} \times \mathbb{R} \times \mathbb{R}^3 \times (-\pi, \pi)$.

The proof, similar to the proof of Proposition 4, is given in Section 2.8.7.

2.4.1.6 Control with unidirectional thrust

In many applications the thrust direction cannot be inverted. This means that only a positive (resp. negative) or null control u can be applied. For the control laws given in Propositions 2–5, this sign constraint is satisfied in the neighborhood of the stabilized equilibrium point (since $u \approx |\gamma|$ and $|\gamma| > 0$ from Assumption 5). However, it is not satisfied in the entire domain of attraction of this equilibrium. The following proposition points out how the position control law (2.21) in Proposition 4 can be modified to comply with the constraint $u \geq 0$, without consequences on the stability issue.

Proposition 6 *Let* k_1, k_2, k_3 *denote some positive constants, and* $\overline{v}$ *and* γ *as defined in Proposition 4. Let* $\sigma : \mathbb{R} \to \mathbb{R}$ *denote a strictly increasing smooth function such that* $\sigma(0) = 0$ *and* $\sigma(s) > -1/k_1$, $\forall s \in \mathbb{R}$. *Apply the control law*

$$\begin{cases} u = |\gamma| + |\gamma|k_1\sigma(\overline{v}_3) \quad (> 0) \\ \omega_1 = -|\gamma|k_2\left(\overline{v}_2 - \dfrac{\overline{v}_3\overline{\gamma}_2}{|\gamma| + \overline{\gamma}_3}\right) - \dfrac{k_3|\gamma|\overline{\gamma}_2}{(|\gamma| + \overline{\gamma}_3)^2} - \dfrac{1}{|\gamma|^2}\gamma^{\top}S(Re_1)\dot{\gamma} \\ \omega_2 = |\gamma|k_2\left(\overline{v}_1 - \dfrac{\overline{v}_3\overline{\gamma}_1}{|\gamma| + \overline{\gamma}_3}\right) + \dfrac{k_3|\gamma|\overline{\gamma}_1}{(|\gamma| + \overline{\gamma}_3)^2} - \dfrac{1}{|\gamma|^2}\gamma^{\top}S(Re_2)\dot{\gamma} \end{cases} \tag{2.27}$$

to System (2.8). *Suppose that Assumptions i)–iv) of Proposition 4 are satisfied. Then the asymptotic stability result of Proposition 4 still holds.*

The proof, similar to the proof of Proposition 4, is given in Section 2.8.8. The proposed modification of the control law can directly apply to the control law of Proposition 5. It can also apply to the control laws of Propositions 2 and 3 by simply replacing $\overline{v}$ in the control law (2.27) by $\widetilde{v}$. A possible choice for the function σ is given, *e.g.*, by

$$\sigma(s) \triangleq \frac{\alpha}{k_1} \tanh\left(\frac{k_1 s}{\alpha}\right), \text{ or } \sigma(s) \triangleq \frac{s}{\sqrt{1 + \dfrac{k_1^2 s^2}{\alpha^2}}}, \text{ with } 0 < \alpha \leq 1.$$

2.4.1.7 Control with variable gains

By loosening the condition that the gains k_1, k_2, k_3 involved in the control laws proposed previously are constant, one has more possibilities for the gain tuning procedure. In what follows a modification is proposed for the control law of Proposition 6 to comply with a new condition of gains. Other control laws can be modified analogously.

Proposition 7 *Let k_1, k_2, k_3 denote some smooth bounded functions which are lower bounded by some positive constant, and $\overline{v}$ and γ as defined in Proposition 4. Let $\sigma :$ $\mathbb{R} \to \mathbb{R}$ denote a strictly increasing smooth function such that $\sigma(0) = 0$ and $\forall s \in \mathbb{R}$, $\sigma(s) > -1/inf(k_1)$. Apply the control law*

$$
\begin{cases}
u \; = \; |\gamma| + |\gamma| k_1(|\gamma|) \sigma(\overline{v}_3) \quad (>0) \\[2mm]
\omega_1 \; = \; -|\gamma| k_2(|\gamma|) \left(\overline{v}_2 - \dfrac{\overline{v}_3 \overline{\gamma}_2}{|\gamma| + \overline{\gamma}_3} \right) - \dfrac{k_3(|\gamma|)|\gamma| \overline{\gamma}_2}{(|\gamma| + \overline{\gamma}_3)^2} - \dfrac{1}{|\gamma|^2} \gamma^\top S(Re_1)\dot{\gamma} + \dfrac{\dot{k}_2(|\gamma|)\overline{\gamma}_2}{k_2(|\gamma|)(|\gamma| + \overline{\gamma}_3)} \\[3mm]
\omega_2 \; = \; |\gamma| k_2(|\gamma|) \left(\overline{v}_1 - \dfrac{\overline{v}_3 \overline{\gamma}_1}{|\gamma| + \overline{\gamma}_3} \right) + \dfrac{k_3(|\gamma|)|\gamma| \overline{\gamma}_1}{(|\gamma| + \overline{\gamma}_3)^2} - \dfrac{1}{|\gamma|^2} \gamma^\top S(Re_2)\dot{\gamma} - \dfrac{\dot{k}_2(|\gamma|)\overline{\gamma}_1}{k_2(|\gamma|)(|\gamma| + \overline{\gamma}_3)}
\end{cases}
$$

$$\text{(2.28)}$$

to System (2.8). Suppose that Assumptions i)–iv) of Proposition 4 are satisfied. Then the asymptotic stability result of Proposition 4 still holds.

The proof, similar to the proof of Proposition 6, is given in Section 2.8.9.

2.4.2   Control robustification

The control results obtained previously rely upon the satisfaction of Assumption 5 which unconditionally guarantees the existence and local uniqueness of the desired thrust direction in the velocity and position control cases. For most underactuated vehicles, this assumption is too strong. Let us illustrate this on a simple example.

Example 1 (Spherical vehicle) *Consider a spherical vehicle, with its center of mass coinciding with the sphere's center, submitted to the action of gravity, drag forces, and added-mass effects. The translational dynamics of the vehicle are given by Eq. (2.2) with $F_e(\dot{x}, \ddot{x}) = -c_a |\dot{x}|\dot{x} - m_a \ddot{x} + mge_3$, and c_a, m_a positive constant associated with drag forces and added-mass effects respectively. This equation can be rewritten as (compare with Eq. (2.2))*

$$\overline{m}\ddot{x} = -TRe_3 + \overline{F}_e(\dot{x}),$$

with $\overline{m} \triangleq m + m_a$ and $\overline{F}_e(\dot{x}) = -c_a |\dot{x}|\dot{x} + mge_3$. The term $\gamma(\dot{x}, t)$ of Eq. (2.9) is thus given by

$$\gamma(\dot{x}, t) = \frac{\overline{F}_e(\dot{x})}{\overline{m}} - \ddot{x}_r = -\frac{c_a}{\overline{m}}|\dot{x}|\dot{x} + \frac{mg}{\overline{m}}e_3 - \ddot{x}_r.$$

When drag effects can be neglected (i.e. $(c_a/\overline{m})|\dot{x}|\dot{x} \approx 0$), Assumption 5 is not satisfied when the reference acceleration vector $\ddot{x}_r$ is equal to $(m/\overline{m})ge_3$. As a matter of fact, the above relation points out that there always exists a velocity $\dot{x}$ such that $\gamma(\dot{x}, t) = 0$.

Even though one may hope that the set of "bad" velocities does not belong to the nominal operational domain of the vehicle, the above example indicates that, in some cases, Assumption 5 does not hold. Moreover, when $|\gamma| = 0$ the control is no longer defined. Now, to ensure *local* stability it is sufficient that γ does not vanish near the considered reference velocity $\dot{x}_r$. This suggests to replace Assumption 5 by the following weaker assumption.

Assumption 6 *There exists a constant $\delta > 0$ such that $|\gamma_e(\dot{x}_r(t), t) - \ddot{x}_r(t)| \geq \delta$, $\forall t \in \mathbb{R}_+$.*

Under this assumption, the control laws proposed in Section 2.4.1 are locally well-defined and ensure *local* asymptotic stability of the desired reference velocity/position trajectory. This may be sufficient for many applications. However, for practical purposes one would like to ensure that the control calculation is always well-posed and that the tracking errors can never diverge explosively, whatever the adverse environmental conditions or poorly chosen reference trajectories for which γ approaches the null vector at some time-instant. Accordingly, the objective of this section is to modify the controllers of Section 2.4.1 in order to have the three following properties satisfied simultaneously:

PI. *local asymptotic stability when Assumption 6 is satisfied;*

PII. *well-posedness of the expression of the control even when Assumption 6 is not satisfied;*

PIII. *global uniform ultimate boundedness of the system's velocities $\dot{x}$ and ω even when Assumption 6 is violated.*

The modifications are carried out for the velocity control objective of Proposition 2, but they are also valid for the other control laws proposed in Section 2.4.1 modulo straightforward transpositions which are shortly commented upon at the end of this section. Property *PII* is simply obtained by multiplying the unbounded terms $1/|\gamma|$ and $1/(|\gamma| + \overline{\gamma}_3)$ in the control expression (2.11) by an adequate function taking the value one inside a neighborhood of the reference trajectory and zero at $\gamma = 0$. For instance, one can use the class $\mathcal{C}^1$ function $\mu_\tau : [0, +\infty) \longrightarrow [0, 1]$ defined by

$$\mu_\tau(s) \triangleq \begin{cases} \sin\left(\dfrac{\pi s^2}{2\tau^2}\right), & \text{if } s \leq \tau \\ 1, & \text{otherwise} \end{cases} \tag{2.29}$$

for some constant $\tau > 0$. This yields the modified control expressions

$$\begin{cases} u = \overline{\gamma}_3 + |\gamma| k_1 \widetilde{v}_3 \\ \omega_1 = -|\gamma| k_2 \widetilde{v}_2 - \mu_\tau(|\gamma| + \overline{\gamma}_3) \dfrac{k_3 |\gamma| \overline{\gamma}_2}{(|\gamma| + \overline{\gamma}_3)^2} - \mu_\tau(|\gamma|) \dfrac{1}{|\gamma|^2} \gamma^\top S(Re_1)\dot{\gamma} \\ \omega_2 = |\gamma| k_2 \widetilde{v}_1 + \mu_\tau(|\gamma| + \overline{\gamma}_3) \dfrac{k_3 |\gamma| \overline{\gamma}_1}{(|\gamma| + \overline{\gamma}_3)^2} - \mu_\tau(|\gamma|) \dfrac{1}{|\gamma|^2} \gamma^\top S(Re_2)\dot{\gamma} \end{cases} \tag{2.30}$$

The fact that

$$\lim_{s \to 0} \frac{\mu_\tau(s)}{s^2} = \lim_{s \to 0} \sin\left(\frac{\pi s^2}{2\tau^2}\right) s^{-2} = \frac{\pi}{2\tau^2}$$

implies that the control law (2.30) is well-defined even when Assumption 6 is not satisfied. This control modification does not destroy the satisfaction of Property *PI*. The fulfillment of Property *PIII* is more involved. It relies in the first place on the following lemma which is a direct consequence of the dissipativity of drag forces (*i.e.* Assumption 3) and whose proof is given in Section 2.8.10.

Lemma 3 *Consider the following system*

$$\ddot{x} = -uRe_3 + \gamma_e(\dot{x}, t). \tag{2.31}$$

Suppose that Assumption 3 is satisfied and that u is calculated according to a feedback law such that, for some constants β_1, β_2,

$$|u| \leq \beta_1 + \beta_2|\dot{x}|. \tag{2.32}$$

Then, the linear velocity $\dot{x}$ of the controlled vehicle is u.u.b.. Moreover, under Assumption 1, γ_e, $\dot{\gamma}_e$ and the linear acceleration $\ddot{x}$ are also u.u.b..

The objective is now to modify the expression (2.9) of $\gamma(\dot{x}, t)$ so that u, as given by Eq. (2.30), can satisfy inequality (2.32) without destroying the property of local asymptotic stability. To this purpose let $\overline{\mathrm{sat}}_M$ denote a continuous "saturation function" satisfying Properties *P1, P2, P3* of the function sat_Δ (with Δ replaced by M) and also the following property:

P4. There exists a continuous function $\phi : \mathbb{R}^3 \longrightarrow \mathbb{R}$ such that $\forall (\xi, \gamma) \in \mathbb{R}^3 \times \mathbb{R}^3$, $\phi(\gamma) \leq 1$ and $\xi^\top \overline{\mathrm{sat}}_M(\gamma) = \phi(\gamma)\xi^\top\gamma$.

A possible choice of $\overline{\mathrm{sat}}_M$ is the saturation function defined by Eq. (2.17).

Let $\gamma_d : \mathbb{R} \longrightarrow \mathbb{R}^3$ denote any bounded function of class $\mathcal{C}^1$ whose derivative is also bounded. The role and choice of this function will be commented upon further, along with some examples. Define now γ as follows

$$\gamma(\dot{x}, t) \triangleq \gamma_d(t) + \overline{\mathrm{sat}}_M(\gamma_{e,d}(\dot{x}, t)) - \ddot{x}_r(t), \tag{2.33}$$

with

$$\gamma_{e,d}(\dot{x}, t) \triangleq \gamma_e(\dot{x}, t) - \gamma_d(t), \tag{2.34}$$

and M a positive real number the choice of which is discussed further. From Eq. (2.33), Assumption 4, the boundedness of γ_d, and the boundedness of the function $\overline{\mathrm{sat}}_M$, it follows that there exists a finite value $Q > 0$ such that, whatever $(\dot{x}, t)$,

$$|\gamma(\dot{x}, t)| \leq Q. \tag{2.35}$$

Therefore, in view of the expression of u in the control law (2.30), inequality (2.32) is now satisfied. Prior to stating the main stabilization result of this section we need to introduce some extra notation. Since γ_d is bounded by assumption, it follows from Assumptions 2 and 3 (recall that $\gamma_e = F_e/m$) and Eq. (2.34) that there exist constant numbers $\overline{c}_1 \geq 0$, $\overline{c}_2 > 0$, $\overline{c}_3 \geq 0$, $\overline{c}_4 > 0$ such that, $\forall (\dot{x}, t) \in \mathbb{R}^3 \times \mathbb{R}$,

$$\begin{cases} |\gamma_{e,d}(\dot{x}, t)| & \leq & \overline{c}_1 + \overline{c}_2|\dot{x}|^2 \\ \dot{x}^\top \gamma_{e,d}(\dot{x}, t) & \leq & \overline{c}_3|\dot{x}| - \overline{c}_4|\dot{x}|^3 \end{cases} \tag{2.36}$$

Consider the following polynomial in s

$$P(s) \triangleq \overline{c}_4 s^3 - \overline{c}_2 \overline{\mathbf{v}}_{\mathbf{r}} s^2 - \overline{c}_3 s - \overline{c}_1 \overline{\mathbf{v}}_{\mathbf{r}}, \text{ with } \overline{\mathbf{v}}_{\mathbf{r}} \geq 0.$$

Since $\overline{c}_4 > 0$, there exists a number $\kappa(\overline{c}_i, \overline{\mathbf{v}}_{\mathbf{r}}) \geq \overline{\mathbf{v}}_{\mathbf{r}}$ such that $s \geq \kappa(\overline{c}_i, \overline{\mathbf{v}}_{\mathbf{r}}) \Rightarrow P(s) \geq 0$.

The following theorem, proved in Section 2.8.11, is the main result of this section.

Theorem 1 *Let k_1, k_2, k_3 denote some positive constants. Apply the control law (2.30) to System (2.8), with μ_τ and γ given by Eqs. (2.29) and (2.33) respectively. Suppose that $0 < \tau < \delta$, where τ and δ are the constants involved in relation (2.29) and Assumption 6 respectively. Suppose that Assumptions 1, 2, 3, 4, and 6 are satisfied. Then, the following properties hold:*

1) u and ω are well-defined and bounded along any solution of the controlled system;

2) $\dot{x}$ is u.u.b. along any solution of the controlled system;

3) for Subsystem (2.8b)–(2.8c), the equilibrium point $(\widetilde{v}, \widetilde{\theta}) = (0,0)$ of the controlled system is locally asymptotically stable if $M > \overline{c}_1 + \overline{c}_2 \overline{\mathbf{v}}_\mathbf{r}$, with M the constant associated with the function $\overline{\mathrm{sat}}_M$ intervening in γ. Furthermore, if $M \geq \overline{c}_1 + \overline{c}_2(\kappa(\overline{c}_i, \overline{\mathbf{v}}_\mathbf{r}))^2$ and $|\gamma(\dot{x}, t)| \geq \tau \; \forall(\dot{x}, t)$, the attraction domain is equal to $\mathbb{R}^3 \times (-\pi, \pi)$.

By comparison with the control laws of Section 2.4.1, the control law (2.30) depends on extra design terms (τ, and the functions $\overline{\mathrm{sat}}_M$ and γ_d) which can be tuned so as to maximize the domain of stability of the closed-loop system. Let us illustrate this tuning possibility in the case of the spherical vehicle already considered in Example 1.

Example 2 (Spherical vehicle, continued) *To simplify we assume that the desired velocity $\dot{x}_r$ is constant, i.e. $\ddot{x}_r = 0$. In this case,*

$$\gamma_e(\dot{x}) = \gamma(\dot{x}) = \gamma_g + \gamma_{ae}(\dot{x}),$$

with $\gamma_g = (mg/\overline{m})e_3$ the gravity acceleration vector field, and $\gamma_{ae}(\dot{x}) = -(c_a/\overline{m})|\dot{x}|\dot{x}$ ($c_a > 0$) the acceleration vector associated with aerodynamic forces. Let us assume that the function $\overline{\mathrm{sat}}_M$ is defined by $\overline{\mathrm{sat}}_M(x) = x \min(1, M/|x|) \; \forall x \in \mathbb{R}^3$, and consider two possible choices for γ_d (among others). Firstly, let $\gamma_d = \gamma_g$. Then $\gamma = \gamma_g + \overline{\mathrm{sat}}_M(\gamma_{e,d})$ and $\gamma_{e,d} = \gamma_{ae}$. Since the norm of γ_g is non-zero and constant, and $\overline{\mathrm{sat}}_M$ is bounded by M, Assumption 6 is satisfied if $M < mg/\overline{m}$. In this case, $|\gamma(\dot{x}, t)| \geq mg/\overline{m} - M > 0$. Moreover, if $\tau < mg/\overline{m} - M$, the equilibrium $(\widetilde{v}, \widetilde{\theta}) = (0,0)$ is "globally" asymptotically stable (i.e. the domain of attraction is $\mathbb{R}^3 \times (-\pi, \pi)$). However, imposing this inequality on M may not be compatible with the satisfaction of the condition $M \geq \overline{c}_1 + \overline{c}_2(\kappa(\overline{c}_i, \overline{\mathbf{v}}_\mathbf{r}))^2$ which guarantees the largest possible domain of attraction. Indeed, in this case one has $\overline{c}_1 = \overline{c}_3 = 0$, $\overline{c}_2 = \overline{c}_4 = c_a$, and $\kappa(\overline{c}_i, \overline{\mathbf{v}}_\mathbf{r}) = \overline{\mathbf{v}}_\mathbf{r}$, so that the condition $M \geq \overline{c}_1 + \overline{c}_2(\kappa(\overline{c}_i, \overline{\mathbf{v}}_\mathbf{r}))^2$ is now equivalent to $M \geq c_a \overline{\mathbf{v}}_\mathbf{r}^2$. Therefore, the satisfaction of Assumption 6 and global asymptotic stability are guaranteed provided that $\sup |\dot{x}_r(t)| < \sqrt{mg/(\overline{m}c_a)}$. Now, to stabilize larger reference velocities which do not satisfy this inequality it is necessary to use values of M larger than $mg/\overline{m}$. However the positivity of $|\gamma(\dot{x}, t)|$ can no longer be guaranteed locally around any reference velocity. In this case, instead of choosing $\gamma_d = \gamma_g$, one might as well set $\gamma_d = 0$, so that

$$\gamma = \overline{\mathrm{sat}}_M(\gamma_e) = \overline{\mathrm{sat}}_M(\gamma_g + \gamma_{ae}).$$

With this choice the positivity of $|\gamma(\dot{x}, t)|$ is not unconditional, but it is satisfied in the neighborhood of any reference velocity such that $\dot{x}_r \neq \sqrt{mg/(\overline{m}c_a)} \, e_3$. From Theorem 1 local asymptotic stability is also obtained if $M \geq g + c_a \overline{\mathbf{v}}_\mathbf{r}^2$.

Remark 3 *The controllers of Propositions 3-6 can be modified in a similar way. Consider for example the position control law of Proposition 4. One can define (compare with Eq.* (2.20)*)*

$$\gamma \triangleq \gamma_d + \overline{\mathrm{sat}}_M(\widehat{\gamma}_{e,d}) - \ddot{x}_r + h(|y|^2)y + \ddot{z},$$

with $\widehat{\gamma}_{e,d} \triangleq \widehat{\gamma}_e - \gamma_d$, and state stability results as in Theorem 1. The sole difference concerns the condition $M > \overline{c}_1 + \overline{c}_2(\kappa(\overline{c}_i, \overline{\mathbf{v}}_\mathbf{r}))^2$ of Theorem 1 which yields global asymptotic stability. It has to be replaced by the stronger condition $M > \overline{c}_1 + \overline{c}_2(\kappa(\overline{c}_i, \overline{\mathbf{v}}_\mathbf{r} + 2\eta_z))^2$.

2.4.3 Complementary control studies

In what follows we complete this control design section with a control law ω_3 for the yaw motion and a gain tuning procedure for the controllers proposed in Section 2.4.1.

2.4.3.1 Yaw motion control

The control variable ω_3 is not involved in the control design of the above control objectives. It is only required to be bounded. This variable constitutes another degree of freedom to be exploited for complementary control objectives. Besides the possibilities mentioned at the beginning of Section 2.4.1, we here consider the heading tracking objective, and let $\overrightarrow{\alpha}$ denote a reference unit vector for the heading direction lying on the horizontal inertial plane $\{O; \overrightarrow{\imath_o}, \overrightarrow{\jmath_o}\}$. Let α denote the vector of coordinates of $\overrightarrow{\alpha}$ expressed in the inertial frame $\mathcal{I}$. In practice this desired vector may be specified by a manual joystick. The control objective is the stabilization of the projection of the vector $\overrightarrow{\alpha}$ onto the vehicle's plane $\{G; \overrightarrow{\imath}, \overrightarrow{\jmath}\}$ about the vector $\overrightarrow{\imath}$ in steady flight regimes (*i.e.* $\omega_{1,2} = 0$). This control objective can be interpreted as the stabilization of $\beta \triangleq \pi_{e_3}R^\top\alpha$, with $\pi_{e_3} \triangleq \mathbf{diag}(1,1,0)$, about $|\beta|e_1$ in steady flight regimes. The control result is stated next (see Section 2.8.12 for the proof).

Lemma 4 *Let k_α denote a positive constant, and apply the control law*

$$\omega_3 = k_\alpha e_2^\top R^\top \alpha \qquad (2.37)$$

to System (2.5)*. Then,*

1) ω_3 remains bounded;

2) in steady flight regimes (i.e. $\omega_{1,2} = 0$), if α is constant and $\beta(0) \neq -|\beta(0)|e_1$, then the equilibrium $\beta = |\beta|e_1$ is asymptotically stable.

2.4.3.2 Gain tuning

Gain tuning is an essential procedure for any feedback controller because the closed-loop system's behavior is strictly related to the chosen set of gains. In linear control theory, many powerful techniques can be found like pole-zero placement, H_∞ pole placement, *etc.*. However, the gain tuning for a nonlinear control law is less obvious and is normally overlooked in the literature. In what follows, we show how the gain tuning for our proposed controllers can be done by using existing gain tuning techniques in linear control theory. A way to determine the control gains consists in considering the linearization of System (2.8) complemented with System (2.16) at the equilibrium ($z = 0, \dot{z} = 0, \widetilde{x} = 0, \widetilde{v} = 0, R = I_3,$

$u = g$, $\omega = 0$) for the particular case where the reference trajectory is a fixed point, $F_e = mge_3$, and the desired yaw angular velocity is equal to zero. Here the gain tuning is performed for the position controller of Proposition 6, and the same technique applies to the other controllers. Near the desired equilibrium, γ as given by Eq. (2.20) can be approximated by

$$\gamma \approx ge_3 + (h(0) + k_z h_z(0))\widetilde{x} + h(0)z - 2k_z\dot{z}.$$

Setting $w \triangleq \dot{z}$ and using the fact that $(\partial\sigma(s)/\partial s)|_{s=0} = 1$, one deduces from the control law (2.27) that

$$\begin{cases} u \approx g + (h(0) + k_z h_z(0))\widetilde{x}_3 + gk_1\widetilde{v}_3 + h(0)z_3 + (gk_1 - 2k_z)w_3 \\ \omega_1 \approx -\dfrac{k_3}{4g}(h(0) + k_z h_z(0))\widetilde{x}_2 - gk_2\widetilde{v}_2 - \dfrac{k_3 h(0)}{4g}z_2 - (gk_2 - \dfrac{k_3 k_z}{2g})w_2 - \dfrac{k_3}{4}(e_2^\top R^\top e_3) \\ \omega_2 \approx \dfrac{k_3}{4g}(h(0) + k_z h_z(0))\widetilde{x}_1 + gk_2\widetilde{v}_1 + \dfrac{k_3 h(0)}{4g}z_1 + (gk_2 - \dfrac{k_3 k_z}{2g})w_1 + \dfrac{k_3}{4}(e_1^\top R^\top e_3) \\ \omega_3 \approx 0 \end{cases}$$

Define $\theta_1 \triangleq e_1^\top R^\top e_3$, and $\theta_2 \triangleq e_2^\top R^\top e_3$. It comes from $\dot{R}^\top = -S(\omega)R^\top$, $\omega_3 \approx 0$, and $R \approx I_3$ that $\dot{\theta}_1 \approx -\omega_2$ and $\dot{\theta}_2 \approx \omega_1$. From here one obtains the following linear system which is the linear approximation of the controlled error system (2.8) complemented with System (2.16)

$$\begin{cases} \dot{z} = w \\ \dot{w} = -2k_z w + k_z h_z(0)\widetilde{x} \\ \dot{\widetilde{x}} = \widetilde{v} \\ \dot{\widetilde{v}} = (g\theta_1, g\theta_2, -(h(0) + k_z h_z(0))\widetilde{x}_3 - gk_1\widetilde{v}_3 - h(0)z_3 - (gk_1 - 2k_z)w_3)^\top \\ \dot{\theta}_1 = -\dfrac{k_3}{4g}(h(0) + k_z h_z(0))\widetilde{x}_1 - gk_2\widetilde{v}_1 - \dfrac{k_3 h(0)}{4g}z_1 - (gk_2 - \dfrac{k_3 k_z}{2g})w_1 - \dfrac{k_3}{4}\theta_1 \\ \dot{\theta}_2 = -\dfrac{k_3}{4g}(h(0) + k_z h_z(0))\widetilde{x}_2 - gk_2\widetilde{v}_2 - \dfrac{k_3 h(0)}{4g}z_2 - (gk_2 - \dfrac{k_3 k_z}{2g}))w_2 - \dfrac{k_3}{4}\theta_2 \end{cases}$$

This system can be decomposed into three independent subsystems

$$(\Sigma_3): \begin{cases} \dot{z}_3 = w_3 \\ \dot{w}_3 = -2k_z w_3 + k_z h_z(0)\widetilde{x}_3 \\ \dot{\widetilde{x}}_3 = \widetilde{v}_3 \\ \dot{\widetilde{v}}_3 = -(h(0) + k_z h_z(0))\widetilde{x}_3 - gk_1\widetilde{v}_3 - h(0)z_3 - (gk_1 - 2k_z)w_3 \end{cases}$$

$$(\Sigma_{i\,(i=1,2)}): \begin{cases} \dot{z}_i = w_i \\ \dot{w}_i = -2k_z w_i + k_z h_z(0)\widetilde{x}_i \\ \dot{\widetilde{x}}_i = \widetilde{v}_i \\ \dot{\widetilde{v}}_i = g\theta_i \\ \dot{\theta}_i = -\dfrac{k_3}{4g}(h(0) + k_z h_z(0))\widetilde{x}_i - gk_2\widetilde{v}_i - \dfrac{k_3 h(0)}{4g}z_i - (gk_2 - \dfrac{k_3 k_z}{2g})w_i - \dfrac{k_3}{4}\theta_i \end{cases}$$

whose characteristic polynomials are given by

$$P_3(\lambda) = \lambda^4 + (2k_z + gk_1)\lambda^3 + (h(0) + 2gk_zk_1 + k_zh_z(0))\lambda^2$$
$$+ (2k_zh(0) + gk_zh_z(0)k_1)\lambda + k_zh_z(0)h(0),$$

$$P_i(\lambda) = \lambda^5 + \left(2k_z + \frac{k_3}{4}\right)\lambda^4 + \left(g^2k_2 + \frac{k_zk_3}{2}\right)\lambda^3 + \left(2g^2k_zk_2 + \frac{h(0)k_3}{4} + \frac{k_zh_z(0)k_3}{4}\right)\lambda^2$$
$$+ \left(g^2k_zh_z(0)k_2 + \frac{k_zh(0)k_3}{2}\right)\lambda + \frac{k_zh_z(0)h(0)k_3}{4}.$$

Among many possibilities one can, for instance, proceed as follows. Take

$$h(0) = 2gk_1k_z - 4k_z^2, \quad k_2 = \frac{k_1k_3}{4g}, \quad k_z < \frac{gk_1}{2}.$$

Then,

$$P_3(\lambda) = (\lambda + 2k_z)\left(\lambda^3 + gk_1\lambda^2 + (2gk_1k_z - 4k_z^2 + k_zh_z(0))\lambda + \frac{1}{2}h_z(0)(2gk_1k_z - 4k_z^2)\right),$$

$$P_i(\lambda) =$$
$$(\lambda + 2k_z)\left(\lambda^4 + \frac{k_3}{4}\left(\lambda^3 + gk_1\lambda^2 + (2gk_1k_z - 4k_z^2 + k_zh_z(0))\lambda + \frac{1}{2}h_z(0)(2gk_1k_z - 4k_z^2)\right)\right).$$

By taking $2k_z < gk_1$, one obtains by application of the Routh–Hurwitz criterion that all roots of $P_3(\lambda)$ have negative real parts. The complementary possibility of having all roots of $P_3(\lambda)$ real negative and equal leads to choose k_1, k_z, $h_z(0)$ as follows

$$k_1 = \frac{3\lambda_0}{g}, \quad k_z = \lambda_0, \quad h_z(0) = \lambda_0,$$

with λ_0 denoting an arbitrary positive number. Note that $h(0) = 2\lambda_0^2$ and $k_2 = 3\lambda_0k_3/(4g^2)$ in this case. One obtains

$$P_3(\lambda) = (\lambda + \lambda_0)^4,$$
$$P_i(\lambda) = (\lambda + \lambda_0)\left(\lambda^4 + \frac{k_3}{4}(\lambda + \lambda_0)^3\right).$$

Then, it suffices to choose k_3 such that $k_3 \gg 4\lambda_0$ in order to get the roots of $P_i(\lambda)$ near those of $\bar{P}_i(\lambda) \triangleq (\lambda + \lambda_0)^3(\lambda + k_3/4)$. The gains k_1, k_2, k_z, $h_z(0)$, $h(0)$ used for the simulations of Section 2.6 have been calculated with $\lambda_0 = 0.8$ and $k_3 = 9.6$.

2.5   Estimation of the external force

As mentioned previously, the information available on $\overrightarrow{F}_e$ or, equivalently, on γ_e is central to the design of effective feedback control laws. Some of the external forces (like gravity or buoyancy) are often known in advance with a good accuracy. Others (like drag or lift forces) are much more difficult to model and/or measure. Unpredictable aero/hydro-dynamic effects induced by wind gusts or sea-currents complicate the matter even more. In practice, accelerometers can be used to measure γ_e when the thrust force and the vehicle's orientation are available to measurement. More precisely, from the accelerometer

measurement $a_\mathcal{B}$, one obtains $\ddot{x} = ge_3 + Ra_\mathcal{B}$. Then, γ_e can be deduced from this relation and Eq. (2.2) as follows

$$\gamma_e = R\left(a_\mathcal{B} + ue_3\right) + ge_3 \tag{2.38}$$

It is also possible to design an observer of γ_e based on thrust, linear velocity, and orientation measurements. This may seem difficult, especially in the absence of a good model of γ_e. However, when the time-derivative of γ_e is bounded, a simple solution to this problem, based on the use of large estimation gains, exists. This boundedness property is in turn granted when the thrust power cannot exceed the power of the dissipative forces. More precisely, if the thrust control input u satisfies inequality (2.32) then $\dot{\gamma}_e$ is $u.u.b.$ as a consequence of Lemma 3.

Now, consider the following observer of γ_e, assuming that $u, \dot{x}, R$ are measured

$$\begin{cases} \dfrac{d}{dt}\widehat{\dot{x}} = -uRe_3 + \widehat{\gamma}_e + k_o(\dot{x} - \widehat{\dot{x}}) \\[2mm] \dot{\widehat{\gamma}}_e = a^2 k_o^2(\dot{x} - \widehat{\dot{x}}) \end{cases} \tag{2.39}$$

with $\widehat{\dot{x}}$ an estimate of $\dot{x}$, $\widehat{\gamma}_e$ the estimate of γ_e, and a, k_o some positive gains. From here the main result of this section is stated next.

Proposition 8 *Consider System* (2.31) *complemented with System* (2.39) *and assume that $\dot{\gamma}_e$ is u.u.b.. Then, for any $a \in \left(1 - \sqrt{2}/2, 1 + \sqrt{2}/2\right)$,*

i) The estimation errors $\dot{x} - \widehat{\dot{x}}$ and $\gamma_e - \widehat{\gamma}_e$ are u.u.b. by a constant $\varepsilon(k_o)$ which tends to zero when k_o tends to $+\infty$;

ii) $\dot{\widehat{\gamma}}_e$ is u.u.b. by a constant independent of k_o.

The proof is given in Section 2.8.13. Lemma 3 and Proposition 8 indicate that if the thrust control u satisfied inequality (2.32), then one can "theoretically" obtain an arbitrarily good estimate of γ_e by increasing the observer gain k_o as much as needed [3]. This suggests a type of "separation principle" allowing to address the observer and controller design problems separately.

2.6   Simulation results

In this section we illustrate through simulations the performance and robustness of the proposed controllers for the following models of rotary-wing VTOL vehicle:

i) a nonlinear model of a ducted fan tailsitter;

ii) a simulator of the ducted fan tailsitter HoverEye, developed by Bertin Technologies;

iii) a nonlinear model of a reduced scale helicopter.

---

3. In practice, there are also well-known reasons such as control discretization, measurements noise, *etc.* for not choosing too high gains, so that a compromise must be done.

2.6.1   Simulation with a model of a ducted fan tailsitter

In this section the proposed controllers are applied for a model of a ducted fan tailsitter similar to the HoverEye whose shape roughly corresponds to the one depicted in Fig. 2.1. It is symmetric along a privileged axis taken as the axis $\{G; \overrightarrow{k}\}$. In the first approximation, its inertia matrix J is diagonal and $J \approx \mathbf{diag}(J_1, J_1, J_3)$.

   The system's equations of motion used for simulations are given by Eq. (2.1) with (see Section 1.4.2)

$$F_e = mge_3 + R\Sigma_R\Gamma + RF_{ae}^{\mathcal{B}}, \ \Gamma_e = \Gamma_{ae}^{\mathcal{B}}, \tag{2.40}$$

with Σ_R defined by Eq. (1.12), and $F_{ae}^{\mathcal{B}}$, $\Gamma_{ae}^{\mathcal{B}}$ defined by Eq. (1.10). Note that $F_{ae}^{\mathcal{B}}$ is the vector of coordinates expressed in the body frame $\mathcal{B}$ of $\overrightarrow{F}_{ae}$ representing the sum of all aerodynamic reaction forces (lift, drag, and momentum drag), and $\Gamma_{ae}^{\mathcal{B}}$ is the torque vector of coordinates expressed in the body frame $\mathcal{B}$ induced by these external forces. Aerodynamic and physical parameters of the vehicle are given by

$$k_1^e = 0.13, \ k_2^e = 0.03, \ k_3^e = 0.03, \ k_4^e = 0.005, \ k_5^e = 0.28,$$
$$\varepsilon_{ae} = \varepsilon_m = 0.05 \, (m),$$
$$m = 3.2 \, (kg), \ J = \mathbf{diag}(0.13, 0.13, 0.04) \, (kg \, m^2), \ L = 0.2 \, (m).$$

By setting

$$\gamma_e \triangleq F_e/m, \tag{2.41}$$

the subsystem Σ_1^{3d} of System (2.1) takes the form of System (2.5). However, Assumption 1 is violated because F_e depends on the vehicle's attitude R, and also because Γ is related to the angular acceleration so that γ_e depends also on these variables. Discrepancies like this one between the ideal model used for the control design and the physical system represent an opportunity to test by simulation the robustness of the proposed controllers. The complete vehicle's pose (*i.e.* x and R) is measured together with all velocity components (*i.e.* v and ω). The simulation results presented next have been obtained with the following estimated physical parameters of the vehicle

$$\widehat{m} = 3 \, (kg), \ \widehat{J}_1 = 0.1 \, (kg \, m^2), \ \widehat{J}_3 = 0.03 \, (kg \, m^2).$$

This allows to test the robustness of the proposed controllers with respect to static modeling errors.

   Among the four control modes considered in the paper, position stabilization is the most advanced one and simulations are only presented for this mode. For the first subsystem Σ_1 the controller of Proposition 6, modified as proposed in Section 2.4.2, is applied to yield u, $\omega_{d,1}$, and $\omega_{d,2}$. Then, the applied thrust force control is given by

$$T = \widehat{m}u.$$

The desired yaw angular velocity (*i.e.* $\omega_{d,3}$) is the controller (2.37) given in Lemma 4, with

$$k_\alpha = 5, \ \alpha = e_1.$$

A high gain controller is applied to the second subsystem Σ_2^{3d} of System (2.1) in order to stabilize the angular velocity at the desired value ω_d whose first two components are generated by the first controller. Note that the choice of a high gain controller is here

justified by the fact that Γ_{ae} is neither measured nor estimated. The applied control torque is calculated according to

$$\Gamma = S(\omega)\widehat{J}\omega_d - \widehat{J}K_\omega(\omega - \omega_d),$$

with $\widehat{J} = \mathbf{diag}(\widehat{J}_1, \widehat{J}_1, \widehat{J}_3)$ and K_ω a positive symmetric gain matrix here chosen diagonal. The following gains and functions are used

- $k_1 = 0.245$, $k_2 = 0.06$, $k_3 = 9.6$, $K_\omega = \mathrm{diag}(20; 20; 20)$,

- $h(s) = \beta/\sqrt{1 + \beta^2 s/\eta^2}$ with $\beta = 1.28$ and $\eta = 12$,

- $\sigma(s) = \alpha/k_1 \tanh(k_1 s/\alpha)$ with $\alpha = 0.9$,

- $k_z = 0.8$, $h_z(s) = \beta_z/\sqrt{1 + \beta_z^2 s/\eta_z^2}$ with $\beta_z = 0.8$ and $\eta_z = 0.8$,

- sat_Δ and $\overline{\mathrm{sat}}_M$ as given by Eq. (2.17) with $\Delta = 8$, $M = 50$,

- $\gamma_d = 0$, μ_τ as given by Eq. (2.29) with $\tau = 1$.

The gains k_1, k_2, k_3, $h(0)$, k_z, $h_z(0)$ have been determined via a pole placement procedure performed on the linearized system of System (2.8)–System (2.16) at the equilibrium $(z = 0, \dot{z} = 0, \widetilde{x} = 0, \widetilde{v} = 0, R = I_3, \omega_3 = 0)$ in the particular case of a reference trajectory consisting of a fixed point, with all external forces being neglected. Details are given in Section 2.4.3.2.

Some simulation cases are reported.

▷ **Simulation 1 − Stabilization at a stationary point.**

The control objective is to stabilize the vehicle's center of mass G, initially resting at the position $x(0) = [8, 5, -8]^\top$. The initial vehicle's attitude is given by $R(0) = I_3$. This corresponds to the equilibrium attitude associated with a fixed desired position in the absence of wind. The desired position is $x_r = [0, 0, 0]^\top$. Initially there is no wind, but a horizontal wind step velocity $\dot{x}_f = [4, 0, 0]^\top$ is introduced between the time-instants $30\,s$ and $70\,s$, followed by a larger one ($\dot{x}_f = [8, 0, 0]^\top$) thereafter. This simulation was devised to test the robustness of the proposed controller when neither measurement nor estimation of aerodynamic reaction forces is available. To this purpose we have used $\widehat{\gamma}_e = ge_3$ in the control calculation, whereas the real value of γ_e is given by Eqs. (2.40)-(2.41). It matters also to illustrate the role and importance of the integrator defined by System (2.16). In this respect two control versions are used for comparison purposes. The first one does not incorporate a position integral action. This corresponds to setting the terms z, $\dot{z}$, and $\ddot{z}$ equal to zero. The second one contains the integral action resulting from the calculation of z and its first and second order time-derivatives from Eq. (2.16). The evolution of the vehicle's position and attitude is shown on Fig. 2.2 and Fig. 2.3. With both control versions, the position of the vehicle's center of mass G converges to a fixed position. However, in the no-integral action case (see Fig. 2.2) the position error does not converge to zero due to estimation errors on the vehicle's physical parameters and poorly modeled aerodynamic reaction forces. Fig. 2.3 shows that the incorporation of the proposed integral action makes this error converge to zero. Note that Assumption *iv)* of Proposition 6 ($\lim_{s \to +\infty} h(s^2)s > |c|$,

with $c = \widehat{\gamma}_e - \gamma_e$) must be satisfied to guarantee the stability of the controlled system and

compensate for large wind-induced perturbations. When η, the upper-bound of $h(s^2)s$, is smaller than 10 and the wind velocity is "strong" ($\dot{x}_f = 8e_1$) (*i.e.* when modeling errors on external forces are very large) we have observed, in simulation, the divergence of the position error despite the integral action. This explains the use of a larger value of η (*i.e.* $\eta = 12$) in the reported simulations. Recall however that, as discussed in Section 2.4.1.3, using a large value of η has the side drawback of increasing the risk of $|\gamma|$ evolving close to zero. It also contributes to increasing the magnitude of γ defined by Eq. (2.20), and thus also of the control inputs defined by (2.21). This in turn increases the risk of saturating the actuators, with known associated destabilizing effects. To comply with actuators power limitations a small value of η is preferable. This in turn militates in favor of the on-line measurement or estimation of the apparent acceleration γ_e. The high gain observer of this force, based on the measurement of the vehicle's translational velocity $\dot{x}$ and orientation R, and of the thrust intensity T, proposed in Section 2.5 will be used. More precisely, the observer of γ_e, *i.e.* System (2.39), is used with $a = 1$, $k_o = 10$.
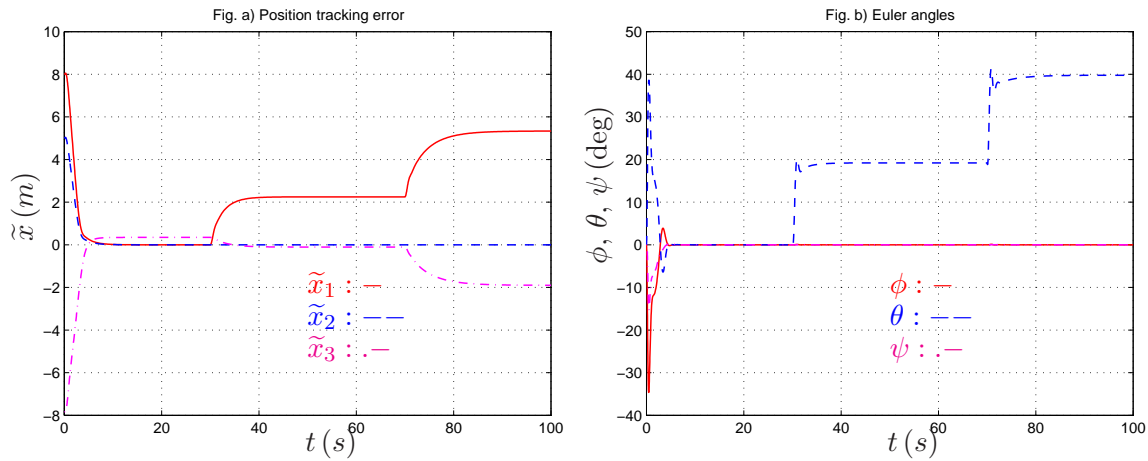
Figure 2.2: Vehicle's pose vs. time, fixed reference position, no integral correction, $\eta = 12$.
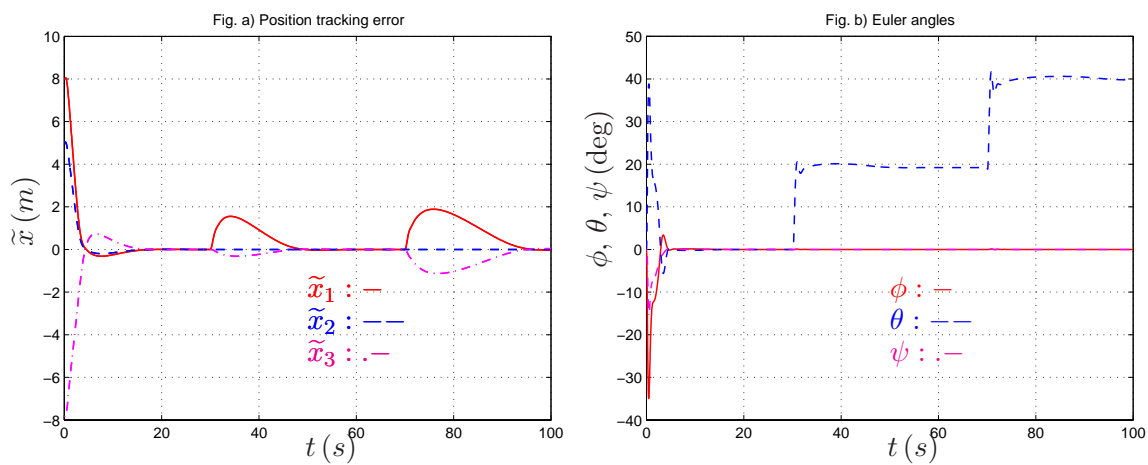
Figure 2.3: Vehicle's pose vs. time, fixed reference position, integral correction, $\eta = 12$, and $\Delta = 8$.

Fig. 2.4 shows simulation results of the controller with integral correction when using such an observer. Smaller values of η and Δ, *i.e.* the value associated with the function sat_Δ, are also applied: $\eta = 4$, $\Delta = 1$. The improved tracking performance of this controller, which is also used in the next simulation case, shows the interest of complementing the integral correction action with the estimation of the apparent acceleration.
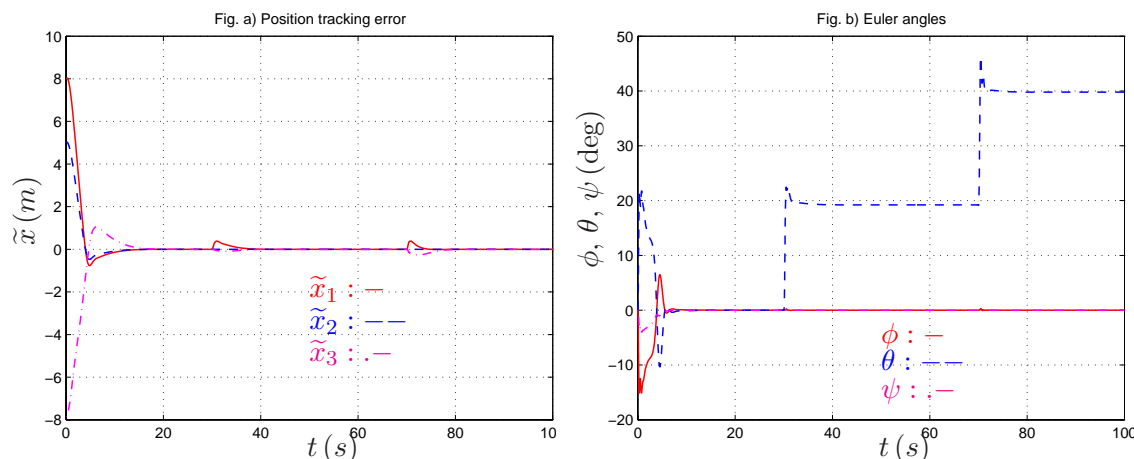
Figure 2.4: Vehicle's pose vs. time, fixed reference position, integral correction, $\eta = 4$, and $\Delta = 1$, on-line estimation of aerodynamic forces.

▷ **Simulation 2 – Trajectory tracking with strong variable wind, large initial position error, and on-line estimation of aerodynamic forces.**

The control objective is to track the following reference trajectory

$$x_r(t) = [10\cos(\pi t/10),\ 10\sin(\pi t/10),\ -t]^\top\ (m/s). \tag{2.42}$$

The vehicle initial position and attitude are given by $x(0) = [45, 50, -10]^\top\ (m)$ and $R(0) = I_3$ respectively. Integral correction in position is used. To test the robustness of the controller with respect to aerodynamic perturbations a "strong" variable wind is simulated with velocity intensity variations represented on Fig. 2.5. Actual and estimated apparent accelerations are shown on Fig. 2.6. The error of estimation of the apparent acceleration is also shown on this figure. Limitations of the actuators are also taken into account by saturating the applied thrust force and torque components according to the following inequality constraints

$$0 \leq T \leq 1.8mg,$$

$$|\Gamma_{i=1,2,3}| \leq 0.3TL.$$

The control results of Fig. 2.7 illustrate the robustness of the controller with respect to strong and rapidly varying wind-induced perturbations and modeling errors. The tracking position errors decrease almost linearly from large initial values and remain small thereafter (see Fig. 2.7.c). At the beginning of the simulation, due to the small value of η (*i.e.* $\eta = 6$) the thrust input remains unsaturated (see Fig. 2.7.e) despite large initial position errors. The saturation occurring later on during short time intervals, as a consequence of strong wind gusts, marginally affects the overall tracking performance.
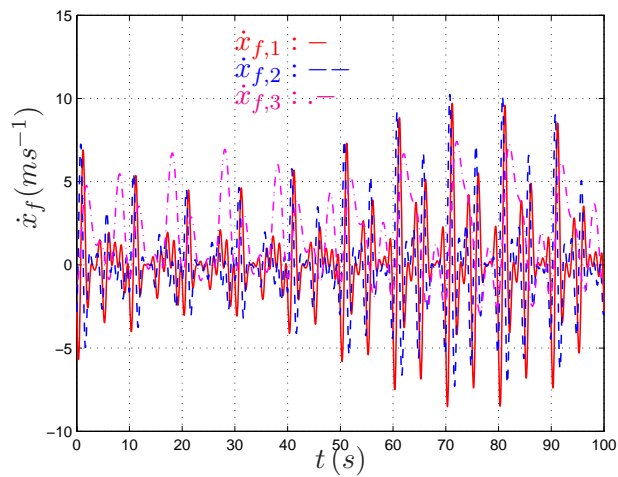
Figure 2.5: Wind velocities vs. time.
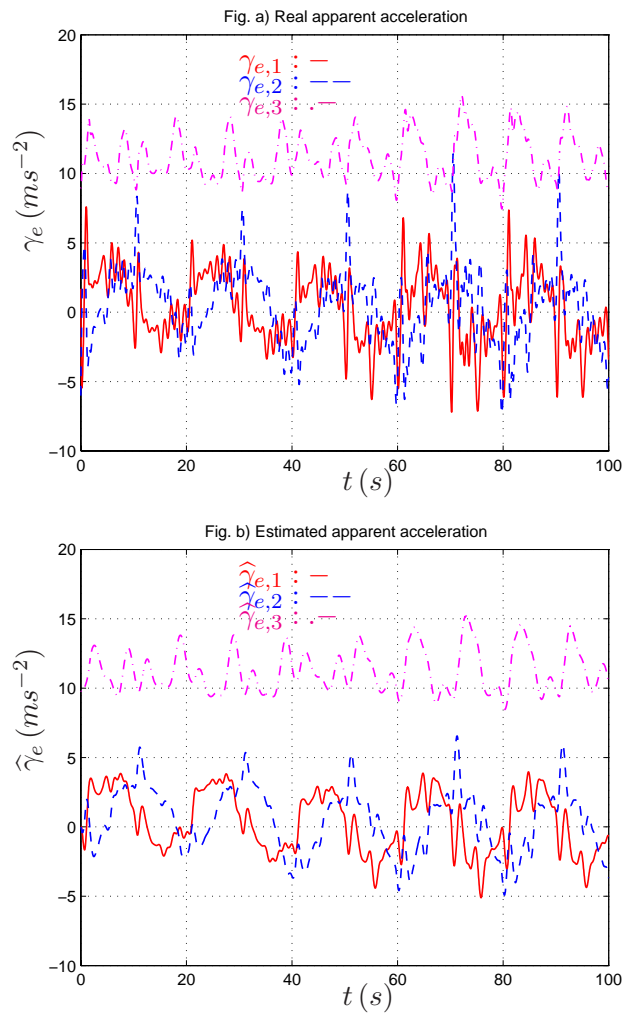
Figure 2.6: Real (γ_e) and estimated ($\widehat{\gamma}_e$) apparent accelerations.
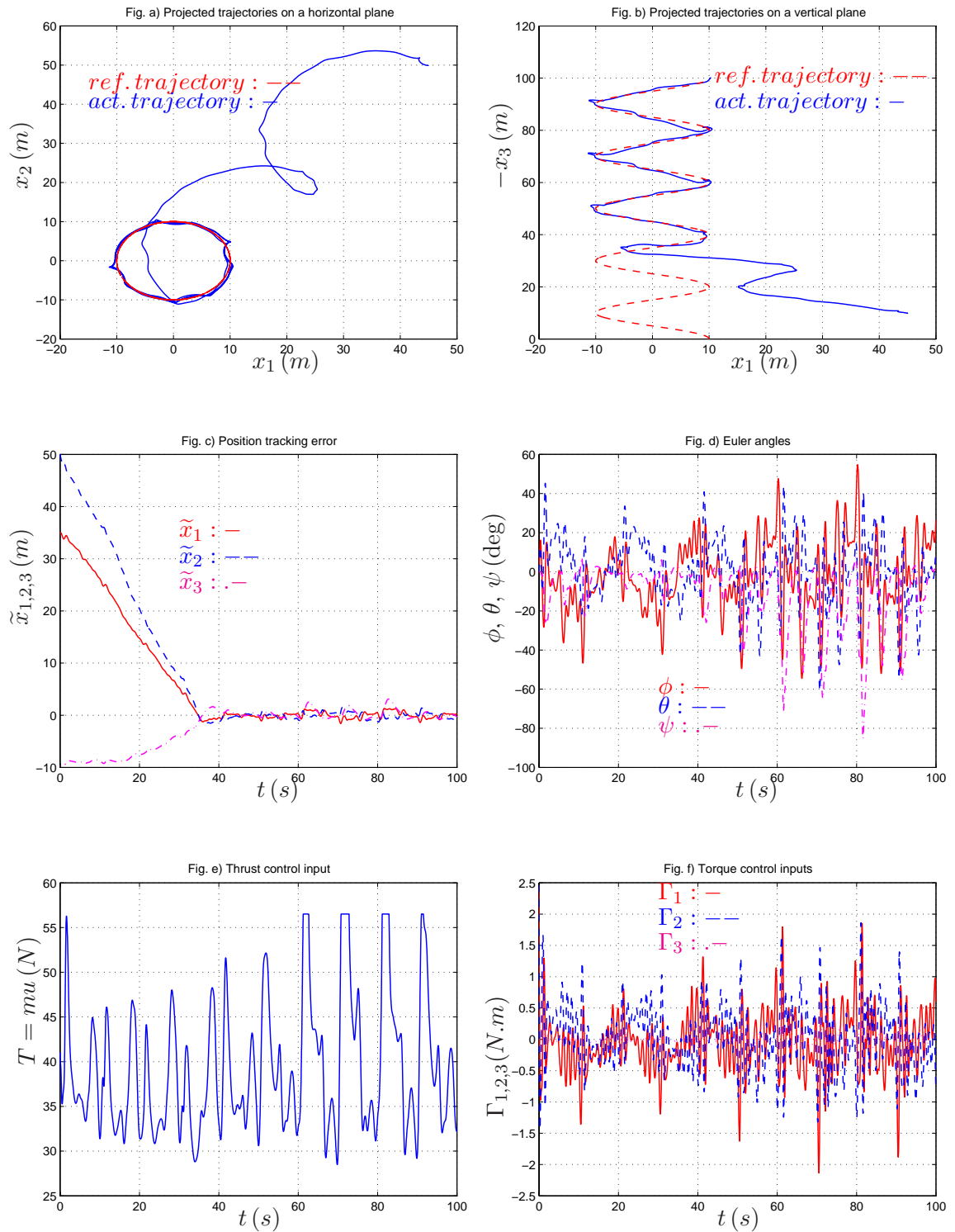
Figure 2.7: Ascending reference spiral and vehicle's trajectory in the presence of strong variable wind and large initial position errors. Control with integral correction, $\eta = 4$, $\Delta = 1$, and on-line estimation of γ_e.

2.6.2   Simulation with the HoverEye simulator

As part of the ANR collaborative project SCUAV, Bertin Technologies has placed its simulator of the ducted fan tailsitter HoverEye at our disposal for testing the performance and robustness of the proposed control laws. The following parts of the simulator make it more representative with respect to a real physical system.

- A model of aerodynamic forces and moments, acting on the ducted structure, has been obtained through intense wind tunnel tests. These aerodynamics effects have been tabulated as functions of the relative wind velocity, angle of attack, and sideslip angle. Models of the thrust of the propellers and of the forces and moments generated by the system of flaps, obtained through wind tunnel tests, are also included in the simulator.

- The dynamics of the engine and servo controllers are modeled.

- Models of wind gusts and of interaction effects when the vehicle touches the ground are included in the dynamical model of the vehicle. This can be useful to test the robustness of the proposed control laws in take-off flight.

The vehicle is initially on the ground at the position $x(0) = 0$ and its initial attitude is I_3. The control objective is to track the following reference trajectory

$$x_r(t) = \begin{cases} [0, 0, -20]^\top, & \text{if } t \leq 20 \\ [10\cos(\pi(t-20)/10),\, 10\sin(\pi(t-20)/10),\, -(t-20) - 20]^\top, & \text{otherwise.} \end{cases}$$

The position tracking controller, together with the observer of the apparent acceleration γ_e, used for Simulation 2 in the previous subsection is applied. To test the robustness of the proposed controllers with respect to static modeling errors, 10% errors in the vehicle's mass and inertia matrix are introduced. We also want to illustrate through simulation that our control approach provides good robustness with respect to errors on attitude estimation. To this end the true attitude is corrupted by bias, such that in terms of Euler angles $\{\phi, \theta, \psi\}$ it is given by $\{5, 5, 10\}$ (deg), to obtain the estimated attitude. Two simulations are reported.

▷ **Simulation 1 – No wind.**

In the absence of wind, simulation results are shown in Figs. 2.8 and 2.9. The vehicle achieved take-off flight. From 10 to 20 (s) the yaw angle ψ converges to -10 (deg) (instead of 0 (deg)) due to the yaw estimation error (see Fig. 2.9.d). However, good position tracking performance is obtained despite important errors in the estimation of the vehicle's attitude and physical parameters.

▷ **Simulation 2 – With strong variable wind.**

In this simulation, we would like to further test the robustness of the proposed controller with respect to aerodynamic perturbations. To this purpose a strong variable wind, shown in Fig. 2.10, is simulated. The simulation proceeds like the previous one, and simulation results are reported in Figs. 2.11 and 2.12. The vehicle achieved take-off flight. Good tracking performance and robustness are obtained despite strong wind-induced perturbations and important errors in the estimation of the vehicle's attitude and physical parameters.
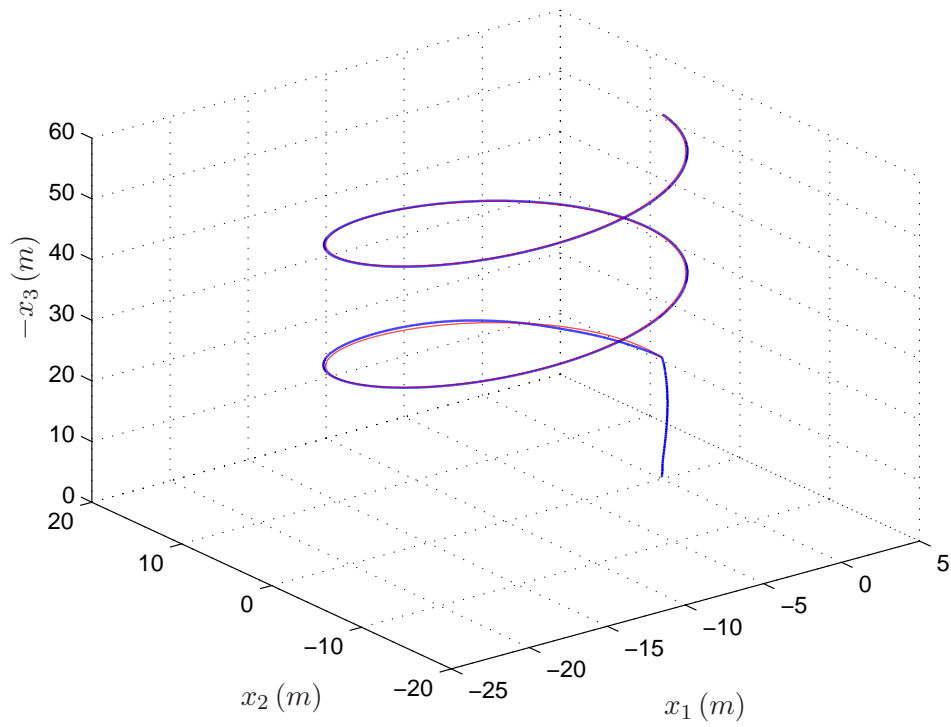
Figure 2.8: Reference and actual trajectories of the HoverEye in the absence of wind.

Figure 2.9: Simulation results with the HoverEye simulator. Take-off flight. Ascending reference spiral and vehicle's trajectory in the absence of wind.

Figure 2.10: Wind velocities vs. time.
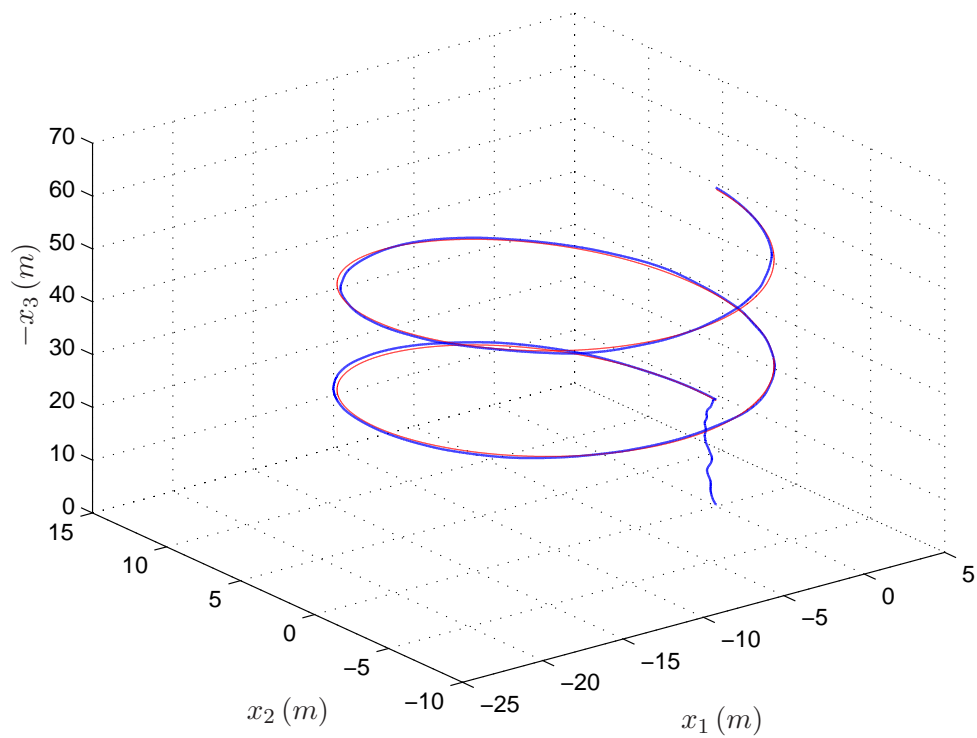
Figure 2.11: Reference and actual trajectories of the HoverEye in the presence of strong variable wind.

Figure 2.12: Simulation results with the HoverEye simulator. Take-off flight. Ascending reference spiral and vehicle's trajectory in the presence of strong variable wind.

2.6.3   Simulation with a model of a reduced scale helicopter

In this section simulations are carried out for a helicopter model given in Section 1.4.1. The helicopter's equations of motion are given by Eq. (1.2), where $F_{\mathcal{B}}$ and $\Gamma_{\mathcal{B}}$ are defined by Eq. (1.3), and

- T_M, T_T, a, b are the available control inputs,

- $F_{ae}^{\mathcal{B}}$ and $\Gamma_{ae}^{\mathcal{B}}$ are given by Eq. (1.4),

- Q_M and Q_T are modeled as in (Koo and Sastry, 1998), $i.e.$ $Q_i = C_i^Q T_i^{1.5} + D_i^Q$, for $i = M, T$, with C_i^Q, D_i^Q some parametric constants,

- $\dfrac{\partial R_M}{\partial b} = \dfrac{\partial M_M}{\partial a} = c_M T_M.$

The physical and aerodynamic parameters of the helicopter are given in Tab. 2.1.

$m = 4.9\,(\mathrm{kg})$, $J = \mathbf{diag}(0.1424, 0.2712, 0.2715)\,(\mathrm{kg\,m^2})$
$(l_M,\, y_M,\, h_M,\, l_T,\, y_T,\, h_T) = (-0.015,\, 0,\, -0.2943,\, -0.8715,\, 0,\, -0.1154)\,(\mathrm{m})$
$C_M^Q = 0.004452$, $D_M^Q = 0.6304$, $C_T^Q = 0.005066$, $D_T^Q = 0.008488$, $c_M = 0.5254$
$k_1^f = 0.055$, $k_2^f = 0.11$, $k_3^f = 0.083$, $k_2^a = 0.066$, $k_3^a = 0.055$
$\rho = 1.25\,(\mathrm{kg\,m^{-3}})$, $A_{disk} = 1.767\,(\mathrm{m^2})$

Table 2.1: Parameters of a single rotor helicopter.

To test the robustness of the proposed controllers with respect to static errors, we multiply the real parameters m, J, l_M, y_M, h_M, l_T, y_T, h_T by 0.8 to obtain the estimated parameters $\widehat{m}$, $\widehat{J}$, $\widehat{l}_M$, $\widehat{y}_M$, $\widehat{h}_M$, $\widehat{l}_T$, $\widehat{y}_T$, $\widehat{h}_T$. The position tracking control law used for Simulation 2 of Section 2.6.1 is applied to obtain the thrust force control T ($i.e.$ T_M) and the torque control Γ. Because Γ is not the true control variable, it needs to be converted into the true control variables T_T, a, and b. To avoid using models of Q_M, Q_T, $\partial R_M/\partial b$ and $\partial M_M/\partial a$, we simply set (see (1.6) in Section 1.4.1 for details)

$$\begin{bmatrix} (bT_M)_d \\ (aT_M)_d \\ T_T \end{bmatrix} = \widehat{A}^{-1}\Gamma\,, \tag{2.43}$$

with

$$\widehat{A} \triangleq \begin{bmatrix} -\widehat{h}_M & 0 & \widehat{h}_T \\ 0 & -\widehat{h}_M & 0 \\ \widehat{l}_M & \widehat{y}_M & -\widehat{l}_T \end{bmatrix}$$

In view of Eq. (2.43), if $T_M \neq 0$ the true control variables a and b can be obtained via

$$a = \frac{(aT_M)_d}{T_M}, \; b = \frac{(bT_M)_d}{T_M}. \tag{2.44}$$

However, if $T_M = 0$ they are no longer well-defined. To avoid this issue of singularities and also to take limitations of the actuators and the swashplate mechanism into account, the control variables T_M, T_T, a, and b are calculated as follows:

- T_M, T_T are saturated according to the following constraints

$$4.8 = 0.1\,mg \leq T_M \leq 69.48 = 1.4454\,mg,$$
$$-5.26 \leq T_T \leq 5.26.$$

- Then, a and b are calculated by (2.44) and saturated according to the following constraints

$$|a| \leq \frac{20\pi}{180}, \quad |b| \leq \frac{20\pi}{180}.$$

The control objective is to track the reference trajectory defined by Eq. (2.42), in the absence of wind. The vehicle initial position and attitude are given by $x(0) = [0, 0, -5]^\top\,(m)$ and $R(0) = \mathbf{diag}(1, -1, -1)$. Note that the vehicle's attitude makes a π-rotation with respect to that in the hovering flight.

Some simulation cases are reported.

- **Simulation 1 – No wind and without estimation of γ_e (*i.e.* $\widehat{\gamma}_e = ge_3$).** To test the robustness of the controller when neither measurement nor estimation of aerodynamic forces is available, the term $\widehat{\gamma}_e$ involved in the control expressions is set to $\widehat{\gamma}_e = ge_3$. Simulation results in the absence of wind are reported in Fig. 2.13.

- **Simulation 2 – No wind and with estimation of γ_e.** This simulation is similar to the previous one. The sole difference concerns the estimation of aerodynamic forces. The estimator of these effects is the one used for Simulation 2 of Section 2.6.1. Simulation results are reported in Fig. 2.14.

- **Simulation 3 – With wind gusts and without estimation of γ_e.** Strong variable wind gusts, as illustrated in Fig. 2.5, are introduced, and the estimate of γ_e is set to $\widehat{\gamma}_e = ge_3$. Simulation results are reported in Fig. 2.15.

In view of these simulations, one observes that incorporating an on-line estimation of aerodynamic forces allows to improve the tracking performance. However, by simply setting $\widehat{\gamma}_e = ge_3$ one also obtains rather good tracking performance and robustness towards uncertainties and unmodeled dynamics.
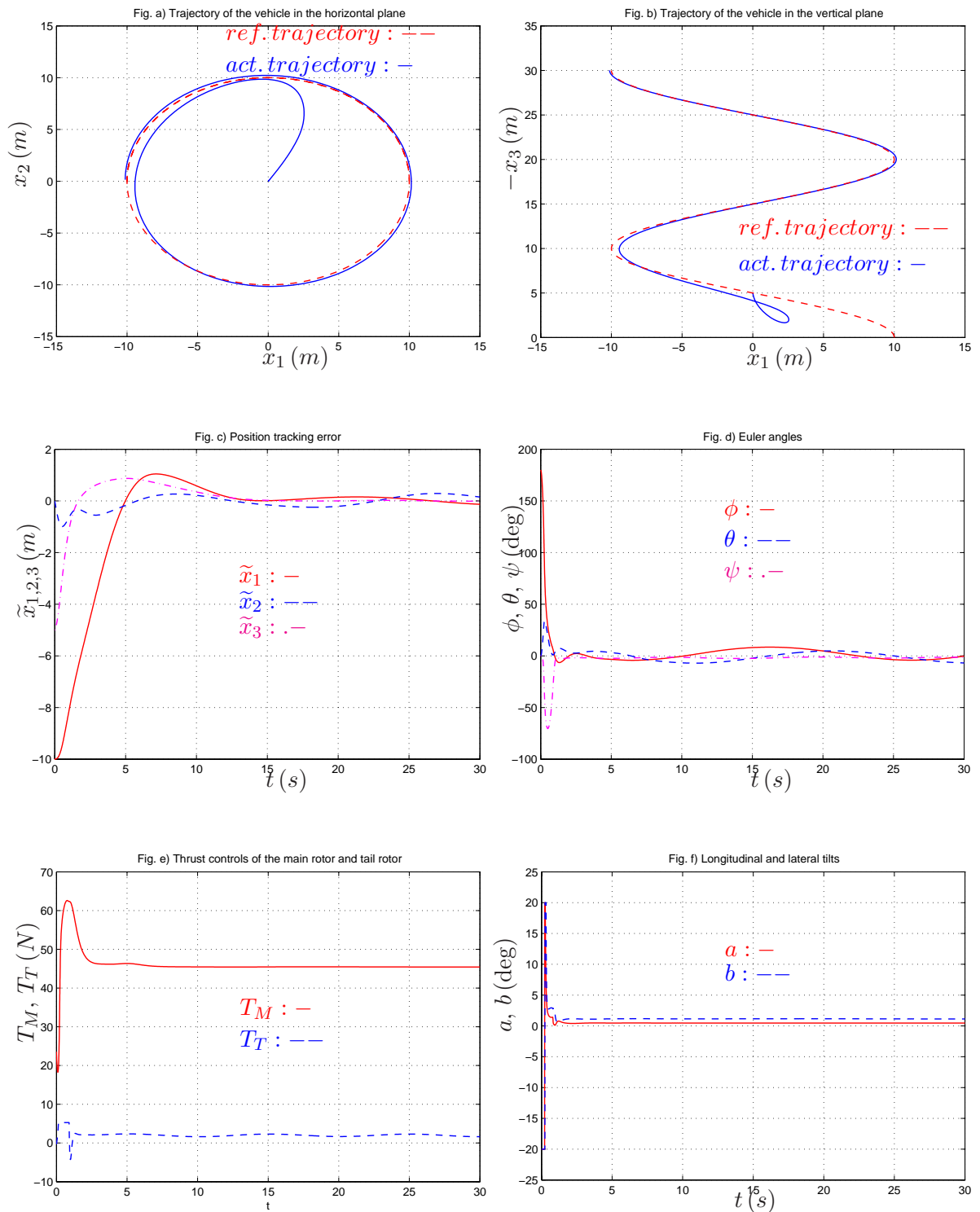
Figure 2.13: Simulation results with a helicopter model. Ascending reference spiral and vehicle's trajectory in the absence of wind. No estimation of aerodynamic forces.
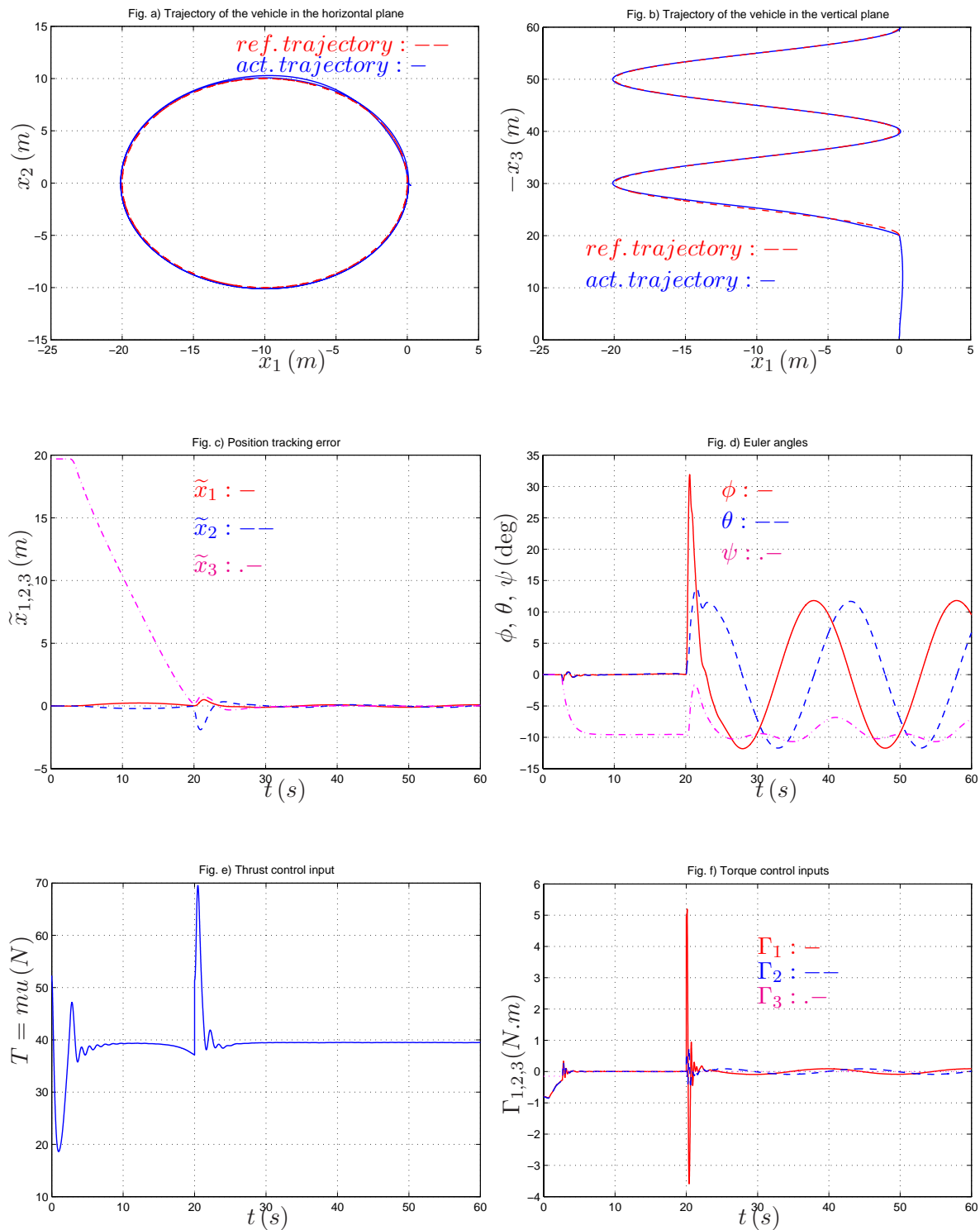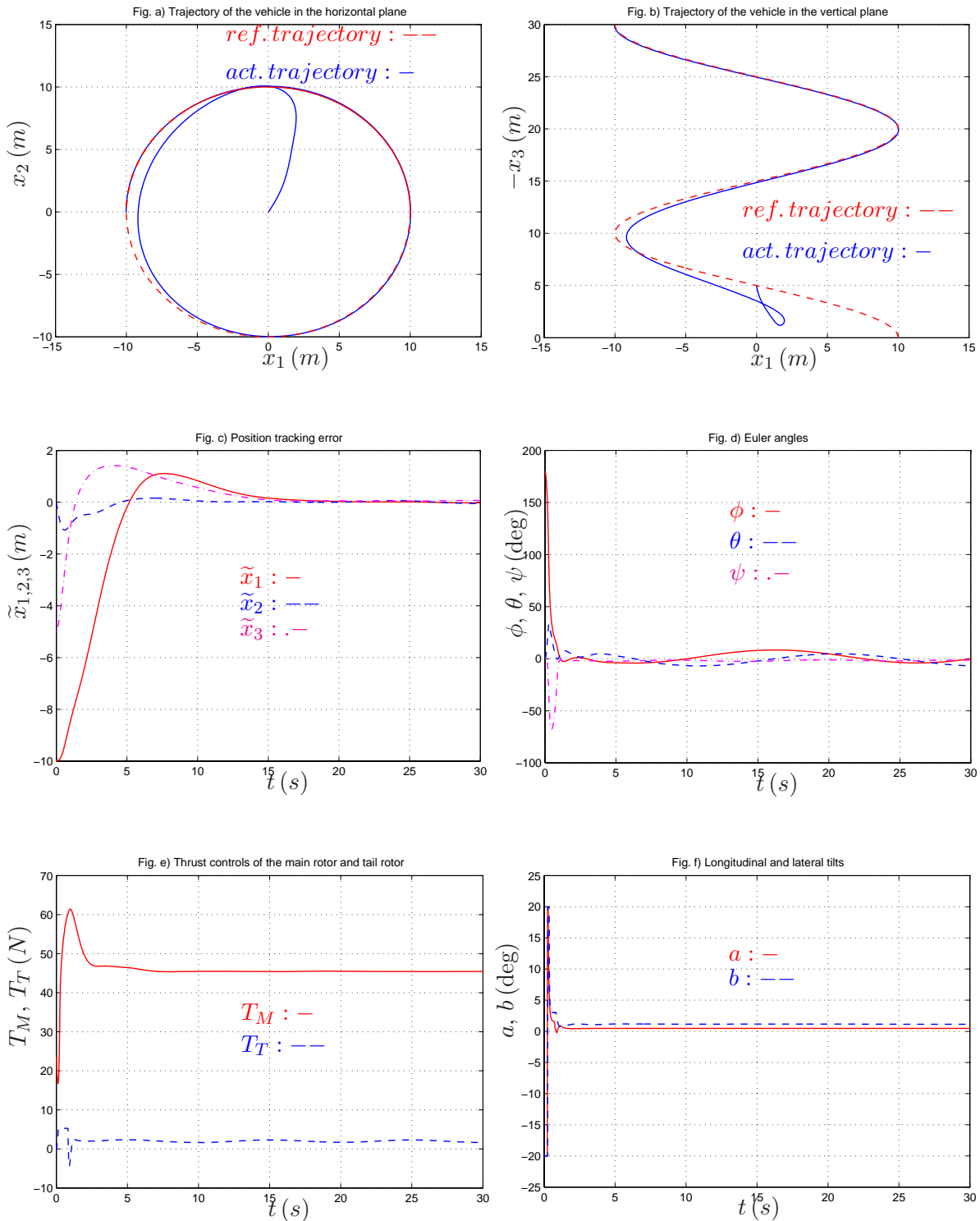
Figure 2.14: Simulation results with a helicopter model. Ascending reference spiral and vehicle's trajectory in the absence of wind. With estimation of aerodynamic forces.
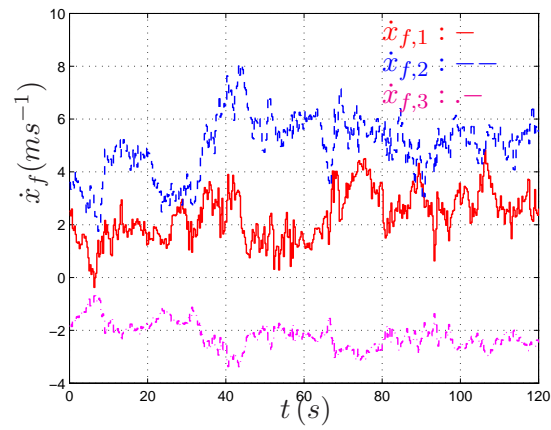
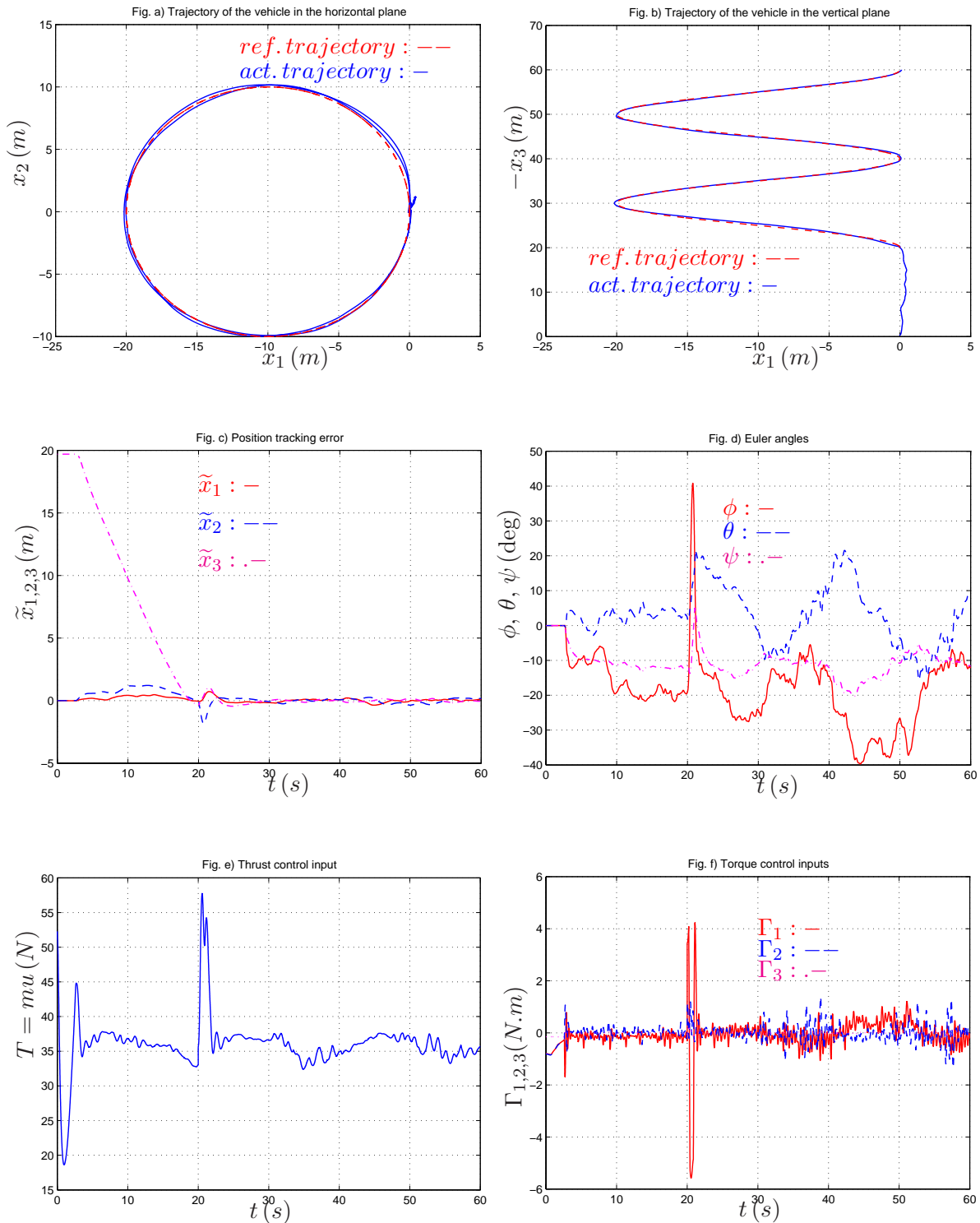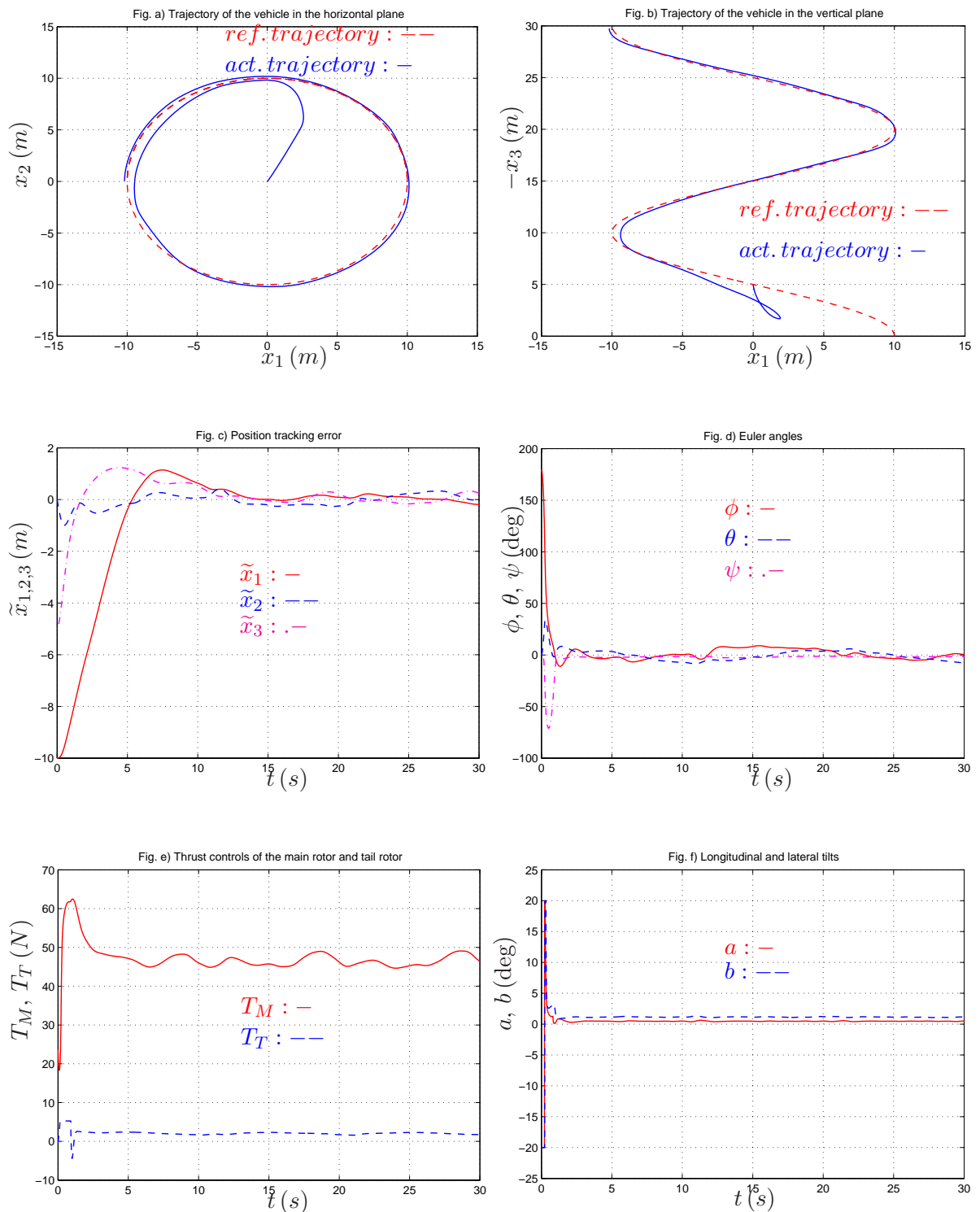Figure 2.15: Simulation results with a helicopter model. Ascending reference spiral and vehicle's trajectory in the presence of strong variable wind. Without estimation of aerodynamic forces.

2.7   Control design for the 2D-plane case

In this section the control design for the 2D-plane case is directly derived from the proposed control approach for the 3D-space case presented previously. Quite naturally, this development consists in considering this case as a degenerate case of the 3D-space case.

2.7.1   Notation

The following notation is introduced for the 2D-plane case.
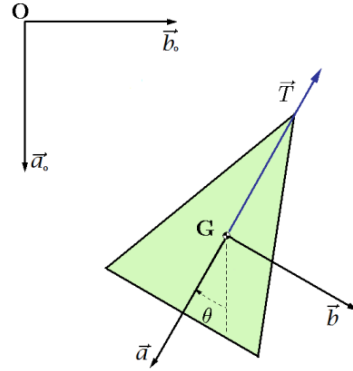
Figure 2.16: Inertial frame $\mathcal{F}_o$ and body frame $\mathcal{F}$ (the 2D-space case).

- G is the vehicle's center of mass, $m \in \mathbb{R}$ its mass, and $J \in \mathbb{R}$ its inertia.

- $\mathcal{F}_o = \{O; \overrightarrow{a}_o, \overrightarrow{b}_o\}$ is a fixed frame with respect to which the vehicle's absolute pose is measured.

- $\mathcal{F} = \{G; \overrightarrow{a}, \overrightarrow{b}\}$ is a frame attached to the body, with the vector $\overrightarrow{a}$ parallel to the thrust force axis as illustrated in Fig. 2.16.

- The vector of coordinates of G in the basis of the fixed frame $\mathcal{F}_o$ is denoted as $x = (x_1, x_2)^\top$. Therefore, $\overrightarrow{OG} = x_1 \overrightarrow{a}_o + x_2 \overrightarrow{b}_o$, i.e. $\overrightarrow{OG} = (\overrightarrow{a}_o, \overrightarrow{b}_o)x$.

- The vehicle's orientation is characterized by the oriented angle θ between $\overrightarrow{a}_o$ and $\overrightarrow{a}$. The rotation matrix associated with the angle θ is denoted as $R(\theta) \in \mathbb{R}^{2\times2}$, with

$$R(\theta) \triangleq \begin{bmatrix} \cos\theta & -\sin\theta \\ \sin\theta & \cos\theta \end{bmatrix}.$$

- The vector of coordinates associated with the linear velocity of G with respect to $\mathcal{F}_o$ is denoted as $\dot{x} = (\dot{x}_1, \dot{x}_2)^\top$ when expressed in the fixed frame $\mathcal{F}_o$, and as $v = (v_1, v_2)^\top$ when expressed in the basis of $\mathcal{F}$, i.e. $\overrightarrow{v} = \frac{d}{dt}\overrightarrow{OG} = (\overrightarrow{a}_o, \overrightarrow{b}_o)\dot{x} = (\overrightarrow{a}, \overrightarrow{b})v$.

- The angular velocity vector of the body frame $\mathcal{F}$ relative to the fixed frame $\mathcal{F}_o$, expressed in the body frame $\mathcal{F}$, is denoted as $\omega \in \mathbb{R}$.

2.7.2   System modeling

The system modeling for the 2D-plane case proceeds analogously to Section 2.3. The thrust force $\overrightarrow{T}$ is assumed to be $\overrightarrow{T} = -T\overrightarrow{a}$. Alike the 3D-space case, the mathematical model of the 2D-plane case, derived from the Newton-Euler formalism, is given by

$$\begin{cases} \Sigma_1^{2d} : & \begin{bmatrix} \dot{x} \\ m\dot{v} \\ \dot{\theta} \end{bmatrix} = \begin{bmatrix} R(\theta)v \\ -m\omega S_2 v - Ti_1 + R(\theta)^\top F_e(\dot{x}, \ddot{x}, \theta, \omega, \dot{\omega}, t) \\ \omega \end{bmatrix} \\ \Sigma_2^{2d} : & J\dot{\omega} \;=\; \Gamma + \Gamma_e(\dot{x}, \ddot{x}, \theta, \omega, \dot{\omega}, t) \end{cases} \tag{2.45}$$

with Γ the scalar torque input, $F_e \in \mathbb{R}^2$ the vector of coordinates of $\overrightarrow{F}_e$ expressed in the inertial frame $\mathcal{F}_o$, Γ_e the external scalar torque induced by $\overrightarrow{F}_e$, $i_1 \triangleq [0, 1]^\top$, and $S_2 \triangleq \begin{bmatrix} 0 & -1 \\ 1 & 0 \end{bmatrix}$.

Now, Assumptions 1–4 are introduced with $\dot{x}$, $\dot{x}_r$, F_e defined in $\mathbb{R}^2$. From here, the subsystem Σ_1^{2d} of System (2.45) can be simplified as follows

$$\begin{cases} \dot{x} &=& R(\theta)v \\ \dot{v} &=& -\omega S_2 v - ui_1 + R(\theta)^\top \gamma_e(\dot{x}, t) \\ \dot{\theta} &=& \omega \end{cases} \tag{2.46}$$

with $\gamma_e(\dot{x}, t) \triangleq F_e(\dot{x}, t)/m$ called the "apparent acceleration", and $u \triangleq T/m$ the new control input. Note that Assumptions 1–3 are still satisfied when F_e is replaced by γ_e and each c_i is replaced by c_i/m.

Alike the 3D-space case, we focus our control design studies on System (2.46) with u and ω used hereafter as the control inputs, and we assume also that the apparent acceleration γ_e and its time-derivative are available for control design. Note that γ_e and $\dot{\gamma}_e$ can be estimated using the estimation solution proposed in Section 2.5 modulo straightforward modifications. More precisely, one must only replace System (2.31) by

$$\ddot{x} = -uR(\theta)i_1 + \gamma_e,$$

and state the uniform boundedness results as in Lemma 3. The results of Proposition 8 still hold with the observer of γ_e (assuming that u, $\dot{x}$, θ are measured) given by

$$\begin{cases} \dfrac{d}{dt}\widehat{\dot{x}} = -uR(\theta)i_1 + \widehat{\gamma}_e + k_o(\dot{x} - \widehat{\dot{x}}) \\ \dot{\widehat{\gamma}}_e = a^2 k_o^2 (\dot{x} - \widehat{\dot{x}}) \end{cases} \tag{2.47}$$

with $\widehat{\dot{x}}$ an estimate of $\dot{x}$, $\widehat{\gamma}_e$ the estimate of γ_e, and a, k_o some positive gains.

2.7.3   Control design

To gain control insight one may view a vehicle moving on a plane with two control inputs (one force and one torque) as a degenerate case of the 3D-space case where the vehicle moves on a plane with two control inputs and two other torque control inputs are

desactivated. For instance, consider *the 3D-space case* where the vehicle is constrained to moving on the plane $\{O; \overrightarrow{k}_o, \overrightarrow{\imath}_o\}$. In this case, one has

$$v_2 \equiv \omega_1 \equiv \omega_3 \equiv \gamma_{e,2} \equiv 0,$$

$$R = \begin{bmatrix} \cos\theta & 0 & -\sin\theta \\ 0 & 1 & 0 \\ \sin\theta & 0 & \cos\theta \end{bmatrix},$$

with θ the angle between $\overrightarrow{k}$ and $\overrightarrow{k}_o$. Then the control law, *e.g.*, proposed in Proposition 2 (*i.e.* the control expression (2.11)) can be simplified as follows

$$\begin{cases} u &= \overline{\gamma}_3 + |\gamma|k_1\widetilde{v}_3 \\ \omega_2 &= |\gamma|k_2\widetilde{v}_1 + \dfrac{k_3|\gamma|\overline{\gamma}_1}{(|\gamma| + \overline{\gamma}_3)^2} - \dfrac{\gamma_{3,1}^\top S_2\dot{\gamma}_{3,1}}{|\gamma|^2} \end{cases}$$

with $\gamma_{3,1} \triangleq (\gamma_3, \gamma_1)^\top$. Therefore, in *the 2D-plane case* by choosing the inertial frame $\mathcal{F}_o = \{O; \overrightarrow{a}_o, \overrightarrow{b}_o\} \equiv \{O; \overrightarrow{k}_o, \overrightarrow{\imath}_o\}$ one may hope that the following control law (note that here $\gamma \in \mathbb{R}^2$)

$$\begin{cases} u = \overline{\gamma}_1 + |\gamma|k_1\widetilde{v}_1 \\ \omega = |\gamma|k_2\widetilde{v}_2 + \dfrac{k_3|\gamma|\overline{\gamma}_2}{(|\gamma| + \overline{\gamma}_1)^2} - \dfrac{\gamma^\top S_2\dot{\gamma}}{|\gamma|^2} \end{cases} \tag{2.48}$$

provides the same asymptotic stability result as Proposition 2. In what follows we rigorously prove that this intuition is correct.

In this section the basics control laws developed in Section 2.4.1 for the 3D-space case will be used with adaptations for the 2D-plane case. The process of robustification given in Section 2.4.2 can be directly applied, and therefore is omitted in this section. We consider now the following control objectives: *i)* thrust direction control, *ii)* velocity control, *iii)* position control, and *iv)* the extension of these control laws by taking into account the unilaterality of the thrust direction. The control design for the 2D-plane case relies in the first place on the following lemma (see Section 2.8.15 for the proof) which is reminiscent of Lemma 1.

Lemma 5 *Let $\overline{\gamma} \triangleq R(\theta)^\top \gamma$, with $\gamma \in \mathbb{R}^2$ a non-zero time-dependent vector and θ the solution to the equation $\dot{\theta} = \omega$. Then*

$$\frac{d}{dt}\left(\frac{\overline{\gamma}}{|\gamma|}\right) = -\frac{S_2\overline{\gamma}}{|\gamma|}\left(\omega + \frac{\gamma^\top S_2\dot{\gamma}}{|\gamma|^2}\right),$$

$$\frac{d}{dt}\left(1 - \frac{\overline{\gamma}_1}{|\gamma|}\right) = -\frac{\overline{\gamma}_2}{|\gamma|}\left(\omega + \frac{\gamma^\top S_2\dot{\gamma}}{|\gamma|^2}\right).$$

▷ **Thrust direction control**

The objective is to stabilize the vehicle's thrust direction $\overrightarrow{a}$ about a desired thrust direction $\overrightarrow{\gamma}$. In practice this desired direction may be specified by a manual joystick. Let $\gamma \in \mathbb{R}^2$ denote the normalized vector ($|\gamma| = 1$) of coordinates of $\overrightarrow{\gamma}$, expressed in the

inertial frame $\mathcal{F}_l$. Then, the control objective is equivalent to stabilizing $R(\theta)^\top \gamma$ about i_1. Define

$$\overline{\gamma} \triangleq R(\theta)^\top \gamma, \tag{2.49}$$

and let $\widetilde{\theta} \in (-\pi; \pi]$ denote the angle between the two unit vectors i_1 and $\overline{\gamma}$, so that $\cos \widetilde{\theta} = \overline{\gamma}_1$, the first component of $\overline{\gamma}$. More precisely, $\widetilde{\theta}$ is defined by $\widetilde{\theta} \triangleq \mathrm{atan2}(-\overline{\gamma}_2, \overline{\gamma}_1)$. The control objective is also equivalent to the asymptotic stabilization of $\widetilde{\theta} = 0$. The control result is stated next.

Proposition 9 *Let k denote a positive constant, and apply the control law*

$$\omega = \frac{k\overline{\gamma}_2}{(1 + \overline{\gamma}_1)^2} - \gamma^\top S_2 \dot{\gamma} \tag{2.50}$$

to the system $\dot{\theta} = \omega$. Then the equilibrium point $\widetilde{\theta} = 0$ of the controlled system is exponentially stable with domain of attraction equal to $(-\pi, \pi)$.

The proof is given in Section 2.8.16.

▷ **Velocity control**

Let $\dot{x}_r$ denote the reference velocity expressed in the inertial frame $\mathcal{F}_o$, $\ddot{x}_r$ its time-derivative, and $\widetilde{v} \triangleq R(\theta)^\top (\dot{x} - \dot{x}_r)$ the velocity error expressed in the body frame $\mathcal{F}$. The problem of asymptotic stabilization of the linear velocity error $\dot{x} - \dot{x}_r$ to zero is equivalent to the asymptotic stabilization of $\widetilde{v}$ to zero. Using System (2.46), one obtains the error system

$$\dot{\widetilde{x}} = R(\theta)\widetilde{v} \tag{2.51a}$$

$$\dot{\widetilde{v}} = -\omega S_2 \widetilde{v} - u i_1 + R(\theta)^\top (\gamma_e(\dot{x}, t) - \ddot{x}_r(t)) \tag{2.51b}$$

$$\dot{\theta} = \omega \tag{2.51c}$$

with either $\widetilde{x} \triangleq \int_0^t (\dot{x}(s) - \dot{x}_r(s))\, ds$, the integral of the velocity error, or $\widetilde{x} \triangleq x - x_r$, the position tracking error when a reference trajectory x_r is specified.

Let $\widehat{\gamma}_e$ denote the measure or estimate of γ_e and define now γ as follows (instead of defining γ as a reference unit vector like previously)

$$\gamma \triangleq \widehat{\gamma}_e - \ddot{x}_r(t) + h(|I_v|^2)I_v, \tag{2.52}$$

where h is a smooth bounded positive function satisfying Properties (2.13) and Eq. (2.14) for some positive constants η, β, and $I_v \in \mathbb{R}^2$ is defined by Eq. (2.12). From here the control results stated next asymptotically stabilize $\widetilde{v}$ to zero.

Proposition 10 *Apply the control law (2.48) to System (2.51), with k_1, k_2, k_3 some positive constants, and γ defined by Eq. (2.52). Suppose that*

i) Assumptions 1, 4, and 5, with γ given by Eq. (2.52), are satisfied;

ii) the measurement (or estimation) error $c \triangleq \gamma_e - \widehat{\gamma}_e$ is constant;

iii) $\lim\limits_{s \to +\infty} h(s^2)s > |c|$.

Then, for System (2.51b)–(2.51c) complemented with the equation $\dot{I}_v = R(\theta)\widetilde{v}$, there exists a constant vector $I_v^* \in \mathbb{R}^2$ such that equilibrium point $(I_v, \widetilde{v}, \widetilde{\theta}) = (I_v^*, 0, 0)$ of the controlled system is asymptotically stable, with domain of attraction equal to $\mathbb{R}^2 \times \mathbb{R}^2 \times (-\pi, \pi)$.

The proof is given in Section 2.8.17. Now to further comply with the constraint of positivity of the thrust control u (*i.e.* T) one can apply the following controller.

Proposition 11 *Let k_1, k_2, k_3 denote some positive constants, and γ as defined by Eq. (2.52). Let $\sigma : \mathbb{R} \to \mathbb{R}$ denote a strictly increasing smooth function such that $\sigma(0) = 0$ and $\sigma(s) > -1/k_1$, $\forall s \in \mathbb{R}$. Apply the control law*

$$\begin{cases} u = |\gamma| + |\gamma| k_1 \sigma(\widetilde{v}_1) \quad (> 0) \\ \omega = |\gamma| k_2 \left(\widetilde{v}_2 - \dfrac{\widetilde{v}_1 \overline{\gamma}_2}{|\gamma| + \overline{\gamma}_1} \right) + \dfrac{k_3 |\gamma| \overline{\gamma}_2}{(|\gamma| + \overline{\gamma}_1)^2} - \dfrac{\gamma^\top S_2 \dot{\gamma}}{|\gamma|^2} \end{cases} \quad (2.53)$$

to System (2.51). Suppose that Assumptions i)–iii) of Proposition 10 are satisfied. Then the asymptotic stability result of Proposition 10 still holds.

The proof, similar to the proof of Proposition 10, is given in Section 2.8.18.

▷ Position control with unidirectional thrust

The control objective is the combined stabilization of the velocity error $\widetilde{v}$ (or $\dot{x} - \dot{x}_r$) and the position error $\widetilde{x} = x - x_r$ to zero. Similar to the design of the position control of the 3D-space case, the nonlinear integrator bounding technique proposed in Proposition 4 (*i.e.* System (2.16)) and the control structure proposed in Propositions 4 and 6 are reused. The control result, whose proof is given in Section 2.8.19, is stated next.

Proposition 12 *Let k_1, k_2, k_3 denote some positive constants. Let $\sigma : \mathbb{R} \to \mathbb{R}$ denote a strictly increasing smooth function such that $\sigma(0) = 0$ and $\sigma(s) > -1/k_1$, $\forall s \in \mathbb{R}$. Apply the following control law*

$$\begin{cases} u = |\gamma| + |\gamma| k_1 \sigma(\overline{v}_1) \quad (> 0) \\ \omega = |\gamma| k_2 \left(\overline{v}_2 - \dfrac{\overline{v}_1 \overline{\gamma}_2}{|\gamma| + \overline{\gamma}_1} \right) + \dfrac{k_3 |\gamma| \overline{\gamma}_2}{(|\gamma| + \overline{\gamma}_1)^2} - \dfrac{\gamma^\top S_2 \dot{\gamma}}{|\gamma|^2} \end{cases} \quad (2.54)$$

to System (2.51) where $\overline{v}$, γ, and y (which intervenes in the definition of γ) are defined by Eqs. (2.19), (2.20), and (2.18) respectively, and z (which also intervenes in the definition of γ) is the solution to System (2.16). Suppose that

i) Assumptions 1, 4, and 5, with γ given by Eq. (2.20), are satisfied;

ii) the measurement (or estimation) error $c \triangleq \gamma_e - \widehat{\gamma}_e$ is constant;

iii) $\lim\limits_{s \to +\infty} h(s^2)s > |c|$;

iv) $\Delta > |z^*|$, where z^* denote the unique solution to the equation $h(|z^*|^2)z^* = c$ and Δ is the positive constant intervening in the function sat_Δ (which involves in System (2.16)).

Then, for System (2.51) complemented with System (2.16), the equilibrium point $(z, \dot{z}, \widetilde{x}, \widetilde{v}, \widetilde{\theta}) = (z^*, 0, 0, 0, 0)$ of the controlled system is asymptotically stable, with domain of attraction equal to $\mathbb{R}^2 \times \mathbb{R}^2 \times \mathbb{R}^2 \times \mathbb{R}^2 \times (-\pi, \pi)$.

2.8 Analyses for Chapter 2

2.8.1 Recalls on Barbalat's lemma

Lemma 6 *(Barbalat, see e.g. (Micaelli and Samson, 1993)) Let $x(t)$ denote a solution to the differential equation $\dot{x} = a(t) + b(t)$ with $a(t)$ a uniformly continuous function. Assume that $\lim_{t \to +\infty} x(t) = c$ and $\lim_{t \to +\infty} b(t) = 0$, with c a constant value. Then, $\lim_{t \to +\infty} \dot{x}(t) = 0$.*

The case $b = 0$ corresponds to the classical version of Barbalat's lemma (see *e.g.* (Khalil, 2002)).

2.8.2 Proof of Lemma 1

One verifies that

$$\frac{d}{dt}\left(\frac{\gamma}{|\gamma|}\right) = \frac{(|\gamma|^2 I_3 - \gamma\gamma^\top)\dot{\gamma}}{|\gamma|^3} = -\frac{S(\gamma)^2\dot{\gamma}}{|\gamma|^3}.$$

Thus,

$$R^\top \frac{d}{dt}\left(\frac{\gamma}{|\gamma|}\right) = -\frac{1}{|\gamma|^3} R^\top S(\gamma)^2 \dot{\gamma} = -\frac{1}{|\gamma|^3} S(\overline{\gamma}) R^\top S(\gamma)\dot{\gamma}.$$

Using this relation and noting that $\overline{\gamma}/|\gamma| = R^\top \gamma/|\gamma|$ one gets

$$\begin{aligned}
\frac{d}{dt}\left(\frac{\overline{\gamma}}{|\gamma|}\right) &= -S(\omega)R^\top \frac{\gamma}{|\gamma|} + R^\top \frac{d}{dt}\left(\frac{\gamma}{|\gamma|}\right) \\
&= -S(\omega)\frac{\overline{\gamma}}{|\gamma|} + R^\top \frac{d}{dt}\left(\frac{\gamma}{|\gamma|}\right) \\
&= \frac{1}{|\gamma|}S(\overline{\gamma})\omega + R^\top \frac{d}{dt}\left(\frac{\gamma}{|\gamma|}\right) \\
&= \frac{1}{|\gamma|}S(\overline{\gamma})\left(\omega - \frac{1}{|\gamma|^2}R^\top S(\gamma)\dot{\gamma}\right).
\end{aligned}$$

Then, this result is used to obtain

$$\begin{aligned}
\frac{d}{dt}\left(1 - \frac{\overline{\gamma}_3}{|\gamma|}\right) &= -\frac{1}{|\gamma|}e_3^\top S(\overline{\gamma})\left(\omega - \frac{1}{|\gamma|^2}R^\top S(\gamma)\dot{\gamma}\right) \\
&= -\frac{1}{|\gamma|}\begin{bmatrix} -\overline{\gamma}_2 & \overline{\gamma}_1 & 0 \end{bmatrix}\left(\omega - \frac{1}{|\gamma|^2}S(\overline{\gamma})R^\top\dot{\gamma}\right) \\
&= \frac{1}{|\gamma|}\overline{\gamma}_{1,2}^\top\begin{bmatrix} -\omega_2 \\ \omega_1 \end{bmatrix} + \frac{1}{|\gamma|^3}\overline{\gamma}_{1,2}^\top\begin{bmatrix} -\gamma^\top S(Re_2)\dot{\gamma} \\ \gamma^\top S(Re_1)\dot{\gamma} \end{bmatrix}.
\end{aligned}$$

2.8.3 Proof of Proposition 1

Consider the following candidate Lyapunov function

$$V \triangleq 1 - \overline{\gamma}_3 = 1 - \cos\widetilde{\theta}.$$

Differentiating V along the solutions of the system $\dot{R} = RS(\omega)$ and using Lemma 1 with $|\gamma| = 1$ one has

$$\dot{V} = \overline{\gamma}_{1,2}^\top \left(\begin{bmatrix} -\omega_2 \\ \omega_1 \end{bmatrix} + \begin{bmatrix} -\gamma^\top S(Re_2)\dot{\gamma} \\ \gamma^\top S(Re_1)\dot{\gamma} \end{bmatrix} \right),$$

with $\overline{\gamma}_{1,2} \triangleq (\overline{\gamma}_1, \overline{\gamma}_2)^\top$. Using expressions (2.7) of ω_1, ω_2 one gets

$$\dot{V} = -k\frac{|\overline{\gamma}_{1,2}|^2}{(1 + \overline{\gamma}_3)^2} = -k\frac{1 - \overline{\gamma}_3}{1 + \overline{\gamma}_3} = -\frac{kV}{1 + \overline{\gamma}_3} \le -\frac{kV}{2} \le 0.$$

This relation points out that V converges exponentially to zero. This in turn implies the exponential convergence of $\widetilde{\theta}$ to zero. The stability of the equilibrium $\widetilde{\theta} = 0$ is a direct consequence of the definition of V, the decrease of V along the system's solutions, and the fact that this point is the unique minimum of V.

2.8.4 Proof of Proposition 2

It follows from the definition of $\widetilde{\theta}$ that

$$\tan^2(\widetilde{\theta}/2) = \frac{|\overline{\gamma}_{1,2}|^2}{(|\gamma| + \overline{\gamma}_3)^2} = \frac{|\gamma| - \overline{\gamma}_3}{|\gamma| + \overline{\gamma}_3}. \tag{2.55}$$

Consider the candidate Lyapunov function V defined by

$$V \triangleq \frac{1}{2}|\widetilde{v}|^2 + \frac{1}{k_2}\left(1 - \frac{\overline{\gamma}_3}{|\gamma|}\right) = \frac{1}{2}|\widetilde{v}|^2 + \frac{1}{k_2}(1 - \cos\widetilde{\theta}). \tag{2.56}$$

Differentiating V along the solutions of System (2.8b)–(2.8c) and using Lemma 1 one gets

$$\dot{V} = \widetilde{v}^\top(-ue_3 + \overline{\gamma}) + \frac{1}{|\gamma|k_2}\overline{\gamma}_{1,2}^\top \left(\begin{bmatrix} -\omega_2 \\ \omega_1 \end{bmatrix} + \frac{1}{|\gamma|^2}\begin{bmatrix} -\gamma^\top S(Re_2)\dot{\gamma} \\ \gamma^\top S(Re_1)\dot{\gamma} \end{bmatrix} \right)$$

$$= \widetilde{v}_3(-u + \overline{\gamma}_3) + \frac{1}{|\gamma|k_2}\overline{\gamma}_{1,2}^\top \left(\begin{bmatrix} -\omega_2 \\ \omega_1 \end{bmatrix} + \frac{1}{|\gamma|^2}\begin{bmatrix} -\gamma^\top S(Re_2)\dot{\gamma} \\ \gamma^\top S(Re_1)\dot{\gamma} \end{bmatrix} + |\gamma|k_2\widetilde{v}_{1,2} \right),$$

with $\widetilde{v}_{1,2} \triangleq (\widetilde{v}_1, \widetilde{v}_2)^\top$ and $\overline{\gamma}_{1,2} \triangleq (\overline{\gamma}_1, \overline{\gamma}_2)^\top$. Substituting the expressions of u, ω_1, ω_2 in (2.11) and using Eq. (2.55) one obtains

$$\dot{V} = -|\gamma|k_1\widetilde{v}_3^2 - \frac{k_3}{k_2}\frac{|\overline{\gamma}_{1,2}|^2}{(|\gamma| + \overline{\gamma}_3)^2} = -|\gamma|k_1\widetilde{v}_3^2 - \frac{k_3}{k_2}\tan^2(\widetilde{\theta}/2). \tag{2.57}$$

Since $\dot{V}$ is negative semi-definite, the velocity error term $\widetilde{v}$ is bounded. The next step of the proof consists in showing that $\dot{V}$ is uniformly continuous along every system's solution in order to deduce, by application of Barbalat's lemma (*i.e.* Lemma 6), the convergence of $\widetilde{v}_3$ and $\widetilde{\theta}$ to zero [4]. To this purpose it suffices to show that $\ddot{V}$ is bounded. In view of Eq. (2.57), Assumption 5, and the boundedness of $\widetilde{v}$, this condition is satisfied if γ, $\dot{\gamma}$, $\dot{\widetilde{v}}_3$, and $d/dt\tan^2(\widetilde{\theta}/2)$ are bounded.

From Assumption 4, the boundedness of $\widetilde{v}$, and the relation $\widetilde{v} = R^\top(\dot{x} - \dot{x}_r)$, it follows that $\dot{x}$ is bounded. Therefore, using Assumptions 1 and 4 one deduces that γ_e, γ and $\overline{\gamma}$ are

---

4. Note that LaSalle's theorem does not apply since the closed-loop dynamics is not autonomous.

also bounded, and that u (given by (2.11)) is also well-defined and bounded. This implies that $\ddot{x}$ given by Eq. (2.31) is bounded. Since

$$\dot{\gamma}_e(\dot{x}, t) = \frac{\partial \gamma_e}{\partial \dot{x}}(\dot{x}, t)\ddot{x} + \frac{\partial \gamma_e}{\partial t}(\dot{x}, t),$$

it comes from Assumptions 1 and 4 and the fact that $\dot{x}$ and $\ddot{x}$ are bounded that $\dot{\gamma}_e$ and $\dot{\gamma}$ are also bounded. Let us now show that along each system's solution there exists $\varepsilon > 0$ such that

$$|\widetilde{\theta}(t)| \leq \pi - \varepsilon, \ \forall t. \tag{2.58}$$

It follows from Eqs. (2.11), (2.55), and Lemma 1 that

$$\frac{d}{dt}(1 - \cos\widetilde{\theta}) = -k_2(\overline{\gamma}_1\widetilde{v}_1 + \overline{\gamma}_2\widetilde{v}_2) - k_3\frac{|\gamma| - \overline{\gamma}_3}{|\gamma| + \overline{\gamma}_3} = -k_2(\overline{\gamma}_1\widetilde{v}_1 + \overline{\gamma}_2\widetilde{v}_2) - k_3\tan^2(\widetilde{\theta}/2).$$

Since $\overline{\gamma}$ and $\widetilde{v}$ are bounded, there exists $\varepsilon_1 > 0$ such that

$$|\widetilde{\theta}| > \pi - \varepsilon_1 \implies \frac{d}{dt}(1 - \cos\widetilde{\theta}) < 0.$$

Eq. (2.58) is thus satisfied with $\varepsilon = \min\{\varepsilon_1, \pi - |\widetilde{\theta}(0)|\}$ (> 0). This implies the boundedness of $\tan(\widetilde{\theta}/2)$ and also, from (2.55), of $1/(|\gamma| + \overline{\gamma}_3)$. Along with Assumption 5 and the fact that $\widetilde{v}$, γ, $\overline{\gamma}$, $\dot{\gamma}$ are bounded, this ensures that the control inputs ω_1 and ω_2, and thus ω, are well-defined and bounded. Since γ, $\widetilde{v}$, ω, u are bounded, it follows from Eq. (2.8b) that $\dot{\widetilde{v}}$ is also bounded. Finally, since both $\dot{\gamma}$ and ω are bounded, one deduces that $\dot{\overline{\gamma}}$ is bounded. The boundedness of $d/dt\tan^2(\widetilde{\theta}/2)$ then follows from Eq. (2.55) and from the boundedness of $1/(|\gamma| + \overline{\gamma}_3)$. This concludes the proof of uniform continuity of $\dot{V}$ and of the convergence of $\widetilde{v}_3$ and $\widetilde{\theta}$ to zero. Note from Eq. (2.55) that $\overline{\gamma}_1$ and $\overline{\gamma}_2$ also converge to zero.

It remains to show that $\widetilde{v}_1$ and $\widetilde{v}_2$ converge to zero. By a direct calculation, one deduces from Lemma 1 and the control law (2.11) that

$$\frac{d}{dt}\frac{\overline{\gamma}_{1,2}}{|\gamma|} = a(t) + b(t), \tag{2.59}$$

with

$$a(t) \triangleq -k_2\overline{\gamma}_3\widetilde{v}_{1,2} - k_3\overline{\gamma}_3\frac{\overline{\gamma}_{1,2}}{(|\gamma| + \overline{\gamma}_3)^2},$$

$$b(t) \triangleq \frac{1}{|\gamma|}\left(\omega_3 + \frac{1}{|\gamma|^2}\gamma^{\top}S(Re_3)\dot{\gamma}\right)\begin{bmatrix} \overline{\gamma}_2 \\ -\overline{\gamma}_1 \end{bmatrix}.$$

It is straightforward to verify that $\dot{a}(t)$ is bounded (so that $a(t)$ is uniformly continuous) by using the boundedness of $\dot{\widetilde{v}}$, $\overline{\gamma}$, $\dot{\overline{\gamma}}$, and $1/(|\gamma| + \overline{\gamma}_3)$). Since $b(t)$ is not necessarily uniformly continuous (because of the terms ω_3 and $\dot{\gamma}$), the classical version of Barbalat's lemma does not apply. This explains the use of the slightly generalized version given in Lemma 6 (see Section 2.8.1). Using the boundedness of ω_3, Assumption 5, and the properties obtained previously (i.e. convergence of $\overline{\gamma}_{1,2}$ to zero and boundedness of $\dot{\gamma}$) one verifies that $b(t)$ converges to zero. Direct application of Lemma 6 to System (2.59) ensures the convergence of $d/dt\,(\overline{\gamma}_{1,2}/|\gamma|)$ to zero. Since $\overline{\gamma}_{1,2}$ converges to zero and $|\gamma| + \overline{\gamma}_3 > 0$, the convergence of $\widetilde{v}_1, \widetilde{v}_2$ to zero follows. As for the stability of the equilibrium $(\widetilde{v}, \widetilde{\theta}) = (0, 0)$, it is a direct consequence of relations (2.56) and (2.57).

2.8.5   Proof of Proposition 3

From the definition of γ, given by Eq. (2.15), Eq. (2.8b) can be rewritten as

$$\dot{\widetilde{v}} = -S(\omega)\widetilde{v} - ue_3 + R^\top \gamma - R^\top h(|I_v|^2)I_v + R^\top c. \qquad (2.60)$$

Define the continuous function $f : s \longmapsto h(s^2)s$. From Property (2.14), f is strictly increasing. Young's inequality (see (Boas et al., 1974), (Witkowski, 2006)) then allows to establish the following relation

$$c^\top I_v \le |c||I_v| \le \int_0^{|I_v|} f(s)\,ds + \int_0^{|c|} f^{-1}(s)\,ds,$$

with f^{-1} the inverse of f. This leads us to consider the following candidate Lyapunov function

$$V \triangleq \frac{1}{2}|\widetilde{v}|^2 + \frac{1}{k_2}\left(1 - \frac{\overline{\gamma}_3}{|\gamma|}\right) + \int_0^{|I_v|} f(s)\,ds - c^\top I_v + \int_0^{|c|} f^{-1}(s)\,ds. \qquad (2.61)$$

It is straightforward to verify that this function is positive and proper with respect to $\widetilde{v}$. One verifies also that V is proper with respect to I_v by verifying that the Hessian matrix of V with respect to I_v is definite positive, $i.e.$ $\partial^2 V/\partial I_v^2 > 0$, using Property (2.14) of the function h. Using Eq. (2.60), Lemma 1, and $\dot{I}_v = R\widetilde{v}$ one gets

$$\dot{V} = \widetilde{v}^\top\left(-ue_3 + \overline{\gamma}\right) + \frac{1}{|\gamma|k_2}\overline{\gamma}_{1,2}^\top\left(\begin{bmatrix} -\omega_2 \\ \omega_1 \end{bmatrix} + \frac{1}{|\gamma|^2}\begin{bmatrix} -\gamma^\top S(Re_2)\dot{\gamma} \\ \gamma^\top S(Re_1)\dot{\gamma} \end{bmatrix}\right), \qquad (2.62)$$

with $\overline{\gamma}_{1,2} \triangleq (\overline{\gamma}_1, \overline{\gamma}_2)^\top$. Substituting the control law (2.11) into Eq. (2.62) one verifies that $\dot{V}$ satisfies the equality (2.57). Then, the proof of convergence of $(I_v, \widetilde{v}, \widetilde{\theta})$ to $(I_v^*, 0, 0)$ proceeds like the proof of Proposition 2. Note in particular that Property (2.14) of the function h is useful to ensure the boundedness of $\dot{\gamma}$, and that its combination with Assumption $iii)$ of Proposition 3 implies the existence of a unique vector $I_v^* \in \mathbb{R}^3$ such that $h(|I_v^*|^2)I_v^* = c$. Furthermore, to prove that I_v converges to I_v^* one can apply Barbalat's lemma ($i.e.$ Lemma 6 in Section 2.8.1) to Eq. (2.60) with

$$a(t) \triangleq - R^\top h(|I_v|^2)I_v + R^\top c, \text{ and } b(t) \triangleq - S(\omega)\widetilde{v} - ue_3 + R^\top \gamma.$$

As for the stability of the equilibrium point $(I_v, \widetilde{v}, \widetilde{\theta}) = (I_v^*, 0, 0)$, it is a direct consequence of relation (2.61), the decrease of V along the system's solutions, and the fact that this point is the unique minimum of V.

2.8.6   Proof of Proposition 4

From Eqs. (2.8b) and (2.19) it follows that the time-derivative of $\overline{v}$ satisfies the equation

$$\dot{\overline{v}} = -S(\omega)\overline{v} - ue_3 + R^\top \ddot{z} + R^\top(\gamma_e - \ddot{x}_r),$$

which can be rewritten as

$$\dot{\overline{v}} = -S(\omega)\overline{v} - ue_3 - R^\top h(|y|^2)y + R^\top \gamma + R^\top c, \qquad (2.63)$$

with γ defined by Eq. (2.20). Consider the candidate Lyapunov function

$$V \triangleq \frac{1}{2}|\overline{v}|^2 + \frac{1}{k_2}\left(1 - \frac{\overline{\gamma}_3}{|\gamma|}\right) + \int_0^{|y|} f(s)\,ds - c^\top y + \int_0^{|c|} f^{-1}(s)\,ds\,. \tag{2.64}$$

where f is specified in the proof of Proposition 3 and $\overline{\gamma}$ is given by Eq. (2.6). Analogously to the proof of Proposition 3 (see Section 2.8.5), one verifies that V is positive and proper with respect to $\overline{v}$ and y. Using Eq. (2.63), the control law (2.21), and the relation $\dot{y} = R\overline{v}$ one gets

$$\dot{V} = -|\gamma|k_1\overline{v}_3^2 - \frac{k_3}{k_2}\frac{|\overline{\gamma}_{1,2}|^2}{(|\gamma| + \overline{\gamma}_3)^2}\,. \tag{2.65}$$

From System (2.16) one verifies that z, $\dot{z}$, and $\ddot{z}$ are bounded. From Eqs. (2.64) and (2.65) one deduces that y and $\overline{v}$ are bounded. Since z and $\dot{z}$ are bounded, the relations $y = \widetilde{x} + z$ and $\overline{v} = \widetilde{v} + R^\top \dot{z}$ imply that $\widetilde{x}$ and $\widetilde{v}$ are also bounded. Then it follows from Property $P1$ of the function sat_Δ, Property (2.14) of the function h_z, and System (2.16) that $z^{(3)}$ remains bounded. Denote z^* the unique solution to $h(|z^*|^2)z^* = c$. From here with the same arguments as in the proof of Proposition 3 one deduces the convergence of $(y, \overline{v}, \widetilde{\theta})$ to $(z^*, 0, 0)$ and the stability of this equilibrium for the corresponding subsystem. Now, let us define

$$\overline{y} \triangleq y - z^*, \ \overline{z} \triangleq z - z^*, \ w \triangleq \dot{z},$$
$$g_z(\overline{y}, \overline{z}) \triangleq h_z(|\overline{y} - \overline{z}|^2)(\overline{y} - \overline{z}) + h_z(|\overline{z}|^2)\overline{z}.$$

Note that $g_z(\overline{y}, \overline{z})$ is bounded and vanishes ultimately since $\overline{y}$ converges to zero. Note also that $\widetilde{x} = y - z = \overline{y} - \overline{z}$. Then, System (2.16) can be rewritten as

$$\begin{cases} \dot{\overline{z}} = w \\ \dot{w} = -2k_z w - k_z^2\overline{z} + k_z^2(\mathrm{sat}_\Delta(\overline{z} + z^*) - z^*) - k_z h_z(|\overline{z}|^2)\overline{z} + k_z g_z(\overline{y}, \overline{z}), \end{cases}$$

or in the more compact form

$$\dot{Z} = F(Z) + G(\overline{y}, Z), \tag{2.66}$$

with $Z \triangleq (\overline{z}, w)^\top$, $F(Z) \triangleq (w, -2k_z w - k_z^2\overline{z} + k_z^2(\mathrm{sat}_\Delta(\overline{z} + z^*) - z^*) - k_z h_z(|\overline{z}|^2)\overline{z})^\top$, and $G(\overline{y}, Z) \triangleq (0, k_z g_z(\overline{y}, \overline{z}))^\top$ (a "perturbation" which vanishes ultimately). One verifies that $Z = 0$ is the globally asymptotically stable point of the system $\dot{Z} = F(Z)$ by considering the candidate Lyapunov function

$$U \triangleq \frac{1}{2k_z}\int_0^{|\overline{z}|^2} h_z(s)\,ds + \frac{1}{2}|\overline{z}|^2 + \frac{1}{2}\left|\overline{z} + \frac{w}{k_z}\right|^2\,. \tag{2.67}$$

Indeed, differentiating U along the solution of the system $\dot{Z} = F(Z)$ and using Property $P4$ of the function sat_Δ and Assumption $iv)$ of Proposition 4 one obtains

$$\dot{U} = -h_z(|\overline{z}|^2)|\overline{z}|^2 - k_z|\overline{z}|^2 - k_z\left(\left|\overline{z} + \frac{w}{k_z}\right|^2 - (\overline{z} + (\mathrm{sat}_\Delta(\overline{z} + z^*) - z^*))^\top\left(\overline{z} + \frac{w}{k_z}\right)\right)$$

$$\leq -h_z(|\overline{z}|^2)|\overline{z}|^2 - k_z|\overline{z}|^2 - k_z\left|\overline{z} + \frac{w}{k_z}\right|^2 + 2k_z|\overline{z}|\left|\overline{z} + \frac{w}{k_z}\right|\,.$$

$$\tag{2.68}$$

Since z is bounded, $\overline{z}$ is also bounded from its definition. As a consequence, since h_z is a smooth positive function, there exists $\delta_z > 0$ such that $h_z(|\overline{z}|^2) > \delta_z$ in such a compact set. This, along with relation (2.68), implies the existence of some positive constants α_z, α_w, α_u such that

$$\dot{U} \leq -\alpha_z|\overline{z}|^2 - \alpha_w \left| \overline{z} + \frac{w}{k_z} \right|^2 \leq -\alpha_u U. \tag{2.69}$$

Therefore, $Z = 0$ is an exponentially stable equilibrium of the unperturbed system $\dot{Z} = F(Z)$. Since $G(\overline{y}, Z)$ converges to zero, this in turn implies that the solutions to System (2.66) converge to zero. The convergence of $(\overline{z}, \dot{z})$ to $(0, 0)$ follows. Then, the convergence of $\overline{y} = \overline{z} + \widetilde{x}$ to zero (proved previously) implies that $\widetilde{x}$ converges to zero. Finally, since $\overline{v} = \widetilde{v} + R^\top \dot{z}$ and $\dot{z}$ converge to zero, $\widetilde{v}$ also converges to zero.

Let us finally establish the stability of the equilibrium $(z, \dot{z}, \widetilde{x}, \widetilde{v}, \widetilde{\theta}) = (z^*, 0, 0, 0, 0)$. In view of Eqs. (2.64) and (2.65) $(\overline{v}, \overline{y}, \widetilde{\theta}) = (0, 0, 0)$ is a stable equilibrium of the controlled system. From relations (2.67) and (2.69) $Z = 0$ is an asymptotically stable equilibrium point of the system $\dot{Z} = F(Z)$. Since the function G in Eq. (2.66) is continuous and identically equal to zero when $\overline{y} = 0$, one deduces that $(\overline{v}, \overline{y}, \widetilde{\theta}, Z) = (0, 0, 0, 0)$ is also a stable equilibrium of the controlled system. The stability of the equilibrium $(z, \dot{z}, \widetilde{x}, \widetilde{v}, \widetilde{\theta}) = (z^*, 0, 0, 0, 0)$ follows directly.

2.8.7 Proof of Proposition 5

One verifies that the time-derivative of $\overline{v}$ satisfies Eq. (2.63) and that $\dot{y} = R\overline{v}$. From here one verifies that the time-derivative of the candidate Lyapunov function V defined by Eq. (2.61) satisfies Eq. (2.65). From here using the same arguments as in the proof of Proposition 4 one deduces the convergence of $(y, \overline{v}, \widetilde{\theta})$ to $(z^*, 0, 0)$ and the stability of this equilibrium for the corresponding subsystem. Then, from Eq. (2.24) one deduces that $(I_{v,1}, I_{v,2}, \widetilde{x}_3 + z)^\top$ converges to z^*. Since $\overline{v}$ converges to zero, one deduces that $\dot{\widetilde{x}}_1$, $\dot{\widetilde{x}}_2$, and $\dot{\widetilde{x}}_3 + \dot{z}$ converge to zero (noting that $\dot{\widetilde{x}}_3 = \dot{\widetilde{x}}_3$). Now, alike the proof of Proposition 4, let us define

$$\overline{y} \triangleq y_3 - z_3^*, \ \overline{z} \triangleq z - z_3^*, \ w \triangleq \dot{z}_3,$$
$$g_z(\overline{y}, \overline{z}) \triangleq h_z((\overline{y} - \overline{z})^2)(\overline{y} - \overline{z}) + h_z(\overline{z}^2)\overline{z}.$$

Note that $g_z(\overline{y}, \overline{z})$ is bounded and vanishes ultimately since $\overline{y}$ converges to zero. Note also that $\widetilde{x}_3 = y_3 - z = \overline{y} - \overline{z}$. Then, System (2.23) can be rewritten as

$$\begin{cases} \dot{\overline{z}} = w \\ \dot{w} = -2k_z w - k_z^2 \overline{z} + k_z^2(\mathrm{sat}_\Delta(\overline{z} + z_3^*) - z_3^*) - k_z h_z(\overline{z}^2)\overline{z} + k_z g_z(\overline{y}, \overline{z}), \end{cases}$$

or in the more compact form

$$\dot{Z} = F(Z) + G(\overline{y}, Z),$$

with $Z \triangleq (\overline{z}, w)^\top$, $F(Z) \triangleq (w, -2k_z w - k_z^2 \overline{z} + k_z^2(\mathrm{sat}_\Delta(\overline{z} + z_3^*) - z_3^*) - k_z h_z(\overline{z}^2)\overline{z})^\top$, and $G(\overline{y}, Z) \triangleq (0, k_z g_z(\overline{y}, \overline{z}))^\top$ (a "perturbation" which vanishes ultimately). From here by proceeding like the proof of Proposition 4 one deduces the convergence of $(z, \dot{z})$ to $(z_3^*, 0)$. This implies the convergence of $\dot{\widetilde{x}}$ and thus of $\widetilde{v}$ to zero. Furthermore, since $\widetilde{x}_3 + z$ converges to z_3^* (as proved previously), the convergence of $\widetilde{x}_3$ to zero is trivial. Finally, the proof of stability of the equilibrium point $((I_{v,1}, I_{v,2}, z)^\top, \dot{z}, \widetilde{x}_3, \widetilde{v}, \widetilde{\theta}) = (z^*, 0, 0, 0, 0)$ proceeds like the proof of Proposition 4.

2.8.8   Proof of Proposition 6

The proof of this proposition is similar to the proof of Proposition 4. The positivity of the thrust input u results from the definition of u given in the control law (2.27) and the assumptions on σ in Proposition 6. Consider now the candidate Lyapunov function defined by Eq. (2.64). Using Eq. (2.63), Lemma 1, and the control law (2.27) one gets

$$
\begin{aligned}
\dot{V} &= \overline{v}^\top \left(-u e_3 + \overline{\gamma} \right) + \frac{1}{|\gamma| k_2} \overline{\gamma}_{1,2}^\top \left(\begin{bmatrix} -\omega_2 \\ \omega_1 \end{bmatrix} + \frac{1}{|\gamma|^2} \begin{bmatrix} -\gamma^\top S(Re_2)\dot{\gamma} \\ \gamma^\top S(Re_1)\dot{\gamma} \end{bmatrix} \right) \\
&= \overline{v}_3 \left(-u + |\gamma| \right) - \overline{v}_3 \left(|\gamma| - \overline{\gamma}_3 \right) + \frac{1}{|\gamma| k_2} \overline{\gamma}_{1,2}^\top \left(\begin{bmatrix} -\omega_2 \\ \omega_1 \end{bmatrix} + \frac{1}{|\gamma|^2} \begin{bmatrix} -\gamma^\top S(Re_2)\dot{\gamma} \\ \gamma^\top S(Re_1)\dot{\gamma} \end{bmatrix} + |\gamma| k_2 \overline{v}_{1,2} \right) \\
&= \overline{v}_3 \left(-u + |\gamma| \right) + \frac{1}{|\gamma| k_2} \overline{\gamma}_{1,2}^\top \left(\begin{bmatrix} -\omega_2 \\ \omega_1 \end{bmatrix} + \frac{1}{|\gamma|^2} \begin{bmatrix} -\gamma^\top S(Re_2)\dot{\gamma} \\ \gamma^\top S(Re_1)\dot{\gamma} \end{bmatrix} + |\gamma| k_2 \overline{v}_{1,2} - \frac{|\gamma| k_2 \overline{v}_3}{|\gamma| + \overline{\gamma}_3} \overline{\gamma}_{1,2} \right),
\end{aligned}
$$
$$(2.70)$$

with $\overline{v}_{1,2} \triangleq (\overline{v}_1, \overline{v}_2)^\top$ and $\overline{\gamma}_{1,2} \triangleq (\overline{\gamma}_1, \overline{\gamma}_2)^\top$. Substituting the control law (2.27) into Eq. (2.70) one obtains

$$
\dot{V} = -|\gamma| k_1 \sigma(\overline{v}_3) \overline{v}_3 - \frac{k_3}{k_2} \frac{|\overline{\gamma}_{1,2}|^2}{\left(|\gamma| + \overline{\gamma}_3 \right)^2}.
$$

From this equality the proof proceeds like the proof of Proposition 4.

2.8.9   Proof of Proposition 7

The proof of this proposition is similar to the proof of Proposition 4. The positivity of the thrust input u results from the definition of u given in the control law (2.28) and the assumptions on σ in Proposition 7. Consider now the candidate Lyapunov function defined by Eq. (2.64) with k_2 now a $\mathcal{C}^1$ function lower bounded by some positive constant. Using Eq. (2.63), Lemma 1, and the control law (2.28) one gets

$$
\begin{aligned}
\dot{V} &= \overline{v}^\top \left(-u e_3 + \overline{\gamma} \right) + \frac{1}{|\gamma| k_2} \overline{\gamma}_{1,2}^\top \left(\begin{bmatrix} -\omega_2 \\ \omega_1 \end{bmatrix} + \frac{1}{|\gamma|^2} \begin{bmatrix} -\gamma^\top S(Re_2)\dot{\gamma} \\ \gamma^\top S(Re_1)\dot{\gamma} \end{bmatrix} \right) - \frac{\dot{k}_2 (|\gamma| - \overline{\gamma}_3)}{k_2^2 |\gamma|} \\
&= \overline{v}_3 \left(-u + |\gamma| \right) - \overline{v}_3 \left(|\gamma| - \overline{\gamma}_3 \right) \\
&\quad + \frac{1}{|\gamma| k_2} \overline{\gamma}_{1,2}^\top \left(\begin{bmatrix} -\omega_2 \\ \omega_1 \end{bmatrix} + \frac{1}{|\gamma|^2} \begin{bmatrix} -\gamma^\top S(Re_2)\dot{\gamma} \\ \gamma^\top S(Re_1)\dot{\gamma} \end{bmatrix} + |\gamma| k_2 \overline{v}_{1,2} - \frac{\dot{k}_2 \overline{\gamma}_{1,2}}{k_2(|\gamma| + \overline{\gamma}_3)} \right) \\
&= \overline{v}_3 \left(-u + |\gamma| \right) \\
&\quad + \frac{1}{|\gamma| k_2} \overline{\gamma}_{1,2}^\top \left(\begin{bmatrix} -\omega_2 \\ \omega_1 \end{bmatrix} + \frac{1}{|\gamma|^2} \begin{bmatrix} -\gamma^\top S(Re_2)\dot{\gamma} \\ \gamma^\top S(Re_1)\dot{\gamma} \end{bmatrix} + |\gamma| k_2 \overline{v}_{1,2} - \frac{|\gamma| k_2 \overline{v}_3 \overline{\gamma}_{1,2}}{|\gamma| + \overline{\gamma}_3} - \frac{\dot{k}_2 \overline{\gamma}_{1,2}}{k_2(|\gamma| + \overline{\gamma}_3)} \right),
\end{aligned}
$$
$$(2.71)$$

with $\overline{v}_{1,2} \triangleq (\overline{v}_1, \overline{v}_2)^\top$ and $\overline{\gamma}_{1,2} \triangleq (\overline{\gamma}_1, \overline{\gamma}_2)^\top$. Substituting the control law (2.28) into Eq. (2.71) one obtains

$$
\dot{V} = -|\gamma| k_1 \sigma(\overline{v}_3) \overline{v}_3 - \frac{k_3}{k_2} \frac{|\overline{\gamma}_{1,2}|^2}{\left(|\gamma| + \overline{\gamma}_3 \right)^2}.
$$

From this equality the proof proceeds like the proof of Proposition 4.

2.8.10   Proof of Lemma 3

The uniform ultimate boundedness of $\dot{x}$ results from inequality (2.32) and Assumption 3 by calculating the time-derivative of $V \triangleq |\dot{x}|^2/2$ and showing that it is negative when $|\dot{x}|$ exceeds a certain threshold. More precisely, one has

$$\dot{V} = \dot{x}^{\top}(-uRe_3 + \gamma_e(\dot{x},t)).$$

Using Assumption 3 and inequality (2.32), one obtains

$$\dot{V} \leq |\dot{x}||u| + \frac{c_3}{m}|\dot{x}| - \frac{c_4}{m}|\dot{x}|^3 \leq |\dot{x}|\left(\beta_1 + (\beta_2 + \frac{c_3}{m})|\dot{x}| - \frac{c_4}{m}|\dot{x}|^2\right),$$

so that $\dot{x}$ is $u.u.b.$ by

$$-\frac{1}{2}\left(\beta_2 + \frac{c_3}{m}\right) + \frac{1}{2}\sqrt{\left(\beta_2 + \frac{c_3}{m}\right)^2 + \frac{4\beta_1 c_4}{m}}.$$

In view of Assumption 1, the uniform ultimate boundedness of γ_e follows. Since $\dot{x}$ is $u.u.b.$, the thrust input u is also $u.u.b.$. Then, one deduces from Eq. (2.31) that $\ddot{x}$ is $u.u.b.$. Combining with Assumption 1, this implies that $\dot{\gamma}_e$ is also $u.u.b.$.

2.8.11   Proof of Theorem 1

The proof relies on the following technical lemma.

Lemma 7 *Let $\gamma_{e,d}$ as defined by (2.34). If $M \geq \overline{c}_1 + \overline{c}_2(\kappa(\overline{c}_i, \overline{\mathbf{v}}_{\mathbf{r}}))^2$, then $\forall(\dot{x},t)$,*

$$\widetilde{v}^{\top} R^{\top}(\gamma_{e,d}(\dot{x},t) - \overline{\mathrm{sat}}_M(\gamma_{e,d}(\dot{x},t))) \leq 0. \tag{2.72}$$

Proof If $|\gamma_{e,d}(\dot{x},t)| < M$, Property *P2* of the saturation function $\overline{\mathrm{sat}}_M$ implies that $\gamma_{e,d}(\dot{x},t) = \overline{\mathrm{sat}}_M(\gamma_{e,d}(\dot{x},t))$, and the result follows. If $|\gamma_{e,d}(\dot{x},t)| \geq M$, it follows from (2.36) and the choice of M that $|\dot{x}| > \kappa(\overline{c}_i, \overline{\mathbf{v}}_{\mathbf{r}})$. Then, by using Property *P4* of the saturation function $\overline{\mathrm{sat}}_M$, relation (2.36), the relations $\phi(\gamma_{e,d}(\dot{x},t)) \leq 1$ and $R\widetilde{v} = \dot{x} - \dot{x}_r$ one gets

$$\begin{aligned}
\widetilde{v}^{\top} R^{\top}(\gamma_{e,d}(\dot{x},t) - \overline{\mathrm{sat}}_M(\gamma_{e,d}(\dot{x},t))) &= (1 - \phi(\gamma_{e,d}(\dot{x},t)))(\dot{x} - \dot{x}_r)^{\top}\gamma_{e,d}(\dot{x},t) \\
&\leq (1 - \phi(\gamma_{e,d}(\dot{x},t)))(\dot{x}\gamma_{e,d}(\dot{x},t) + \overline{\mathbf{v}}_{\mathbf{r}}|\gamma_{e,d}(\dot{x},t)|) \\
&\leq -(1 - \phi(\gamma_{e,d}(\dot{x},t)))(\overline{c}_4|\dot{x}|^3 - \overline{c}_2\overline{\mathbf{v}}_{\mathbf{r}}|\dot{x}|^2 - \overline{c}_3|\dot{x}| - \overline{c}_1\overline{\mathbf{v}}_{\mathbf{r}}).
\end{aligned}$$

From the definition of the function κ, the inequality $|\dot{x}| > \kappa(\overline{c}_i, \overline{\mathbf{v}}_{\mathbf{r}})$ implies that

$$\overline{c}_4|\dot{x}|^3 - \overline{c}_2\overline{\mathbf{v}}_{\mathbf{r}}|\dot{x}|^2 - \overline{c}_3|\dot{x}| - \overline{c}_1\overline{\mathbf{v}}_{\mathbf{r}} \geq 0.$$

Then, inequality (2.72) follows.   ∎

From the control law (2.30) and inequality (2.35), relation (2.32) holds true for some positive constants β_1, β_2. Property 2 of Theorem 1 (together with the completeness of the system's solutions) then directly follows by application of Proposition 3. Since Assumption 1 holds, Proposition 3 implies also that γ_e, $\dot{\gamma}_e$, $\ddot{x}$ are bounded. Since $\dot{\gamma}_d(t)$ is bounded, one deduces from Eq. (2.34) that $\dot{\gamma}_{e,d}(\dot{x},t)$ remains bounded. Combined with Assumption 4, Eq. (2.33), and Property *P1* of the function $\overline{\mathrm{sat}}_M$, this result implies that $\dot{\gamma}(\dot{x},t)$ is also

bounded. As a consequence, it follows from the control law (2.30) that u, ω_1, and ω_2 are well-defined and bounded along every system's solution. This and the boundedness of ω_3 yield Property 1 of the theorem. Let us now establish Property 3. Omitting the arguments for γ and $\gamma_{e,d}$, one has

$$\dot{\widetilde{v}} = -S(\omega)\widetilde{v} - ue_3 + R^\top \gamma + R^\top (\gamma_{e,d} - \overline{\mathrm{sat}}_M(\gamma_{e,d})).$$

Therefore, the time-derivative of the function V defined by Eq. (2.56) along the system's solutions is given by

$$\dot{V} = \widetilde{v}_3 \left(-u + \overline{\gamma}_3 \right) + \widetilde{v}^\top R^\top (\gamma_{e,d} - \overline{\mathrm{sat}}_M(\gamma_{e,d}))$$
$$+ \frac{1}{|\gamma|k_2} \overline{\gamma}_{1,2}^\top \left(\begin{bmatrix} -\omega_2 \\ \omega_1 \end{bmatrix} + \frac{1}{|\gamma|^2} \begin{bmatrix} -\gamma^\top S(Re_2)\dot{\gamma} \\ \gamma^\top S(Re_1)\dot{\gamma} \end{bmatrix} + |\gamma|k_2 \widetilde{v}_{1,2} \right).$$

Replacing u, ω_1, ω_2 by their expressions in (2.30) one obtains

$$\dot{V} = -|\gamma|k_1\widetilde{v}_3^2 - \mu_\tau(|\gamma| + \overline{\gamma}_3)\frac{k_3}{k_2}\frac{|\overline{\gamma}_{1,2}|^2}{(|\gamma| + \overline{\gamma}_3)^2}$$
$$+ \widetilde{v}^\top R^\top (\gamma_{e,d} - \overline{\mathrm{sat}}_M(\gamma_{e,d})) + \frac{(1 - \mu_\tau(|\gamma|))}{|\gamma|^3 k_2}(-\overline{\gamma}_1\gamma^\top S(Re_2) + \overline{\gamma}_2\gamma^\top S(Re_1))\dot{\gamma}, \tag{2.73}$$

with $\widetilde{v}_{1,2} \triangleq (\widetilde{v}_1, \widetilde{v}_2)^\top$ and $\overline{\gamma}_{1,2} \triangleq (\overline{\gamma}_1, \overline{\gamma}_2)^\top$. It follows from (2.36) and Assumption 4 that $\overline{\mathrm{sat}}_M(\gamma_{e,d}(\dot{x}_r(t), t)) = \gamma_{e,d}(\dot{x}_r(t), t)$, when $M \geq \overline{c}_1 + \overline{c}_2\overline{\mathbf{v}}_{\mathbf{r}}^2$. Using Assumption 2 one deduces that $\overline{\mathrm{sat}}_M(\gamma_{e,d}(\dot{x}, t)) = \gamma_{e,d}(\dot{x}, t)$ for $\dot{x}$ in a neighborhood of $\dot{x}_r$, when $M > \overline{c}_1 + \overline{c}_2\overline{\mathbf{v}}_{\mathbf{r}}^2$. Furthermore, since $\tau \in (0, \delta)$ by assumption, one deduces from Eq. (2.29) that $\mu_\tau(|\gamma|) = 1$ in a neighborhood of $\dot{x}_r$. Eq. (2.73) becomes

$$\dot{V} = -|\gamma|k_1\widetilde{v}_3^2 - \mu_\tau(|\gamma| + \overline{\gamma}_3)\frac{k_3}{k_2}\frac{|\overline{\gamma}_{1,2}|^2}{(|\gamma| + \overline{\gamma}_3)^2},$$

and the proof of local asymptotic stability proceeds like the proof of Proposition 2. Let us now consider the case when $M \geq \overline{c}_1 + \overline{c}_2(\kappa(\overline{c}_i, \overline{\mathbf{v}}_{\mathbf{r}}))^2$ and $|\gamma(\dot{x}, t)| \geq \tau$, $\forall(\dot{x}, t)$. This latter condition implies that $\mu_\tau(|\gamma|) = 1$, $\forall(\dot{x}, t)$. Therefore, Eq. (2.73) becomes

$$\dot{V} = -|\gamma|k_1\widetilde{v}_3^2 - \mu_\tau(|\gamma| + \overline{\gamma}_3)\frac{k_3}{k_2}\frac{|\overline{\gamma}_{1,2}|^2}{(|\gamma| + \overline{\gamma}_3)^2} + \widetilde{v}^\top R^\top (\gamma_{e,d} - \overline{\mathrm{sat}}_M(\gamma_{e,d}))$$
$$\leq -|\gamma|k_1\widetilde{v}_3^2 - \mu_\tau(|\gamma| + \overline{\gamma}_3)\frac{k_3}{k_2}\frac{|\overline{\gamma}_{1,2}|^2}{(|\gamma| + \overline{\gamma}_3)^2},$$

where the inequality follows from Lemma 7. From here the proof proceeds like the proof of Proposition 2.

2.8.12   Proof of Lemma 4

The boundedness of ω_3 is straightforward. Let us now prove the second property. Consider the following candidate Lyapunov function

$$V \triangleq |\beta| - e_1^\top \beta,$$

whose time-derivative satisfies

$$\dot{V} = \frac{1}{|\beta|}(\beta - |\beta|e_1)^\top \dot{\beta}$$

$$= \frac{1}{|\beta|}((\beta_1 - |\beta|)e_1 + \beta_2 e_2)^\top (-S(\omega)R^\top \alpha + R^\top \dot{\alpha}).$$

By assumption $\omega_{1,2} = 0$ and $\dot{\alpha} = 0$. Then using the control law (2.37), one obtains

$$\dot{V} = -\frac{\omega_3}{|\beta|} \left((\beta_1 - |\beta|)e_1 + \beta_2 e_2\right)^\top S(e_3)R^\top \alpha$$

$$= -\frac{\omega_3}{|\beta|} \left((\beta_1 - |\beta|)e_2^\top R^\top \alpha + \beta_2 e_1^\top R^\top \alpha\right)$$

$$= -\omega_3 \beta_2$$

$$= -k_\alpha \beta_2^2$$

From here LaSalle's theorem ensures the convergence of β_2 to zero. The decreasing of V and that $\beta(0) \neq -|\beta(0)|e_1$ imply that β converges to $|\beta|e_1$.

2.8.13   Proof of Proposition 8

By denoting $\tilde{\dot{x}} \triangleq \dot{x} - \hat{\dot{x}}$ and $\tilde{\gamma}_e \triangleq \gamma_e - \hat{\gamma}_e$, one gets

$$\begin{cases} \dfrac{d}{dt}\tilde{\dot{x}} &=& \tilde{\gamma}_e - k_o \tilde{\dot{x}} \\ \tilde{\dot{\gamma}}_e &=& -a^2 k_o^2 \tilde{\dot{x}} + \dot{\gamma}_e \end{cases}$$

Consider now the following candidate Lyapunov function

$$V \triangleq \frac{1}{2}\left(a^2 k_o^2 |\tilde{\dot{x}}|^2 - a k_o \tilde{\gamma}_e^\top \tilde{\dot{x}} + |\tilde{\gamma}_e|^2\right),$$

which is positive definite because

$$\frac{1}{4}\left(a^2 k_o^2 |\tilde{\dot{x}}|^2 + |\tilde{\gamma}_e|^2\right) \leq V \leq \frac{3}{4}\left(a^2 k_o^2 |\tilde{\dot{x}}|^2 + |\tilde{\gamma}_e|^2\right). \qquad (2.74)$$

The time-derivative of V satisfies

$$\dot{V} = -\frac{a k_o}{2}\left(|\tilde{\dot{x}}|^2 k_o^2 (2a - a^2) + |\tilde{\gamma}_e|^2 - k_o \tilde{\gamma}_e^\top \tilde{\dot{x}} + \tilde{\dot{x}}^\top \dot{\gamma}_e - \frac{2}{a k_o}\tilde{\gamma}_e^\top \dot{\gamma}_e\right).$$

From the Young inequality one obtains

$$|\tilde{\gamma}_e^\top \tilde{\dot{x}}| \leq \frac{1}{2k_o}\left(|\tilde{\gamma}_e|^2 + k_o^2 |\tilde{\dot{x}}|^2\right),$$

$$|\tilde{\gamma}_e^\top \dot{\gamma}_e| \leq \frac{a k_o}{4}\left(\frac{1}{2}|\tilde{\gamma}_e|^2 + \frac{8}{a^2 k_o^2}|\dot{\gamma}_e|^2\right),$$

$$|\tilde{\dot{x}}^\top \dot{\gamma}_e| \leq \frac{1}{2}\left(\varepsilon^2 k_o^2 |\tilde{\dot{x}}|^2 + \frac{|\dot{\gamma}_e|^2}{\varepsilon^2 k_o^2}\right),$$

with ε some positive constant. So that

$$\dot{V} \leq -\frac{ak_o}{2}\left(|\tilde{\tilde{x}}|^2 k_o^2 \left(2a - a^2 - \frac{1}{2} - \frac{\varepsilon^2}{2}\right) + \frac{1}{4}|\tilde{\gamma}_e|^2 - |\dot{\gamma}_e\|^2 \frac{1}{k_o^2}\left(\frac{1}{2\varepsilon^2} + \frac{4}{a^2}\right)\right). \quad (2.75)$$

For all $a \in \left(1 - \sqrt{2}/2, 1 + \sqrt{2}/2\right)$, one has $2a - a^2 - 1/2 > 0$, so that there exists a positive constant $\varepsilon(a)$ such that $2a - a^2 - 1/2 - \varepsilon(a)^2/2 > 0$. Let us choose $\varepsilon = \varepsilon(a)$. Therefore, in view of (2.75) and (2.74) there exists a positive constant $\tau(a)$ (independent of k_o) such that

$$\dot{V} \leq -\frac{ak_o}{2}\left(\tau(a)V - |\dot{\gamma}_e|^2 \frac{1}{k_o^2}\left(\frac{1}{2\varepsilon(a)^2} + \frac{4}{a^2}\right)\right).$$

From here one deduces that

$$\text{ub}(V) \leq \frac{1}{\tau(a)k_o^2}(\text{ub}(\dot{\gamma}_e))^2 \left(\frac{1}{2\varepsilon(a)^2} + \frac{4}{a^2}\right).$$

This inequality and (2.74) imply that

$$\text{ub}(|\tilde{\tilde{x}}|) \leq \frac{2}{ak_o^2}\sqrt{\frac{1}{\tau(a)}\left(\frac{1}{2\varepsilon(a)^2} + \frac{4}{a^2}\right)}\,\text{ub}(\dot{\gamma}_e),$$

$$\text{ub}(|\tilde{\gamma}_e|) \leq \frac{2}{k_o}\sqrt{\frac{1}{\tau(a)}\left(\frac{1}{2\varepsilon(a)^2} + \frac{4}{a^2}\right)}\,\text{ub}(\dot{\gamma}_e),$$

which also imply the first property of the proposition and that $\dot{\hat{\gamma}}_e$ is *u.b.* by

$$\text{ub}(|\dot{\hat{\gamma}}_e|) \leq 2a\sqrt{\frac{1}{\tau(a)}\left(\frac{1}{2\varepsilon(a)^2} + \frac{4}{a^2}\right)}\,\text{ub}(\dot{\gamma}_e).$$

2.8.14   Other technical lemmas

Lemma 8 *Consider the saturation function* sat_Δ *defined by* (2.17). *Then,* $\forall(c, x) \in \mathbb{R}^n \times \mathbb{R}^n$ *such that* $|c| \leq \Delta$, *with* Δ *a positive constant associated with the function* sat_Δ, *one verifies that* $|\text{sat}_\Delta(x + c) - c| \leq |x|$.

Proof If $|x+c| \leq \Delta$, one directly deduces from the definition of sat_Δ that $|\text{sat}_\Delta(x+c)-c| = |x|$. Now, consider the case $|x + c| > \Delta$. In this case, using this inequality and the fact that $|c| \leq \Delta$ one gets

$$\begin{aligned}
|\text{sat}_\Delta(x + c) - c|^2 - |x|^2 &= \left|(x + c)\frac{\Delta}{|x + c|} - c\right|^2 - |x|^2 \\
&= \left(1 - \frac{\Delta}{|x + c|}\right)\left(|c|^2 - |x|^2 - \Delta|x + c|\right) \\
&\leq -\left(1 - \frac{\Delta}{|x + c|}\right)|x|^2 \leq 0.
\end{aligned}$$

This concludes the proof.   ∎

Lemma 9 *Consider the differential equation (2.16) driven by $\widetilde{x}$, where h_z denotes a smooth bounded positive function satisfying (2.13)–(2.14) for some positive constants η_z, β_z, and sat_Δ is a continuous "saturation function" bounded by $\overline{\Delta}$. Then, $|z|, |\dot{z}|$, and $|\ddot{z}|$ are u.u.b. by $\overline{\Delta} + \eta_z/k_z$, $2(k_z\overline{\Delta} + \eta_z)$, and $6k_z(k_z\overline{\Delta} + \eta_z)$ respectively.*

Proof Equation (2.16) can be rewritten as

$$
\begin{cases}
\dot{z} = -k_z z + k_z w \\
\dot{w} = -k_z w + k_z \mathrm{sat}_\Delta(z) + h_z(|\widetilde{x}|^2)\widetilde{x},
\end{cases}
\tag{2.76}
$$

with w an intermediary variable and $z(0) = \dot{z}(0) = w(0) = 0$. Since $h_z(|\widetilde{x}|^2)\widetilde{x}$ and $\mathrm{sat}_\Delta(z)$ are bounded by η_z and $\overline{\Delta}$ respectively, System (2.76) indicates that w is u.u.b. by $\overline{\Delta} + \eta_z/k_z$, and as a consequence z is *u.u.b.* by $\overline{\Delta} + \eta_z/k_z$. From here using (2.76) and (2.16) one deduces that

$$
\mathrm{ub}(\dot{z}) \leq k_z \mathrm{ub}(z) + k_z \mathrm{ub}(w) \leq 2(k_z\overline{\Delta} + \eta_z),
$$

and

$$
\mathrm{ub}(\ddot{z}) \leq 2k_z \mathrm{ub}(\dot{z}) + k_z^2 \mathrm{ub}(z) + k_z(k_z\overline{\Delta} + \eta_z) \leq 6k_z(k_z\overline{\Delta} + \eta_z).
$$

∎

2.8.15   Proof of Lemma 5

One verifies that $R(\theta)$ satisfies the differential equation $\dot{R}(\theta) = \omega R(\theta)S_2$, which implies that $\dot{R}(\theta)^\top = -\omega S_2 R(\theta)^\top$. One also verifies that

$$
R(\theta)^\top S_2 \gamma = S_2 \overline{\gamma},
$$

and

$$
\frac{d}{dt}\left(\frac{\gamma}{|\gamma|}\right) = \frac{(|\gamma|^2 I_2 - \gamma\gamma^\top)\dot{\gamma}}{|\gamma|^3} = \frac{S_2\gamma(S_2\gamma)^\top\dot{\gamma}}{|\gamma|^3}.
$$

Thus,

$$
R(\theta)^\top \frac{d}{dt}\left(\frac{\gamma}{|\gamma|}\right) = \frac{S_2\overline{\gamma}(S_2\gamma)^\top\dot{\gamma}}{|\gamma|^3}.
$$

Using these above relations and noting that $S_2^\top = -S_2$, one gets

$$
\frac{d}{dt}\left(\frac{\overline{\gamma}}{|\gamma|}\right) = -\omega S_2 R(\theta)^\top \frac{\gamma}{|\gamma|} + R(\theta)^\top \frac{d}{dt}\left(\frac{\gamma}{|\gamma|}\right) = -\frac{S_2\overline{\gamma}}{|\gamma|}\left(\omega + \frac{\gamma^\top S_2\dot{\gamma}}{|\gamma|^2}\right).
$$

Then, this result is used to deduce that

$$
\frac{d}{dt}\left(1 - \frac{\overline{\gamma}_1}{|\gamma|}\right) = i_1^\top \frac{S_2\overline{\gamma}}{|\gamma|}\left(\omega + \frac{\gamma^\top S_2\dot{\gamma}}{|\gamma|^2}\right) = -\frac{\overline{\gamma}_2}{|\gamma|}\left(\omega + \frac{\gamma^\top S_2\dot{\gamma}}{|\gamma|^2}\right).
$$

2.8.16 Proof of Proposition 9

The proof is based on the candidate Lyapunov function

$$V \triangleq 1 - \overline{\gamma}_1 = 1 - \cos\widetilde{\theta} = 2\sin^2(\widetilde{\theta}/2),$$

whose time-derivative along the solutions to the controlled system verifies (using Lemma 5 with $|\gamma| = 1$)

$$\dot{V} = -\overline{\gamma}_2\left(\omega + \gamma^\top S_2 \dot{\gamma}\right) = -k\frac{\overline{\gamma}_2^2}{(1+\overline{\gamma}_1)^2} = -k\frac{1-\overline{\gamma}_1}{1+\overline{\gamma}_1} = -\frac{kV}{1+\overline{\gamma}_1} \le -\frac{kV}{2}.$$

From here the exponential stability of $\widetilde{\theta}$ to zero is straightforward.

2.8.17 Proof of Proposition 10

Using (2.52), Eq. (2.51b) can be rewritten as

$$\dot{\widetilde{v}} = -\omega S_2 \widetilde{v} - ui_1 + R(\theta)^\top \gamma - R(\theta)^\top h(|I_v|^2)I_v + R(\theta)^\top c. \qquad (2.77)$$

Analogously to the proof of Proposition 3, consider the following Lyapunov function

$$V \triangleq \frac{1}{2}|\widetilde{v}|^2 + \frac{1}{k_2}\left(1 - \frac{\overline{\gamma}_1}{|\gamma|}\right) + \int_0^{|I_v|} f(s)\,ds - c^\top I_v + \int_0^{|c|} f^{-1}(s)\,ds, \qquad (2.78)$$

with $f : s \longmapsto h(s^2)s$ and f^{-1} the inverse of f. Using (2.77), Lemma 5, the relation $\dot{I}_v = R(\theta)\widetilde{v}$, and the control expression (2.48) one gets

$$\begin{aligned}
\dot{V} &= \widetilde{v}^\top\left(-ui_1 + \overline{\gamma}\right) - \frac{\overline{\gamma}_2}{|\gamma|k_2}\left(\omega + \frac{\gamma^\top S_2\dot{\gamma}}{|\gamma|^2}\right) \\
&= \widetilde{v}_1(-u + \overline{\gamma}_1) - \frac{\overline{\gamma}_2}{|\gamma|k_2}\left(\omega + \frac{\gamma^\top S_2\dot{\gamma}}{|\gamma|^2} - |\gamma|k_2\widetilde{v}_2\right) \\
&= -|\gamma|k_1\sigma(\widetilde{v}_1)\widetilde{v}_1 - \frac{k_3\overline{\gamma}_2^2}{k_2(|\gamma| + \overline{\gamma}_1)^2}.
\end{aligned}$$

From here one completes the proof by proceeding like the proofs of Propositions 2 and 3.

2.8.18 Proof of Proposition 11

The proof of this proposition is similar to the proof of Proposition 10. The positivity of the thrust control u results from the definition of u given in the control law (2.53) and the assumptions on σ in Proposition 11. Now, using Eq. (2.77), Lemma 5, the relation $\dot{I}_v = R(\theta)\widetilde{v}$, and the control law (2.53) one verifies that the time-derivative of the candidate Lyapunov function V (defined by (2.78)) satisfies

$$\begin{aligned}
\dot{V} &= \widetilde{v}^\top\left(-ui_1 + \overline{\gamma}\right) - \frac{\overline{\gamma}_2}{|\gamma|k_2}\left(\omega + \frac{\gamma^\top S_2\dot{\gamma}}{|\gamma|^2}\right) \\
&= \widetilde{v}_1(-u + |\gamma|) - \widetilde{v}_1(|\gamma| - \overline{\gamma}_1) - \frac{\overline{\gamma}_2}{|\gamma|k_2}\left(\omega + \frac{\gamma^\top S_2\dot{\gamma}}{|\gamma|^2} - |\gamma|k_2\widetilde{v}_2\right) \\
&= \widetilde{v}_1(-u + |\gamma|) - \frac{\overline{\gamma}_2}{|\gamma|k_2}\left(\omega + \frac{\gamma^\top S_2\dot{\gamma}}{|\gamma|^2} - |\gamma|k_2\widetilde{v}_2 + \frac{|\gamma|k_2\widetilde{v}_1\overline{\gamma}_2}{|\gamma| + \overline{\gamma}_1}\right) \\
&= -|\gamma|k_1\sigma(\widetilde{v}_1)\widetilde{v}_1 - \frac{k_3\overline{\gamma}_2^2}{k_2(|\gamma| + \overline{\gamma}_1)^2}.
\end{aligned}$$

From this equality the proofs proceeds like the proof of Proposition 10.

2.8.19   Proof of Proposition 12

The proof of this proposition is similar to the proofs of Propositions 11 and 4. The candidate Lyapunov function is

$$V \triangleq \frac{1}{2}|\overline{v}|^2 + \frac{1}{k_2}\left(1 - \frac{\overline{\gamma}_1}{|\gamma|}\right) + \int_0^{|y|} f(s)\,ds - c^\top y + \int_0^{|c|} f^{-1}(s)\,ds,$$

with $f : s \longmapsto h(s^2)s$ and f^{-1} the inverse of f. Using Eqs. (2.20) and (2.51b) one gets

$$\dot{\overline{v}} = -\omega S_2 \overline{v} - u i_1 + R(\theta)^\top \gamma - R(\theta)^\top h(|y|^2)y + R(\theta)^\top c. \qquad (2.79)$$

Then, similar to the proof of Proposition 11 one verifies that along the solutions to the controlled system the time-derivative of V is

$$\dot{V} = -|\gamma|k_1\sigma(\overline{v}_1)\overline{v}_1 - \frac{k_3\overline{\gamma}_2^2}{k_2(|\gamma| + \overline{\gamma}_1)^2}.$$

From here the proof proceeds like the proof of Proposition 4.

Chapter 3

Attitude estimation

3.1 Survey on attitude estimation

The *attitude* represents the orientation of a frame, attached to the moving rigid body, relative to an inertial reference frame. It can be described by a rotation matrix, an element of the Lie group SO(3). In the literature two definitions of the attitude can be found. It is either the rotation matrix which carries the body reference frame into the inertial reference frame, or, conversely, the rotation matrix which carries the inertial reference frame into the body reference frame. While the earliest definition, *i.e.* the latter one, originates from the aerospace field, the robotics field adopts the first definition. These rotation matrices are just the transposes of each other, and the first definition is adopted throughout this dissertation. By denoting $R \in$ SO(3) such a matrix of rotation, R satisfies the matrix differential equation

$$\dot{R} = RS(\omega), \tag{3.1}$$

with $\omega = [\omega_1, \omega_2, \omega_3]^\top \in \mathbb{R}^3$ the angular velocity vector of the body frame relative to the inertial frame, expressed in the body frame.

In view of the control design in the previous chapter, a good estimation of the vehicle's attitude is very important for feedback control laws. It is even more so for small and light VTOL vehicles whose attitude can rapidly vary in large proportions due to wind-induced perturbations. In the present work we focus on the problem of attitude estimation based on measurements provided by a GPS and an IMU embarked on the vehicle. The vehicle's position and linear velocity are directly measured by the GPS, but the reconstruction of its attitude poses difficulties. In fact, estimating the vehicle's attitude by just integrating the rigid body kinematics equation of rotation (*i.e.* Eq. (3.1)) is not safe in long-term applications due to gyro drifts and noises. Several alternative solutions have been proposed in the last decades. The surveys of nonlinear attitude estimation methods based on vector measurements (*i.e.* vector observations) (Crassidis et al., 2007), (Mahony et al., 2008), (Choukroun, 2003), which contain a large number of literature citations, are useful sources to start a research on the topic. The paper (Shuster, 2006) by one of the pioneers in the domain is also interesting. The author provides many intriguing anecdotes about the history of attitude estimation, and especially the QUEST (*i.e.* QUaternion ESTimator) that he gave birth to and which has become one of the most widely-used spacecraft attitude estimation algorithms. Throughout this chapter, the terms *"filter"* and *"estimator"* are used synonymously when noisy measurements are involved. On the other hand,

when perfect observations are provided, the term *"observer"* is adopted.

The first solution to the problem of attitude estimation from vector observations is the TRIAD algorithm, proposed by Black in 1964 (see *e.g.* (Shuster, 1978), (Shuster and Oh, 1981), (Shuster, 2006)). It is also known as the Algebraic Method. It straightforwardly constructs the attitude matrix from the information in both the body frame and the inertial frame of two non-collinear unit vectors. More precisely, by denoting v_1, v_1^*, v_2, v_2^* as the vectors of coordinates, expressed in the inertial frame and the body frame respectively, of two unit vectors $\overrightarrow{v_1}$ and $\overrightarrow{v_2}$, one has $v_1 = Rv_1^*$, $v_2 = Rv_2^*$, and the TRIAD algorithm provides the attitude matrix R as

$$R = \begin{bmatrix} s_1 & s_2 & s_3 \end{bmatrix} \begin{bmatrix} r_1 & r_2 & r_3 \end{bmatrix}^\top,$$

with two orthonormal triads

$$s_1 = v_1, \; s_2 = \frac{v_1 \times v_2}{|v_1 \times v_2|}, \; s_3 = s_1 \times s_2,$$

$$r_1 = v_1^*, \; r_2 = \frac{v_1^* \times v_2^*}{|v_1^* \times v_2^*|}, \; r_3 = r_1 \times r_2.$$

This algorithm is very simple to implement, but it can accommodate only two vector observations. This may lead to the difficulty of treating information when the observation of more than two vectors are available. For instance, in this case one may not know *a priori* the observation of which pair of vectors provides the best attitude estimate using the TRIAD algorithm. Additionally, it does not take the relative reliability of the vector observations into account, even in the case of two vector observations. These drawbacks of the TRIAD algorithm disappear in optimal algorithms which calculate the best attitude estimate based on a cost function for which all vector observations are taken into account simultaneously. Optimal algorithms are, however, computationally more expensive than the TRIAD algorithm. The first and also best-known optimal attitude estimation problem is the least-square problem, named *Wahba's problem*, proposed in (Wahba, 1965). It consists in finding a rotation matrix $\widehat{A} \in \mathrm{SO}(3)$ which minimizes the cost function

$$J(A) \triangleq \frac{1}{2} \sum_{i=1}^{n \geq 2} a_i ||v_i^* - Av_i||^2, \tag{3.2}$$

where A corresponds to the transpose of the estimated attitude $\widehat{R}$; $\{v_i^*\}$ is a set of measurements of $n\,(\geq 2)$ unit vectors, expressed in the body frame; $\{v_i\}$ are the corresponding unit vectors, expressed in the inertial frame; and $\{a_i\}$ is a set of non-negative weights whose values can be designed based on the reliability of the corresponding measurements. Wahba's problem allows arbitrary weighting of vector observations. In (Shuster, 1989a), the author proposes the particular choice $a_i = \sigma_i^{-2}$, the inverse variance of the measurement v_i^*, in order to relate Wahba's problem to Maximum Likelihood Estimation of the attitude based on an uncorrelated noise model (Shuster and Oh, 1981), (Shuster, 1989a). In fact, the cost function $J(A)$ defined by Eq. (3.2) can be rewritten as

$$J(A) = \frac{1}{2} \sum_{i=1}^{n \geq 2} a_i \mathbf{tr}\left((v_i^* - Av_i)(v_i^* - Av_i)^\top\right) = \frac{1}{2} \sum_{i=1}^{n \geq 2} a_i \left(|v_i^*|^2 + |v_i|^2\right) - \frac{1}{2}\mathbf{tr}(AB^T), \tag{3.3}$$

with

$$B \triangleq \sum_{i=1}^{n \geq 2} a_i v_i^* v_i^\top. \tag{3.4}$$

It is, thus, obvious that finding a rotation matrix $\widehat{A}$ which minimizes $J(A)$ is equivalent to finding a rotation matrix $\widehat{A}$ which maximizes $\mathbf{tr}(AB^T)$. The first solutions to Wahba's problem, based on this observation, were proposed in 1966 by Farrell and Stuelpnagel (Wahba, 1966), and by Wessner, Velman, Brock in the same paper [1]. However, these solutions, being computationally expensive, are not well suited to real-time applications. For instance, Farrell and Stuelpnagel's method requires a polar decomposition of the matrix B into a product $B = UP$ (with U a orthogonal matrix [2] and P a symmetric and positive semidefinite matrix) and a diagonalization of P into $P = WDW^\top$ [3] (with W a orthogonal matrix and D a diagonal matrix whose diagonal elements are arranged in decreasing order, i.e. $D = \mathbf{diag}(d_1, d_2, d_3)$ with $d_1 \geq d_2 \geq d_3$). The optimal rotation matrix $\widehat{A}$ is then given by

$$\widehat{A} = UW\mathbf{diag}(1, 1, \mathbf{det}(U))W^\top.$$

As for Wessner's solution, which is a particular case of Farrell and Stuelpnagel's solution, the optimal rotation matrix $\widehat{A}$ is calculated according to

$$\widehat{A} = \left(B^\top\right)^{-1} \left(B^\top B\right)^{1/2}.$$

This solution, due to the inverse of $B^\top$, indicates that a minimum of three (non-collinear) vector observations must be available, knowing that two vector observations are sufficient for attitude estimation. Besides, the calculation of the square root of the matrix $B^\top B$ also requires expensive computation. For example, one needs to diagonalize $B^\top B$ as $B^\top B = W_B D_B W_B^\top$ to obtain $\left(B^\top B\right)^{1/2} = W_B D_B^{1/2} W_B^\top$.

No solution to Wahba's problem was able to replace the TRIAD algorithm in practice, until Davenport's q-method (Davenport, 1968) and the numerical technique QUEST (Shuster, 1978), (Shuster and Oh, 1981) were proposed. By using the quaternion parametrization, Davenport transformed Wahba's problem into the problem of finding the largest eigenvalue λ_{max} of the symmetric Davenport matrix $K \in \mathbb{R}^{4 \times 4}$ defined by

$$K \triangleq \begin{bmatrix} C - \gamma I_3 & z \\ z^\top & \gamma \end{bmatrix},$$

with $C \triangleq B + B^\top$, $\gamma \triangleq \mathbf{tr}(B)$, $z \triangleq \sum_{i=1}^{n \geq 2} a_i v_i^* \times v_i$, and B defined by Eq. (3.4). The optimal quaternion, corresponding to the optimal rotation matrix $\widehat{A}$ of Wahba's problem, is the normalized eigenvector q_{max} of K associated with the eigenvalue λ_{max}. In fact, the largest eigenvalue λ_{max} may be obtained by solving analytically, as proposed in (Davenport, 1968), the largest zero of the fourth-degree characteristic polynomial $\mathbf{det}(K - \lambda I_4)$. However, Davenport's q-method is also computationally complex. This leads to the development of the QUEST algorithm (Shuster, 1978), (Shuster and Oh, 1981) on the basis of Davenport's q-method. QUEST consists in solving numerically the equation $\mathbf{det}(K - \lambda I_4) = 0$, or equivalently (see (Shuster, 1978))

$$\lambda^4 - (a + b)\lambda^2 - c\lambda + (ab + c\gamma - d) = 0, \tag{3.5}$$

---

1. These solutions were sent to Wahba and he presented them in that paper.
2. $\mathbf{det}(U)$ can be either 1 or -1.
3. Note that any symmetric matrix is diagonalizable.

with $a \triangleq \gamma^2 - \mathbf{tr}(\mathbf{adj}(C))$ [4], $b \triangleq \gamma^2 + |z|^2$, $c \triangleq \mathbf{det}(C) + z^\top C z$, $d \triangleq z^\top C^2 z$. More precisely, based on Shuster's observation that λ_{max} is close to $\lambda_o \triangleq \sum_{i=1}^{n \geq 2} a_i$, QUEST makes use of the Newton-Raphson iteration method to solve Eq. (3.5), with λ_o as the initial estimate. It thus avoids the computation of all eigenvalues of K (*i.e.* all solutions to Eq. (3.5)). Theoretically, QUEST is less robust than Davenport's q-method, but it is clearly faster (normally one iteration is sufficient) and has proved itself reliable in practice (*e.g.* QUEST was implemented in the Magsat satellite in 1979). Many alternative numerical solutions for QUEST and Davenport's q-method to Wahba's problem have been proposed like, for instance, the Singular Value Decomposition (SVD), the Fast Optimal Attitude Matrix (FOAM), the Estimator of the Optimal Quaternion (ESOQ), ESOQ-1, ESOQ-2 algorithms (Markley and Mortari, 2000). These solutions, along with QUEST, for Wahba's problem require a trade-off between computational time and precision; for instance, the number of iterations has to be defined in advance. Additionally, their main shortcoming concerns the memoryless characteristic, that is the information contained in measurements of past attitudes is loss.

Because a filtering algorithm is usually preferred when measurements are obtained over a range of times, many alternative solutions have been proposed. They combine the vector measurements with the kinematic model of rotation and the angular velocity measurements (*i.e.* rate or gyro measurements). We will use the term *"model-based attitude filtering methods"* to distinguish them from the solutions presented previously which are based solely on vector observations. In this manner, the attitude estimation methods such as TRIAD, QUEST, SVD, FOAM, ESOQ, *etc.* can still be of use as a preprocessor (*i.e.* the role of an attitude sensor) for a certain number of model-based attitude filtering methods, like in many Kalman filters (KFs), extended Kalman filters (EKFs), or Kalman-like filters (*e.g.* (Farrell, 1964), (Lefferts et al., 1982), (Markley, 2003), (Crassidis et al., 2007), (Bonnabel, 2007) and the references therein), or nonlinear filters (*e.g.* (Mahony et al., 2005), (Mahony et al., 2008), (Thienel and Sanner, 2003), (Vik and Fossen, 2001)). However, this process is not a prerequisite. It is loosened in many model-based attitude filtering methods, including KFs and EKFs, as proposed in (Shuster, 1989b), (Shuster, 1990), (Bar-Itzhack, 1996), (Hamel and Mahony, 2006), (Mahony et al., 2008), (Mahony et al., 2009), (Martin and Salaun, 2007), (Vasconcelos et al., 2008), (Crassidis et al., 2007), *etc..* This leads to simpler, faster, and (probably) more accurate methodologies. For instance, consider the filter QUEST algorithm (a recursive discrete-time Kalman-like estimator) proposed in (Shuster, 1989b), (Shuster, 1990). The author proposes to calculate the estimated attitude using QUEST algorithm and by propagating and updating the matrix B (which is, itself, involved in the Davenport matrix K) as

$$B(t_k) = \mu \Phi_{3 \times 3}(t_k, t_{k-1}) B(t_{k-1}) + \sum_{i=1}^{n_k} a_i v_i^* v_i^\top,$$

where $\Phi_{3 \times 3}(t_k, t_{k-1}) B(t_{k-1})$ is the state transition matrix of the transpose of the rotation matrix R, μ is a fading memory factor, and n_k is the number of vector observations at time t_k. An alternative sequential algorithm for the filter QUEST is the recursive quaternion estimator (REQUEST) (Bar-Itzhack, 1996) which propagates and updates the Davenport

---

4. Recall that $\mathbf{adj}(A)\, A = A\, \mathbf{adj}(A) = \mathbf{det}(A) I_n$, for an $n \times n$ matrix A.

matrix K by

$$K(t_k) = \mu\Phi_{4\times4}(t_k, t_{k-1})B(t_{k-1}) + \sum_{i=1}^{n_k} a_i K_i,$$

where $\Phi_{4\times4}(t_k, t_{k-1})B(t_{k-1})$ is the quaternion state transition matrix and K_i is the Davenport matrix for a single vector observation

$$K_i = \begin{bmatrix} v_i^* v_i^\top + v_i v_i^{*\top} - (v_i^{*\top} v_i)I_3 & (v_i^* \times v_i) \\ (v_i^* \times v_i)^\top & v_i^{*\top} v_i \end{bmatrix}.$$

The main shortcoming of the filter QUEST and REQUEST algorithms concerns the fading memory factor μ which, being arbitrarily chosen, makes these solutions *suboptimal* filters. This leads to the development of the Optimal-REQUEST algorithm (Choukroun, 2003)[Ch.3] which, being essentially based on the REQUEST algorithm, further optimally calculates the fading memory factor μ in the update stage of REQUEST according to a covariance optimization argument. Note that the filter QUEST, REQUEST, and Optimal-REQUEST algorithm, being based on QUEST, are numerical gradient methods. Another interesting example is the nonlinear *explicit complementary filter* proposed in (Mahony et al., 2008)). This method is basically inspired by the *Luenberger observer* (Luenberger, 1971) in the sense that the dynamics of the estimated attitude, denoted as $\widehat{R}$, contains two parts: a main part copying the dynamics of the real attitude (*i.e.* Eq. (3.1)), and an innovation part allowing the correction of the estimated attitude to the real attitude. For instance, if the gyro measurements are not affected by biases, the observer dynamics is given by

$$\dot{\widehat{R}} = \widehat{R}S\left(\omega + \sum_{i=1}^{n} k_i v_i^* \times \widehat{R}^\top v_i\right),$$

with k_i positive constants. An important issue of the attitude filtering concerns the gyro drifts, leading to a complementary approach in which the gyroscopes are used to filter the vector measurements and the vector measurements are in turn used to estimate the gyro drifts (*e.g.* (Mahony et al., 2008), (Thienel and Sanner, 2003), (Vik and Fossen, 2001), (Lefferts et al., 1982)). By making a *constant gyro drift assumption* (*i.e.* $\omega_m = \omega + b$, with ω_m the gyro measurement and b the constant gyro drift vector), a complete version of the *explicit complementary filter* is proposed in (Mahony et al., 2008)) as

$$\begin{cases} \dot{\widehat{R}} &= \widehat{R}S(\omega_m - \widehat{b} + \sigma) \\ \dot{\widehat{b}} &= -k_b\sigma \\ \sigma &= \sum_{i=1}^{n} k_i v_i^* \times \widehat{R}^\top v_i \end{cases}$$

with k_b, k_i positive constants. This is a continuous version; however, a discrete version can be easily derived. It can also be conveniently rewritten in quaternion form. The authors proved that with at least two non-collinear vector observations the estimated attitude exponentially converges to the real one, for almost all initial conditions. Furthermore, a fast attitude estimation method from vector observations like TRIAD or QUEST can be used for a good initial attitude estimate. Note also that in the case of a single vector observation, the solutions to this filter are still well-posed whereas analytically reconstructing the attitude from a single vector observation is not possible.

In view of the above survey, one notes that most of existing methods of attitude estimation make use of the measurements of at least two known vectors. However, an important issue encountered in practice concerns the difficulty of obtaining measurements of two known vectors. As a matter of fact, it has been shown that a single vector observation is sufficient for attitude estimation under a condition of *"persistent excitation"* (*i.e.* if the vector's direction or the vehicle's attitude is permanently varying) (see *e.g.* (Mahony et al., 2009)). But this assumption is rather restrictive from an application point of view. Other remedies are approximative nonlinear solutions (see *e.g.* (Mahony et al., 2008), (Martin and Salaun, 2007), (Pflimlin et al., 2005)) based on measurement data of an embedded IMU which consists of gyroscopes, accelerometers, and magnetometers [5]. They approximate the accelerometer measurements by the measurement of the gravity, under a *"weak acceleration assumption"*. In fact, they provide rather good experimental results in indoor operations, for a certain number of prototypes of VTOL vehicles (see *e.g.* (Mahony et al., 2008), (Pflimlin et al., 2005)). However, the quality of the estimated attitude provided by these methods is far from satisfying when the vehicle is subjected to important accelerations. To cope with strong accelerations, a complementary GPS measurement of the vehicle's linear velocity can be used to estimate the vehicle's linear acceleration and, subsequently, to improve the precision of the estimated attitude [6]. In this manner, a nonlinear observer for GPS-based Attitude and Heading Reference System (AHRS) has been proposed recently in (Martin and Salaun, 2008), based on the construction of an *invariant observer* (Bonnabel et al., 2008). It exhibits interesting physical properties, illustrated by convincing simulation and experimental results. However, the stability and convergence analysis given in (Martin and Salaun, 2008), based on the linearized estimation error system, only guarantees local convergence and stability. Motivated by this result, we propose in this thesis two other attitude observers with associated Lyapunov-based convergence and stability analyses. The first observer ensures semi-global exponential convergence and stability and suggests that a high-gain observer is the price to pay for a large basin of attraction. In turn, the second observer ensures almost global convergence without the *"high-gain assumption"*. An inconvenience, however, is that its stability has yet to be derived for the case when the vehicle's linear acceleration is not constant. Which of these observers is best in practice may depend on sensor characteristics. So far, simulation results show similar performance between the two solutions proposed here and the solution proposed in (Martin and Salaun, 2008). It has also been observed that all these three solutions outperform approximation based ones proposed in the literature when the vehicle's linear acceleration is not small compared to the gravitational acceleration.

This chapter is organized as follows. Attitude parametrizations are recalled in Section 3.2. Directional sources and sensors are described in Section 3.3. Section 3.4 is devoted to our contributions to attitude estimation.

3.2   Recalls on attitude parametrizations

Let us first introduce some definitions. A k-dimensional parametrization of the group of rotation SO(3) is the process of finding a subset U^k of Euclidean space $\mathbb{R}^k$, and an

---

5. The magnetometers provide the measurement of the geomagnetic direction, but the accelerometers only measure the gravity direction during non-accelerated motion.

6. The involvement of the GPS measurement is in turn a price to pay.

associated smooth function $\gamma : U^k \longrightarrow \mathrm{SO}(3)$ such that around each point $p_o \in U^k$, γ is locally subjective (*i.e.* γ send any neighborhood of $p_o \in U^k$ into a neighborhood of $\gamma(p_o)$ in SO(3)). A parametrization is 1-1 if the function γ is a global diffeomorphism. It is 2-1 if the function γ is a local diffeomorphism and for any $R \in \mathrm{SO}(3)$ there exist two and only two elements $u_1, u_2 \in U^k$ such that $\gamma(u_1) = \gamma(u_2) = R$. A parametrization is singular if there exists an element $R \in \mathrm{SO}(3)$ such that the solution to the equation $\gamma(u) = R$ is not well-posed (*i.e.* there does not exist any solution or there exists an infinity of solutions).

Studies about the rotation group SO(3) started in the eighteenth century. As a matter of fact, the problem of parametrization of the group of rotation of the Euclidean 3D-space has been of interest since 1776, when Euler first showed that this group is a three-dimensional manifold. A rotation matrix has nine scalars components. However, it is possible to represent an element of the group of rotation by a set of less than nine parameters, and three is the minimum number of parameters needed for this. Nevertheless, it was shown that no three-dimensional parametrization can be 1-1 (Stuelpnagel, 1964). Previously in 1940 Hopf showed that no four-dimensional parametrization can be 1-1, and that a five-dimensional parametrization can be used to represent the rotation group in a 1-1 global manner. However, the greatest inconvenience of Hopf's five-dimensional parametrization concerns the nonlinearity of the associated differential equations (see *e.g.* (Stuelpnagel, 1964)). On the other hand, four-dimensional parametrizations (see *e.g.* (Stuelpnagel, 1964), (Robinson, 1958)), alike the quaternions parametrization, only represent the rotation group in a 2-1 way. Nevertheless, although the quaternion parametrization is not 1-1, no difficulty arises for practical purposes because the transformation of a unit quaternion to SO(3) is everywhere a local diffeomorphism. Hereafter, the Euler angles and the quaternion parametrizations are recalled and discussed. These parametrizations, and many others, are also discussed in the survey papers (Stuelpnagel, 1964), (Shuster, 1993).

3.2.1 Euler angles parametrization

A number of three-dimensional parametrizations can be found in the literature (see *e.g.* (Stuelpnagel, 1964)), among which the Euler angles parametrization is most widely-used. As a matter of fact, the definition of the Euler angles depends on the problem to be solved and on the chosen systems of coordinates. The definition adopted here is the definition commonly used in the aerospace field for which the Euler angles ϕ, θ, ψ correspond to the parameters of roll, pitch, and yaw (see *e.g.* (Stuelpnagel, 1964), (Mayer, 1960)). The corresponding Euler angles are defined by

$$
\begin{cases}
\cos\phi = \dfrac{r_{3,3}}{\sqrt{r_{1,1}^2 + r_{2,1}^2}}, & \sin\phi = \dfrac{r_{3,2}}{\sqrt{r_{1,1}^2 + r_{2,1}^2}}, \\[3mm]
\cos\theta = \sqrt{r_{1,1}^2 + r_{2,1}^2}, & \sin\theta = -r_{3,1}, \\[3mm]
\cos\psi = \dfrac{r_{1,1}}{\sqrt{r_{1,1}^2 + r_{2,1}^2}}, & \sin\psi = \dfrac{r_{2,1}}{\sqrt{r_{1,1}^2 + r_{2,1}^2}}.
\end{cases}
$$

with $r_{i,j}$ the component of row i and column j of the rotation matrix R. The Euler angles allows to factorize R into a product of three matrices of rotation about three axes of the

body frame, as

$$
\begin{aligned}
R &= \begin{bmatrix} \cos\psi & -\sin\psi & 0 \\ \sin\psi & \cos\psi & 0 \\ 0 & 0 & 1 \end{bmatrix} \begin{bmatrix} \cos\theta & 0 & \sin\theta \\ 0 & 1 & 0 \\ -\sin\theta & 0 & \cos\theta \end{bmatrix} \begin{bmatrix} 1 & 0 & 0 \\ 0 & \cos\phi & -\sin\phi \\ 0 & \sin\phi & \cos\phi \end{bmatrix} \\
&= \begin{bmatrix} \cos\theta\cos\psi & \sin\theta\sin\phi\cos\psi - \sin\psi\cos\phi & \sin\theta\cos\phi\cos\psi + \sin\psi\sin\phi \\ \cos\theta\sin\psi & \sin\theta\sin\phi\sin\psi + \cos\psi\cos\phi & \sin\theta\cos\phi\sin\psi - \cos\psi\sin\phi \\ -\sin\theta & \cos\theta\sin\phi & \cos\theta\cos\phi \end{bmatrix}.
\end{aligned}
\tag{3.6}
$$

From Eq. (3.1) and Eq. (3.6), a direct calculation gives (see *e.g.* (Stuelpnagel, 1964), (Mayer, 1960))

$$
\begin{cases}
\dot{\phi} = \omega_1 + \sin\phi\tan\theta\,\omega_2 + \cos\phi\tan\theta\,\omega_3 \\
\dot{\theta} = \cos\phi\,\omega_2 - \sin\phi\,\omega_3 \\
\dot{\psi} = \dfrac{\sin\phi}{\cos\theta}\omega_2 + \dfrac{\cos\phi}{\cos\theta}\omega_3
\end{cases}
$$

If $r_{1,1}^2 + r_{2,1}^2 = 0$, *i.e.* $r_{3,1} = \pm 1$, then $\theta = \pm\pi/2$, but ϕ and ψ are no longer well-defined. Therefore, the Euler angles constitute a parametrization of the rotation group, except at points (on the subset) corresponding to $\theta = \pm\pi/2$. Furthermore, when $\theta = \pm\pi/2$, $\dot{\phi}$ and $\dot{\psi}$ are not well-defined either. The problem of singularities is a weakness of the Euler angles parametrization and, as a matter of fact, of all three-dimensional parametrization techniques.

3.2.2 Quaternion parametrization

Compared to three-dimensional parametrizations, four-dimensional parametrizations allow to avoid singularities. The earliest formulation of the four-dimensional parametrization, as pointed out in (Robinson, 1958), was given by Euler in 1776. Earlier in 1775, he stated that in three dimensions, every rotation has an axis. This statement can be reformulated as follows (see *e.g.* (Robinson, 1958), (Palais and Palais, 2007) for the proof)

Euler's theorem: *For any $R \in SO(3)$, there is a non-zero vector* v *satisfying Rv $=$ v.*

This theorem implies that the attitude of a body can be specified in terms of a rotation by some angle about some fixed axis. It also indicates that any rotation matrix has an eigenvalue equal to one. A number of four-dimensional parametrizations can be found in the literature (see *e.g.* (Robinson, 1958), (Shuster, 1993), (Borgne, 1987)) such as the Euler parameters, the quaternion parameters, the Rodrigues parameters, and the Cayley-Klein parameters. Here, only the quaternion parameters are presented.

The quaternions were first invented by Hamilton in 1843 (Hamilton, 1843), (Hamilton, 1844), and further studied by Cayley and Klein. A unit quaternion has the form

$$
q = s + ir_1 + jr_2 + kr_3,
$$

where s, r_1, r_2, r_3 are real numbers satisfying $s^2 + r_1^2 + r_2^2 + r_3^2 = 1$, called *constituents* of the quaternion q; and i, j, k are *imaginary units* which satisfy

$$
i^2 = j^2 = k^2 = -1,\ ij = -ji = k,\ jk = -kj = i,\ ki = -ik = j.
$$

In the literature the quaternion q can be represented in a more concise way as $q = [s, r]^\top$, with $s \in \mathbb{R}$ the real part of the quaternion q and $r = [r_1, r_2, r_3]^\top \in \mathbb{R}^3$ its pure part or

imaginary part. The quaternions are not commutative, but associative, and they form a group known as the quaternion group where the unit element is $\mathbf{1} \triangleq [1, 0]^\top$ and the quaternion product $\star$ associated with this group is defined by

$$\begin{bmatrix} s \\ r \end{bmatrix} \star \begin{bmatrix} \bar{s} \\ \bar{r} \end{bmatrix} = \begin{bmatrix} s\bar{s} - r^\top \bar{r} \\ s\bar{r} + \bar{s}r + r \times \bar{r} \end{bmatrix}.$$

The transformed rotation matrix R is uniquely defined from the unit quaternion q as follows

$$R = \begin{bmatrix} s^2 + r_1^2 - r_2^2 - r_3^2 & -2sr_3 + 2r_1r_2 & 2sr_2 + 2r_1r_3 \\ 2sr_3 + 2r_1r_2 & s^2 - r_1^2 + r_2^2 - r_3^2 & -2sr_1 + 2r_2r_3 \\ -2sr_2 + 2r_1r_3 & 2sr_1 + 2r_2r_3 & s^2 - r_1^2 - r_2^2 + r_3^2 \end{bmatrix}. \tag{3.7}$$

This relation is equivalent to Rodrigues' rotation formula

$$R = I_3 + 2s\, S(r) + 2S(r)^2, \tag{3.8}$$

with I_3 the 3×3 identity matrix. Besides, if the rotation matrix R is represented by a rotation by an angle θ about a fixed axis specified by a unit vector $u \in \mathbb{R}^3$, then the above equation is equivalent to

$$R = I_3 + \sin\theta\, S(u) + 2\sin^2(\theta/2)\, S(u)^2$$

On the other hand, converting a rotation matrix to a quaternion is less direct. Using Eq. (3.7) one obtains

$$\begin{cases} s^2 = \dfrac{1 + r_{1,1} + r_{2,2} + r_{3,3}}{4}, \; r_1^2 = \dfrac{1 + r_{1,1} - r_{2,2} - r_{3,3}}{4}, \\[2mm] r_2^2 = \dfrac{1 - r_{1,1} + r_{2,2} - r_{3,3}}{4}, \; r_3^2 = \dfrac{1 - r_{1,1} - r_{2,2} + r_{3,3}}{4}, \\[2mm] sr_1 = \dfrac{r_{3,2} - r_{2,3}}{4}, \; sr_2 = \dfrac{r_{1,3} - r_{3,1}}{4}, \; sr_3 = \dfrac{r_{2,1} - r_{1,2}}{4}, \\[2mm] r_1r_2 = \dfrac{r_{2,1} + r_{1,2}}{4}, \; r_2r_3 = \dfrac{r_{2,3} + r_{2,3}}{4}, \; r_3r_1 = \dfrac{r_{3,1} + r_{1,3}}{4}. \end{cases} \tag{3.9}$$

There always exists at least one component of the unit quaternion q different from zero. Once this component is identified, the quaternion can be directly deduced from the relations given in Eq. (3.9). Note that only two values of the quaternion q correspond to the rotation matrix R, and that they have opposed signs. For example, if $\mathbf{tr}(R) \neq -1$, then

$$s = \pm\frac{1}{2}\sqrt{1 + \mathbf{tr}(R)}, \; S(r) = \frac{R - R^\top}{4s}.$$

It matters now to express the time-derivative of the quaternion q. One has

$$\begin{bmatrix} \dot{s} \\ \dot{r}_1 \\ \dot{r}_2 \\ \dot{r}_3 \end{bmatrix} = \frac{1}{2} \begin{bmatrix} 0 & -\omega_1 & -\omega_2 & -\omega_3 \\ \omega_1 & 0 & \omega_3 & -\omega_2 \\ \omega_2 & -\omega_3 & 0 & \omega_1 \\ \omega_3 & \omega_2 & -\omega_1 & 0 \end{bmatrix} \begin{bmatrix} s \\ r_1 \\ r_2 \\ r_3 \end{bmatrix},$$

or, equivalently

$$\dot{q} = \frac{1}{2}q \star \begin{bmatrix} 0 \\ \omega \end{bmatrix}.$$

The quaternion parametrization involves four parameters (*i.e.* only one redundant parameter) and is free of singularities. The associated differential equation is linear in q. Furthermore, the structure of the quaternion group is, by itself, of great interest. In view of the above remarks, one may wonder why the Euler angles parametrization is still widely used especially for aircraft control. Robotists and automaticians working on nonlinear control and estimation are not fond of the Euler angles parametrization due to the associated singularities and increased nonlinearity of the representation. On the contrary, engineers and automaticians used to linear control techniques for aircrafts find reasons to defend this parametrization. For instance, most of aircrafts are designed and controlled in such a way that the pitch and roll Euler angles are limited to small values, away from singularities. When applying linear control techniques based on first order approximations, the Euler angles parametrization equally allows for the decoupling of the altitude control and the longitudinal control. Historical and security issues may also impede the replacement of existing linear control techniques by any nonlinear control technique without costly and long-term validation procedures. Such a debate never ends, and changing habits is never simple.

3.3   Vector measurements and sensors

As a result of evolution, living beings possess several natural means of orientation with respect to the surrounding environment. Vision is perhaps the most versatile one, despite several shortcomings and pitfalls. Quite useful directional input is the earth's gravity field which can be sensed by many living beings. Some species, like birds or whales, are also able to sense and use the geomagnetic field for navigation purposes. Human beings unfortunately do not possess this ability. However, human inventions allow to bypass this shortcoming. The magnetic compass is known as the very first orientation measurement instrument invented by mankind. It was probably first made in China during the Qin dynasty (221-206 B.C.) (see Fig. 3.1), and Zheng He (1371-1435) was the first person recorded to have used the compass as a navigational aid during his seven ocean voyages between 1405 and 1433 (Ding et al., 2007). Early inclinometers for measuring angles of tilt, elevation, or inclination of an object with respect to the earth's gravity include Well's inclinometer, Rufus Porter's inclinometer, Gibson's inclinometer, *etc.*. They are direct descendants of the oldest form of leveling device: the plumb bob. Since the last decades, a considerable number of direction measurement instruments have been invented, as a result of great demands for aerospace and maritime navigation and control, and of fast technological development. One can mention magnetometers (Hall effect magnetometer, Giant Magnetoresistance (GMR) magnetometer, Proton precession magnetometer, Fluxgate magnetometer, Overhauser magnetometer, Cesium vapor magnetometer, SQUID magnetometer, *etc.*), inclinometers (accelerometer, liquid capacitive, electrolytic, *etc.*), orbital gyrocompasses, sun sensors, star trackers, cameras, *etc.* as examples. Last but not least, the Global Positioning System (GPS) can be used as an orientation measurement sensor.

The appearance of the GPS (in 1978, initially for the United States Air Force) and especially its availability for civil applications (since 1995) have revolutionized the aerospace and maritime Guidance, Navigation and Control. Beside its well-known utility as a positioning device, or for linear velocity and time measurements (see *e.g.* (Grewal et al., 2001),
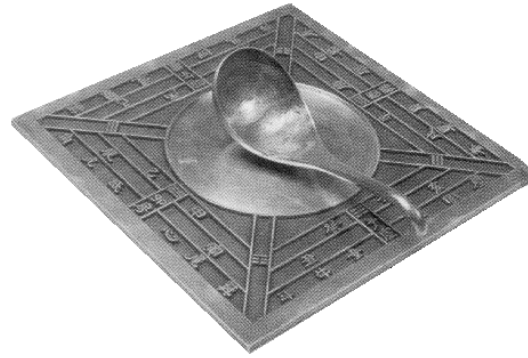
Figure 3.1: The first compass of the world: a Chinese "spoon compass".

(El-Rabbany, 2002), (Tsui, 2005)), the GPS is also one of the most widely-used sensors for attitude estimation. The problem of attitude estimation from GPS-measurements has been addressed in several studies (Ellis and Creswell, 1979), (Brown, 1981), (Brown, 1992), (Cohen, 1992), (Lu, 1995), (Crassidis and Markley, 1997), (Bar-Itzhack et al., 1998), (Li et al., 2004). Basically, the proposed methods rely on the use of a GPS multi-antenna system which integrates three or more GPS antennas into a simple system with a proper antenna configuration on a platform. These antennas form at least two non-collinear baseline vectors [7], where a baseline vector is the relative position vector from one antenna to another expressed in the vehicle's body frame. The GPS multi-antenna system provides vector measurements, *e.g.* the baseline vectors or the vectors from the platform to the observed satellites, using the differential carrier phase measurements with integer ambiguity resolution. From these measurements, numerous methods can be applied to estimate the platform attitude (see Section 3.1). For illustration purposes let us consider a simple example given in (Bar-Itzhack et al., 1998). In this example three integrated antennas form
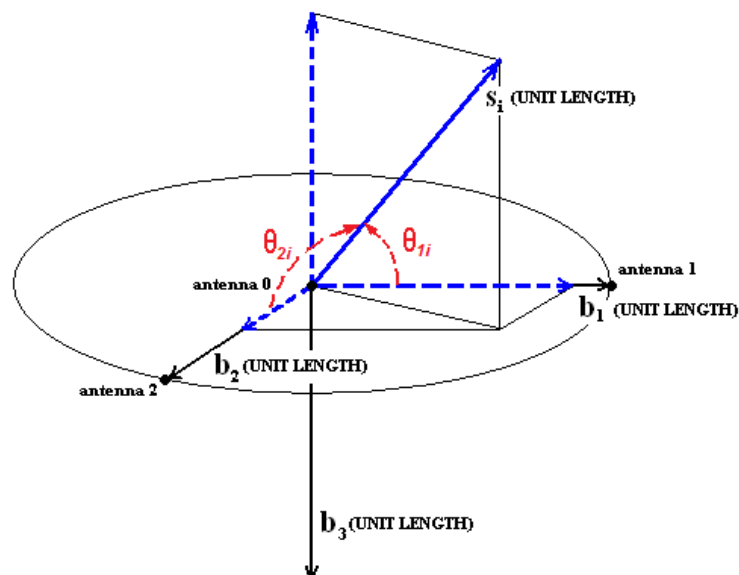
Figure 3.2: Definition of the antenna coordinate system.

7. Note that only one baseline is needed for heading estimation in 2D-plane.

two baselines which lie on two axis of a Cartesian triad as follows: the origin of this system is at antenna 0, the system x-axis corresponding to the baseline unit vector b_1 is along the line connecting antenna 0 and antenna 1, and the y-axis corresponding to the baseline unit vector b_2 is along the line connecting antenna 0 and antenna 2 (see Fig. 3.2). Let s_i be a unit vector (expressed in the inertial reference frame) in the direction of the observed GPS satellite i (*i.e.* ith sightline), and θ_{ji} be the angle between b_j ($j = 1, 2$) and s_i, one has

$$\cos \theta_{ji} = b_j^\top R^\top s_i.$$

Besides, $\cos \theta_{ji}$ is related to the phase difference ϕ_{ji} between simultaneous phase measurements at antenna 0 and antenna j of the carrier wave broadcasted by the GPS satellite i as follows

$$\phi_{ji} = \frac{l_j}{\lambda} \cos \theta_{ji},$$

with l_j the length of the baseline j and λ the wavelength of the GPS signal. Therefore, if ϕ_{ji} is known, then $\cos \theta_{ji}$ is also known. However, by performing the carrier-phase differencing, one only obtains the measurement of $\phi'_{ji} \in [0; 1)$, the fraction of wavelength, which satisfies

$$\phi_{ji} = \phi'_{ji} + n_{ji},$$

with n_{ji} the unknown integer ambiguity. This integer ambiguity has to be removed. This problem has constituted a research topic up to now since the early stages of the GPS development. Let us cite, for instance, in the case of GPS position measurements, (Hatch, 1990), (Hwang, 1990), (Chen, 1994), (Teunissen, 1994), (Chen and Lachapelle, 1995), (Han and Rizos, 1996), (Lightsey et al., 1999), (Kim and Langley, 2000)). Extensions of these integer ambiguity resolution methods have been developed for attitude estimation purposes (Cohen, 1992), (Lu, 1995), (Hill and Euler, 1996), (Pervan and Parkinson, 1997), (Crassidis et al., 1999), (Sutton, 1997), (Sutton, 2002). Now, assuming that n_{ji}, and thus that the measurement of ϕ_{ji} are available, one deduces the calculation of the unit vector s_i^* (expressed in the body frame) in the direction of the GPS satellite i (see Fig. 3.2) as

$$s_i^* = \begin{bmatrix} \dfrac{\lambda}{l_1} \phi_{1i} \\[2mm] \dfrac{\lambda}{l_2} \phi_{2i} \\[2mm] -\sqrt{1 - \left(\dfrac{\lambda}{l_1}\phi_{1i}\right)^2 - \left(\dfrac{\lambda}{l_2}\phi_{2i}\right)^2} \end{bmatrix}.$$

Note that the calculation of s_i is also available if the positions of the GPS satellite i and of the vehicle are known. Therefore, if at least two GPS sightlines are observed, then the vehicle's attitude can be estimated from this GPS multi-antenna system.

Attitude estimation based on GPS multi-antenna systems has found several applications. Nevertheless, it has also a few drawbacks which require close attention:

1. As a general rule, the accuracy of the estimated attitude is inversely proportional to the baseline lengths. This means that the antenna separation within a multi-antenna system should be as long as possible in order to obtain accurate attitude parameters. Limited accuracy of the estimated attitude is thus to be expected for small-size vehicles.

2. GPS measurements are subjected to several error sources (*e.g.* measurement noise, satellite clock bias, receiver clock bias, multipath, ionospheric refraction, tropospheric refraction, *etc.*) of which the carrier phase multipath is almost inevitable. It is also most troublesome because the vector measurements are based on the differential carrier phase measurements (see *e.g.* (Cohen, 1992), (Lu, 1995, Ch.2), (Treichler and Agee, 1983), (Axelrad et al., 1996)). As a consequence, the estimated attitude in urban zones can be very erroneous. An informative discussion about the carrier phase multipath effect on the platform attitude estimation is given in (Lu, 1995, Ch.2). Another survey on GPS error sources are available in (Chen, 1994, Ch.2).

3. All existing methods of integer ambiguity resolution for GPS multi-antenna systems are iterative search methods. The number of required searches can be excessive and it rapidly increases with the baseline lengths. As a consequence, computational time, which depends on the calculation capacity, may impede real time applications. Furthermore, it is worth noting that existing methods may fail to provide exact solutions (see (Teunissen, 1998), (Teunissen, 1999), (Teunissen, 2000)).

These are the three main weaknesses of GPS multi-antenna systems for vector measurements and, therefore, for attitude estimation. However, despite their weaknesses GPS multi-antenna systems remain interesting for the following reasons:

1. Other types of direction measurement sensors have also their own shortcomings. For instance, sun sensors, star trackers, or gyrocompasses are hindered by their high price, important weight, and limited operational conditions. A magnetometer can be strongly influenced by magnetic perturbations generated by electric engines or other sources. An inclinometer does not exactly measure the gravity direction during accelerated motions. A sensor like a magnetometer or an inclinometer only provides the measurement of a simple vector (*i.e.* the geomagnetic field, the gravity) so that it needs to be combined with another sensor capable of measuring a second, non-collinear, vector in order to satisfy the condition of uniform observability for the attitude estimation problem. Cameras provide only relative direction measurements with respect to the observed environment, *etc.*.

2. GPS multi-antenna systems provide simultaneously measurements of many vectors (at least of the two baselines). Long term stability and high accuracy of vector measurements can be obtained if the considered vehicle is large enough to yield large antennas separation and if powerful processors are available to implement integer ambiguity resolution algorithms on line.

Sources (either natural or artificial) providing orientation information and associated sensors have been outlined in this section. They are complementary and they can be combined to design an effective and reliable attitude sensor. But, it is important to keep in mind that no universal solution for attitude estimation is available today. For instance, a GPS multi-antenna system is a good choice for large vehicles such as airplanes or cargo ships, while a combination of magnetometers and inclinometers is likely preferable in the case of small flying drones. This choice is thus made case-by-case, depending on many factors such as the considered application, the required precision, the sensors' price and weight, the system dynamics, *etc.*. Furthermore, the method used for attitude estimation directly impacts on the quality of the estimated attitude which itself impacts on the control performance.

3.4 Attitude estimation based on GPS/INS fusion

We have seen in the previous sections that the attitude can be estimated via the use of many types of sensors. In the present study we have opted for the GPS/INS fusion solution for a certain number of reasons which, beyond economic and practical motivations, include the theoretical challenge [8] associated with the fact that accelerometers do not directly measure the gravity direction during accelerated motions.

3.4.1 Preliminary

A rigid body moving inside the earth's gravity field satisfies the following equations (see *e.g.* (Mahony et al., 2008), (Martin and Salaun, 2008))

$$
\begin{cases}
\dot{v}_{\mathcal{I}} &= ge_3 + Ra_{\mathcal{B}} \\
\dot{R} &= RS(\omega)
\end{cases}
\tag{3.10}
$$

where $v_{\mathcal{I}} \in \mathbb{R}^3$ is the body's linear velocity expressed in the inertial frame $\mathcal{I}$; $a_{\mathcal{B}}$ is the so-called *"specific acceleration"* representing the sum of all non-gravitational forces applied to the body divided by its mass, expressed in the body frame $\mathcal{B}$; ge_3 is the gravitational acceleration expressed in the inertial frame $\mathcal{I}$.

Supposing that the embedded GPS and IMU on the vehicle are well-calibrated, the following measurements are assumed to be available:

- *GPS-velocity:* measures the linear velocity $v_{\mathcal{I}}$.

- *Gyroscopes:* measure the angular velocity ω.

- *Accelerometers:* measure the specific acceleration $a_{\mathcal{B}}$. By defining

$$
a_{\mathcal{I}} \triangleq \dot{v}_{\mathcal{I}} - ge_3,
\tag{3.11}
$$

  one has $a_{\mathcal{B}} = R^\top a_{\mathcal{I}}$.

- *Magnetometers:* whose measurements are normalized to obtain $m_{\mathcal{B}}$, the normalized geomagnetic field expressed in the body frame $\mathcal{B}$. One has $m_{\mathcal{B}} = R^\top m_{\mathcal{I}}$, with $m_{\mathcal{I}}$ the normalized geomagnetic field expressed in the inertial frame $\mathcal{I}$.

Let $\widehat{v}_{\mathcal{I}}$ and $\widehat{R}$ denote estimates of $v_{\mathcal{I}}$ and R respectively. Define the error variables

$$
\widetilde{v} \triangleq v_{\mathcal{I}} - \widehat{v}_{\mathcal{I}}, \; \widetilde{R} \triangleq R\widehat{R}^\top.
\tag{3.12}
$$

The objective of observer design can be stated as the combined stabilization of $\widetilde{v}$ to zero and $\widetilde{R}$ to I_3.

Let us first recall a particular case of the attitude observer proposed in (Hamel and Mahony, 2006), (Mahony et al., 2008) by fusing the measurements in the body frame $\mathcal{B}$ of two non-collinear directions $\overrightarrow{\alpha}$, $\overrightarrow{\beta}$ with the angular velocity measurements. Denote $\alpha_{\mathcal{I}}$,

---

8. After all "Math is fun" as stated Terence Tao.

$\alpha_{\mathcal{B}}$, $\beta_{\mathcal{I}}$, $\beta_{\mathcal{B}}$ as the vectors of coordinates of $\overrightarrow{\alpha}$ and $\overrightarrow{\beta}$, expressed in the inertial frame $\mathcal{I}$ and the body frame $\mathcal{B}$ respectively. This observer has the form

$$\begin{cases} \dot{\widehat{R}} &= \widehat{R}S(\omega + \sigma) \\ \sigma &= k_\alpha \alpha_{\mathcal{B}} \times \widehat{R}^\top \alpha_{\mathcal{I}} + k_\beta \beta_{\mathcal{B}} \times \widehat{R}^\top \beta_{\mathcal{I}} \end{cases} \tag{3.13}$$

with k_α, k_β some positive constant gains. It is shown that if all measurements are perfect, $\alpha_{\mathcal{I}}$ and $\beta_{\mathcal{I}}$ are constant, and $|\alpha_{\mathcal{I}} \times \beta_{\mathcal{I}}| \neq 0$, then the estimated attitude exponentially converges to the real one for almost all initial conditions (see *e.g.* (Mahony et al., 2008) for the proof). It is also important to note that this observer still provides the exponential stability property when $\alpha_{\mathcal{I}}$ and $\beta_{\mathcal{I}}$ are time-varying and bounded. In the following proposition we prove this property.

Proposition 13 *Consider the kinematic equation of rotation $\dot{R} = RS(\omega)$ and the attitude observer* (3.13). *Define the set $\mathbb{U} \in SO(3)$ as*

$$\mathbb{U} = \{R \in SO(3) \,|\, \mathbf{tr}(R) = -1\}. \tag{3.14}$$

Suppose that for all $t \in \mathbb{R}_+ \triangleq [0, +\infty)$, $\alpha_{\mathcal{I}}(t)$ and $\beta_{\mathcal{I}}(t)$ are bounded, and there exists a constant $\eta > 0$ such that $|\alpha_{\mathcal{I}}(t) \times \beta_{\mathcal{I}}(t)| \geq \eta$. Then, the equilibrium $\widetilde{R} = I_3$ is exponentially stable with domain of attraction equal to $SO(3)\backslash\mathbb{U}$.

The proof is reported in Section 3.5.2. In our situation, two vectorial measurements are provided by the magnetometers and accelerometers, *i.e.* $m_{\mathcal{B}} = R^\top m_{\mathcal{I}}$ and $a_{\mathcal{B}} = R^\top a_{\mathcal{I}}$. However, since $\dot{v}$ and therefore $a_{\mathcal{I}}$ are not known a priori the above attitude observer (3.13) does not directly apply. Thus, an *approximative attitude observer* has been proposed in (Hamel and Mahony, 2006), (Mahony et al., 2008) which consists in approximating the gravity direction expressed in the body frame $\mathcal{B}$ by the accelerometer measurements (*i.e.* $a_{\mathcal{B}} \approx -gR^\top e_3$), and then applying the attitude observer (3.13) with $\alpha_{\mathcal{I}} = m_{\mathcal{I}}$, $\alpha_{\mathcal{B}} = m_{\mathcal{B}}$, $\beta_{\mathcal{I}} = -ge_3$, $\beta_{\mathcal{B}} = a_{\mathcal{B}}$. This is equivalent to the approximation $a_{\mathcal{I}} \approx -ge_3$, as obtained by Eq. (3.11) when $\dot{v}_{\mathcal{I}} \approx 0$. Unsurprisingly, this solution ensures good performance when $\dot{v}_{\mathcal{I}}$ is small compared to the gravitational acceleration (*i.e.* $|\dot{v}_{\mathcal{I}}| \ll g$), but its performance can become very poor in the case of permanent stronger accelerations. Consequently, the measurements of the linear velocity $v_{\mathcal{I}}$ can be used in order to improve the attitude estimation. An observer of this nature has been recently proposed in (Martin and Salaun, 2008). When measurements are not affected by bias, it is given by

$$\begin{cases} \dot{\widehat{v}}_{\mathcal{I}} = k_1(v_{\mathcal{I}} - \widehat{v}_{\mathcal{I}}) + ge_3 + \widehat{R}a_{\mathcal{B}} \\ \dot{\widehat{R}} = \widehat{R}S(\omega + \sigma) \\ \sigma = k_2((m_{\mathcal{B}} \times \widehat{R}^\top m_{\mathcal{I}})^\top a_{\mathcal{B}})a_{\mathcal{B}} + k_3 a_{\mathcal{B}} \times \widehat{R}^\top(v_{\mathcal{I}} - \widehat{v}_{\mathcal{I}}) \end{cases} \tag{3.15}$$

This defines an *invariant* observer ((Bonnabel et al., 2008), (Lageman et al., 2010)) in the sense that it preserves the (Lie group) invariance properties of System (3.10) with respect to constant velocity translation $v_{\mathcal{I}} \mapsto v_{\mathcal{I}} + v_0$ and constant rotation of the body frame $R \mapsto RR_0$. Another practical advantage of this solution is the (local) decoupling of the roll and pitch angles estimation from the measurements of the earth's magnetic field (which may be rather erroneous due to magnetic perturbations). On the other hand, only local exponential stability of the estimation error is proved in (Martin and Salaun, 2008) (based on the linearized estimation error dynamics), under some assumptions on the reference motion (*i.e.* "smooth trajectory"). We propose next some modifications on observer (3.15) along with associated analyses of convergence and stability.

3.4.2 Invariant attitude observer

The following "weak" assumptions are introduced and discussed.

Assumption 7 *There exist four positive constants $\underline{c}_a$, $\overline{c}_a$, c_v, and c_ω such that $\forall t \in \mathbb{R}_+ \triangleq [0, +\infty)$,*

$$\underline{c}_a \leq |a_\mathcal{I}(t)| \leq \overline{c}_a, \; |\ddot{v}_\mathcal{I}(t)| \leq c_v, \; |\omega(t)| \leq c_\omega.$$

Assumption 8 *(Observability) There exists a constant $c_{obs} > 0$ such that $\forall t \in \mathbb{R}_+$,*
$$\left| m_\mathcal{I}(t) \times \frac{a_\mathcal{I}(t)}{|a_\mathcal{I}(t)|} \right| \geq c_{obs}.$$

Assumption 7 indicates that the body's acceleration is bounded and different from ge_3, and that the time-derivative of the body's acceleration is bounded. These properties are satisfied in "normal" flight conditions. As for Assumption 8, it indicates that the geomagnetic field direction and the direction given by $a_\mathcal{I}$ are never collinear. This condition guarantees the system's observability. From here, the main result of this section is stated next.

Theorem 2 *Consider System (3.10) and the observer system*

$$\begin{cases} \dot{\widehat{v}}_\mathcal{I} &= k_1(v_\mathcal{I} - \widehat{v}_\mathcal{I}) + ge_3 + \widehat{R}a_\mathcal{B} \\ \dot{\widehat{R}} &= \widehat{R}S(\omega + \sigma) \\ \sigma &= k_2 m_\mathcal{B} \times \widehat{R}^\top m_\mathcal{I} + k_3 a_\mathcal{B} \times \widehat{R}^\top(v_\mathcal{I} - \widehat{v}_\mathcal{I}) \end{cases} \quad (3.16)$$

with k_1, k_2, k_3 positive constant gains. Suppose that Assumptions 7 and 8 are satisfied. Then, for any $k_2, k_3 > 0$,

1. *for any $k_1 > 0$, the equilibrium $(\widetilde{v}, \widetilde{R}) = (0, I_3)$ is locally exponentially stable;*

2. *for any closed neighborhood $\mathbb{V}$ of $(0, I_3)$ with $\mathbb{V} \subset \mathbb{R}^3 \times SO(3) \backslash \mathbb{U}$ and $\mathbb{U}$ defined by Eq. (3.14), there exists a constant $\Bbbk_1 > 0$ such that for all $k_1 > \Bbbk_1$ and $(\widetilde{v}(0), \widetilde{R}(0)) \in \mathbb{V}$, the set point $(\widetilde{v}(t), \widetilde{R}(t))$ exponentially converges to the equilibrium $(0, I_3)$.*

The proof is given in Section 3.5.3. Observer (3.16) is very similar to Observer (3.15) which is a simplified version of the observer proposed in (Martin and Salaun, 2008) suited to the case without gyroscope biases. The sole difference between observers (3.15) and (3.16) lies in the definition of σ where the term $k_2((m_\mathcal{B} \times \widehat{R}^\top m_\mathcal{I})^\top a_\mathcal{B})a_\mathcal{B}$ in Observer (3.15) is replaced in Observer (3.16) by $k_2(m_\mathcal{B} \times \widehat{R}^\top m_\mathcal{I})$. Note that Observer (3.16) also defines an invariant observer ((Bonnabel et al., 2008), (Lageman et al., 2010)).

Property 1 of Theorem 2 concerning the local exponential stability is similar to the stability property proved in (Martin and Salaun, 2008), but the present assumptions upon the reference trajectory (Assumptions 1 and 2) are more explicit and less restrictive than those given in (Martin and Salaun, 2008). As for Property 2, it ensures the semi-global stability property under a "high-gain"-like condition on k_1 (see Remark 5 in Section 3.5.3 for details). This condition indicates that the size of the basin of attraction is proportional to the size of k_1, but k_1 tends to infinity only when the initial attitude estimate makes a π-rotation with the true attitude. In practice it should never happen as the initial guess of the body's attitude is never that bad. Furthermore, let us remind that this condition is

only sufficient. Simulation results seem to indicate that the basin of attraction does not depend on the value of k_1 (> 0). But the proof of this property remains an open problem.

Finally, contrary to Observer (3.15), Observer (3.16) does not locally ensure the decoupling of the estimation of the roll and pitch (Euler) angles from the magnetic measurements. More precisely, if we consider motions for which the body's acceleration is negligible against the gravitational acceleration (*i.e.* $a_\mathcal{I} \approx -ge_3$), and linearize the estimation error dynamics, we can verify that the estimation errors of the roll and pitch (Euler) angles, corresponding to Observer (3.15), do not depend upon the magnetic measurements. However, this is not the case with Observer (3.16). More details can be found in Remark 6 in Section 3.5.3. This suggests, as an open problem, the design of an observer combining the advantages of both observers (3.15) and (3.16).

3.4.3 Cascaded attitude observer

In this section we propose another observer for which the associated convergence and stability analyses do not rely on "high-gain" conditions. The design of this observer relies on the following lemma.

Lemma 10 *Consider System (3.10) and the observer*

$$\begin{cases} \dot{\widehat{v}}_\mathcal{I} &= k_1(v_\mathcal{I} - \widehat{v}_\mathcal{I}) + ge_3 + Qa_\mathcal{B} \\ \dot{Q} &= QS(\omega) + k_v(v_\mathcal{I} - \widehat{v}_\mathcal{I})a_\mathcal{B}^\top \end{cases} \tag{3.17}$$

with k_1, k_v some positive constant gains, and $Q \in \mathbb{R}^{3\times3}$ a virtual matrix. Suppose that $\forall t \in \mathbb{R}_+$, $\omega(t)$, $\dot{v}_\mathcal{I}(t)$, and $\ddot{v}_\mathcal{I}(t)$ are bounded. Then,

1. *$\forall (\widehat{v}_\mathcal{I}(0), Q(0)) \in \mathbb{R}^3 \times \mathbb{R}^{3\times3}$, $(\widetilde{v}(t), (a_\mathcal{I} - Qa_\mathcal{B})(t))$ converges to zero;*

2. *furthermore, if the acceleration $\dot{v}_\mathcal{I}$ is constant and $|a_\mathcal{I}| > 0$, then the equilibrium $(\widetilde{v}, a_\mathcal{I} - Qa_\mathcal{B}) = (0, 0)$ is globally exponentially stable.*

The proof is given in Section 3.5.4. Since $(\widetilde{v}, Qa_\mathcal{B})$ converges to $(0, a_\mathcal{I})$, one can view either $Qa_\mathcal{B}$ or $\widehat{v}_\mathcal{I} - ge_3$ ($= k_1\widetilde{v} + Qa_\mathcal{B}$) as the estimate of $a_\mathcal{I}$. Simulation results show that the latter provides better performance. From here, the main result of this section is stated next.

Theorem 3 *Consider System (3.10) and the observer system (3.17) complemented with the following attitude observer*

$$\begin{cases} \dot{\widehat{R}} = \widehat{R}S(\omega + \sigma) \\ \sigma = k_2\, m_\mathcal{B} \times \widehat{R}^\top m_\mathcal{I} + k_3\, a_\mathcal{B} \times \widehat{R}^\top(Qa_\mathcal{B} + k_1(v_\mathcal{I} - \widehat{v}_\mathcal{I})) \end{cases} \tag{3.18}$$

with k_2, k_3 some positive gains, and Q, $\widehat{v}_\mathcal{I}$ given by System (3.17). Define $\xi \triangleq a_\mathcal{I} - Qa_\mathcal{B}$. Suppose that Assumptions 7 and 8 are satisfied. Then,

1. *for any initial condition $(\widehat{v}_\mathcal{I}(0), Q(0), \widehat{R}(0)) \in \mathbb{R}^3 \times \mathbb{R}^{3\times3} \times SO(3)$, $(\xi, \widetilde{v}, \widetilde{R})$ asymptotically converges to the set $\mathbb{E} = \mathbb{E}_u \cup \mathbb{E}_s$ with $\mathbb{E}_u = \{0\} \times \{0\} \times \mathbb{U}$, $\mathbb{E}_s = (0, 0, I_3)$, and $\mathbb{U} \in SO(3)$ defined by Eq. (3.14);*

2. *furthermore, if the acceleration $\dot{v}_{\mathcal{I}}$ is constant, then $\mathbb{E}$ is an equilibrium set with the subset $\mathbb{E}_u$ unstable and the subset $\mathbb{E}_s$ stable.*

The proof is given in Section 3.5.5. The observer given in Theorem 3 uses an auxiliary matrix Q which (surprisingly) is not a rotation matrix. But this matrix is such that $Qa_{\mathcal{B}} - Ra_{\mathcal{B}}$ tends to zero. Thus Q allows an estimation of the specific acceleration in the inertial frame $\mathcal{I}$ (*i.e.* $a_{\mathcal{I}}$). Once this is done, the mathematical problem is very close to the case where the approximation $a_{\mathcal{I}} \approx -ge_3$ is made. Indeed the images by the rotation R of two distinct vectors of the body frame are now known. The form of the attitude observer (3.18) is close to the nonlinear observers already proposed in the literature (*e.g.* (Mahony et al., 2008)) for the attitude estimation problem under the approximation $a_{\mathcal{I}} \approx -ge_3$. Note that Observer (3.18) also defines an invariant observer ((Bonnabel et al., 2008), (Lageman et al., 2010)).

The stability property established in Theorem 3 is weaker than that of Theorem 2 but the convergence result, being independent of the gain values, is stronger. Furthermore, when $\dot{v}_{\mathcal{I}}$ is constant, one obtains the strongest possible result, *i.e.*, stability of the desired equilibrium $\mathbb{E}_s = (0, 0, I_3)$, instability of the "undesired" equilibrium set $\mathbb{E}_u$, and convergence to $\mathbb{E}_u \cup \mathbb{E}_s$. Note that there does not exist any smooth globally asymptotically stable observer due to the topology of the Lie group SO(3). To our knowledge, the simultaneous achievement of these stability and convergence properties in the case of constant accelerations is a new result. Additionally, let us remind that for Observer (3.15) (*i.e.* as proposed in (Martin and Salaun, 2008)) specifying the domain of attraction is not easy to achieve, even in the case of constant accelerations.

In view of the proof of Lemma 10, one ensures that $||Q||$ –the Frobenius norm of Q– remains bounded in the case of perfect measurements. In practice, however, sensor noises and drifts and numerical errors can drive $||Q||$ arbitrarily large which possibly yields large estimation errors. This suggests us to replace the expression of $\dot{Q}$ in System (3.17) by the following

$$\begin{cases} \dot{Q} &= QS(\omega) + k_v(v_{\mathcal{I}} - \hat{v}_{\mathcal{I}})a_{\mathcal{B}}^\top - \rho Q \\ \rho &= k_q \max(0, ||Q|| - \sqrt{3}), \text{ with } k_q > 0 \end{cases} \tag{3.19}$$

Since $a_{\mathcal{I}} = Ra_{\mathcal{B}}$ can be estimated via the vector $Qa_{\mathcal{B}}$, $||Q||$ can be theoretically bounded by $\sqrt{3}$ (*i.e.* the value of the Frobenius norm of any rotation matrix R). The term $-\rho Q$ in the expression of $\dot{Q}$ in System (3.19) creates a dissipative effect when $||Q||$ becomes larger than $\sqrt{3}$, allowing it to be driven back to this threshold and thus avoiding numerical drifts of Q. This astute of robustification does not destroy the convergence properties of Lemma 10 and Theorem 3 (see Remark 7 in Section 3.5.4 for the detailed proof). However, the stability has yet to be derived within this context.

3.4.4 Simulation results

In this section we illustrate through simulation results the performance and robustness of the observers here proposed compared to other solutions proposed in the literature. Simulations are conducted on a model of a small VTOL vehicle. The vehicle's motion consists of a circular trajectory on a horizontal plane. The vehicle's linear velocity is

$$v = [-15\alpha\sin(\alpha t), 15\alpha\cos(\alpha t), 0]^\top \ (m/s) \text{ with } \alpha = 2\sqrt{30}/15.$$

Note that the magnitude of the linear acceleration is equal to eight, a significant value compared to the gravitational acceleration. The normalized earth's magnetic field is taken as $m_\mathcal{I} = [0.434, -0.0091, 0.9008]^\top$ (i.e. the normalized geomagnetic field in Paris). Simulations are carried on for the four following observers:

Observer 1: is the explicit complementary attitude observer (3.13) (proposed in (Hamel and Mahony, 2006), (Mahony et al., 2008)) with $\alpha_\mathcal{I} = m_\mathcal{I}$, $\alpha_\mathcal{B} = m_\mathcal{B}$, $\beta_\mathcal{I} = -ge_3$, and $\beta_\mathcal{B} = a_\mathcal{B}$. The gains have been chosen as $k_\alpha = 3$, $k_\beta = 0.03$. The initial estimation error is $\widetilde{R}(0) = I_3$.

Observer 2: is the invariant observer (3.15) as proposed in (Martin and Salaun, 2008). The gains have been chosen as $k_1 = 3$, $k_2 = 0.03$, and $k_3 = 0.03$. The initial estimation errors are $\widetilde{v}(0) = [-19.7, -14.1, -10]^\top (m/s)$ and $\widetilde{R}(0) = \mathbf{diag}(1, -1, -1)$.

Observer 3: is the observer of Theorem 2. The gains have been chosen as $k_1 = 3$, $k_2 = 3$, and $k_3 = 0.03$. The initial estimation errors are $\widetilde{v}(0) = [-19.7, -14.1, -10]^\top (m/s)$ and $\widetilde{R}(0) = \mathbf{diag}(1, -1, -1)$.

Observer 4: is the observer of Theorem 3 with $\dot{Q}$ defined by System (3.19). The gains have been chosen as $k_1 = 3$, $k_2 = 3$, $k_3 = 0.03$, and $k_v = 0.12, k_q = 1$. The initial conditions are $Q(0) = I_3$, $\widetilde{v}(0) = [-19.7, -14.1, -10]^\top (m/s)$, and $\widetilde{R}(0) = \mathbf{diag}(1, -1, -1)$.

Note that the initial values of Observers 2, 3, and 4 are chosen very far from the real values, so as to test the extent of the associated domains of convergence. Note also that the gains k_α, k_β of Observer 1 and k_2, k_3 of Observers 2, 3, and 4 are chosen so that the four observers possess "similar performance" when $\dot{v} \approx 0$. Three simulations are reported.

▷ **Simulation 1:** allows to compare the performance of these four observers in the case of perfect measurements.

Fig. 3.3: The estimated and real Euler angles (i.e. roll, pitch, and yaw) are shown on Fig. 3.3. Poor performance of Observer 1 can be observed, despite the fact that $\widehat{R}(0) = R(0)$. In turn, Observers 2, 3, and 4 ensure the asymptotic convergence of the estimated attitude to the real one despite the very large initial estimation errors. Note that the sufficient condition for the observer gain k_1 of the observer proposed in Theorem 2, which is given by Eq. (3.45), is based on a number of majorations. Thus, estimating the domain of attraction for a given k_1 is quite conservative. Note also that, with the given initial conditions, the gain k_1 involved in Observer 3 does not correspond to the limit corresponding to the sufficient condition (i.e. Eq. (3.45)) given in the proof of Theorem 2. Furthermore, simulations results tend to indicate that the domain of attraction is (quasi) global for any positive value of k_1. The same observation through simulation results is made for Observer 2 (i.e. the observer proposed in (Martin and Salaun, 2008)), recalling that no proof is available in this respect. On the other hand, the closed-loop stability of Observers 2 and 3 are quite sensitive and exhibit poor performance compared to Observer 4 for "very small" values of k_1.

Fig. 3.4: illustrates an example case with $k_1 = 0.03$ (a very small value). It shows that the convergence rates of Observers 2, 3 are rather slow while Observer 4 still provides a good performance. It also implies that in the case where the GPS velocity measurement is rather erroneous (i.e. noisy) the observer in Theorem 3 can be more advantageous than

the one in Theorem 2 and the one proposed in (Martin and Salaun, 2008) because a small gain k_1 can be used to limit the influence of GPS velocity measurement noise.

▷ **Simulation 2:** illustrates the robustness of Observers 2, 3, and 4 towards sensor noises, biases, and output rates. To get realistic measurements of v, ω, $a_\mathcal{B}$, and $m_\mathcal{B}$ we discretize the real values and corrupt them with noise in accordance with the sensors characteristics described in Tab. 3.1. Furthermore, the measurements of the gyroscopes are corrupted by a constant bias $\omega_b = [1, 1, 1]^\top (\text{deg/s})$. Observers 2, 3, and 4 are simulated with $k_1 = 3$. To better view the influence of the sensors characteristics on these observers' performance, their initial estimated variables are now chosen as $\widetilde{v}(0) = [0.3, -0.1, 0]^\top (m/s)$, $\widetilde{R}(0) = R(0)$ (*i.e.* $\widehat{R}(0) = I_3$), knowing that the initial Euler angles are $\phi(0) = -34.5(\text{deg})$, $\theta(0) = 47(\text{deg})$, $\psi(0) = 11(\text{deg})$. For these three observers, one observes from Fig. 3.5 good convergence rates of the estimated Euler angles to the true ones and small ultimate estimation errors despite the significant magnetometer and gyroscope noises, the high gyroscope bias, and the low GPS output rate. One also observes from Fig. 3.5 the less accurate estimation of the Euler yaw angle given by Observer 2 (with a maximum absolute error of 7.4(deg) after 10 (s)) compared to that given by Observers 3 and 4 (with maximum absolute errors less than 4.8(deg) after 10 (s)).

	Accelerometers	Gyroscopes
Sensor noise (1σ)	$0.1\,(\text{m/s}^2)$	$1\,(\text{deg/s})$
Output rate	$100\,(\text{Hz})$	$100\,(\text{Hz})$

	Magnetometers (normalized measure)	GPS-velocity
Sensor noise (1σ)	0.1	$0.1\,(\text{m/s})$
Output rate	$100\,(\text{Hz})$	$5\,(\text{Hz})$

Table 3.1: Sensors characteristics

▷ **Simulation 3:** illustrates the discussion made previously about the influence of magnetic perturbations on the estimated attitude provided by Observers 2, 3, and 4 for the case of weak accelerations. We suppose that magnetic perturbations are such that the normalized (total) magnetic field becomes $m_\mathcal{I} = [0.7076, 0.4328, 0.5586]^\top$ while the value $m_\mathcal{I} = [0.434, -0.0091, 0.9008]^\top$ is still taken into account in the three observers. It is also assumed that all measurements are perfect. In this simulation the VTOL is in a hovering flight where its velocity is null and its attitude is equal to the identity matrix. One observes from Fig. 3.6 that for Observer 2 (*i.e.* the one proposed in (Martin and Salaun, 2008)) the magnetic perturbations only influence on the precision of the estimated yaw angle whereas for our proposed solutions (*i.e.* Observers 3 and 4) the magnetic perturbations also make the estimated pitch angle erroneous.

Remark 4 *Simulation results show similar performance between our approaches and the one proposed in (Martin and Salaun, 2008), and in the cases of strong accelerations all of them outperform approximative solutions proposed in the literature (e.g. (Hamel and Mahony, 2006), (Mahony et al., 2008), (Martin and Salaun, 2007)). However, we are aware that our approaches (involving GPS velocity measurements) can not replace approximative solutions like (Hamel and Mahony, 2006), (Mahony et al., 2008), (Martin and Salaun, 2007) for many applications (e.g. indoor flight) where GPS signal is not available.*
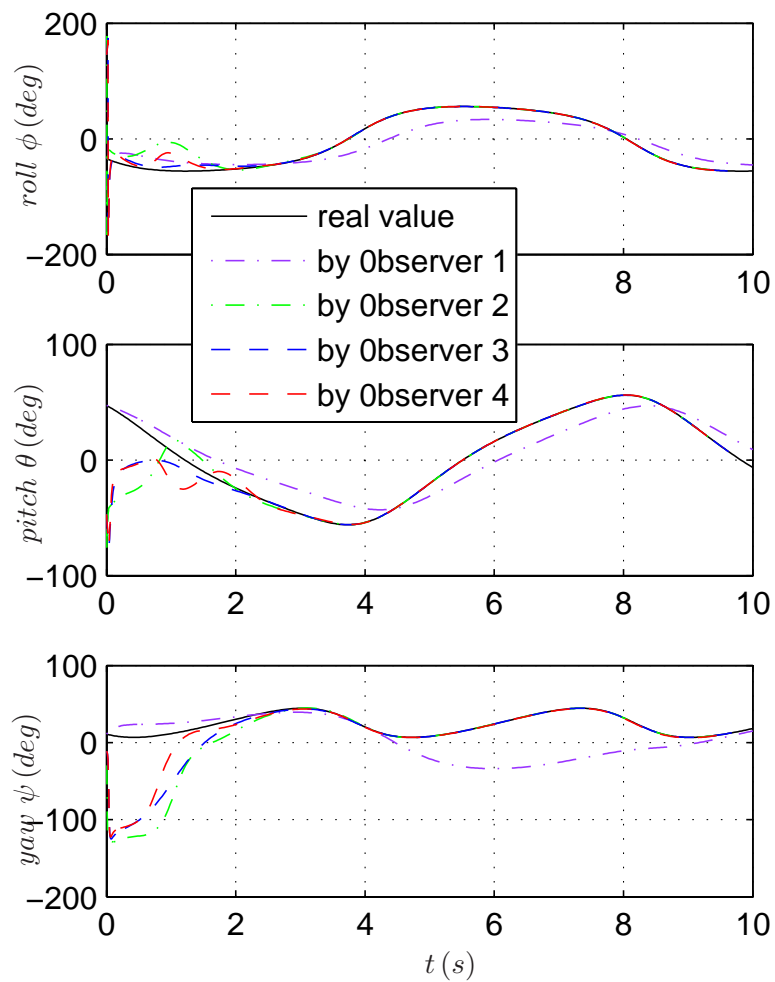
Figure 3.3: Estimated and real Euler angles (simulation 1, $k_1 = 3$)
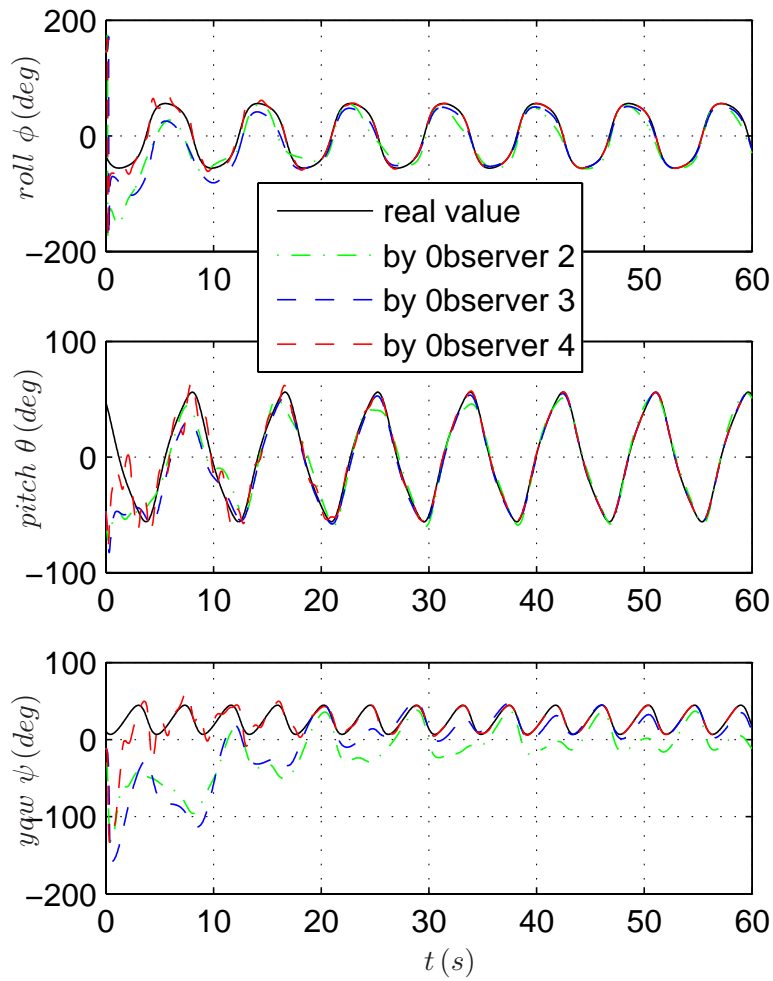
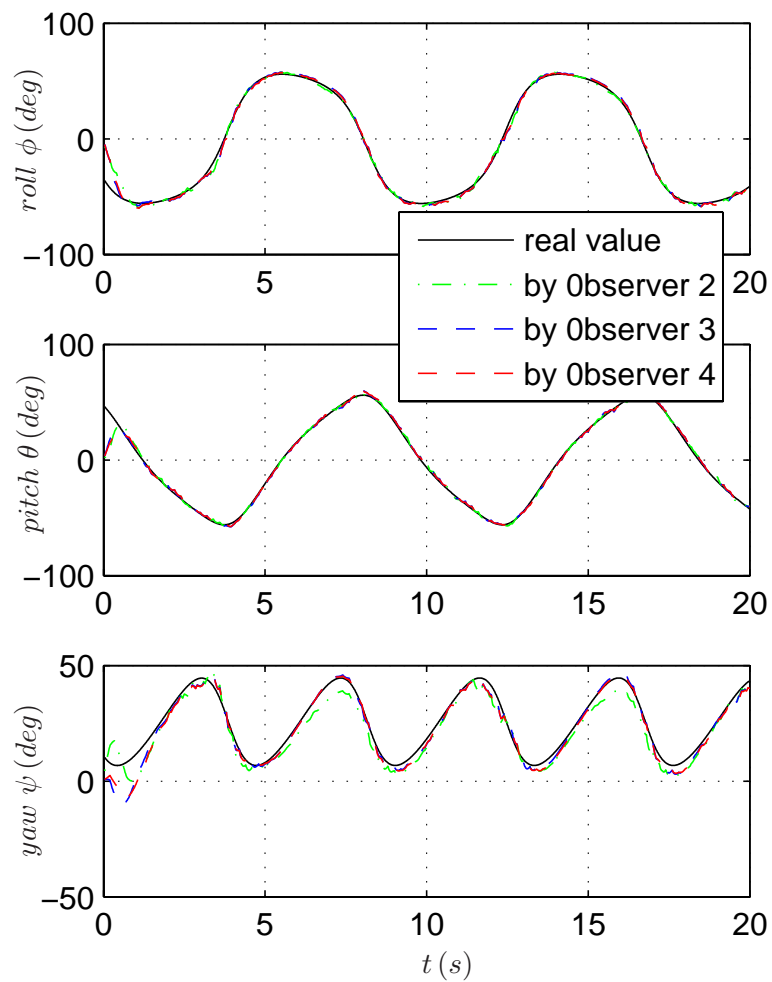Figure 3.4: Estimated and real Euler angles (simulation 1, $k_1 = 0.03$)

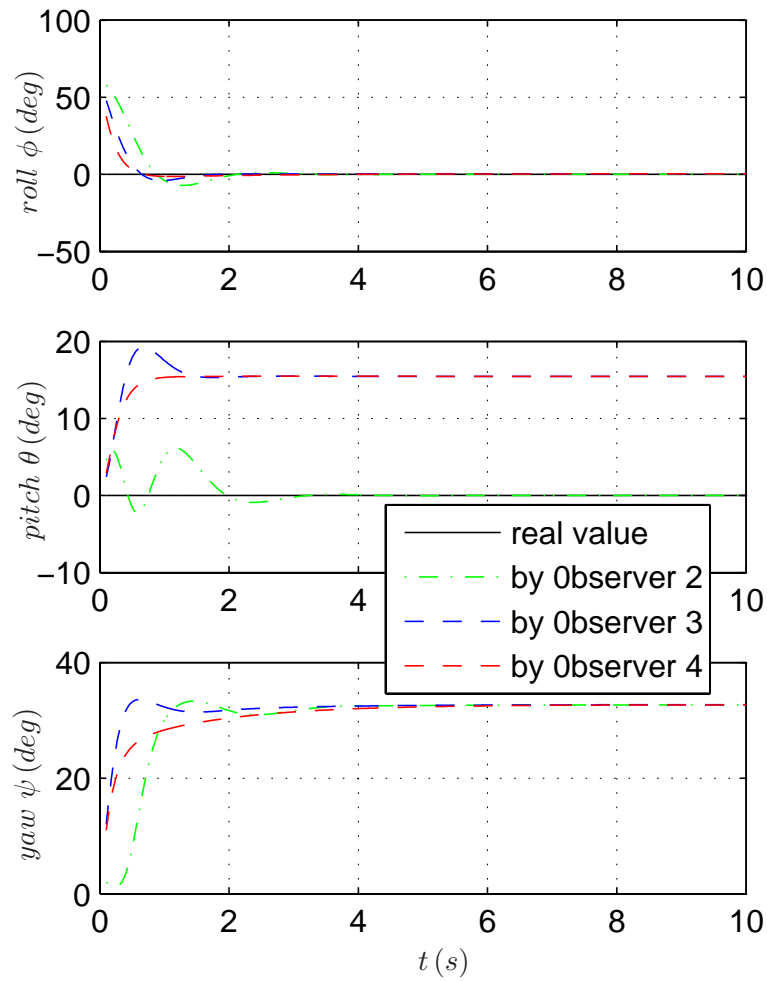Figure 3.5: Estimated and real Euler angles (simulation 2, $k_1 = 3$)

Figure 3.6: Estimated and real Euler angles (simulation 3, $k_1 = 3$)

3.5   Analyses for Chapter 3

3.5.1   Technical Lemma

Lemma 11 *Given two unit vectors $e_a, e_b \in \mathbb{R}^3$ and two positive numbers k_a, k_b, $\forall u \in \mathbb{R}^3$,*

$$k_a|u \times e_a|^2 + k_b|u \times e_b|^2 \geq \frac{k_a k_b}{k_a + k_b}|u|^2|e_a \times e_b|^2.$$

Proof   If $|e_a \times e_b| = 0$, one directly obtains this inequality. Consider now the case $|e_a \times e_b| \neq 0$. In this case $\forall u \in \mathbb{R}^3$ there exist three real numbers α, β, γ such that

$$u = \alpha e_a + \beta e_b + \gamma(e_a \times e_b). \tag{3.20}$$

Using Eq. (3.20) and the fact that $|e_a \times e_b| \leq 1$ one deduces that

$$
\begin{aligned}
|u|^2 &= \alpha^2 + \beta^2 + \gamma^2|e_a \times e_b|^2 + 2\alpha\beta e_a^\top e_b \\
&\leq \left(1 + \frac{k_b}{k_a}\right)\alpha^2 + \left(1 + \frac{k_a}{k_b}\right)\beta^2 + \gamma^2|e_a \times e_b|^2 \\
&\leq \frac{k_a + k_b}{k_a k_b}\left(k_b\alpha^2 + k_a\beta^2 + \frac{k_a k_b}{k_a + k_b}\gamma^2\right).
\end{aligned}
\tag{3.21}
$$

From (3.20) and (3.21) one verifies that

$$
\begin{aligned}
k_a|u \times e_a|^2 + k_b|u \times e_b|^2 &= (k_b\alpha^2 + k_a\beta^2 + (k_a + k_b)\gamma^2)|e_a \times e_b|^2 \\
&\geq \left(k_b\alpha^2 + k_a\beta^2 + \frac{k_a k_b}{k_a + k_b}\gamma^2\right)|e_a \times e_b|^2 \\
&\geq \frac{k_a k_b}{k_a + k_b}|u|^2|e_a \times e_b|^2.
\end{aligned}
$$

∎

3.5.2   Proof of Proposition 13

One verifies that

$$\dot{\widetilde{R}} = -S\left(k_\alpha\,\alpha_\mathcal{I} \times \widetilde{R}\alpha_\mathcal{I} + k_\beta\,\beta_\mathcal{I} \times \widetilde{R}\beta_\mathcal{I}\right)\widetilde{R}.$$

Denote $\widetilde{q} \triangleq (\widetilde{s}, \widetilde{r})^\top$ the quaternion associated with the matrix of rotation $\widetilde{R}$. Note that $\widetilde{r} = 0$ corresponds to $\widetilde{R} = I_3$ and $\widetilde{s} = 0$ corresponds to $\mathrm{tr}(\widetilde{R}) = -1$ (*i.e.* $\widetilde{R} \in \mathbb{U}$). From Rodrigues' rotation formula (3.8) one obtains

$$\mathbf{tr}(I_3 - \widetilde{R}) = 4|\widetilde{r}|^2, \quad \mathbf{P_a}(\widetilde{R}) = 2\widetilde{s}S(\widetilde{r}), \quad I_3 - \widetilde{R}^\top = 2\widetilde{s}S(\widetilde{r}) - 2S(\widetilde{r})^2. \tag{3.22}$$

Along the solutions of the closed-loop system, the time-derivative of the following candidate Lyapunov function

$$\mathcal{V} \triangleq \mathbf{tr}(I_3 - \widetilde{R}) = 4|\widetilde{r}|^2 \tag{3.23}$$

satisfies

$$\dot{\mathcal{V}} = \mathbf{tr}\left(k_\alpha S(\alpha_\mathcal{I} \times \widetilde{R}\alpha_\mathcal{I})\widetilde{R} + k_\beta S(\beta_\mathcal{I} \times \widetilde{R}\beta_\mathcal{I})\widetilde{R}\right) \tag{3.24}$$

Using Eq. (3.24), the following mathematical properties

$$\forall x, y \in \mathbb{R}^3, \mathbf{tr}(xy^\top) = x^\top y, \text{ and } S(x \times y) = yx^\top - xy^\top, \tag{3.25}$$

and Lemma 11 one obtains

$$
\begin{aligned}
\dot{\mathcal{V}} &= k_\alpha \mathbf{tr}(\widetilde{R}\alpha_\mathcal{I}\alpha_\mathcal{I}^\top \widetilde{R} - \alpha_\mathcal{I}\alpha_\mathcal{I}^\top) + k_\beta \mathbf{tr}(\widetilde{R}\beta_\mathcal{I}\beta_\mathcal{I}^\top \widetilde{R} - \beta_\mathcal{I}\beta_\mathcal{I}^\top) \\
&= -k_\alpha \left(|\alpha_\mathcal{I}|^2 - \alpha_\mathcal{I}^\top \widetilde{R}^2 \alpha_\mathcal{I} \right) - k_\beta \left(|\beta_\mathcal{I}|^2 - \beta_\mathcal{I}^\top \widetilde{R}^2 \beta_\mathcal{I} \right) \\
&= -2k_\alpha \left| \mathbf{P_a}(\widetilde{R})\alpha_\mathcal{I} \right|^2 - 2k_\beta \left| \mathbf{P_a}(\widetilde{R})\beta_\mathcal{I} \right|^2 \\
&= -8\widetilde{s}^2 \left(k_\alpha |\widetilde{r} \times \alpha_\mathcal{I}|^2 + k_\beta |\widetilde{r} \times \beta_\mathcal{I}|^2 \right) \\
&\leq -8\widetilde{s}^2 \left(\frac{k_\alpha k_\beta}{k_\alpha + k_\beta} |\alpha_\mathcal{I} \times \beta_\mathcal{I}|^2 |\widetilde{r}|^2 \right) \\
&\leq -\frac{8 k_\alpha k_\beta \eta^2}{k_\alpha + k_\beta} \widetilde{s}^2 |\widetilde{r}|^2.
\end{aligned}
\tag{3.26}
$$

Since $\widetilde{R}(0) \notin \mathbb{U}$, there exists a constant ε $(0 < \varepsilon \leq 1)$ such that $|\widetilde{s}(0)| \geq \varepsilon$. Let us prove (by contradiction) that for all $t \in \mathbb{R}_+$ $|\widetilde{s}(t)| \geq \varepsilon$. Assume that there exists $T > 0$ such that $|\widetilde{s}(T)| < \varepsilon$. In view of (3.23), one has $\mathcal{V}(T) > \mathcal{V}(0)$ which implies that there exists $\tau \in (0, T)$ such that $\dot{\mathcal{V}}(\tau) > 0$. But this contradicts with inequality (3.26). Using this property, the definition of $\mathcal{V}$ given by Eq. (3.23), and inequality (3.26) one ensures the existence of a constant $\kappa > 0$ such that

$$\dot{\mathcal{V}} \leq -\kappa \mathcal{V}. \tag{3.27}$$

The exponential stability of $\mathcal{V}$ and $\widetilde{r}$ to zero then follows which implies also the exponential stability of $\widetilde{R}$ to I_3.

3.5.3 Proof of Theorem 2

Let us first prove the second statement of Theorem 2. From Eqs. (3.10), (3.16), and (3.12) one obtains the error system

$$
\begin{cases}
\dot{\widetilde{v}} &= -k_1 \widetilde{v} + (I_3 - \widetilde{R}^\top) a_\mathcal{I} \\
\dot{\widetilde{R}} &= -k_2 S(m_\mathcal{I} \times \widetilde{R} m_\mathcal{I}) \widetilde{R} - k_3 S(a_\mathcal{I} \times \widetilde{R}\widetilde{v}) \widetilde{R}
\end{cases}
\tag{3.28}
$$

Consider the following candidate Lyapunov function

$$\mathcal{L} \triangleq \frac{1}{2} \mathbf{tr}(I_3 - \widetilde{R}) + \frac{l_1}{2} |\widetilde{v}|^2 - \frac{k_3}{k_1} \widetilde{v}^\top \mathbf{P_a}(\widetilde{R}) \widetilde{R}^\top a_\mathcal{I}, \tag{3.29}$$

with l_1 some positive constant specified hereafter. Denote $\widetilde{q} \triangleq (\widetilde{s}, \widetilde{r})^\top$ the quaternion associated with the matrix of rotation $\widetilde{R}$. Using Eqs. (3.22) one verifies that $\mathcal{L}$ defined by Eq. (3.29) can be rewritten as

$$\mathcal{L} = 2|\widetilde{r}|^2 + \frac{l_1}{2} |\widetilde{v}|^2 + \frac{2k_3}{k_1} \widetilde{s}(\widetilde{R}^\top a_\mathcal{I})^\top (\widetilde{r} \times \widetilde{v}). \tag{3.30}$$

Using Eq. (3.30) and Assumption 7 one deduces that

$$2|\widetilde{r}|^2 + \frac{l_1}{2}|\widetilde{v}|^2 + \frac{2\overline{c}_a k_3}{k_1}|\widetilde{v}||\widetilde{r}| \geq \mathcal{L} \geq 2|\widetilde{r}|^2 + \frac{l_1}{2}|\widetilde{v}|^2 - \frac{2\overline{c}_a k_3}{k_1}|\widetilde{v}||\widetilde{r}| \geq 2\left(1 - \frac{\overline{c}_a^2 k_3^2}{l_1 k_1^2}\right)|\widetilde{r}|^2. \quad (3.31)$$

The candidate Lyapunov function $\mathcal{L}$ is positive and proper with respect to $\widetilde{v}$ and $\widetilde{r}$ if $k_1 > \overline{c}_a k_3/\sqrt{l_1}$. Now, let us calculate the time-derivative of $\mathcal{L}$. To this purpose and the clarity of the calculation, we first calculate the time-derivative of intermediary terms. Using System (3.28) and the mathematical properties in (3.25) one verifies that

$$\begin{aligned}
\frac{d}{dt}\mathbf{tr}(I - \widetilde{R}) &= k_2\mathbf{tr}(S(m_{\mathcal{I}} \times \widetilde{R}m_{\mathcal{I}})\widetilde{R}) + k_3\mathbf{tr}(S(a_{\mathcal{I}} \times \widetilde{R}\widetilde{v})\widetilde{R}) \\
&= k_2\mathbf{tr}(\widetilde{R}m_{\mathcal{I}}m_{\mathcal{I}}^\top\widetilde{R} - m_{\mathcal{I}}m_{\mathcal{I}}^\top) + k_3\mathbf{tr}(\widetilde{R}\widetilde{v}a_{\mathcal{I}}^\top\widetilde{R} - a_{\mathcal{I}}\widetilde{v}^\top) \\
&= -k_2(|m_{\mathcal{I}}|^2 - m_{\mathcal{I}}^\top\widetilde{R}^2 m_{\mathcal{I}}) - k_3\widetilde{v}^\top(I_3 - (\widetilde{R}^\top)^2)a_{\mathcal{I}} \\
&= -2k_2|\mathbf{P_a}(\widetilde{R})m_{\mathcal{I}}|^2 - 2k_3\widetilde{v}^\top\mathbf{P_a}(\widetilde{R})\widetilde{R}^\top a_{\mathcal{I}},
\end{aligned} \quad (3.32)$$

$$\frac{d}{dt}|\widetilde{v}|^2 = -2k_1|\widetilde{v}|^2 + 2\widetilde{v}^\top(I_3 - \widetilde{R}^\top)a_{\mathcal{I}}, \quad (3.33)$$

$$\widetilde{v}^\top\mathbf{P_a}(\widetilde{R})\widetilde{R}^\top\dot{a}_{\mathcal{I}} = \widetilde{v}^\top\mathbf{P_a}(\widetilde{R})\widetilde{R}^\top\ddot{v}_{\mathcal{I}}, \quad (3.34)$$

$$\begin{aligned}
\dot{\widetilde{v}}^\top\mathbf{P_a}(\widetilde{R})\widetilde{R}^\top a_{\mathcal{I}} &= -k_1\widetilde{v}^\top\mathbf{P_a}(\widetilde{R})\widetilde{R}^\top a_{\mathcal{I}} + \frac{1}{2}a_{\mathcal{I}}^\top(I_3 - \widetilde{R})(\widetilde{R} - \widetilde{R}^\top)\widetilde{R}^\top a_{\mathcal{I}} \\
&= -k_1\widetilde{v}^\top\mathbf{P_a}(\widetilde{R})\widetilde{R}^\top a_{\mathcal{I}} + \frac{1}{2}a_{\mathcal{I}}^\top(I_3 - (\widetilde{R}^\top)^2 - \widetilde{R} + \widetilde{R}^\top)a_{\mathcal{I}} \\
&= -k_1\widetilde{v}^\top\mathbf{P_a}(\widetilde{R})\widetilde{R}^\top a_{\mathcal{I}} + \frac{1}{2}a_{\mathcal{I}}^\top(I_3 - (\widetilde{R}^\top)^2)a_{\mathcal{I}} \\
&= -k_1\widetilde{v}^\top\mathbf{P_a}(\widetilde{R})\widetilde{R}^\top a_{\mathcal{I}} + |\mathbf{P_a}(\widetilde{R})a_{\mathcal{I}}|^2,
\end{aligned} \quad (3.35)$$

$$\begin{aligned}
\widetilde{v}^\top\frac{d}{dt}\left(\mathbf{P_a}(\widetilde{R})\widetilde{R}^\top\right)a_{\mathcal{I}} &= a_{\mathcal{I}}^\top\frac{d}{dt}\left(\widetilde{R}\mathbf{P_a}(\widetilde{R})^\top\right)\widetilde{v} = -\frac{1}{2}a_{\mathcal{I}}^\top\left(\widetilde{R}\dot{\widetilde{R}} + \dot{\widetilde{R}}\widetilde{R}\right)\widetilde{v} \\
&= \frac{k_2}{2}a_{\mathcal{I}}^\top S((\widetilde{R} + I_3)(m_{\mathcal{I}} \times \widetilde{R}m_{\mathcal{I}}))\widetilde{R}^2\widetilde{v} + \frac{k_3}{2}a_{\mathcal{I}}^\top S((\widetilde{R} + I_3)(a_{\mathcal{I}} \times \widetilde{R}\widetilde{v}))\widetilde{R}^2\widetilde{v}.
\end{aligned} \quad (3.36)$$

One has

$$\begin{aligned}
(\widetilde{R} + I_3)(m_{\mathcal{I}} \times \widetilde{R}m_{\mathcal{I}}) &= (I_3 + \widetilde{R}^\top)(m_{\mathcal{I}} \times \widetilde{R}m_{\mathcal{I}}) + 2\mathbf{P_a}(\widetilde{R})(m_{\mathcal{I}} \times \widetilde{R}m_{\mathcal{I}}) \\
&= 2m_{\mathcal{I}} \times \mathbf{P_a}(\widetilde{R})m_{\mathcal{I}} + 2\mathbf{P_a}(\widetilde{R})(m_{\mathcal{I}} \times \widetilde{R}m_{\mathcal{I}}).
\end{aligned} \quad (3.37)$$

Using Eqs. (3.36), (3.37) and the fact that $|m_{\mathcal{I}}| = 1$ one deduces that

$$\left|\widetilde{v}^\top\frac{d}{dt}\left(\mathbf{P_a}(\widetilde{R})\widetilde{R}^\top\right)a_{\mathcal{I}}\right| \leq k_2|a_{\mathcal{I}}||\widetilde{v}|\left(|\mathbf{P_a}(\widetilde{R})m_{\mathcal{I}}| + |\mathbf{P_a}(\widetilde{R})(m_{\mathcal{I}} \times \widetilde{R}m_{\mathcal{I}})|\right) + k_3|a_{\mathcal{I}}|^2|\widetilde{v}|^2. \quad (3.38)$$

From relations (3.29), (3.32), (3.33), (3.34), (3.35), (3.36), and (3.38) one verifies that

$$\begin{aligned}
\dot{\mathcal{L}} \leq &-\left(k_1 l_1 - \frac{k_3^2|a_{\mathcal{I}}|^2}{k_1}\right)|\widetilde{v}|^2 - k_2|\mathbf{P_a}(\widetilde{R})m_{\mathcal{I}}|^2 - \frac{k_3}{k_1}|\mathbf{P_a}(\widetilde{R})a_{\mathcal{I}}|^2 \\
&+ l_1\widetilde{v}^\top(I_3 - \widetilde{R}^\top)a_{\mathcal{I}} + \frac{k_3}{k_1}|\widetilde{v}||\mathbf{P_a}(\widetilde{R})\widetilde{R}^\top\ddot{v}_{\mathcal{I}}| \\
&+ \frac{k_2 k_3}{k_1}|a_{\mathcal{I}}||\widetilde{v}|\left(|\mathbf{P_a}(\widetilde{R})m_{\mathcal{I}}| + |\mathbf{P_a}(\widetilde{R})(m_{\mathcal{I}} \times \widetilde{R}m_{\mathcal{I}})|\right).
\end{aligned} \quad (3.39)$$

Using relations (3.39), (3.22), Assumptions 7 and 8, and Lemma 11 (see Section 3.5.1) one deduces that

$$
\begin{aligned}
\dot{\mathcal{L}} \leq & -\left(k_1 l_1 - \frac{\bar{c}_a^2 k_3^2}{k_1}\right)|\widetilde{v}|^2 - 4k_2\widetilde{s}^2|\widetilde{r} \times m_{\mathcal{I}}|^2 - \frac{4\underline{c}_a^2 k_3}{k_1}\widetilde{s}^2\left|\widetilde{r} \times \frac{a_{\mathcal{I}}}{|a_{\mathcal{I}}|}\right|^2 \\
& + 2\bar{c}_a l_1|\widetilde{v}|(|\widetilde{s}| + |\widetilde{r}|)|\widetilde{r}| + \frac{2c_v k_3}{k_1}|\widetilde{v}||\widetilde{s}||\widetilde{r}| + \frac{2\bar{c}_a k_2 k_3}{k_1}(|m_{\mathcal{I}}| + |m_{\mathcal{I}} \times \widetilde{R}m_{\mathcal{I}}|)|\widetilde{v}||\widetilde{s}||\widetilde{r}| \\
\leq & -\left(k_1 l_1 - \frac{\bar{c}_a^2 k_3^2}{k_1}\right)|\widetilde{v}|^2 - 4k_2\widetilde{s}^2|\widetilde{r} \times m_{\mathcal{I}}|^2 - \frac{4\underline{c}_a^2 k_3}{k_1}\widetilde{s}^2\left|\widetilde{r} \times \frac{a_{\mathcal{I}}}{|a_{\mathcal{I}}|}\right|^2 \\
& + 2\sqrt{2}\bar{c}_a l_1|\widetilde{v}||\widetilde{r}| + \frac{2(c_v + 2k_2\bar{c}_a)k_3}{k_1}|\widetilde{v}||\widetilde{s}||\widetilde{r}| \\
\leq & -\left(k_1 l_1 - \frac{\bar{c}_a^2 k_3^2}{k_1}\right)|\widetilde{v}|^2 - \frac{4\underline{c}_a^2 k_2 k_3}{k_1 k_2 + \underline{c}_a^2 k_3}\left|m_{\mathcal{I}} \times \frac{a_{\mathcal{I}}}{|a_{\mathcal{I}}|}\right|^2\widetilde{s}^2|\widetilde{r}|^2 \\
& + 2\sqrt{2}\bar{c}_a\left(l_1 + \frac{k_3(c_v + 2k_2\bar{c}_a)}{\sqrt{2}\bar{c}_a k_1}\right)|\widetilde{v}||\widetilde{r}| \\
\leq & -\left(k_1 l_1 - \frac{\bar{c}_a^2 k_3^2}{k_1}\right)|\widetilde{v}|^2 - \frac{4\underline{c}_a^2 c_{obs}^2 k_2 k_3}{k_1 k_2 + \underline{c}_a^2 k_3}\widetilde{s}^2|\widetilde{r}|^2 + 2\sqrt{2}\bar{c}_a\left(l_1 + \frac{k_3(c_v + 2k_2\bar{c}_a)}{\sqrt{2}\bar{c}_a k_1}\right)|\widetilde{v}||\widetilde{r}|.
\end{aligned} \tag{3.40}
$$

Define

$$
\alpha_1 \triangleq \frac{k_3(c_v + 2k_2\bar{c}_a)}{\sqrt{2}\bar{c}_a}, \quad \alpha_2 \triangleq \frac{2\underline{c}_a^2 c_{obs}^2 k_3}{\bar{c}_a^2}, \quad \alpha_3 \triangleq \frac{\underline{c}_a^2 k_3}{k_2}.
$$

Choosing $k_1 > \bar{c}_a k_3/\sqrt{l_1}$, and using inequality (3.40) one obtains

$$
\begin{aligned}
\dot{\mathcal{L}} \leq & -\left(k_1 l_1 - \frac{\bar{c}_a^2 k_3^2}{k_1}\right)|\widetilde{v}|^2 - \frac{2\bar{c}_a^2 \alpha_2}{k_1 + \alpha_3}\widetilde{s}^2|\widetilde{r}|^2 + 2\sqrt{2}\bar{c}_a\left(l_1 + \frac{\alpha_1}{k_1}\right)|\widetilde{v}||\widetilde{r}| \\
\leq & -2\sqrt{2}\bar{c}_a\left(\sqrt{\frac{\alpha_2(k_1^2 l_1 - \bar{c}_a^2 k_3^2)}{k_1(k_1 + \alpha_3)}}|\widetilde{s}| - \frac{k_1 l_1 + \alpha_1}{k_1}\right)|\widetilde{v}||\widetilde{r}|.
\end{aligned} \tag{3.41}
$$

Define

$$
\varepsilon \triangleq \min\left(1 - |\widetilde{r}(0)|, \frac{1}{2}\right). \tag{3.42}
$$

Since $\widetilde{R}(0) \notin \mathbb{U}$ with $\mathbb{U}$ defined by (3.14), $|\widetilde{r}(0)| < 1$. Therefore, ε is strictly positive. One verifies that $|\widetilde{r}(0)| \leq 1 - \varepsilon$. Now let us choose l_1 as follows

$$
l_1 \triangleq \min\left(\frac{4\varepsilon(1 - \varepsilon)\left(\sqrt{3/2 - \varepsilon} - \sqrt{1 - \varepsilon}\right)^2}{|\widetilde{v}(0)|^2}, \frac{\alpha_2\varepsilon}{2}\right). \tag{3.43}
$$

Note that l_1 is well-defined and strictly positive even in the case $|\widetilde{v}(0)| = 0$. It follows from Eq. (3.43) that $\alpha_2\varepsilon l_1 > l_1^2$, so that there exists $\kappa_1(l_1, \varepsilon) > 0$ such that for all $k_1 > \kappa_1(l_1, \varepsilon)$ the following inequality is satisfied

$$
(\alpha_2\varepsilon l_1 - l_1^2)k_1^3 - (2\alpha_1 l_1 + \alpha_3 l_1^2)k_1^2 - \left(\alpha_1^2 + 2\alpha_1\alpha_3 l_1 + \bar{c}_a^2 k_3^2\alpha_2\varepsilon\right)k_1 - \alpha_1^2\alpha_3 > 0,
$$

which is equivalent to

$$
\varepsilon\alpha_2 l_1(k_1^2 l_1 - \bar{c}_a^2 k_3^2) > (k_1 l_1 + \alpha_1)^2(k_1 + \alpha_3). \tag{3.44}
$$

Therefore, with the choice of k_1 satisfying

$$k_1 > \Bbbk_1 \triangleq \max\left(\frac{\sqrt{2}\,\overline{c}_a k_3}{\sqrt{\varepsilon l_1}}, \kappa_1(l_1, \varepsilon)\right) \tag{3.45}$$

inequality (3.44) holds. Note that the choice of k_1 in (3.45) verifies the inequality $k_1 > \overline{c}_a k_3/\sqrt{l_1}$. From (3.31) and (3.45) one verifies that

$$
\begin{aligned}
\mathcal{L}(0) &\leq 2|\widetilde{r}(0)|^2 + \frac{l_1}{2}|\widetilde{v}(0)|^2 + \frac{2\overline{c}_a k_3}{k_1}|\widetilde{v}(0)||\widetilde{r}(0)| \\
&\leq 2(1-\varepsilon)^2 + \frac{|\widetilde{v}(0)|^2}{2}l_1 + 2\sqrt{\varepsilon}(1-\varepsilon)|\widetilde{v}(0)|\sqrt{l_1}\,.
\end{aligned}
\tag{3.46}
$$

Now consider the following equation (with s the variable)

$$
\begin{aligned}
&\frac{|\widetilde{v}(0)|^2}{2}s^2 + 2\sqrt{\varepsilon}(1-\varepsilon)|\widetilde{v}(0)|s + 2(1-\varepsilon)^2 - 2\left(1-\frac{\varepsilon}{2}\right)(1-\varepsilon) = 0 \\
\Leftrightarrow \quad &\frac{|\widetilde{v}(0)|^2}{2}s^2 + 2\sqrt{\varepsilon}(1-\varepsilon)|\widetilde{v}(0)|s - \varepsilon(1-\varepsilon) = 0\,.
\end{aligned}
$$

Using Eq. (3.42) one easily verifies that this equation possess two real solutions with one negative and one positive. The positive one is given by

$$s_{max} = \frac{2}{|\widetilde{v}(0)|}\sqrt{\varepsilon}\sqrt{1-\varepsilon}\left(\sqrt{3/2-\varepsilon} - \sqrt{1-\varepsilon}\right).$$

Note that s_{max} tends to $+\infty$ when $|\widetilde{v}(0)|$ tends to zero. Thus, $\forall s \in [0, s_{max}]$,

$$\frac{|\widetilde{v}(0)|^2}{2}s^2 + 2\sqrt{\varepsilon}(1-\varepsilon)|\widetilde{v}(0)|s + 2(1-\varepsilon)^2 \leq 2\left(1-\frac{\varepsilon}{2}\right)(1-\varepsilon).$$

This relation and inequality (3.46) and the definition of l_1 in (3.43) imply that

$$\mathcal{L}(0) \leq 2\left(1-\frac{\varepsilon}{2}\right)(1-\varepsilon). \tag{3.47}$$

As a consequence of (3.44) and (3.45) one has

$$1 - \frac{(k_1 l_1 + \alpha_1)^2(k_1 + \alpha_3)}{\alpha_2 k_1(k_1^2 l_1 - \overline{c}_a^2 k_3^2)} > 1 - \varepsilon \tag{3.48}$$

and

$$1 - \frac{\overline{c}_a^2 k_3^2}{k_1^2 l_1} \geq 1 - \frac{\varepsilon}{2}. \tag{3.49}$$

Then, one deduces from inequalities (3.47), (3.48), and (3.49) that

$$\mathcal{L}(0) < 2\left(1 - \frac{\overline{c}_a^2 k_3^2}{k_1^2 l_1}\right)\left(1 - \frac{(k_1 l_1 + \alpha_1)^2(k_1 + \alpha_3)}{\alpha_2 k_1(k_1^2 l_1 - \overline{c}_a^2 k_3^2)}\right). \tag{3.50}$$

Using inequalities (3.50) and (3.31) one deduces that

$$\widetilde{s}(0)^2 > \delta \triangleq \frac{(k_1 l_1 + \alpha_1)^2(k_1 + \alpha_3)}{\alpha_2 k_1(k_1^2 l_1 - \overline{c}_a^2 k_3^2)}.$$

Let us now prove (by contradiction) that $\forall t \in \mathbb{R}_+$, $\widetilde{s}(t)^2 > \delta$. Assume that there exists $T > 0$ such that $\widetilde{s}(T)^2 \leq \delta$ and $\forall t \in [0, T)$, $\widetilde{s}(t)^2 > \delta$. This supposition and inequality (3.31) imply that

$$\mathcal{L}(T) > 2 \left(1 - \frac{\bar{c}_a^2 k_3^2}{k_1^2 l_1}\right) \left(1 - \frac{(k_1 l_1 + \alpha_1)^2 (k_1 + \alpha_3)}{\alpha_2 k_1 (k_1^2 l_1 - \bar{c}_a^2 k_3^2)}\right).$$

Then, this relation and inequality (3.50) imply that $\mathcal{L}(T) > \mathcal{L}(0)$, so that there exists a time-instant $\tau \in (0, T)$ such that $\dot{\mathcal{L}}(\tau) > 0$. But this contradicts inequality (3.41) since $\widetilde{s}(\tau)^2 > \delta$. This result and inequality (3.41) imply the existence of positive constants κ_v, κ_r, κ such that

$$\dot{\mathcal{L}} \leq -\kappa_v |\widetilde{v}|^2 - \kappa_r |\widetilde{r}|^2 \leq -\kappa \mathcal{L}. \tag{3.51}$$

From here the exponential convergence of $\mathcal{L}$ to zero follows. The exponential convergence of $(\widetilde{v}, \widetilde{r})$ to zero, $i.e.$ of $(\widetilde{v}, \widetilde{R})$ to $(0, I_3)$, then directly follows. The stability of the equilibrium $(\widetilde{v}, \widetilde{R}) = (0, I_3)$ is a direct consequence of relations (3.29) and (3.51). Now, to prove the first statement of the theorem let us consider the linearized system of System (3.28) about the equilibrium $(\widetilde{v}, \widetilde{r}) = (0, 0)$ which is given by (using (3.28) and the fact that $\widetilde{R} - I_3 \approx 2S(\widetilde{r}) \approx I_3 - \widetilde{R}^\top$)

$$\begin{cases} \dot{\widetilde{v}} = -k_1 \widetilde{v} + 2\widetilde{r} \times a_\mathcal{I} \\ \dot{\widetilde{r}} = -k_2 m_\mathcal{I} \times S(\widetilde{r}) m_\mathcal{I} - \dfrac{k_3}{2} a_\mathcal{I} \times \widetilde{v} \end{cases} \tag{3.52}$$

Consider the candidate Lyapunov function

$$\mathcal{L}_1 \triangleq \frac{1}{2} |\widetilde{r}|^2 + \frac{\gamma_1}{2} |\widetilde{v}|^2 - \frac{k_3 - 4\gamma_1}{2k_1} \widetilde{v}^\top (\widetilde{r} \times a_\mathcal{I}), \tag{3.53}$$

with $0 < \gamma_1 < k_3/4$, $k_1 > (k_3 - 4\gamma_1)\bar{c}_a/(2\sqrt{\gamma_1})$ (to ensure that $\mathcal{L}_1$ is positive and proper with respect to $\widetilde{r}$ and $\widetilde{v}$). The time-derivative of $\mathcal{L}_1$ along the solutions to (3.52) satisfies (proceeding majorations like in (3.39) and (3.40))

$$\dot{\mathcal{L}}_1 = -k_1 \gamma_1 |\widetilde{v}|^2 + \frac{k_3(k_3 - 4\gamma_1)}{4k_1} |\widetilde{v} \times a_\mathcal{I}|^2 - k_2 |\widetilde{r} \times m_\mathcal{I}|^2 - \frac{k_3 - 4\gamma_1}{k_1} |\widetilde{r} \times a_\mathcal{I}|^2$$
$$- \frac{k_2(k_3 - 4\gamma_1)}{2k_1} (m_\mathcal{I} \times S(\widetilde{r}) m_\mathcal{I})^\top (\widetilde{v} \times a_\mathcal{I}) - \frac{k_3 - 4\gamma_1}{2k_1} \widetilde{v}^\top (\widetilde{r} \times \ddot{v}_\mathcal{I})$$
$$\leq -\frac{4k_1^2 \gamma_1 - k_3(k_3 - 4\gamma_1)\bar{c}_a^2}{4k_1} |\widetilde{v}|^2$$
$$- k_2 |\widetilde{r} \times m_\mathcal{I}|^2 - \frac{k_3 - 4\gamma_1}{k_1} \underline{c}_a^2 \left|\widetilde{r} \times \frac{a_\mathcal{I}}{|a_\mathcal{I}|}\right|^2 + \frac{(k_3 - 4\gamma_1)(c_v + k_2 \bar{c}_a)}{2k_1} |\widetilde{v}||\widetilde{r}|$$
$$\leq -\frac{4k_1^2 \gamma_1 - k_3(k_3 - 4\gamma_1)\bar{c}_a^2}{4k_1} |\widetilde{v}|^2 - \frac{\underline{c}_a^2 c_{obs}^2 k_2(k_3 - 4\gamma_1)}{k_1 k_2 + \underline{c}_a^2(k_3 - 4\gamma_1)} |\widetilde{r}|^2 + \frac{(k_3 - 4\gamma_1)(c_v + k_2 \bar{c}_a)}{2k_1} |\widetilde{v}||\widetilde{r}|. \tag{3.54}$$

Denote $\kappa_0(\gamma_1) \in \mathbb{R}_+$ the largest positive solution to the equation

$$f(\kappa) \triangleq \kappa^3 - \left(k_3 \bar{c}_a^2 + \frac{(c_v + k_2 \bar{c}_a)^2}{4\underline{c}_a^2 c_{obs}^2}\right) \frac{k_3 - 4\gamma_1}{4\gamma_1} \kappa - \frac{(c_v + k_2 \bar{c}_a)^2 (k_3 - 4\gamma_1)^2}{16 c_{obs}^2 k_2 \gamma_1} = 0.$$

The existence of $\kappa_0(\gamma_1)$ is a direct consequence of $f(0) < 0$ and $\lim_{\kappa \to +\infty} f(\kappa) = +\infty$. From here choosing k_1 satisfying

$$k_1 > \mathbb{k}_0(\gamma_1) \triangleq \max\left(\frac{(k_3 - 4\gamma_1)\bar{c}_a}{2\sqrt{\gamma_1}}, \kappa_0(\gamma_1)\right) \tag{3.55}$$

one ensures that $f(k_1) > 0$ or, equivalently

$$\sqrt{\frac{(4k_1^2\gamma_1 - k_3(k_3 - 4\gamma_1)\bar{c}_a^2)\underline{c}_a^2 c_{obs}^2 k_2(k_3 - 4\gamma_1)}{k_1(k_1 k_2 + \underline{c}_a^2(k_3 - 4\gamma_1))}} > \frac{(k_3 - 4\gamma_1)(c_v + k_2\bar{c}_a)}{2k_1}.$$

This inequality, relations (3.53) and (3.54), and Young's inequality ensure the existence of three positive constants γ_r, γ_v, $\gamma_{\mathcal{L}}$ such that $\dot{\mathcal{L}}_1 \leq -\gamma_r|\tilde{r}|^2 - \gamma_v|\tilde{v}|^2 \leq -\gamma_{\mathcal{L}}\mathcal{L}_1$. Then, the latter inequality and the definition of $\mathcal{L}_1$ imply the exponential stability of the equilibrium $(\tilde{v}, \tilde{r}) = (0, 0)$, *i.e.* of $(\tilde{v}, \tilde{R}) = (0, I_3)$. Now, it's important to prove that for any $k_1 \, (> 0)$ there exists a positive constant γ_1 such that $k_1 > \mathbb{k}_0(\gamma_1)$. One verifies from (3.55) that when $\gamma_1 \, (< k_3/4)$ tends to $k_3/4$, $\kappa_0(\gamma_1)$ and $\mathbb{k}_0(\gamma_1)$ tend to zero. Therefore, by continuity of the functions $\kappa_0(\gamma_1)$ and $\mathbb{k}_0(\gamma_1)$ one deduces that for any $k_1 > 0$ there exists a positive value of $\gamma_1 \, (< k_3/4)$ such that $\kappa_0(\gamma_1) < k_1$ and $\mathbb{k}_0(\gamma_1) < k_1$. This concludes the proof.

Remark 5 *A sufficient condition for the gain k_1 is provided (i.e. inequality (3.45)) ensuring the convergence and stability results. One also deduces that k_1 must tend to $+\infty$ to guarantee the satisfaction of the sufficient condition when $|\tilde{r}(0)|$ tends to one (the value for which $\tilde{R}(0) \in \mathbb{U}$). One also remarks that the size of k_1 is proportional to the size of the domain of initial estimation errors for which the sufficient condition is satisfied.*

Remark 6 *Now, let us discuss the influence of magnetic measurements on Observer (3.15) compared to Observer (3.16). Similar to System (3.52), one easily verifies that the linearized error system of Observer (3.15) (using quaternion parametrization) for the case of "week accelerations" (i.e. $a_{\mathcal{I}} \approx -ge_3$) is*

$$\begin{cases} \dot{\tilde{v}} = -k_1\tilde{v} + 2g\, e_3 \times \tilde{r} \\ \dot{\tilde{r}} = -k_2 g^2 \left((m_{\mathcal{I}} \times S(\tilde{r})m_{\mathcal{I}})^\top e_3\right) e_3 + \frac{k_3 g}{2} e_3 \times \tilde{v} \end{cases} \tag{3.56}$$

One can verify from System (3.56) that the dynamics of $\tilde{r}_1$ and $\tilde{r}_2$ are independent upon the magnetic information, and only the dynamics of $\tilde{r}_3$ depends on this information. On the contrary, for System (3.52) the magnetic information involves in the dynamics of all three components of $\tilde{r}$ even in the case $a_{\mathcal{I}} \approx -ge_3$. Now, let us parameterize the rotation matrix R by the Euler angles parametrization (ϕ, θ, ψ) corresponding to the parameters of roll, pitch, and yaw, and verifying the relation (3.6). Denote $\left(\hat{\phi}, \hat{\theta}, \hat{\psi}\right)$ as the Euler angles parametrization of $\hat{R}$, and define $\tilde{\phi} \triangleq \phi - \hat{\phi}$, $\tilde{\theta} \triangleq \theta - \hat{\theta}$, $\tilde{\psi} \triangleq \psi - \hat{\psi}$ as the Euler angles estimation errors. Using the fact that $\tilde{R} = R\hat{R}^\top \approx I_3 + 2S(\tilde{r})$, one can verify that in a first order approximation

$$\begin{cases} \tilde{r}_1 = (\cos\theta\,\cos\psi\,\sin\tilde{\phi} - \sin\psi\,\sin\tilde{\theta})/2 \\ \tilde{r}_2 = (\sin\theta\,\sin\psi\,\sin\tilde{\phi} + \cos\psi\,\sin\tilde{\theta})/2 \\ \tilde{r}_3 = (-\sin\theta\,\sin\tilde{\phi} + \sin\tilde{\psi})/2 \end{cases}$$

From these relations, one remarks that $\widetilde{\phi}$ and $\widetilde{\theta}$ depend on $\widetilde{r}_1$ and $\widetilde{r}_2$ and do not depend on $\widetilde{r}_3$ (and only $\widetilde{\psi}$ depends on $\widetilde{r}_3$). These remarks together with those made previously (i.e. local independency (resp. dependency) of the dynamics of $\widetilde{r}_1$ and $\widetilde{r}_2$ on magnetic information for Observer (3.15) (resp. Observer (3.16))) allow to conclude that in the case of "weak accelerations" Observer (3.15) locally ensures the decoupling of the roll and pitch angles estimation from the magnetic measurements, whereas Observer (3.16) does not.

3.5.4   Proof of Lemma 10

Using Eqs. (3.10) and (3.17) one obtains

$$\dot{\widetilde{v}} = -k_1\widetilde{v} + (R - Q)a_{\mathcal{B}}. \tag{3.57}$$

Along the solutions of the closed-loop system, the time-derivative of the candidate Lyapunov function

$$\mathcal{W} \triangleq \frac{1}{2}|\widetilde{v}|^2 + \frac{1}{2k_v}||R - Q||^2 \tag{3.58}$$

satisfies

$$\begin{aligned}
\dot{\mathcal{W}} &= -k_1|\widetilde{v}|^2 + \widetilde{v}^\top(R - Q)a_{\mathcal{B}} - \mathbf{tr}((R - Q)^\top \widetilde{v}a_{\mathcal{B}}^\top) + \frac{1}{k_v}\mathbf{tr}((R-Q)^\top(R-Q)S(\omega)) \\
&= -k_1|\widetilde{v}|^2.
\end{aligned} \tag{3.59}$$

The time-derivative of $\mathcal{W}$ is negative semi-definite, so that $\widetilde{v}$ and Q are bounded. In view of Eq. (3.57) and the boundedness of $\widetilde{v}$, Q, $a_{\mathcal{B}}$ (since $\dot{v}_{\mathcal{I}}$ is bounded from assumption), one deduces the boundedness of $\dot{\widetilde{v}}$. Then, one deduces from Eq. (3.59) the boundedness of $\ddot{\mathcal{W}}$, *i.e.* $\dot{\mathcal{W}}$ is uniformly continuous along every system's solution. Then, the application of Barbalat's lemma ensures the convergence of $\dot{\mathcal{W}}$ to zero which implies the convergence of $\widetilde{v}$ to zero. The boundedness of $\ddot{v}_{\mathcal{I}}$ and ω from Assumption 7 implies the boundedness of $\dot{a}_{\mathcal{B}}$ since $a_{\mathcal{B}} = R^\top(\dot{v}_{\mathcal{I}} - g)$. This along with Eq. (3.57) and the properties obtained previously (*i.e.* the boundedness of $\widetilde{v}$, $\dot{\widetilde{v}}$, Q, $\dot{Q}$, $\dot{R}$) implies that $\ddot{\widetilde{v}}$ is bounded, *i.e.* $\dot{\widetilde{v}}$ is uniformly continuous. Since $\widetilde{v}$ converges to zero and $\dot{\widetilde{v}}$ is uniformly continuous, the application of Barbalat's lemma ensures the convergence of $\dot{\widetilde{v}}$ to zero which implies the convergence of $Qa_{\mathcal{B}}$ to $a_{\mathcal{I}}$. It remains to show the last statement of the lemma. If $\dot{v}_{\mathcal{I}}$ is constant, one has

$$\frac{d}{dt}\left((R - Q)a_{\mathcal{B}}\right) = -k_v|a_{\mathcal{I}}|^2\widetilde{v}. \tag{3.60}$$

From Eqs. (3.57) and (3.60), the exponential stability of $(\widetilde{v}, a_{\mathcal{I}} - Qa_{\mathcal{B}})$ to zero is straightforward.

Remark 7 *With $\dot{Q}$ given by System (3.19), the time-derivative of $\mathcal{W}$ defined by Eq. (3.58) satisfies*

$$\dot{\mathcal{W}} = -k_1|\widetilde{v}|^2 + \widetilde{v}^\top (R - Q)a_{\mathcal{B}} - \mathbf{tr}((R - Q)^\top \widetilde{v}a_{\mathcal{B}}^\top)$$

$$+ \frac{1}{k_v}\mathbf{tr}((R - Q)^\top (R - Q)S(\omega) + \rho(R - Q)^\top Q)$$

$$= -k_1|\widetilde{v}|^2 + \frac{\rho}{k_v}(\mathbf{tr}(R^\top Q) - ||Q||^2)$$

$$\leq -k_1|\widetilde{v}|^2 + \frac{\rho}{k_v}\left(\frac{1}{2}\left(||R||^2 + ||Q||^2\right) - ||Q||^2\right)$$

$$\leq -k_1|\widetilde{v}|^2 + \frac{k_q}{2k_v}\max(0, ||Q|| - \sqrt{3})\left(3 - ||Q||^2\right)$$

$$\leq -k_1|\widetilde{v}|^2.$$

From here, the proof of convergence of $(\widetilde{v}, a_{\mathcal{I}} - Qa_{\mathcal{B}})$ to zero does not change. As a consequence, the proof of Property 1 of Theorem 3 is still valid.

3.5.5 Proof of Theorem 3

One verifies that

$$\dot{\widetilde{R}} = -S\left(k_2\, m_{\mathcal{I}} \times \widetilde{R}m_{\mathcal{I}} + k_3\, a_{\mathcal{I}} \times \widetilde{R}a_{\mathcal{I}}\right)\widetilde{R} + E\,, \tag{3.61}$$

with

$$E \triangleq k_3 S\left(a_{\mathcal{I}} \times \widetilde{R}\,(a_{\mathcal{I}} - Qa_{\mathcal{B}} - k_1\widetilde{v})\right)\widetilde{R}\,. \tag{3.62}$$

The convergence of $\widetilde{v}$ to zero is a direct consequence of Lemma 10. Furthermore, one verifies from the proof of Lemma 10 that $\widetilde{v}$, $\dot{\widetilde{v}}$, Q are bounded. From the theorem's assumptions one deduces that $a_{\mathcal{I}}$, $a_{\mathcal{B}}$, $\dot{a}_{\mathcal{I}}$, and $\dot{a}_{\mathcal{B}}$ are bounded, so that E is bounded. From Eq. (3.61) and the boundedness of $a_{\mathcal{I}}$ and E, one ensures the boundedness of $\dot{\widetilde{R}}$. From the expression of $\dot{Q}$ in System (3.17) and the boundedness of $\widetilde{v}$, $a_{\mathcal{B}}$, and Q one ensures the boundedness of $\dot{Q}$. Then, from the definition of E and the boundedness of $\dot{\widetilde{R}}$, $a_{\mathcal{I}}$, $\dot{a}_{\mathcal{I}}$, $a_{\mathcal{B}}$, $\dot{a}_{\mathcal{B}}$, Q, $\dot{Q}$ one deduces that $\dot{E}$ is bounded. Thus, E is uniformly continuous, bounded, and converges to zero as a consequence of Lemma 10 (*i.e.* $\widetilde{v}$ and $a_{\mathcal{I}} - Qa_{\mathcal{B}}$ converge to zero).

Denote $(\widetilde{\theta}, \widetilde{a}) \in (-\pi, \pi] \times \{\widetilde{a} \in \mathbb{R}^3 : |\widetilde{a}| = 1\}$ as the angle-coordinates of $\widetilde{R}$ (see *e.g.* (Murray et al., 1994)). One has $\mathbf{tr}(\widetilde{R}) = 1 + 2\cos(\widetilde{\theta})$ and $\mathbf{P_a}(\widetilde{R}) = \sin(\widetilde{\theta})S(\widetilde{a})$. Note that $\widetilde{\theta} = 0$ corresponds to $\widetilde{R} = I_3$ and $\widetilde{\theta} = \pi$ corresponds to $\mathrm{tr}(\widetilde{R}) = -1$ (*i.e.* $\widetilde{R} \in \mathbb{U}$). Along the solutions to the closed-loop system, the time-derivative of the candidate Lyapunov function

$$\mathcal{V} \triangleq \mathbf{tr}(I_3 - \widetilde{R}) = 4\sin^2(\widetilde{\theta}/2) \tag{3.63}$$

satisfies

$$\begin{aligned}
\dot{\mathcal{V}} &= \mathbf{tr}\left(k_2 S\left(m_{\mathcal{I}} \times \widetilde{R}m_{\mathcal{I}}\right)\widetilde{R} + k_3 S\left(a_{\mathcal{I}} \times \widetilde{R}a_{\mathcal{I}}\right)\widetilde{R} - E\right) \\
&= -k_2\left(|m_{\mathcal{I}}|^2 - m_{\mathcal{I}}^\top \widetilde{R}^2 m_{\mathcal{I}}\right) - k_3\left(|a_{\mathcal{I}}|^2 - a_{\mathcal{I}}^\top \widetilde{R}^2 a_{\mathcal{I}}\right) - \mathbf{tr}(E) \\
&= -2k_2|\mathbf{P_a}(\widetilde{R})m_{\mathcal{I}}|^2 - 2k_3|\mathbf{P_a}(\widetilde{R})a_{\mathcal{I}}|^2 - \mathbf{tr}(E) \\
&= -2\left(k_2\,|\widetilde{a} \times m_{\mathcal{I}}|^2 + k_3\,|\widetilde{a} \times a_{\mathcal{I}}|^2\right)\sin^2(\widetilde{\theta}) - \mathbf{tr}(E).
\end{aligned} \tag{3.64}$$

Then, from (3.64) and Assumption 8 one ensures the existence of a positive constant κ such that

$$\dot{\mathcal{V}} \leq -\kappa \sin^2(\widetilde{\theta}) - \mathbf{tr}(E). \tag{3.65}$$

From Eq. (3.64) one ensures the boundedness of $\dot{\mathcal{V}}$ which implies the uniform continuity of $\mathcal{V}$ and therefore of $\widetilde{\theta}$. Now, let us prove that if $\widetilde{R}$ does not converge to $\mathbb{U}$, then it converges to I_3. Assume that $\widetilde{R}$ does not converge to $\mathbb{U}$ which implies that $\widetilde{\theta}$ does not converge to π. This implies the existence of a constant ε $(0 < \varepsilon < \pi)$ and a strictly increasing sequence of time-instants $\left\{ t_n \,|\, n \in \mathbb{N},\ \lim\limits_{n \to \infty} t_n = +\infty \right\}$ such that $|\widetilde{\theta}(t_n) - \pi| > \varepsilon$, $\forall n \in \mathbb{N}$. Since $E(t)$ uniformly converges to zero, there exists an integer $N > 0$ such that $\forall t \geq t_N$, one has $|\mathbf{tr}(E(t))| < \kappa \sin^2(\pi - \varepsilon)$. Let us prove (by contradiction) that $|\widetilde{\theta}(t) - \pi| > \varepsilon$, $\forall t \geq t_N$. Assume that there exists a first instant $T > t_N$ such that $|\widetilde{\theta}(T) - \pi| = \varepsilon$. This implies that $|\widetilde{\theta}(t) - \pi| > \varepsilon$, $\forall t \in [t_N, T)$. In view of Eq. (3.63), one has $\mathcal{V}(T) > \mathcal{V}(t)$, $\forall t \in [t_N, T)$. This implies that $\dot{\mathcal{V}}(T) > 0$. But this contradicts with inequality (3.65) since $|\mathbf{tr}(E(T))| < \kappa \sin^2(\pi - \varepsilon) = \kappa \sin^2(\widetilde{\theta}(T))$. Therefore, in view of relations (3.63) and (3.65), there exists a constant $\lambda > 0$ such that $\forall t \geq t_N$, $\dot{\mathcal{V}}(t) \leq -\lambda \mathcal{V}(t) - \mathbf{tr}(E(t))$. From this inequality and the fact that the perturbing term $\mathbf{tr}(E(t))$ uniformly converges to zero one deduces that $\mathcal{V}(t)$ globally converges to zero. This implies that if $\widetilde{\theta}$ does not converge to π, then it converges to zero. From here, one deduces the first statement of the theorem. Now, it is important to prove the second statement of the theorem. When the body's acceleration $\dot{v}_{\mathcal{I}}$ is constant, as a consequence of Eqs. (3.57) and (3.60) one has

$$\begin{cases} \dot{\widetilde{v}} = -k_1 \widetilde{v} + \xi \\ \dot{\xi} = -k_v |a_{\mathcal{I}}|^2 \widetilde{v} \end{cases} \tag{3.66}$$

with $\xi \triangleq a_{\mathcal{I}} - Q a_{\mathcal{B}}$. One verifies from Eq. (3.62) and the mathematical properties in (3.25) that

$$\begin{aligned} \mathbf{tr}(E) &= k_3 \mathbf{tr}\left(S\left(a_{\mathcal{I}} \times \widetilde{R}(-k_1 \widetilde{v} + \xi) \right) \widetilde{R} \right) \\ &= k_3 a_{\mathcal{I}}^\top (\widetilde{R}^2 - I_3)(-k_1 \widetilde{v} + \xi) \\ &= 2 k_3 a_{\mathcal{I}}^\top \widetilde{R} \, \mathrm{P_a}(\widetilde{R})(-k_1 \widetilde{v} + \xi) \\ &= 2 k_3 \sin \widetilde{\theta} a_{\mathcal{I}}^\top \widetilde{R} \, S(\widetilde{a})(-k_1 \widetilde{v} + \xi). \end{aligned} \tag{3.67}$$

Define $y \triangleq 1 + \cos \widetilde{\theta}$ and $z \triangleq 1 - \cos \widetilde{\theta}$. One verifies that $\widetilde{\theta} = \pi$ and $\widetilde{\theta} = 0$ corresponds to $y = 0$ and $z = 0$ respectively. Note that $y = 2 - \mathcal{V}/2$ and $z = \mathcal{V}/2$. Using Eq. (3.64) one obtains

$$\dot{y} = 2 \left(k_2 |\widetilde{a} \times m_{\mathcal{I}}|^2 + k_3 |\widetilde{a} \times a_{\mathcal{I}}|^2 \right) \left(1 - \frac{y}{2} \right) y + \frac{1}{2} \mathbf{tr}(E), \tag{3.68}$$

$$\dot{z} = -2 \left(k_2 |\widetilde{a} \times m_{\mathcal{I}}|^2 + k_3 |\widetilde{a} \times a_{\mathcal{I}}|^2 \right) \left(1 - \frac{z}{2} \right) z - \frac{1}{2} \mathbf{tr}(E). \tag{3.69}$$

From Eqs. (3.66), (3.67), (3.68), (3.69) it is straightforward to verify that $(\xi, \widetilde{v}, y) = (0, 0, 0)$ and $(\xi, \widetilde{v}, z) = (0, 0, 0)$ are equilibrium points. This implies that $\mathbb{E}$ is an equilibrium set of $(\xi, \widetilde{v}, \widetilde{R})$. From the definition of y and z, and from Eq. (3.67) one verifies that the first order approximation of $\mathbf{tr}(E)$ about the equilibrium point $(\xi, \widetilde{v}, y) = (0, 0, 0)$ or

$(\xi, \widetilde{v}, z) = (0, 0, 0)$ is equal to zero. Therefore, the linearization of system (3.68) about the equilibrium $(\xi, \widetilde{v}, y) = (0, 0, 0)$ is

$$\dot{y} = 2 \left(k_2 \left| \widetilde{a} \times m_{\mathcal{I}} \right|^2 + k_3 \left| \widetilde{a} \times a_{\mathcal{I}} \right|^2 \right) y. \qquad (3.70)$$

The linearization of system (3.69) about the equilibrium $(\xi, \widetilde{v}, z) = (0, 0, 0)$ is

$$\dot{z} = -2 \left(k_2 \left| \widetilde{a} \times m_{\mathcal{I}} \right|^2 + k_3 \left| \widetilde{a} \times a_{\mathcal{I}} \right|^2 \right) z. \qquad (3.71)$$

From Eq. (3.70) one directly deduces that the equilibrium $(\xi, \widetilde{v}, y) = (0, 0, 0)$ of the linearized system is unstable. This implies that the equilibrium set $\mathbb{E}_1$ of $(\xi, \widetilde{v}, \widetilde{R})$ is unstable. From Eqs. (3.66) and (3.71) one deduces that the equilibrium $(\xi, \widetilde{v}, z) = (0, 0, 0)$ of the linearized system is stable which also concludes the proof of the theorem.

Epilogue

This thesis has been devoted to two research directions: *i)* control design for a class of thrust-propelled underactuated vehicles, and *ii)* attitude estimation. Both issues are relevant to many robotic applications, especially aerial robotics.

Firstly, the present work attempts to set the foundations of a general approach to the control of a large family of thrust-propelled underactuated vehicles. Developing a control theory for vehicles seemingly as different as a VTOL vehicle, an underwater vehicle, or a space rocket may, at first glance, appears far-fetched and unrealistic. However, a closer look at the model equations of these systems brings evidence that the idea is technically relevant. The initial stage of this work logically focused on gathering information from the existing related literature and extracting the elements, at the modeling and control levels, on which a reasonably sound theory can be worked out. Among them, the basic principle according to which the thrust direction has to be monitored in order to allow for the compensation of the resultant of external forces has been the leading guide. Control laws conceived for incrementally complex objectives (ranging from joystick-augmented-control of the vehicle's attitude to autonomous trajectory tracking) have been derived, with the support of Lyapunov stability and convergence analyses. To cope with imprecise modeling and/or measurement of the forces acting on the vehicle, effective integral and anti-windup correction terms have been introduced, whereas this type of correction is often overlooked in nonlinear control studies. On the other hand, the concern of generality induced a certain number of simplifying assumptions. For instance, the existence of attitude control actuators enough powerful to overcome environmental perturbation torques was assumed, as well as the availability of accurate measurements/estimations of the vehicle's state. Deriving an approach as little dependent as possible on the vehicle particularities goes with the decoupling of the control architecture into inner hardware-dependent and outer control loops. The present study focused on the latter one, and the availability of low-level servo mechanisms in charge of effectively producing the desired thrust force magnitude and angular velocity –the determinant of which constitutes the core of the proposed approach– was not discussed or, equivalently, was assumed. Clearly the validity of these assumptions has to be assessed when considering an application on a physical system. For the genericity of the approach, it is important to extend this study in two directions. The first one concerns the assumption according to which environmental forces only depend on the vehicle's velocity (and the independent time-variable). This assumption needs to be loosened because it is not realistic for a number of vehicles, like airplanes, for which drag and lift forces depend strongly on the angle of attack. The second direction concerns the assumption of non zero-crossing upon the so-called *"apparent acceleration"* –the resultant of external forces and desired accelerations. A route could consist in coupling the present approach with more involved, non-classical, control techniques aiming at the

unconditional practical stability of the system (Morin and Samson, 2006). Besides these conceptual developments, conducting experiments on physical systems is indispensable to consolidate the results of this study with respect to claims of robustness and performance in particular.

The attitude information is needed to apply the proposed control laws for vehicles evolving in the 3D-space. Obtaining accurate estimate of the attitude at high frequency is even more critical for small-size and/or light vehicles because their attitude can vary rapidly and in large proportions due to environmental perturbations or changes of operating mode (*e.g.* hover to forward flight of a ducted fan tailsitter). In practice, the choice of directional sensors is limited by various constraints like, *e.g.*, the small size and limited payload of numerous aerial robotic systems. For instance, limitations of existing measurement systems make the problem of attitude estimation very challenging, especially when the vehicle's linear acceleration is important. In this case, the performance of *classical* methods, based on measurements of an IMU and a "weak acceleration" assumption, can be poor. A remedy to this problem, proposed recently in (Martin and Salaun, 2008), has been a source of inspiration for the two novel algorithms of attitude estimation reported in the present thesis. We believe that the specification of the convergence domain of the proposed solutions, with the support of Lyapunov stability and convergence analyses, is also an original contribution. However, many open problems on this topic remain. Perspectives include the extension of the proposed methods to compensate for measurement biases encountered in practice (gyroscope bias and/or accelerometer bias), and the design of a new observer that combines the advantages of our methods with the one in (Martin and Salaun, 2008). Needless to add that experiments on physical systems have to be carried out to test and validate all solutions.

The work reported in this document addresses a certain number of challenging problems. It is a small step of the quest for robust autonomous robots, and autonomous aerial robots in particular. One may mark a thesis as an ending of a work. For me it was just a beginning. In actual fact [1]

> *"What we call the beginning is often the end*
> *And to make an end is to make a beginning.*
> *The end is where we start from."*

---

[1]. From "Little Gidding" of T.S. Eliot.

Appendix A

About input-output exact linearization for ducted fan tailsitters

In this appendix we study a ducted fan tailsitter whose equations of motions are given in Section 1.4.2. We focus on a near hover flight in the absence of wind. In this situation aerodynamic lift and drag forces which depend on the square of the vehicle velocity can be neglected in first-order approximations. By contrast, the momentum drag force which is proportional to the vehicle's velocity must be taken into account, so that $F_{ae}^{\mathcal{B}} \approx -Qv$, $\Gamma_{ae}^{\mathcal{B}} \approx \varepsilon_m S(e_3) F_{ae}^{\mathcal{B}}$, with $Q\,(>0)$ and ε_m some constants. Therefore, the equations of motion of the vehicle's CoM can be approximated by

$$
\begin{bmatrix} \dot{x} \\ m\dot{v} \\ \dot{R} \\ J\dot{\omega} \end{bmatrix} = \begin{bmatrix} Rv \\ -mS(\omega)v - Te_3 + \Sigma_R\Gamma + R^\top mge_3 + F_{ae}^{\mathcal{B}} \\ RS(\omega) \\ -S(\omega)J\omega + \Gamma + \Gamma_{ae}^{\mathcal{B}} \end{bmatrix}, \tag{A.1}
$$

with $T \in \mathbb{R}$ and $\Gamma \in \mathbb{R}^3$ the thrust force and torque control inputs, $F_{ae}^{\mathcal{B}} = -Qv$, $\Gamma_{ae}^{\mathcal{B}} = \varepsilon_m S(e_3) F_{ae}^{\mathcal{B}}$, and $\Sigma_R = -S(e_3)/L$.

Lemma 12 *The System* (A.1) *is not feedback linearizable.*

Proof: Denote

$$
r_1 \triangleq \frac{Re_1}{mL},\ r_2 \triangleq \frac{Re_2}{mL},\ r_3 \triangleq \frac{Re_3}{mL},
$$
$$
u_1 \triangleq \Gamma_1,\ u_2 \triangleq \Gamma_2,\ u_3 \triangleq \Gamma_3,\ u_4 \triangleq -TL.
$$

Define also

$$
v_{\mathcal{I}} \triangleq Rv
$$

One verifies that

$$
\Gamma_{ae}^{\mathcal{B}} = -\varepsilon_m Q S(e_3) R^\top v_{\mathcal{I}} = c \sum_{i=1,2,3} S(e_3) r_i\, e_i^\top v_{\mathcal{I}},
$$

with $c \triangleq -\varepsilon_m Q m L$. System (A.1) then can be rewritten as

$$
\dot{X} = f(X) + \sum_{i=1,..,4} g_i(X)u_i, \tag{A.2}
$$

with

$$X = \begin{bmatrix} x \\ v_{\mathcal{I}} \\ r_1 \\ r_2 \\ r_3 \\ \omega \end{bmatrix}, \; f(X) = \begin{bmatrix} v_{\mathcal{I}} \\ g e_3 - q v_{\mathcal{I}} \\ \left(r_2 e_3^\top - r_3 e_2^\top \right) \omega \\ \left(r_3 e_1^\top - r_1 e_3^\top \right) \omega \\ \left(r_1 e_2^\top - r_2 e_1^\top \right) \omega \\ -J^{-1} S(\omega) J \omega + c \sum_{i=1,2,3} S(e_3) r_i \, e_i^\top v_{\mathcal{I}} \end{bmatrix},$$

$$g_1(X) = \begin{bmatrix} 0 \\ -r_2 \\ 0 \\ 0 \\ 0 \\ J^{-1} e_1 \end{bmatrix}, \; g_2(X) = \begin{bmatrix} 0 \\ r_1 \\ 0 \\ 0 \\ 0 \\ J^{-1} e_2 \end{bmatrix}, \; g_3(X) = \begin{bmatrix} 0 \\ 0 \\ 0 \\ 0 \\ 0 \\ J^{-1} e_3 \end{bmatrix}, \; g_4(X) = \begin{bmatrix} 0 \\ r_3 \\ 0 \\ 0 \\ 0 \\ 0 \end{bmatrix},$$

and $q \triangleq Q/m$.

Define the distribution

$$\mathcal{D}_1 := \operatorname{span}\{g_1, g_2, g_3, g_4, [f, g_1], [f, g_2], [f, g_3], [f, g_4]\}.$$

To show that System (A.1) is not feedback linearizable, we will show that $\mathcal{D}_1$ is not involutive in any neighborhood of any point $X(0)$ in order to deduce, by application of Jakubczyk-Respondek's theorem, that System (A.2) is not feedback linearizable in any neighborhood of $X(0)$. To this purpose we need to calculate Lie products of vector fields in $\mathcal{D}_1$. This is done by using the classical formula

$$[Z_1, Z_2] = \frac{\partial Z_2}{\partial X} Z_1 - \frac{\partial Z_1}{\partial X} Z_2 \tag{A.3}$$

In this respect, we must be aware of a mathematical subtlety. Formula (A.3) is only valid in a system of (minimal) coordinates $X \in \mathbb{R}^n$. In order to avoid using a minimal parametrization of SO(3) (like, *e.g.*, Euler angles) which complicates calculations, we will view X as a vector in $\mathbb{R}^3 \times \mathbb{R}^3 \times (\mathbb{R}^3)^3 \times \mathbb{R}^3$ (*i.e.* we view r_1, r_2, r_3 as elements of $\mathbb{R}^3$ instead of elements of the unit sphere $\mathbb{S}^2$). This allows us to use formula (A.3) for the calculations. The fact that System A.1 is not feedback linearizable will follow from the fact that *i)* $\mathcal{D}_1$ does not satisfy the involutivity property at any point of the set $\mathbb{E} \triangleq \mathbb{R}^3 \times \mathbb{R}^3 \times (\mathbb{S}^2)^3 \times \mathbb{R}^3$ (this is proved below) and *ii)* because $\mathbb{E}$ is an invariant manifold for System (A.2), there is a one-to-one correspondence between vector fields of System(A.1) and their Lie brackets on one hand, and vector fields of System (A.2) and their Lie brackets restricted to $\mathbb{E}$ on the other hand.

Now let us calculate the Lie products in the span of $\mathcal{D}_1$. First, one verifies that the Jacobian matrix $\partial f(X)/\partial X$ is

$$\frac{\partial f(X)}{\partial X} =$$

$$\begin{bmatrix} 0_{3\times3} & I_3 & 0_{3\times3} & 0_{3\times3} & 0_{3\times3} & 0_{3\times3} \\ 0_{3\times3} & -qI_3 & 0_{3\times3} & 0_{3\times3} & 0_{3\times3} & 0_{3\times3} \\ 0_{3\times3} & 0_{3\times3} & 0_{3\times3} & (e_3^\top\omega)I_3 & -(e_2^\top\omega)I_3 & r_2e_3^\top - r_3e_2^\top \\ 0_{3\times3} & 0_{3\times3} & -(e_3^\top\omega)I_3 & 0_{3\times3} & (e_1^\top\omega)I_3 & r_3e_1^\top - r_1e_3^\top \\ 0_{3\times3} & 0_{3\times3} & (e_2^\top\omega)I_3 & -(e_1^\top\omega)I_3 & 0_{3\times3} & r_1e_2^\top - r_2e_1^\top \\ 0_{3\times3} & c\sum_{i=1,2,3}S(e_3)r_ie_i^\top & c(e_1^\top v_\mathcal{I})S(e_3) & c(e_2^\top v_\mathcal{I})S(e_3) & c(e_3^\top v_\mathcal{I})S(e_3) & J^{-1}S(J\omega) - J^{-1}S(\omega)J \end{bmatrix}$$

with $0_{3\times3}$ a 3×3 matrix with all components equal to zero, and I_3 the 3×3 identity matrix. From here one deduces

$$[f,g_1](X) = \begin{bmatrix} r_2 \\ -\left(r_3e_1^\top - r_1e_3^\top\right)\omega - qr_2 \\ -\left(r_2e_3^\top - r_3e_2^\top\right)J^{-1}e_1 \\ -\left(r_3e_1^\top - r_1e_3^\top\right)J^{-1}e_1 \\ -\left(r_1e_2^\top - r_2e_1^\top\right)J^{-1}e_1 \\ J^{-1}S(\omega)e_1 - J^{-1}S(J\omega)J^{-1}e_1 + c\sum_{i=1,2,3}S(e_3)r_ie_i^\top r_2 \end{bmatrix},$$

$$[f,g_2](X) = \begin{bmatrix} -r_1 \\ \left(r_2e_3^\top - r_3e_2^\top\right)\omega + qr_1 \\ -\left(r_2e_3^\top - r_3e_2^\top\right)J^{-1}e_2 \\ -\left(r_3e_1^\top - r_1e_3^\top\right)J^{-1}e_2 \\ -\left(r_1e_2^\top - r_2e_1^\top\right)J^{-1}e_2 \\ J^{-1}S(\omega)e_2 - J^{-1}S(J\omega)J^{-1}e_2 - c\sum_{i=1,2,3}S(e_3)r_ie_i^\top r_1 \end{bmatrix},$$

$$[f,g_3](X) = \begin{bmatrix} 0 \\ 0 \\ -\left(r_2e_3^\top - r_3e_2^\top\right)J^{-1}e_3 \\ -\left(r_3e_1^\top - r_1e_3^\top\right)J^{-1}e_3 \\ -\left(r_1e_2^\top - r_2e_1^\top\right)J^{-1}e_3 \\ J^{-1}S(\omega)e_3 - J^{-1}S(J\omega)J^{-1}e_3 \end{bmatrix},$$

$$[f,g_4](X) = \begin{bmatrix} -r_3 \\ \left(r_1e_2^\top - r_2e_1^\top\right)\omega + qr_3 \\ 0 \\ 0 \\ 0 \\ -c\sum_{i=1,2,3}S(e_3)r_ie_i^\top r_3 \end{bmatrix}.$$

One verifies that

$$
[[f, g_3], g_1](X) = \begin{bmatrix} 0 \\ \left(r_3 e_1^\top - r_1 e_3^\top \right) J^{-1} e_3 \\ 0 \\ 0 \\ 0 \\ \left(J^{-1} S(e_3) - J^{-1} S(J^{-1} e_3) J \right) J^{-1} e_1 \end{bmatrix}.
$$

If $[[f, g_3], g_1]$ belongs to the distribution $\mathcal{D}_1$, then there exists some constants α_i, β_i, with $i = 1, .., 4$, such that for all X in a neighborhood of $X(0)$ one has

$$
[[f, g_3], g_1](X) = \sum_{i=1,..,4} \left(\alpha_i g_i(X) + \beta_i [f, g_i](X) \right). \tag{A.4}
$$

Now, Eq. (A.4) will be used to deduce these constants. The first component of $[[f, g_3], g_1](X)$ implies that $\beta_1 r_2 - \beta_2 r_1 - \beta_4 r_3 = 0$. This indicates that $\beta_1 = \beta_2 = \beta_4 = 0$. Besides, the third, fourth, and fifth components of $[[f, g_3], g_1](X)$ imply that $\beta_3 = 0$. The second component of $[[f, g_3], g_1](X)$ does not depend on r_2, so that $\alpha_1 = 0$. It also implies that

$$
\alpha_2 = -e_3^\top J^{-1} e_3, \ \alpha_4 = e_1^\top J^{-1} e_3.
$$

Finally, the last component of $[[f, g_3], g_1](X)$ implies that

$$
\begin{aligned}
& \alpha_2 e_2 + \alpha_3 e_3 = S(e_3) J^{-1} e_1 + S(e_1) J^{-1} e_3 \\
\implies \ & e_1^\top S(e_3)(\alpha_2 e_2 + \alpha_3 e_3) = e_1^\top S(e_3)(S(e_3) J^{-1} e_1 + S(e_1) J^{-1} e_3) \\
\implies \ & -\alpha_2 = e_1^\top S(e_3)^2 J^{-1} e_1 + e_3^\top J^{-1} e_3 = -e_1^\top J^{-1} e_1 + e_3^\top J^{-1} e_3 \\
\implies \ & e_1^\top J^{-1} e_1 = 0.
\end{aligned}
$$

From the definition of the moment of inertia, one notes that $e_1^\top J^{-1} e_1$ corresponds to the inverse of the moment of inertia around the x-axis when the vehicle is rotated around the x-axis. The fact that $e_1^\top J^{-1} e_1 = 0$ implies that the vehicle's mass is infinite which is impossible for any physical system. This allows to conclude the proof. ∎

To analyze the internal stability, zero dynamics of the system should be examined.

▷ In **position and heading control mode**, $\{x, \psi\}$ are chosen as outputs. The zero dynamics corresponds to the situation when the chosen outputs reach the reference values and their time derivatives are null. In the absence of wind, the fact that the vehicle's velocity is identically null indicates that $F_{ae}^{\mathcal{B}} = 0$ and $\Gamma_{ae}^{\mathcal{B}} = 0$. Then, the translational dynamics of System (A.1) becomes

$$
T e_3 + \frac{1}{L} S(e_3) \Gamma = mg R^\top e_3 \tag{A.5}
$$

Multiplying both sides of Eq. (A.5) by $S(e_3)$, one obtains

$$
\begin{bmatrix} \Gamma_1 \\ \Gamma_2 \\ 0 \end{bmatrix} = -mg L S(e_3) R^\top e_3.
$$

From the Euler angles parametrization (see Section 3.2.1) the above relation is equivalent to

$$\begin{cases} \Gamma_1 = mgL\cos\theta\sin\phi \\ \Gamma_2 = mgL\sin\theta \end{cases} \tag{A.6}$$

Now, suppose that the vehicle's inertia matrix has a diagonal form, *i.e.* $J = \mathbf{diag}(J_1, J_2, J_3)$. Using (A.6) and the rotational dynamics of System (A.1), it yields

$$\begin{cases} \dot{\omega}_1 = \dfrac{1}{J_1}mgL\cos\theta\sin\phi \\ \dot{\omega}_2 = \dfrac{1}{J_2}mgL\sin\theta \end{cases} \tag{A.7}$$

Moreover, the fact that $\dot{\psi} = 0$ indicates that

$$\omega_3 = -\tan\phi\,\omega_2,$$

and thereby

$$\begin{cases} \dot{\phi} = \omega_1 \\ \dot{\theta} = \dfrac{1}{\cos\phi}\omega_2 \end{cases} \tag{A.8}$$

In view of (A.7) and (A.8), the linearized zero dynamics about the equilibrium point $(\phi, \theta, \omega_1, \omega_2) = (0, 0, 0, 0)$ is

$$\begin{bmatrix} \dot{\phi} \\ \dot{\theta} \\ \dot{\omega}_1 \\ \dot{\omega}_2 \end{bmatrix} = \begin{bmatrix} 0 & 0 & 1 & 0 \\ 0 & 0 & 0 & 1 \\ mgL/J_1 & 0 & 0 & 0 \\ 0 & mgL/J_2 & 0 & 0 \end{bmatrix} \begin{bmatrix} \phi \\ \theta \\ \omega_1 \\ \omega_2 \end{bmatrix} \tag{A.9}$$

From here one obtains the poles of the characteristic polynomial of the linearized zero dynamics

$$\lambda^4 - \lambda^2\, mgL\left(\frac{1}{J_2} + \frac{1}{J_1}\right) + \frac{(mgL)^2}{J_1 J_2}$$

as follows

$$\pm\sqrt{\frac{mgL}{J_1}} \text{ and } \pm\sqrt{\frac{mgL}{J_2}}$$

From here one concludes that the zero dynamics when choosing $\{x, \psi\}$ as outputs is unstable.

▷ In **attitude and altitude control mode**, $\{\phi, \theta, \psi, x_3\}$ are chosen as outputs. The zero dynamics corresponds to the internal dynamics when $Re_3 \equiv e_3$, $v_{\mathcal{I},3} \equiv 0$, $\dot{v}_{\mathcal{I},3} \equiv 0$, $\omega \equiv 0$, $\dot{\omega} \equiv 0$, recalling that $v_{\mathcal{I}} = Rv$. From the rotational dynamics in Eq. (A.1) one obtains

$$\Gamma = -\Gamma_{ae}^{\mathcal{B}} = \varepsilon_m Q S(e_3) R^\top v_{\mathcal{I}} \tag{A.10}$$

Using Eq. (A.10) and the fact that $Re_3 \equiv e_3$, one gets

$$m\dot{v}_{\mathcal{I}} = (-T + mg)e_3 - Qv_{\mathcal{I}} - \frac{\varepsilon_m Q}{L}RS(e_3)^2 R^\top v_{\mathcal{I}}$$

$$= (-T + mg)e_3 - Qv_{\mathcal{I}} - \frac{\varepsilon_m Q}{L}S(e_3)^2 v_{\mathcal{I}}$$

This implies that

$$\dot{v}_{\mathcal{I},1,2} = -\frac{Q}{m}\left(1 - \frac{\varepsilon_m}{L}\right) v_{\mathcal{I},1,2}$$

with $v_{\mathcal{I},1,2} = (v_{\mathcal{I},1}, v_{\mathcal{I},2})^\top$. Therefore, the zero dynamics is given by

$$\begin{cases} \dot{x}_{1,2} = v_{\mathcal{I},1,2} \\ \dot{v}_{\mathcal{I},1,2} = -\dfrac{Q}{m}\left(1 - \dfrac{\varepsilon_m}{L}\right) v_{\mathcal{I},1,2} \end{cases}$$

One pole of this linear system is equal to zero, but interestingly, the sign of the second pole depends on the value of the aerodynamic level arm ε_m. It is:

- negative if $\varepsilon_m < L$,

- null if $\varepsilon_m = L$,

- positive if $\varepsilon_m > L$.

Appendix B

Commande des engins volants de type VTOL: résultats et perspectives

B.1 Introduction

La commande des véhicules de type VTOL (Vertical Take-Off and Landing) suscite depuis plusieurs années un intérêt important dans la communauté roboticienne, notamment française. De nombreux laboratoires de recherche sont maintenant équipés de tels systèmes (hélicoptères, quadrotors, "tailsitters", etc.). Citons par exemple les drones à hélice carénée comme le HoverEye (Pflimlin, 2006), le iStar (Lipera et al., 2001), celui de l'université de Bologne (Naldi, 2008), le GTSpy (Johnson and Turbe, 2005), le SLADe (Peddle et al., 2009); les quadrotor hélicoptères (Hamel et al., 2002), (Tayebi and McGilvray, 2006); et les hélicoptères comme le Vigilant (Fabiani et al., 2007), le Goliath (Vissière et al., 2008), le GTMax (Johnson and Kannan, 2005), ou l'AVATAR (Saripalli et al., 2002). Une raison de cet intérêt tient aux nombreuses applications que ce type de véhicule permet de couvrir, aussi bien dans le secteur civil que militaire (surveillance, inspection d'ouvrages ou de zones dangeureuses pour l'homme, cartographie, œil déporté, etc.). Une autre raison est la récente miniaturisation des capteurs et cartes de traitement de données, permettant d'embarquer sur de petits véhicules tous les éléments nécessaires à leur fonctionnement autonome. Enfin, le fait que ces systèmes évoluent dans un espace tri-dimensionnel (3D) pose de nouveaux problèmes de recherche par rapport au cas 2D de la robotique mobile terrestre (véhicules à roues notamment). Le développement de tels systèmes présente plusieurs défis sur le plan mécanique (conception d'un système doté de bonnes capacités de vol et capable d'embarquer la puissance et les capteurs nécessaires à son fonctionnement) comme au niveau de l'estimation en temps réel de l'état du véhicule (détermination d'algorithmes de traitement des données capteurs efficaces, rapides, et robustes) et de celui de la commande (synthèse de commandes efficaces et robustes aux perturbations aérologiques). Les difficultés sont amplifiées pour les systèmes de petite taille en raison de la complexité des phénomènes aérodynamiques qui entrent en jeu, de leur plus forte sensibilité aux perturbations aérologiques, et des limitations sur la charge utile qui génèrent des contraintes de dimensionnement et de poids pour les capteurs embarqués. Nous nous intéresserons ici essentiellement aux aspects de synthèse de la commande, tout en sachant que les aspects de conception mécanique et d'estimation sont tout autant importants.

Un premier objectif de cette thèse est de présenter une synthèse des techniques de commande par retour d'état (linéaires ou non-linéaires) développées pour ces véhicules

afin de les stabiliser le long de trajectoires désirées. Le point de vue ici adopté est celui de l'automaticien. Différents objectifs de commande, associés à différents modes opérationnels sont considérés, comme la commande en vitesse (typiquement associée à un "mode joystick"), ou la commande en position associée à un fonctionnement complètement autonome. Un autre objectif de cette thèse est de proposer un cadre général pour la synthèse de lois de commande pour un ensemble de systèmes présentant des caractéristiques structurelles et fonctionnelles communes. Plus précisement, de nombreux véhicules conçus par l'homme sont mus par l'intermédiaire d'une force de poussée dans une direction privilégiée du véhicule et d'un vecteur couple permettant un contrôle complet de l'orientation (cette classe de véhicules est parfois désignée par le terme *thrust-propelled vehicles* dans la littérature anglo-saxonne). Outre les VTOLs (hélicoptères, quadrotors, etc.), c'est aussi le cas des avions, dirigeables, fusées, aéroglisseurs, bateaux ou encore sous-marins. Cette similitude structurelle peut être exploitée dans un cadre général de commande. Evidemment, chaque classe de systèmes possède aussi des caractéristiques propres qu'il convient de prendre en compte. Celles-ci sont essentiellement liées à la nature des forces extérieures exercées sur le véhicule. Par exemple, l'avion évolue dans l'air et dans un espace à trois dimensions, tandis que le bateau est en partie immergé dans l'eau et se déplace essentiellement dans un espace à deux dimensions. Le fluide ambiant n'est pas le même et génère des forces aérodynamiques ou hydrodynamiques de réaction ayant des propriétés et amplitudes différentes. La pesanteur n'est pas compensée par la flottabilité dans le cas d'un avion, mais les effets de portance sont plus systématiques et prépondérants. Les masses ajoutées ne concernent essentiellement que les bateaux, sous-marins, et dirigeables, etc.. Cette thèse n'a pas la prétention de couvrir la commande de tous ces systèmes, mais elle essaie de dégager un cadre d'analyse commun et de proposer une approche de commande exploitant la structure d'actionnement commune à tous ces systèmes.

Une des finalités de la commande par retour d'état est d'assurer une certaine robustesse de fonctionnement vis-à-vis d'erreurs de modélisation et de perturbations agissant sur le système. Pour les véhicules de type VTOL cet aspect de robustesse est crucial (la "survie" du système en dépend). Plusieurs facteurs en accroissent la difficulté:

- La complexité des effets aérodynamiques/hydrodynamiques empêche l'obtention d'un modèle dynamique précis et valide dans un grand domaine d'opération.

- Les perturbations externes (rafales de vent, courants de mer, etc.), imprévisibles par nature, peuvent fortement modifier la dynamique du véhicule. Pour des petits véhicules aériens en particulier, la puissance embarquée ne permet pas toujours de contrer ces perturbations.

- Les erreurs d'estimation ou de mesure de la pose peuvent être très importantes et accentuent le besoin de disposer de commandes robustes.

Les aspects de robustesse ont été largement étudiés dans le cadre de la commande linéaire (see e.g. (Abzug and Larrabee, 2002), (Fossen, 1994), (Prouty, 2002), (Stevens and Lewis, 1992)). Les applications aéronautiques ont d'ailleurs joué un rôle important dans le développement de nombreuses méthodes d'automatique linéaire (techniques de type Nyquist (Etkin and Reid, 1996), (Stevens and Lewis, 1992), H_2 et H_∞ (Garg, 1993), (Mammar and Duc, 1992), (Takahashi, 1993), (Civita et al., 2003), (Prempain and Postlethwaite, 2005), commande de type LQR et LQG (Leonard and Graver, 2001),

(Stevens and Lewis, 1992), (Castillo et al., 2005), (Teel et al., 1997), (Stone, 2004), (Bendotti and Morris, 1995), (Mammar, 1992), etc.). Basées sur l'étude de modèles linéarisés de la dynamique du système, ces méthodes ne garantissent cependant qu'un domaine limité de stabilité et sont souvent basées sur des hypothèses restrictives en ignorant les perturbations externes (le vent par exemple). Elles se limitent la plupart du temps à des modes de vol très particuliers: mode quasi-stationnaire pour les véhicules de type VTOL, suivi de trajectoires d'équilibres [1] pour les véhicules de type avion. Pour toutes ces raisons, les méthodes de conception non-linéaires pour la commande (linéarisation entrées-sorties, backstepping, mode glissant, saturations imbriquées, etc.) ont été largement étudiées lors de cette dernière décennie. Elles ont généralement pour but d'accroître la taille du domaine de stabilité, assurant par là même un degré supplémentaire de robustesse. Toutefois, elles sont souvent basées sur des modélisations très simplistes de la dynamique (en particuler des efforts aérodynamiques), et le problème du rejet de perturbations est très rarement abordé. Les études de commande non-linéaire intégrant l'aspect robustesse pour ces systèmes, comme (Mahony and Hamel, 2004), (Pflimlin et al., 2006), (Isidori et al., 2003), (Marconi and Naldi, 2007) par exemple, restent peu nombreuses. Une des motivations de ce travail est aussi de mettre l'accent sur cet aspect et de proposer des pistes/outils pour le développement de nouvelles méthodes.

Ce résumé est organisé de la façon suivante. Dans un premier temps nous revenons sur la modélisation dynamique des systèmes considérés afin d'en discuter quelques propriétés caractéristiques ainsi que les différences que l'on peut rencontrer d'un système à l'autre. Ensuite une synthèse des techniques de commande développées pour la classe des véhicules de type VTOL est présentée: techniques linéaires (placement de pôles, méthodes LQR, LQG, H_2, H_∞, gain scheduling), techniques non-linéaires par feedback statique ou dynamique incluant la linéarisation entrée sortie, les méthodes de type Backstepping, la commande hiérarchique, etc.. Finalement, l'approche de commande non-linéaire proposée dans cette thèse et son utilisation pour les modes de fonctionnement typiquement rencontrés en pratique (télé-opérés ou complètement autonomes) seront brièvement présentés. Cette approche permet d'incorporer des termes de correction intégrale pour le rejet de perturbations statiques. Quelques remarques finales et perspectives concluent ce résumé.

B.2   Modélisation

Nous nous intéressons ici à des véhicules évoluant dans un espace à trois dimensions et pouvant être modélisés comme un corps rigide évoluant dans un fluide. Le contrôle de ces véhicules est réalisé par l'intermédiaire d'une force de poussée $\overrightarrow{T}$ le long d'une direction privilégie du véhicule (que l'on notera $\overrightarrow{k}$) pour générer le mouvement longitudinal et d'un vecteur Γ de couples permettant un contrôle complet de la dynamique de rotation.

Nous supposons que le point d'application de la poussée $\overrightarrow{T} = -T\overrightarrow{k}$ se situe à proximité de l'axe $\{G; \overrightarrow{k}\}$, où G est le centre de masse, de sorte que le couple généré par la poussée soit négligeable. Toutes les forces externes agissant sur le véhicule (pesanteur, flottabilité, masses ajoutées, trainée aérodynamique ou hydrodynamique, vent ou courant, etc.) sont regroupées dans un vecteur $\overrightarrow{F}_e$, de sorte que la force résultante appliquée au

---

1. Ce sont les trajectoires le long desquelles les vitesses linéaires et angulaires du véhicule, exprimées dans le repère corps, sont constantes.
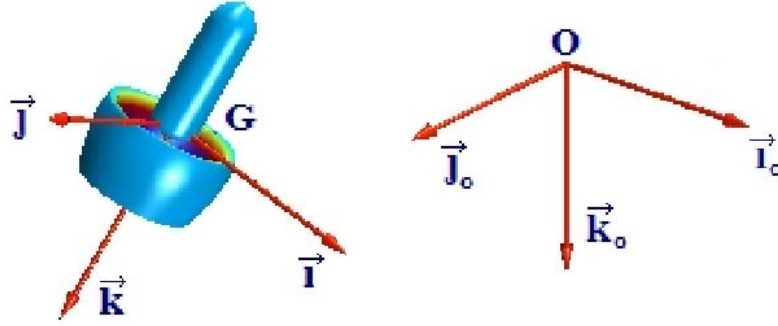
Figure B.1: Repères du drone.

véhicule est $\overrightarrow{F} = -T\overrightarrow{k} + \overrightarrow{F}_e$. En utilisant le formalisme de Newton-Euler, les équations de la dynamique s'écrivent sous la forme suivante:

$$m\ddot{x} = -TRe_3 + F_e(\dot{x}, \ddot{x}, R, \omega, \dot{\omega}, t) + R\Sigma_R\Gamma \qquad (B.1)$$

$$\dot{R} = RS(\omega) \qquad (B.2)$$

$$J\dot{\omega} = -S(\omega)J\omega + \Gamma + \Gamma_e(\dot{x}, \ddot{x}, R, \omega, \dot{\omega}, t) + \Sigma_T Te_3 \qquad (B.3)$$

avec x la position du centre de masse dans le repère inertiel, m la masse totale du véhicule, $J \in \mathbb{R}^{3\times3}$ la matrice d'inertie évaluée au centre de masse et exprimée dans le repère de l'engin, $R \in \mathrm{SO}(3)$ la matrice de rotation du repère du véhicule par rapport au repère inertiel, ω le vecteur de vitesse angulaire du corps exprimé dans son repère local, $S(u)$ la matrice pré-produit vectoriel associée au vecteur u, i.e. pour tout vecteur $u \in R^3$, $S(u)v = u \times v$, et Γ_e le vecteur regroupant tous les couples externes appliqués aux véhicules. La dépendance de F_e et Γ_e vis-à-vis de la variable temporelle t permet de prendre en compte la dynamique du vent ainsi que toute autre perturbation exogène. Les matrices Σ_T et $\Sigma_R \in \mathbb{R}^{3\times3}$ représentent des couplages complémentaires entre les dynamiques de translation et de rotation. Par exemple, l'influence de la translation sur la rotation via Σ_T traduit la contribution de l'excentricité du point d'application de la poussée par rapport au centre de masse. Son effet reste limité si le point d'application de la poussée $\overrightarrow{T}$ se situe à proximité de l'axe $\{G; \overrightarrow{k}\}$. Il peut être complètement éliminé par feedback si l'action du couple le permet. L'influence des couples de commande sur la translation via Σ_R est plus problématique; elle engendre un système à déphasage non minimal à l'origine d'un phénomène de dynamique des zéros. Son expression dépend principalement de la configuration du véhicule et de son mode d'actionnement. Lorsqu'il s'agit d'un hélicoptère à quatre rotors identiques (le cas du X4-flyer) ce couplage est théoriquement nul ($\Sigma_R = 0$). Par contre, dans le cas d'un VTOL, comme le HoverEye par exemple, où le contrôle de la dynamique de rotation est réalisé par l'intermédiaire de la déflexion du jet d'air généré par les hélices, seule la dernière ligne de cette matrice est nulle (Pflimlin et al., 2006).

La modélisation des forces et couples externes (i.e. F_e et Γ_e) reste un problème majeur, en raison de la complexité de la dynamique des fluides et des interactions entre le véhicule (corps rigide, mais muni d'actionneurs en mouvement) et le fluide environnant (voir e.g. (Pflimlin, 2006) pour une discussion de ces aspects sur l'HoverEye

de Bertin). En particulier, la dépendance des forces de traînée et portance par rapport à "l'angle d'attaque" du véhicule est très difficile à modéliser. A l'heure actuelle il n'existe pas de modèles analytiques permettant de représenter précisément ces efforts dans toute l'enveloppe de fonctionnement. Le peu de modèles existants sont supposés obéir au principe de superposition. Ainsi, pour le HoverEye de Bertin par exemple, on distingue (hormis la contribution de la gravité) les efforts de propulsion des hélices, les efforts de portance et de traînée générés par la circulation d'air autour de la cellule, et les efforts générés par les gouvernes. La légitimité d'un tel découpage n'a rien d'évident: en toute rigueur, le véhicule en mouvement dans un fluide exerce, par la rotation de l'hélice et par déflexion des gouvernes, une force sur le fluide qui, en retour, applique une force sur la cellule. La modélisation de ces forces sert en premier lieu à l'évaluation des limites de fonctionnement et à l'optimisation des caractéristiques géométriques et mécaniques de véhicule. Elle est nécessaire pour la simulation de la dynamique, mais la connaissance précise de ces forces et couples n'est pas nécessaire à la conception de lois de commande. Il est possible d'utiliser une approximation, ou même (c'est souvent préférable lorsque les capteurs disponibles le permettent) une estimation en ligne des termes F_e et Γ_e. Le retour d'expérience montre d'ailleurs que dans la pluplart des cas la modélisation explicite de Γ_e n'est pas nécessaire. La possibilité d'obtenir une bonne estimation en ligne de Γ_e, via une inversion dynamique ou un observateur à grands gains, dépend principalement de la qualité de mesure des vitesses de rotation et de leur fréquence d'acquisition. Il demeure que toute analyse de robustesse repose sur une caractérisation des erreurs de modèle par rapport à un modèle nominal. La connaissance fine de la dynamique de vol peut donc servir à l'automaticien pour garantir des niveaux de performance et robustesse acceptables. Ce point n'est pas à négliger en aéronautique puisque les exigences de certification sont souvent draconiennes.

B.3   Stratégies de contrôle dans la littérature

Le système (B.1)–(B.3) fait clairement apparaître une dynamique de rotation complètement actionnée (vecteur de couples Γ de l'équation (B.3)), et une dynamique de translation sous-actionnée (une seule entrée de commande T pour la dynamique de translation (B.1)). Au niveau de la translation, la commandabilité repose sur le couplage non-linéaire TRe_3 entre la commande T et la variable d'état R. C'est ce couplage qu'il faut exploiter pour stabiliser la position du véhicule.

Nous commencerons cette section par un survol des techniques de commande basées sur le linéarisé tangent du système autour du vol quasi-stationnaire.

B.3.1   Linéarisation autour du vol quasi-stationnaire

Afin de poser simplement le problème de la commande de VTOLs, et faire un premier tour des lieux des stratégies de conception de schémas de commande proposés dans la littérature, nous nous intéressons au linéarisé tangent du modèle dynamique du système en vol quasi stationnaire [2]. Nous supposerons que le vent est quasi-nul et nous négligerons les efforts aérodynamiques qui sont essentiellement des termes quadratiques en la vitesse. La résultante et le moment des efforts extérieurs se résument alors à $F_e = mge_3$ et $\Gamma_e = 0$,

---

2. Vol pour lequel les vitesses de translation et de rotation sont faibles

où g est la constante de gravité. Nous supposerons aussi que la matrice de couplage Σ_T est nulle. Au voisinage de l'identité, une approximation linéaire de la matrice de rotation est $R \approx I_3 + S(\eta)$, où $\eta \in \mathbb{R}^3$ est le vecteur des angles d'Euler (η_1 roulis, η_2 tangage, η_3 lacet). Le système linéarisé autour du point d'équilibre ($x = 0, \dot{x} = 0, \eta = 0, \omega = 0, T = mg, \Gamma = 0$) est donné par les équations:

$$m\ddot{x} = -mgS(\eta)e_3 - \widetilde{T}e_3 + \Sigma_R\Gamma \tag{B.4}$$

$$\dot{\eta} = \omega \tag{B.5}$$

$$J\dot{\omega} = \Gamma \tag{B.6}$$

avec $\widetilde{T} \triangleq T - mg$. Sans perte de généralité, nous supposerons que la matrice d'inertie est diagonale: $J = \mathrm{diag}(J_1, J_2, J_3)$. Le couplage $\Sigma_R\Gamma$ est non nul pour la plupart des VTOLs, et en particuler pour l'ensemble de la classe des "*tail-sitters*". Cette force parasite entraîne une dynamique des zéros marginalement stable ou instable (ceci en fonction de la configuration mécanique du VTOL), motivant des travaux de recherche encore d'actualité. En se référant au modèle de l'HoverEye (Pflimlin, 2006), la matrice de couplage Σ_R est

$$\Sigma_R = -\frac{1}{L}S(e_3) \tag{B.7}$$

où L représente la distance séparant le plan des gouvernes du centre de masse (ou bras de levier). Les équations (B.4)–(B.6) font alors apparaître quatre chaînes monoentrées-monosorties dont les deux premières, concernant l'altitude et l'angle de lacet, sont:

$$m\ddot{x}_3 = -\widetilde{T} \tag{B.8}$$

$$J_3\ddot{\eta}_3 = \Gamma_3 \tag{B.9}$$

Il s'agit de deux doubles intégrateurs indépendants dont les deux entrées $\widetilde{T}$ et Γ_3 permettent facilement de stabiliser exponentiellement les états $(x_3, \dot{x}_3)$ et (η_3, ω_3) vers $(0,0)$. Les deux autres chaînes sont:

$$\begin{cases} m\ddot{x}_1 &=& -mg\eta_2 + \frac{1}{L}\Gamma_2 \\ J_2\ddot{\eta}_2 &=& \Gamma_2 \end{cases} \tag{B.10}$$

$$\begin{cases} m\ddot{x}_2 &=& mg\eta_1 - \frac{1}{L}\Gamma_1 \\ J_1\ddot{\eta}_1 &=& \Gamma_1 \end{cases} \tag{B.11}$$

Par une transformation adéquate de coordonnées, il est facile de vérifier que chacun des deux systèmes précédents peut aussi s'écrire:

$$\dot{X}_1 = X_2 \tag{B.12}$$

$$\dot{X}_2 = X_3 + \varepsilon u \tag{B.13}$$

$$\dot{X}_3 = X_4 \tag{B.14}$$

$$\dot{X}_4 = u \tag{B.15}$$

avec $(X_1, X_2, X_3, X_4) \triangleq (x_1, \dot{x}_1, -g\eta_2, -g\dot{\eta}_2)$, $u \triangleq -(g/J_2)\Gamma_2$ et $\varepsilon \triangleq -J_2/(mgL)$ dans le cas du système (B.10), et $(X_1, X_2, X_3, X_4) \triangleq (x_2, \dot{x}_2, g\eta_1, g\dot{\eta}_1)$, $u \triangleq (g/J_1)\Gamma_1$ et $\varepsilon \triangleq -J_1/(mgL)$ dans le cas du système (B.11).

Le système linéaire (B.12)–(B.15) est commandable mais la stabilisation de son origine $x = 0$, même si elle est évidente, mérite que l'on s'y attarde un peu. En effet, les principaux travaux en commande non-linéaire de VTOLs sont inspirés des approches résumées ci-dessous.

1. Une première approche consiste à se focaliser sur la stabilisation de la sortie X_1. Lorsque $\varepsilon \neq 0$ ceci conduit à prendre εu comme entrée du système et à poser $v = X_3 + \varepsilon u$ comme nouvelle variable de contrôle. On obtient alors le double intégrateur:

$$\dot{X}_1 = X_2 \qquad (B.16)$$

$$\dot{X}_2 = v \qquad (B.17)$$

Ce système est commandable et le choix $v = -k_0 X_1 - k_1 X_2$ $(k_{0,1} > 0)$ assure la stabilisation exponentielle de $X_{1,2}$ vers zéro, ainsi que la convergence exponentielle de v vers zéro. Après convergence, il subsiste une dynamique interne des états $X_{3,4}$ dite "dynamique des zéros", qui évolue selon l'équation:

$$\dot{X}_3 = X_4 \qquad (B.18)$$

$$\dot{X}_4 = -\frac{1}{\varepsilon} X_3 \qquad (B.19)$$

Cette dynamique est au mieux marginalement stable (i.e. lorsque $\varepsilon > 0$). Lorsque $\varepsilon < 0$ on obtient une dynamique instable. Il faut préciser que même dans le cas où cette dynamique est marginalement stable (c'est le cas de l'hélicopère par exemple), c'est celle d'un oscillateur à haute fréquence (car ε est souvent très faible). Avec ce type de commande, la moindre perturbation peut alors facilement entraîner un départ en instabilité.

2. La deuxième approche consiste à mettre en œuvre un retour d'état complet $u = -\sum_{i=1}^{4} k_{i-1} X_i$, $(k_i > 0)$ afin de stabiliser l'origine du système (B.12)–(B.15). Dans ce cas, lorsque ε est petit, la présence du terme εu affecte peu la forme du feedback. En effet, pour assurer la stabilité du système, il suffit de faire en sorte que le polynôme caractéristique du système en boucle fermée:

$$p^4 + (k_3 + \varepsilon k_1)p^3 + (k_2 + \varepsilon k_0)p^2 + k_1 p + k_0$$

soit Hurwitz. En imposant, par exemple, que k_2 et k_3 soient grands devant εk_0, la connaissance précise de ε importe peu.

Bien que cette approche paraisse simple et logique, elle n'est que rarement utilisée en pratique. Ceci est dû au fait que le praticien préfère souvent décomposer un système du quatrième ordre, tel que (B.12)–(B.15), en une cascade de sous-systèmes d'ordre deux au plus, afin de faciliter la mise en œuvre de la commande ainsi que le diagnostic en cas de problème. En particulier la hiérarchisation en contrôle de X_1 (guidage) et contrôle de X_3 (pilotage) est souvent adoptée. La justification de ce choix est aussi liée aux cadences de commande qui sont différentes pour chacun des deux niveaux: une dizaine de Hz au plus pour la boucle de guidage et plus de 100 Hz pour la boucle de pilotage. Ceci conduit aux approches de type "hiérarchique".

3. Le principe de la commande hiérarchique consiste essentiellement à ignorer le couplage εu de la dynamique de translation (i.e. en posant $\varepsilon = 0$), et à considérer X_3 comme entrée de commande pour le système (B.12)–(B.13). Cette entrée sert alors de consigne pour le système (B.14)–(B.15). La hiérarchisation peut être de type

backstepping ou de type commande à grands gains. L'utilisation du backstepping par bloc (guidage et pilotage) conduit au système suivant:

$$\begin{cases} \dot{X}_1 = X_2 \\ \dot{X}_2 = X_3^d + \widetilde{X}_3 \\ \dot{\widetilde{X}}_3 = \widetilde{X}_4 \\ \dot{\widetilde{X}}_4 = \ddot{X}_3^d + u \end{cases}$$

où X_3^d représente le contrôle par retour d'état du sous-système $X_{1,2}$, choisi typiquement de la forme $X_3^d = -k_0 X_1 - k_1 X_2$ $(k_{0,1} > 0)$, $\widetilde{X}_3 = X_3 - X_3^d$, $\widetilde{X}_4 = X_4 - \dot{X}_3^d$ avec $\dot{X}_3^d = -k_0 X_2 - k_1 X_3$, et $\ddot{X}_3^d = -k_0 X_3 - k_1 X_4$. Il ne reste qu'à déterminer u pour réguler X_3 autour de X_3^d. Si l'on choisit

$$u = -\ddot{X}_3^d - k_2 \tilde{X}_3 - k_3 \tilde{X}_4 \tag{B.20}$$

le système bouclé présentera un polynôme caractéristique de la forme :

$$p^4 + (k_3 + k_1)p^3 + (k_2 + k_1 k_3 + k_0)p^2 + (k_1 k_2 + k_0 k_3)p + k_0 k_2$$

Les racines sont à partie réelle négative si les gains k_i $(i = 0, \ldots, 3)$ sont tous positifs.

Une variante de la commande par backstepping consiste en l'utilisation de grands gains pour la commande du second sous-système, tout en négligeant la dynamique de la consigne X_3^d, c'est-à-dire en posant $\dot{X}_3^d = \ddot{X}_3^d = 0$ dans l'expression de la commande u. Ceci revient à modifier l'expression (B.20) de la façon suivante: $u = -k_2 \widetilde{X}_3 - k_3 X_4$. Il en résulte un système en boucle fermée de polynôme caractéristique:

$$p^4 + k_3 p^3 + k_2 p^2 + k_1 k_2 p + k_0 k_2$$

Le fait que ce polynôme est Hurwitz si et seulement si $k_3 > k_1$ et $k_2 > \frac{k_3^2 k_0}{k_1(k_3 - k_1)} > 0$ va dans le sens du choix de grands gains k_2 et k_3 pour la commande du second sous-système. Un tel choix n'est possible en pratique que si la dynamique de rotation est suffisamment rapide par rapport à la dynamique de translation, et si l'on dispose de mesures de la rotation et de la vitesse angulaire à une fréquence élevée. En ce qui concerne la vitesse angulaire, de telles mesures peuvent être facilement obtenues grâce à l'utilisation de centrales inertielles. Dans le cas de la rotation, ceci est beaucoup plus difficile et fait l'objet actuellement de travaux de recherche (Martin and Salaun, 2008), (Hua, 2009), (Hua, 2010).

Au delà de ces principes de base, les techniques d'automatique linéaire plus modernes permettent, à partir d'un cahier des charges et d'une architecture de commande, de trouver les gains optimaux en termes de robustesse aux incertitudes, rejet de perturbations, etc.. C'est le cas par exemple de la méthode de commande LQR qui a été appliquée à la commande de la dynamique de rotation d'un X4-flyer et comparée à une approche de type PID (Bouabdallah et al., 2004), ou encore de la synthèse LQG utilisée en ajoutant au critère quadratique un terme pondérant la sensibilité du modèle aux variations paramétriques (Benallegue et al., 2006). Les méthodes de commande traitant de l'atténuation des perturbations, comme la commande H_∞, ont également été utilisées (Luo et al., 2003).

Bien que toutes ces techniques aient été expérimentées avec (plus ou moins de) succès, leur inconvénient réside dans la limitation de leur application au vol quasi-stationnaire et aux trajectoires d'équilibre à faible vitesse. La synthèse linéaire ne constitue donc qu'une étape préalable pour la commande sur l'ensemble du domaine de vol (souvent très en dessous des limites du drone). A partir de là, l'approche classiquement utilisée consiste à synthétiser le feedback pour un ensemble d'approximations linéaires du système autour de divers points du domaine de vol, puis à tabuler les gains en fonction de ce domaine tout en sachant qu'il devient alors quasiment impossible de garantir inconditionnellement la stabilité (ne serait-ce que locale) du schéma de commande ainsi obtenu. Cette technique, dite du *gain scheduling*, a fait ses preuves en pratique pour certains systèmes (souvent dans des conditions aérologiques très favorables). Elle reste toutefois laborieuse à mettre en place et pose un certain nombre de problèmes pour les véhicules de type VTOL:

1. Tout d'abord, la détermination des trajectoires d'équilibre nécessite une connaissance fine et préalable des efforts aérodynamiques. Pour les systèmes de type VTOL, dont les angles d'attaque peuvent varier de façon significative, déterminer une expression analytique de ces efforts est très difficile, et les évaluer de façon expérimentale (essais en soufflerie) est coûteux.

2. En raison des perturbations aérologiques, le système est souvent amené à fonctionner loin de la trajectoire d'équilibre désirée. Le linéarisé n'est alors plus siginificatif de la dynamique réelle du drone.

3. La linéarisation nécessite une paramétrisation minimale de la matrice de rotation. Ceci introduit des singularités de représentation qui limitent artificiellement le domaine de stabilité du contrôleur. A cet égard, certaines paramétrisations (e.g., de type Rodrigues) sont moins mauvaises que d'autres (e.g., de type Euler). Malgré son importance historique et son usage fréquent, la paramétrisation par les angles d'Euler n'est certainement pas la plus judicieuse pour des engins de type VTOL car elle limite significativement le domaine de stabilité.

L'utilisation de techniques de commande non-linéaire permet en grande partie de contourner ces difficultés.

B.3.2   Les stratégies de commande non-linéaire

Les travaux sur la commande non-linéaire des drones sont relativement récents et toujours d'actualité. On peut, pour simplifier, classer les approches existantes en deux catégories.

B.3.2.1   Techniques de commande basées sur l'extension dynamique

Ce type d'approche consiste essentiellement à considérer TRe_3 comme un état du système et à le dériver pour faire apparaître trois variables de commande indépendantes qui permettront de linéariser la dynamique de translation. Les premiers travaux dans cette direction (e.g. (Hauser et al., 1992)) ont porté sur le contrôle d'un avion à décollage et atterrissage vertical (PVTOL). L'approche a ensuite été étendue au cas 3D par Koo et Sastry (Koo and Sastry, 1998). En supposant que le vecteur des forces extérieures est

réduit à la gravité (i.e. $F_e = mge_3$) et en ignorant le terme de couplage $\Sigma_R\Gamma$ dans la dynamique de translation, on déduit facilement de (B.13)–(B.15) les relations suivantes:

$$\begin{cases} \dot{X}_1 = \dfrac{1}{m}X_2 \\ \dot{X}_2 = X_3 \\ \dot{X}_3 = X_4 \\ \dot{X}_4 = U \end{cases} \tag{B.21}$$

avec $X = (X_1, X_2, X_3, X_4) \triangleq (x, m\dot{x}, -TRe_3 + mge_3, -R\delta)$, $\delta \triangleq (T\omega_2, -T\omega_1, \dot{T})^T$, et

$$U \triangleq -R\left(\ddot{T}e_3 - TS(e_3)J^{-1}\Gamma - 2\dot{T}S(e_3)\omega + TS(\omega)^2e_3 + TS(e_3)J^{-1}S(\omega)J\omega\right)$$

Si l'on assimile $\ddot{T}$ à une variable de commande, et si $T \neq 0$, l'application $(\ddot{T}, \Gamma) \longrightarrow U$ est surjective. Ceci permet de considérer U comme une nouvelle variable de commande. Le système (B.21) étant linéaire et commandable, la stabilisation de $x = X_1$ le long d'une trajectoire de référence donnée devient alors triviale.

Cette approche est séduisante à première vue, mais elle pose un certain nombre de problèmes en pratique.

1. Pour des véhicules dont la propulsion est assurée par une hélice, T est fonction de la vitesse de rotation de l'hélice. La consigne d'entrée du moteur de propulsion étant le plus souvent une vitesse de rotation, ceci permet directement de générer la valeur T désirée. Dans le cas où $\ddot{T}$ devient la variable de commande, il faut être capable de générer cette grandeur physiquement. Ceci nécessite d'intégrer la dynamique des moteurs dans la synthèse de la commande.

2. La connaissance de T et $\dot{T}$ est nécessaire pour le calcul de $\ddot{T}$ et Γ. Pour la plupart des plateformes, ces deux grandeurs ne sont pas mesurables, et les estimer via des observateurs dédiés est difficile car ceci nécessite d'utiliser les mesures de position qui ne sont disponibles qu'à faible fréquence (de l'ordre de quelques Hz).

3. La commande n'est bien définie que pour $T \neq 0$. Puisque T devient un état interne du système, rien ne garantit a priori qu'il reste toujours positif.

4. La prise en compte des efforts aérodynamiques avec une telle approche nécessite une expression analytique de ces efforts, très difficile à obtenir.

5. Enfin, la prise en compte du terme de couplage $\Sigma_R\Gamma$ n'est pas évidente. Afin de linéariser le système une possibilité consisterait à intégrer ce terme dans la variable X_3 en posant $X_3 = -TRe_3 + mge_3 + R\Sigma_R\Gamma$. Malheureusement, on retombe alors sur le problème de dynamique des zéros évoqué en Section B.3.1. Pour prendre en compte ce couplage, d'autres approches ont été proposées, basées elles-aussi sur une extension dynamique du système mais sans chercher une linéarisation exacte (Mahony et al., 1999), (Frazzoli et al., 2000). Par exemple, en s'inspirant de (Martin et al., 1994), il est montré dans (Pflimlin et al., 2004) qu'il est possible d'annuler les effets de $\Sigma_R\Gamma$ pour certains véhicules symétriques (comme le Hovereye par exemple), en considérant un point de contrôle déporté par rapport au centre de masse. Toutefois, ces travaux n'apportent pas de solutions aux autres problèmes mentionnés ci-dessus.

B.3.2.2 Commande non-linéaire de systèmes interconnectés

Il ne s'agit plus dans ce cas d'assimiler TRe_3 à un état, mais de garantir qu'il converge vers une valeur de référence $(TRe_3)_r$ choisie de façon à stabiliser la dynamique de translation. Ce type d'approche s'apparente donc à la commande hiérarchique linéaire décrite en Section B.3.1 avec: un contrôle en position de "haut niveau" (guidage) défini par $(TRe_3)_r$, et un contrôle d'attitude de "bas niveau" (pilotage) qui va permettre de faire converger Re_3 vers $(Re_3)_r$. Plus précisément, en supposant que $F_e = mge_3$ et en ignorant le terme de couplage $\Sigma_R\Gamma$ (ou en réduisant son effet par le choix d'un point de contrôle déporté par rapport au centre de masse), la dynamique de translation se réduit à

$$m\ddot{x} = -TRe_3 + mge_3$$

Lorsque l'objectif consiste (par exemple) à stabiliser une position fixe, ceci suggère de définir comme valeur de référence pour TRe_3:

$$(TRe_3)_r = k_0x + k_1\dot{x} + mge_3$$

afin de garantir la stabilisation de x et $\dot{x}$ à zéro lorsque $TRe_3 = (TRe_3)_r$. Puisque Re_3 est un vecteur unitaire, cette valeur de référence permet directement de déterminer:

1. L'expression de la poussée (que l'on supposera non nulle):

$$T = |k_0x + k_1\dot{x} + mge_3| \tag{B.22}$$

2. La direction de poussée désirée:

$$(Re_3)_r = \frac{k_0x + k_1\dot{x} + mge_3}{|k_0x + k_1\dot{x} + mge_3|} \tag{B.23}$$

Bien qu'il soit plus plus simple de réguler seulement la direction de poussée, les travaux existants considèrent dans la plupart des cas toute la dynamique de rotation. Pour cela, une orientation de référence R_r est calculée à partir de la direction $(Re_3)_r$ et d'une autre direction non-colinéaire permettant de définir une valeur de référence pour le lacet (η_3). La matrice R_r est ensuite considérée comme une consigne pour la dynamique de rotation. Comme dans le cas de la commande hiérarchique linéaire (Section B.3.1), la dynamique de la consigne R_r est parfois négligée (i.e., $\dot{R}_r \approx \ddot{R}_r \approx 0$), en invoquant l'utilisation de "grands gains" pour la boucle de commande bas niveau de l'orientation. Les différences que l'on trouve dans la littérature concernent principalement le type de modélisation utilisé (matrice de rotation, quaternions, angles d'Euler), le type de mission visé (asservissement visuel, way-point, etc.), le type de capteur embarqué (mesure complète ou partielle de l'état), etc.. Certains travaux s'intéressent à des aspects de robustesse vis-à-vis, e.g., de la variation de la masse du véhicule ou du champ gravitationnel (Hamel et al., 2002), de rafales de vent, ou encore d'erreurs de mesure (Pflimlin et al., 2006). D'autres intègrent la saturation des actionneurs dans la synthèse de la loi de commande (Guenard, 2007), (Marconi and Naldi, 2007), en se basant la plupart du temps sur la technique des saturations imbriquées développée par Teel (Teel, 1992), (Marconi and Isidori, 2000). D'autres encore se concentrent sur les apports possibles du contrôle par mode glissant (Bouabdallah and Siegwart, 2005), (Xu and Ozguner, 2008), (Lee et al., 2009), ou encore de la commande

prédictive [3] (Jadbabaie et al., 1999), (Kim et al., 2002), (Bertrand et al., 2007). Dans la plupart des cas les efforts aérodynamiques sont complètement négligés, ce qui limite l'utilisation de ces approches au vol quasi-stationnaire. Les rares travaux qui prennent en compte ces efforts, comme (Pflimlin et al., 2006), utilisent un modèle constant qui ne permet pas de modéliser la dépendance de ces efforts par rapport à la vitesse du véhicule.

B.4   Nouvelle approche de commande pour véhicules à propulsion centrale

Nous résumons dans cette section la méthode de commande proposée dans cette thèse (Chapitre 2) pour des véhicules avec une force de poussée et un actionnement complet en couples (i.e. modèle (B.1)–(B.3)). La principale originalité porte sur la prise en compte des efforts aérodynamiques afin d'augmenter la précision de suivi et la robustesse de la commande vis-à-vis des perturbations aérologiques et des dynamiques non-modélisées.

Dans son principe, cette approche s'apparente aux techniques de commande de systèmes interconnectés présentées précédemment. Elle utilise toutefois une hiérarchisation des équations différente, en considérant d'un côté les équations (B.1)–(B.2), et de l'autre l'équation (B.3) (le découpage habituellement utilisé consiste à considérer l'équation (B.1) d'une part, et les équations (B.2)–(B.3) d'autre part). En supposant que le couplage $\Sigma_R\Gamma$ est négligeable, la première étape de cette approche consiste à se ramener à la commande du sous-système

$$\begin{cases} m\ddot{x} &= -TRe_3 + F_e(\dot{x}, \ddot{x}, R, \omega, \dot{\omega}, t) \\ \dot{R} &= RS(\omega) \end{cases} \tag{B.24}$$

en considérant que T et ω sont les variables de commande. Ceci suppose que la dynamique de la vitesse angulaire est suffisament rapide par rapport aux dynamiques de translation et de rotation, et que la fréquence des mesures de vitesse angulaire est suffisament élevée.

Dans l'état actuel de l'approche, il est aussi supposé que F_e ne dépend que de $\dot{x}$ et t, i.e. $F_e(\dot{x}, t)$. Le fait de négliger la dépendance de F_e par rapport à $\ddot{x}$ et $\dot{\omega}$ est réaliste pour la classe des véhicules aériens car les effets de masse ajoutée sont négligeables. La non-dépendance de cette force vis-à-vis de l'attitude du véhicule est une hypothèse beaucoup plus forte puisqu'elle revient à supposer que les forces aérodynamiques ne dépendent pas de cette attitude. En toute rigueur cette hypothèse n'est satisfaite que pour un corps sphérique, c'est à dire sans portance. En pratique, la méthode proposée est bien adaptée au cas des véhicules à faible portance (ce qui est le cas de la plupart des VTOLs), mais son utilisation/extension pour des véhicules à forte portance, comme les avions, reste un problème ouvert. Malgré ces restrictions le modèle (B.24) permet de prendre en compte les effets aérodynamiques de traînée, très souvent ignorés dans les études de commande. La dépendance de F_e par rapport à la variable exogène t permet aussi d'englober les efforts extérieurs associés par exemple à la dynamique du vent. Enfin, cette structure de modèle donne un cadre unique pour traiter le problème de stabilisation en un point et celui de suivi de trajectoires (i.e. "tracking"). Plus précisément, étant donné une trajectoire de référence $x_r(.)$, si l'on note $\widetilde{x} \triangleq x - x_r$ l'erreur de suivi en position, on obtient le modèle

---

3. A notre connaissance, les expérimentations réalisées à ce jour utilisent un calculateur déporté au sol pour l'implémentation des techniques prédictives.

d'erreur suivant:

$$\begin{cases} m\ddot{\tilde{x}} & = & -TRe_3 + F(\dot{x},t) \\ \dot{R} & = & RS(\omega) \end{cases} \tag{B.25}$$

avec $F(\dot{x},t) \triangleq F_e(\dot{x},t) - m\ddot{x}_r(t)$. Modulo la différence d'expression entre F_e et F, les équations des systèmes (B.24) et (B.25) sont identiques.

Plusieurs objectifs de commande, associés a différents modes opératoires (télé-opérés ou complètement autonomes), sont traités dans ce travail de thèse. Nous allons détailler le principe de synthèse de commande pour la stabilisation en vitesse, puis nous indiquerons brièvement comment ce principe s'étend à des objectifs plus complexes, comme par exemple la stabilisation en position avec rejet de perturbations statiques.

B.4.1   Stabilisation en vitesse

Afin de stabiliser l'erreur de vitesse $\dot{\tilde{x}}$ à zéro pour le système (B.25), il faut que $\dot{\tilde{x}} = 0$ soit un équilibre du système en boucle fermée. Il faut donc que $-TRe_3 + F(\dot{x}_r,t) = 0$ lorsque $\dot{\tilde{x}} = 0$. Cette relation est équivalente à

$$TRe_3 = F(\dot{x}_r,t) \tag{B.26}$$

Lorsque $F(\dot{x}_r,t) \neq 0$, il existe seulement deux couples de valeurs (T, Re_3) solutions de cette équation, à savoir

$$(T, Re_3) = \left(|F(\dot{x}_r,t)|, \frac{F(\dot{x}_r,t)}{|F(\dot{x}_r,t)|}\right), \text{ et } (T, Re_3) = \left(-|F(\dot{x}_r,t)|, -\frac{F(\dot{x}_r,t)}{|F(\dot{x}_r,t)|}\right) \tag{B.27}$$

Ces deux solutions (de type "vent de face" et "vent de dos") définissent l'amplitude T et la direction Re_3 de la poussée du véhicule qu'il est nécessaire d'appliquer pour contrer les efforts extérieurs le long de la trajectoire de référence et générer l'accélération associée à cette trajectoire. Notons qu'il reste un degré de liberté non-contraint en orientation (qui correspond typiquement à l'angle de lacet).

Lorsque $F(\dot{x}_r,t) = 0$ en revanche, tout couple (T, Re_3) avec $T = 0$ est solution de l'équation (B.26). Ce cas de figure, dégénéré, n'est pas traité dans ce travail de thèse pour deux raisons:

- Les véhicules de type VTOL étant soumis à l'action de la gravité, lorsque la trajectoire de référence est réduite à un point fixe (et en l'absence de vent), le terme $F(\dot{x}_r,t)$ est réduit au terme de gravité et est donc non nul. Pour que $F(\dot{x}_r,t)$ passe par zéro il faut des conditions très particulières (fortes rafales de vent, trajectoires de référence très agressives, etc.).

- Lorsque $F(\dot{x}_r,.) \equiv 0$, on peut vérifier que le linéarisé du système (B.25) en un équilibre quelconque $(\tilde{x}, \dot{\tilde{x}}, R) = (0, 0, R^*)$ n'est pas commandable (bien que le système lui-même soit commandable). Des techniques spécifiques aux systèmes "très" non-linéaires sont alors nécessaires pour traiter le problème de stabilisation (voir e.g. (Morin and Samson, 2006)).

La synthèse de la commande découle directement de l'analyse des solutions (T, Re_3) de l'équation (B.26) ci-dessus. En supposant, sans perte de généralité, que la poussée T est choisie de signe positif, on définie dans un premier temps

$$T = |F(\dot{x},t)| \tag{B.28}$$

puis, en supposant que $F(\dot{x}, t)$ ne s'anulle jamais[4], on détermine ω_1 et ω_2 de sorte que Re_3 converge vers le vecteur

$$(Re_3)_r = \frac{F(\dot{x}, t)}{|F(\dot{x}, t)|} \tag{B.29}$$

Ceci conduit aux expressions

$$\begin{cases} \omega_1 & = & -k_3 \dfrac{|\gamma|\overline{\gamma}_2}{(|\gamma| + \overline{\gamma}_3)^2} - \dfrac{1}{|\gamma|^2} \gamma^T S(Re_1)\dot{\gamma} \\[2mm] \omega_2 & = & k_3 \dfrac{|\gamma|\overline{\gamma}_1}{(|\gamma| + \overline{\gamma}_3)^2} - \dfrac{1}{|\gamma|^2} \gamma^T S(Re_2)\dot{\gamma} \end{cases} \tag{B.30}$$

avec $k_3 > 0$ un gain de commande, $\gamma \triangleq F(\dot{x}, t)/m$, et $\overline{\gamma} \triangleq R^T\gamma$. Il est important de noter à ce stade que dans les expressions ci-dessus F est évaluée en $(\dot{x}, t)$ et non pas en $(\dot{x}_r, t)$ comme dans l'équation (B.27). En effet, l'expression des efforts aérodynamiques le long de la trajectoire de référence n'est généralement pas connue, et donc $F(\dot{x}_r, t)$ n'est pas connue non plus. Par contre, il est possible d'estimer en temps réel F au point courant, i.e. $F(\dot{x}, t)$, par exemple grâce aux mesures d'accéléromètres ou via la synthèse d'un observateur (voir Chapitre 2, Section 2.5 pour plus de détails).

Les expressions (B.28)–(B.30) ci-dessus permettent de rendre l'équilibre $\dot{\tilde{x}} = 0$ stable, mais pas asymptotiquement stable. Pour stabiliser asymptotiquement $\dot{\tilde{x}}$ à zéro, il suffit alors d'ajouter aux expressions de T, ω_1, et ω_2 ci-dessus des termes de dissipation proportionnels à $\dot{\tilde{x}}$. Finalement, l'expression de commande suivante est obtenue:

$$\begin{cases} T & = & m(\overline{\gamma}_3 + k_1|\gamma|e_3^T R^T\dot{\tilde{x}}) \\[2mm] \omega_1 & = & -k_2|\gamma|e_2^T R^T\dot{\tilde{x}} - k_3 \dfrac{|\gamma|\overline{\gamma}_2}{(|\gamma| + \overline{\gamma}_3)^2} - \dfrac{1}{|\gamma|^2} \gamma^T S(Re_1)\dot{\gamma} \\[2mm] \omega_2 & = & k_2|\gamma|e_1^T R^T\dot{\tilde{x}} + k_3 \dfrac{|\gamma|\overline{\gamma}_1}{(|\gamma| + \overline{\gamma}_3)^2} - \dfrac{1}{|\gamma|^2} \gamma^T S(Re_2)\dot{\gamma} \end{cases} \tag{B.31}$$

avec $k_{1,2,3} > 0$ des gains de commande. Cette commande assure la stabilisation *quasi-globale*[5] de $\widetilde{x}$ vers zéro et Re_3 vers la direction de poussée désirée à l'équilibre.

A ce stade, il est clair que cette approche s'apparente aux techniques présentées en Section B.3.2.2. On peut toutefois noter une différence importante en comparant les expressions (B.22)–(B.23) d'une part avec les équations (B.28)–(B.29) d'autre part. Dans le premier cas, en posant $k_0 = 0$ pour considérer le seul cas de la stabilisation de la vitesse, le terme de retour en vitesse $k_1\dot{x}$ introduit une singularité dans (B.23) lorsque $k_1\dot{x} = -mge_3$. Dans le deuxième cas, les termes de retour en vitesse n'introduisent pas de singularité puisqu'ils n'apparaissent pas dans $F(\dot{x}, t)$. Les singularités de commande n'ont lieu que lorsque $F(\dot{x}, t) = 0$, ou lorsque la direction de poussée est opposée à la direction de poussée désirée[6].

B.4.2   Extensions à d'autres objectifs de stabilisation

La loi de commande (B.31) peut-être facilement modifiée afin de traiter des objectifs de commande plus avancés. Nous illustrons brièvement ce point pour le problème de

---

4. Dans un deuxième temps, il est montré qu'il suffit d'imposer que $F(\dot{x}_r, t)$ ne s'anulle jamais.

5. Pour toute condition initiale telle que la direction de poussée à l'instant initial n'est pas l'opposée de la direction de poussée désirée.

6. Ceci traduit l'impossibilité, de nature topologique, de stabiliser globalement un point d'équilibre sur la sphère de dimension deux via une commande continue.

commande en position. Le système d'erreur (B.25) peut s'écrire

$$\begin{cases} \ddot{\widetilde{x}} & = & -k\widetilde{x} - TRe_3 + (F(\dot{x},t) + k\widetilde{x}) \\ & = & -k\widetilde{x} - TRe_3 + F_x(\widetilde{x},\dot{x},t) \\ \dot{R} & = & RS(\omega) \end{cases}$$

avec $F_x(\widetilde{x},\dot{x},t) \triangleq F(\dot{x},t) + k\widetilde{x}$. Ceci suggère d'appliquer la commande (B.31) avec $\gamma = F_x(\widetilde{x},\dot{x},t)/m$ en lieu et place de l'expression précédente $\gamma = F(\dot{x},t)/m$. On espère ainsi que le terme $-k\widetilde{x}$ introduit dans l'expression de $\ddot{\widetilde{x}}$ apporte la correction nécessaire à la stabilisation de $\widetilde{x}$ à zéro. On peut démontrer que ce raisonnement intuitif est correct au sens où la commande ainsi obtenue stabilise asymptotiquement (localement) $\widetilde{x}$ à zéro. Toutefois ce choix de F_x peut poser problème. En effet, l'analyse de stabilité repose sur l'hypothèse que la fonction F_x ne s'annule pas; la commande (B.31) n'étant pas définie lorsque $F_x = 0$. A cause du terme $k\widetilde{x}$ introduit dans F_x, cette fonction va s'annuller pour certaines valeurs des variables d'état. Afin de circonvenir ce problème, on utilise un terme de retour en position *borné*, i.e. F_x est défini par $F_x(\widetilde{x},\dot{x},t) \triangleq F(\dot{x},t) + h(\widetilde{x})$ où h est une fonction bornée. Typiquement, la norme de h doit rester sensiblement plus petite que mg (qui correspond à la norme de F lorsque le véhicule ne subit aucun effort aérodynamique et $x_r \equiv 0$). Ceci permet d'accroître la taille du domaine de stabilité de façon très significative.

Plusieurs autres questions sont traitées dans ce travail de thèse. Citons en particulier:

1. La commande en position avec retour intégral. Les lois de commande présentées ci-dessus nécessitent en théorie la connaissance du terme F_e, et donc des forces extérieures. En pratique, quelque soit le moyen utilisé pour estimer ce terme (modélisation fonctionelle, estimation en ligne via des capteurs embarqués, etc.), sa connaissance ne peut être précise en toutes circonstances. Afin de conserver de bonnes performances en présence d'erreurs sur la connaissance de F_e, une correction non-linéaire de type intégrale bornée est proposée. Comme pour le terme de correction en position, le principe repose sur une modification de la fonction F limitant les risques d'annulation de cette fonction.

2. La prise en compte de la contrainte de poussée unidirectionelle. Pour de nombreux véhicules aériens la poussée est seulement uni-directionnelle (i.e. T ne peut changer de signe). Les différentes commandes proposées (i.e. en vitesse, en position, etc.) peuvent être adaptées à cette situation, sans conséquences sur le domaine de stabilité.

3. L'analyse des efforts aérodynamiques. En raison des efforts aérodynamiques il est quasiment exclu de pouvoir garantir que la fonction F ne s'annule en aucun point de l'espace d'état. Par contre, il est possible de choisir la trajectoire de référence de sorte que la fonction ne s'annule pas le long de cette trajectoire (i.e. $F(\dot{x}_r,t) \neq 0$). En s'appuyant sur les propriétés de dissipativité des efforts aérodynamiques, des propriétés de stabilité quasi-globale sont obtenues sous la seule condition que $F(\dot{x}_r,t) \neq 0$.

B.5 Conclusion

De nombreuses approches ont été développées pour la commande de véhicules de type VTOL. Il reste pourtant de nombreuses directions à explorer. Une meilleure compréhension de l'aérodynamique de ces systèmes est essentielle pour améliorer la performance et la robustesse des techniques de commande. En effet, la tendance à la miniaturisation des drones conduit à des fonctionnements dans de très larges gammes d'angles d'attaque et fait apparaître des phénomènes aérodynamiques très complexes. De ce point de vue, les modèles utilisés actuellement pour la synthèse de commande sont extrêmement simplistes et, à l'exception du vol quasi-stationnaire, reflètent mal la dynamique de vol de ces systèmes. En pratique, le fonctionnement autonome de petits véhicules de type VTOL reste aujourd'hui limité à des conditions aérologiques très favorables et des mouvements peu "agressifs". Ceci est en partie lié au problème critique de l'estimation de l'état du système. Concernant la partie contrôle/commande, des progrès significatifs peuvent encore êtres réalisés en prenant mieux en compte l'aérodynamique de ces systèmes. La diversité des véhicules aériens est aussi de nature à fournir de nouveaux problèmes de recherche. Par exemple, malgré quelques travaux récents (Azinheira et al., 2006), (Rifai et al., 2008), la commande de dirigeables ou de systèmes à ailes battantes reste une problématique très largement ouverte. Enfin, le couplage entre les aspects estimation d'état et stabilisation, par exemple dans le cadre de la commande référencée capteurs, est aussi un sujet qu'il convient d'étudier plus en détail.

Appendix C

Synthèse bibliographique du problème d'estimation d'attitude

Le terme *"attitude"* est souvent employé afin de représenter l'orientation relative entre un repère corps (*i.e.* celui fixé à un corps rigide) et un repère inertiel. L'attitude peut être décrite par une matrice de rotation – un élément du groupe de Lie SO(3). Dans la littérature, on trouve (parmi plusieurs) deux définitions différentes de l'attitude. Soit elle est définie par la matrice de changement de base entre le repère corps et repère inertiel, soit, au contraire, elle est la matrice de changement de base entre le repère inertiel et le repère corps. Alors que la deuxième définition provient du domaine de l'aéronautique, le domaine de la robotique communément adopte la première. Dans ce travail de thèse, nous utilisont la première définition. En dénotant $R \in$ SO(3) d'une telle matrice de rotation, R satisfait l'équation différentielle suivante:

$$\dot{R} = RS(\omega), \tag{C.1}$$

avec $\omega = [\omega_1, \omega_2, \omega_3]^\top \in \mathbb{R}^3$ le vecteur de vitesse de rotation du repère corps par rapport au repère inertiel exprimé dans le repère corps.

Ce travail de thèse met l'accent sur le problème d'estimation d'attitude en utilisant des mesures fournies par un capteur GPS et un central inertiel embarqués sur le véhicule. Tandis que la position et la vitesse linéaire du véhicule peuvent être directement mesurées par le capteur GPS, la reconstruction de l'attitude du véhicule rencontre certain nombre de difficultés. En effet, estimer l'attitude du véhicule en simplement intégrant l'équation cinématique de rotation du corps principale du véhicule n'est pas une solution fiable pour des applications à long terme en raison de dérives et de bruits de mesure gyroscopique. Plusieurs solutions alternatives ont été proposées dans les dernières décennies. Les synthèses de littérature sur les méthodes non-linéaires d'estimation d'attitude en se basant sur des mesures vectorielles comme (Crassidis et al., 2007), (Mahony et al., 2008), (Choukroun, 2003) sont des sources utiles pour commencer des études sur le sujet. Le document (Shuster, 2006) par un des pionniers du domaine est également intéressante. L'auteur donne de nombreuses anecdotes fascinantes sur l'histoire de l'estimation d'attitude, et surtout la méthode célèbre QUEST (*i.e.* "Quaternion Estimator") qu'il a proposée.

La première solution dans la littérature au problème d'estimation d'attitude à partir des mesures vectorielles est l'algorithme TRIAD proposé par Black en 1964 (voir *ex.* (Shuster, 1978), (Shuster and Oh, 1981), (Shuster, 2006)). Cet algorithme directement construit l'attitude à partir de deux vecteurs unitaires non-colinéaires, connus dans le repère corps

et le repère inertiel. Plus précisément, en dénotant v_1, v_1^*, v_2, v_2^* les vecteurs de coordonnées, exprimés respectivement dans le repère inertiel et le repère corps de deux vecteurs unitaire $\overrightarrow{v}_1$ et $\overrightarrow{v}_2$, on a $v_1 = Rv_1^*$, $v_2 = Rv_2^*$, et l'algorithme TRIAD fournit la matrice de rotation R comme suivant

$$R = \begin{bmatrix} s_1 & s_2 & s_3 \end{bmatrix} \begin{bmatrix} r_1 & r_2 & r_3 \end{bmatrix}^\top,$$

avec deux triades orthonormées

$$s_1 = v_1, \ s_2 = \frac{v_1 \times v_2}{|v_1 \times v_2|}, \ s_3 = s_1 \times s_2,$$

$$r_1 = v_1^*, \ r_2 = \frac{v_1^* \times v_2^*}{|v_1^* \times v_2^*|}, \ r_3 = r_1 \times r_2.$$

TRIAD est très simple à implémenter. Pourtant, comme il utilise uniquement des mesures de deux vecteurs, il n'est donc pas évident à l'utiliser "optimalement" quand des mesures de plus de deux vecteurs sont disponibles. Dans ce cas, les méthodes optimales permettent de calculer la meilleure estimation d'attitude en se basant sur une fonction de coût pour laquelle toutes les mesures vectorielles sont simultanément prises en compte. Pourtant, les algorithmes optimaux sont plus coûteux en calcul que l'algorithme TRIAD. Le premier et aussi le plus connu problème optimal d'estimation d'attitude est le problème Wahba qui est en fait un problème de moindres carrées proposé par Wahba en 1965 (Wahba, 1965). Ce problème s'agit de trouver une matrice de rotation $\widehat{A} \in \text{SO}(3)$ qui minimise la fonction de coût

$$J(A) \triangleq \frac{1}{2} \sum_{i=1}^{n \geq 2} a_i ||v_i^* - Av_i||^2, \tag{C.2}$$

où A correspond à la transposition de l'attitude estimée $\widehat{R}$; $\{v_i^*\}$ est un ensemble de mesures de n (≥ 2) vecteurs de coordonnées unitaires, exprimées dans le repère corps; $\{v_i\}$ sont les vecteurs de coordonnées unitaires correspondants, exprimés dans le repère inertiel; et $\{a_i\}$ est un ensemble de poids positifs dont les valeurs peuvent être conçues en fonction de la fiabilité des mesures correspondantes. En effet, le problème Wahba permet d'une pondération arbitraire des mesures vectorielles. Dans (Shuster, 1989a), l'auteur propose le choix particulier $a_i = \sigma_i^{-2}$, l'inverse de la variance de mesure de v_i^*, afin de transformer le problème Wahba au problème d'estimation par maximum de vraisemblance en se basant sur un modèle de bruit non-corrélé (Shuster and Oh, 1981), (Shuster, 1989a). En fait, la fonction de coût $J(A)$ définie par (C.2) peut s'être exprimée sous la forme suivante

$$J(A) = \frac{1}{2} \sum_{i=1}^{n \geq 2} a_i \left(|v_i^*|^2 + |v_i|^2 \right) - \frac{1}{2}\mathbf{tr}(AB^T), \tag{C.3}$$

avec

$$B \triangleq \sum_{i=1}^{n \geq 2} a_i v_i^* v_i^\top. \tag{C.4}$$

Il est donc évident que la matrix de rotation $\widehat{R}$ qui minimise la fonction de coût $J(A)$ maximise la fonction $\mathbf{tr}(AB^T)$. Des premières solutions du problème Wahba, en se basant sur cette remarque, furent proposées en 1966 par Farrell et Stuelpnagel (Wahba, 1966), et par Wessner, Velman, Brock dans le même document. Toutefois, ces solutions ne sont

pas bien adaptées aux applications temps réel à cause de leurs calculs très coûteux. Par exemple, le méthode proposée par Farrell et Stuelpnagel exige une décomposition polaire de la matrice B en $B = UP$ (avec U une matrix orthogonale et P une matrice symétrique semi-définie positive) et une diagonalisation de la matrice P en $P = WDW^{\top}$ (avec W une matrice orthogonale et D une matrice diagonale dont les éléments diagonaux sont arrangés par ordre décroissant, *i.e.* $D = \mathbf{diag}(d_1, d_2, d_3)$ avec $d_1 \geq d_2 \geq d_3$). En suite, la matrice de rotation optimale $\widehat{A}$ est donnée par

$$\widehat{A} = UW\mathbf{diag}(1, 1, \mathbf{det}(U))W^{\top}.$$

Quant à la solution proposée par Wessner qui est en fait un car particulier de celle de Farrell et Stuelpnagel, la matrice de rotation optimale $\widehat{A}$ est calculée selon l'expression

$$\widehat{A} = \left(B^{\top}\right)^{-1}\left(B^{\top}B\right)^{1/2}.$$

Cette solution, due à l'inverse de $B^{\top}$, indique que les mesures d'au moins trois vecteurs non-colinéaires doivent être disponibles, sachant que l'observation de deux vecteurs non-colinéaires est suffisante pour estimer l'attitude. D'ailleurs, calculer la racine carrée de la matrice $B^{\top}B$ nécessite également un calcul assez coûteux. Par example, on doit diagonaliser $B^{\top}B$ en $B^{\top}B = W_B D_B W_B^{\top}$ afin d'obtenir $\left(B^{\top}B\right)^{1/2} = W_B D_B^{1/2} W_B^{\top}$.

Pour des raisons pratiques, aucune solution n'était capable de remplacer l'algorithme TRIAD jusqu'au moment la q-méthode de Davenport (Davenport, 1968) et la méthode numérique QUEST de Shuster (Shuster, 1978), (Shuster and Oh, 1981) furent proposées. En utilisant des quaternions, Davenport transforma le problème Wahba au problème de recherche de la valeur propre la plus grande λ_{max} de la matrice symétrique Davenport $K \in \mathbb{R}^{4\times 4}$ définie par

$$K \triangleq \begin{bmatrix} C - \gamma I_3 & z \\ z^{\top} & \gamma \end{bmatrix},$$

avec $C \triangleq B + B^{\top}$, $\gamma \triangleq \mathbf{tr}(B)$, $z \triangleq \sum_{i=1}^{n\geq 2} a_i v_i^* \times v_i$, et B défini par (3.4). Le quaternion optimal, associé à la matrice de rotation optimale $\widehat{A}$ du problème Wahba, est en fait le vecteur propre normalisé q_{max} de la matrice K associé à la valeur propre λ_{max}. La valeur propre λ_{max} peut être obtenue, comme proposé dans (Davenport, 1968), en calculant analytiquement le pôle le plus grand du polynôme caractéristique du quatrième degré $\mathbf{det}(K - \lambda I_4)$. Toutefois, la q-méthode de Davenport a aussi un coût de calcul élevé. Cela conduisait à l'élaboration de l'algorithme QUEST (Shuster, 1978), (Shuster and Oh, 1981) sur la base de la q-méthode. QUEST s'agit de résoudre numériquement l'équation $\mathbf{det}(K - \lambda I_4) = 0$, ou de manière équivalente (voir (Shuster, 1978))

$$\lambda^4 - (a + b)\lambda^2 - c\lambda + (ab + c\gamma - d) = 0, \tag{C.5}$$

avec $a \triangleq \gamma^2 - \mathbf{tr}(\mathbf{adj}(C))$, $b \triangleq \gamma^2 + |z|^2$, $c \triangleq \mathbf{det}(C) + z^{\top}Cz$, $d \triangleq z^{\top}C^2z$. Plus précisément, en se basant sur l'observation de Shuster que λ_{max} est proche de $\lambda_o \triangleq \sum_{i=1}^{n\geq 2} a_i$, QUEST fait usage de la méthode d'iteration Newton-Raphson pour résoudre l'équation (C.5), en utilisant λ_o comme une estimation initiale. Cette méthode évite ainsi de calculer toutes les valeurs propres de K (*i.e.* toutes les solutions à l'équation (C.5)). Théoriquement, QUEST est moins robuste que la q-méthode de Davenport, mais elle est clairement plus rapide (normalement une itération est suffisante) et elle s'est avérée fiable dans la pratique

(QUEST fut implémenté dans le satellite Magsat en 1979). Plusieurs solutions alternatives pour QUEST et la q-méthode pour le problème Wahba furent proposées dans la littérature comme, par exemple, les algorithmes suivants: "Singular Value Decomposition" (SVD), "Fast Optimal Attitude Matrix" (FOAM), "Estimator of the Optimal Quaternion" (ESOQ), ESOQ-1, ESOQ-2 (Markley and Mortari, 2000). Ces solutions, et aussi QUEST, nécessitent un compromis entre le temps de calcul et la précision; par exemple, le nombre d'itérations doit être défini à l'avance. En outre, la faiblesse principale de ces solutions concerne leur caractéristique *"sans mémoire"* dans le sens que l'information contenue dans les mesures d'attitudes du passé est perdue.

Puisqu'un algorithme de filtrage est généralement préféré lorsque les mesures sont obtenues sur une plage de temps, plusieurs solutions alternatives ont été proposées. Elles combinent les mesures vectorielles avec le modèle cinématique de rotation et les mesures de vitesse angulaire du corps rigide. Nous utilisons le terme *"méthodes basées modèle"* afin de les distinguer des méthodes présentées précédemment qui se basent uniquement sur des mesures vectorielles. De cette manière, les méthodes d'estimation attitude telle que TRIAD, QUEST, SVD, FOAM, ESOQ peuvent encore être utiles en tant que préprocesseur (*i.e.* le rôle d'un capteur d'attitude) pour un certain nombre de méthodes bassées modèle d'estimation d'attitude, comme dans nombreuses méthodes de filtrage de Kalman, de Kalman étendu, ou de "Kalman-like" ((Farrell, 1964), (Lefferts et al., 1982), (Markley, 2003), (Crassidis et al., 2007), (Bonnabel, 2007)), ou des méthodes de filtrage non-linéaires ((Mahony et al., 2005), (Mahony et al., 2008), (Thienel and Sanner, 2003), (Vik and Fossen, 2001)). Toutefois, ce processus n'est pas une condition préalable. Il est relâché dans nombreuses méthodes basées modèle telles que proposées dans (Shuster, 1989b), (Shuster, 1990), (Bar-Itzhack, 1996), (Hamel and Mahony, 2006), (Mahony et al., 2008), (Mahony et al., 2009), (Martin and Salaun, 2007), (Vasconcelos et al., 2008), (Crassidis et al., 2007), *etc.*. Cela conduit à des méthodologies plus simples, plus rapides, et (probablement) plus précises. Par exemple, considérons l'algorithme *"filter QUEST"* (un estimateur "Kalman-like" récursif à temps discret) proposé dans (Shuster, 1989b), (Shuster, 1990). L'auteur propose d'estimer l'attitude en utilisant l'algorithme QUEST, et en propagant et misant à jour la matrice B (qui est lui-même impliquée dans la matrice Davenport K) comme suivant

$$B(t_k) = \mu \Phi_{3 \times 3}(t_k, t_{k-1}) B(t_{k-1}) + \sum_{i=1}^{n_k} a_i v_i^* v_i^\top,$$

où $\Phi_{3 \times 3}(t_k, t_{k-1}) B(t_{k-1})$ est la matrice de transition de l'état de $R^\top$, μ est un facteur de souvenir dit "fading memory factor" dans la litérature anlo-saxonne, et n_k est le nombre de mesures vectorielles disponibles à l'instant t_k. Un algorithme séquentiel alternatif pour le "filter QUEST" est la méthode REQUEST (Bar-Itzhack, 1996) qui se propage et met à jour la matrice de Davenport K par

$$K(t_k) = \mu \Phi_{4 \times 4}(t_k, t_{k-1}) B(t_{k-1}) + \sum_{i=1}^{n_k} a_i K_i,$$

où $\Phi_{4 \times 4}(t_k, t_{k-1}) B(t_{k-1})$ est la matrice de transition de l'état du quaternion associé à la matrice de rotation R, et K_i est la matrice Davenport calculée à partir d'un seul vecteur

$$K_i = \begin{bmatrix} v_i^* v_i^\top + v_i v_i^{*\top} - (v_i^{*\top} v_i) I_3 & (v_i^* \times v_i) \\ (v_i^* \times v_i)^\top & v_i^{*\top} v_i \end{bmatrix}.$$

La principale lacune des algorithmes *"filter QUEST"* et REQUEST concerne le facteur de souvenir μ qui, arbitrairement choisi, rend ces solutions *sous-optimales*. Cela conduit à l'élaboration de l'algorithme "Optimal-REQUEST" (Choukroun, 2003)[Ch.3] qui, étant essentiellement basée sur l'algorithme REQUEST, calcule en outre de façon optimale le facteur de souvenir μ à l'étape de mise à jour de REQUEST selon un argument d'optimisation de covariance. Il est important à noter que les algorithmes "filter QUEST", REQUEST, "Optimal-REQUEST", étant fondée sur QUEST, sont des méthodes de descente de gradient. Un autre exemple intéressant est le filtre non-linéaire complémentaire explicite (Mahony et al., 2008). Cette méthode est essentiellement inspirée par l'observateur de Luenberger (Luenberger, 1971) dans le sens que la dynamique de l'attitude estimée $\widehat{R}$ contient deux parties: une partie principale copie la dynamique de l'attitude réelle (*i.e.* équation (C.1)), et une partie d'innovation permettant la correction de l'attitude estimée à l'attitude réelle. Si les mesures gyroscopiques ne sont pas affectées par des biais, la dynamique de cet observateur est donnée par

$$\dot{\widehat{R}} = \widehat{R}S\left(\omega + \sum_{i=1}^{n} k_i v_i^* \times \widehat{R}^\top v_i\right),$$

avec k_i des constantes positives. Un problème important de filtrage d'attitude concerne le biais gyroscopique, conduisant à une approche complémentaire dans laquelle les gyroscopes sont utilisés pour filtrer les mesures vectorielles et les mesures vectorielles sont à leur tour utilisées pour estimer le biais gyroscopique (*e.g.* (Mahony et al., 2008), (Thienel and Sanner, 2003), (Vik and Fossen, 2001), (Lefferts et al., 1982)). En faisant l'hypothèse que le biais gyroscopique est constant (*i.e.* $\omega_m = \omega + b$, avec ω_m la mesure de gyroscopes et b le biais gyroscopique constant), la version complète du filtre complémentaire explicite proposé dans (Mahony et al., 2008) s'écrit

$$\begin{cases} \dot{\widehat{R}} &= \widehat{R}S(\omega_m - \widehat{b} + \sigma) \\ \dot{\widehat{b}} &= -k_b\sigma \\ \sigma &= \sum_{i=1}^{n} k_i v_i^* \times \widehat{R}^\top v_i \end{cases}$$

avec k_b, k_i des constantes positives. Ceci s'agit d'une version continue, cependant, une version discrète peut être facilement déduite. Il peut être aussi commodément réécrite sous la forme de quaternion. Les auteurs prouvent que, avec au moins deux observations vectorielles non-colinéaires l'attitude estimée converge exponentiellement vers la vraie, pour presque toutes les conditions initiales. Par ailleurs, une méthode rapide d'estimation d'attitude à partir des mesures vectorielles comme TRIAD ou QUEST peut être utilisée pour une bonne attitude estimée initiale. Il est à noter que dans le cas d'observation d'un seul vecteur, les solutions à ce filtre sont encore bien posé tandis que la reconstruction de l'attitude analytiquement n'est pas possible.

Compte tenu de la synthèse biblioraphique ci-dessus, on constate que la plupart des méthodes d'estimation d'attitude actuelles utilisent des mesures d'au moins deux vecteurs non-colinéaires connus. Cependant, dans la pratique il est souvent très difficile à obtenir des mesures de deux vecteurs connus. En fait, il fut montré que l'observation d'un seul vecteur est suffisante pour estimer l'attitude sous une condition d'excitation persistante (*i.e.* si la direction du vecteur ou l'attitude du véhicule varie de façon permanente)

(Mahony et al., 2009). Mais cette hypothèse est plutôt restrictive d'un point de vue applicatif. D'autres remèdes sont des solutions non-linéaires approximatives (voir *ex.* (Mahony et al., 2008), (Martin and Salaun, 2007), (Pflimlin et al., 2005)) qui se basent sur des mesures d'un central inertiel qui se compose de gyroscopes, d'accéléromètres, et de magnétomètres. Elles se rapprochent les mesures accéléromètres par la mesure de la gravité sous une hypothèse d'accélération faible. En fait, elles donnent plutôt de bons résultats expérimentaux à des opérations à l'intérieur pour un certain nombre de prototypes d'engins volants de type VTOL (voir *ex.* (Mahony et al., 2008), (Pflimlin et al., 2005)). Toutefois, la précision de l'attitude estimée fournie par ces méthodes est loin d'être satisfaisante lorsque le véhicule est soumis à des accélérations importantes. Afin de mieux faire face aux cas de fortes accélérations du véhicule, une mesure complémentaire GPS de vitesse linéaire du véhicule peut être utilisée pour estimer l'accélération linéaire du véhicule et, par conséquent, améliorer la précision de l'attitude estimée. De cette manière, un observateur non-linéaire d'estimation d'attitude basé GPS ("GPS-based Attitude and Heading Reference System" dans la littérature anlo-saxonne) fut proposé récemment dans (Martin and Salaun, 2008) en se basant sur la construction d'un observateur invariant (Bonnabel et al., 2008). Il présente des propriétés intéressantes, illustrées par des résultats convaincants de simulation et d'expérimentation. Pourtant, les analyses de convergence et stabilité dans (Martin and Salaun, 2008), en se basant sur le système d'erreur linéarisé, garantit seulement les propriétés locales de convergence et stabilité. Motivé par ce résultat, nous proposons dans cette thèse deux autres observateurs d'attitude avec des analyses de convergence et stabilité en se basant sur l'approche de Lyapunov (voir Chapitre 3). Le premier observateur assure la convergence et la stabilité exponentielles semi-globales, et suggère qu'un observateur à grand gain est le prix à payer pour un grand bassin d'attraction. Par contre, le deuxième observateur assure la convergence quasi globale sans usage de "grand gain". Cependant, l'inconvénient est que sa propriété de stabilité doit encore être démontrée pour le cas où l'accélération linéaire du véhicule n'est pas constante. Dans la pratique, lequel des deux observateurs est le meilleur doit être dépendre des caractéristiques de capteurs. Jusqu'à présent, les résultats de simulation montrent des performances similaires entre les deux solutions proposées ici et la solution proposée dans (Martin and Salaun, 2008). Nous observons également que la performance de toutes ces trois solutions est meilleure que celle des méthodes approximatives proposées dans la littérature lorsque l'accélération linéaire du véhicule n'est pas négligeable comparé à l'accélération gravitationnelle.

References

Abzug, M. J. and Larrabee, E. E. (2002). *Airplane Stability and Control.* Cambridge University Press, second edition.

Antonelli, G. (2006). *Underwater Robots: Motion and Force Control of Vehicle-Manipulator Systems.* Springer Verlag, second edition.

Axelrad, P., Comp, C. J., and Macdoran, P. F. (1996). SNR-based multipath error correction for GPS differential phase. *IEEE Transactions on Aerospace and Electronic Systems*, 32(2):650–660.

Azinheira, J. R. and Moutinho, A. (2008). Hover control of an UAV with backtepping design including input saturations. *IEEE Transactions on Control Systems Technology*, 16(3):517–526.

Azinheira, J. R., Moutinho, A., and Paiva, E. C. D. (2006). Airship hover stabilization using a backstepping control approach. *AIAA Journal of Guidance, Control, and Dynamics*, 29(4):903–914.

Bar-Itzhack, I. Y. (1996). REQUEST: a recursive QUEST algorithm for sequentiel attitude determination. *AIAA Journal of Guidance, Control, and Dynamics*, 19(5):1034–1038.

Bar-Itzhack, I. Y., Montgomery, P. Y., and Garrick, J. C. (1998). Algorithms for attitude determination using Global Positioning System. *AIAA Journal of Guidance, Control, and Dynamics*, 21(6):846–852.

Benallegue, A., Belaidi, A., and Mokhtari, A. (2006). Polynomial Linear Quadratic Gaussian and Sliding mode observer for a quadrotor Unmanned Aerial Vehicle. *Journal of Robotics and Mechatronics*, 17(3):483–495.

Bendotti, P. and Morris, J. C. (1995). Robust hover control for a model helicopter. In *IEEE American Control Conference*, pages 682–687.

Bertrand, S., Piet-Lahanier, H., and Hamel, T. (2007). Contractive model predictive control of an unmanned aerial vehicle model. In *17th IFAC Symp. on Automatic Control in Aerospace*, volume 17(1).

Boas, R. P., Jr., and Marcus, M. B. (1974). Inverse functions and integration by parts. *The American Mathematical Monthly*, 81(7):760–761.

Bonnabel, S. (2007). Left-invariant extended Kalman filter and attitude estimation. In *IEEE Conference on Decision and Control*, pages 1027–1032.

Bonnabel, S., Martin, P., and Rouchon, P. (2008). Symmetry-preserving observers. *IEEE Transactions on Automatic Control*, 53(11):2514–2526.

Borgne, M. L. (1987). Quaternions et controle sur l'espace de rotation. Technical Report 751, INRIA. Available at http://hal.inria.fr/inria-00075801/en/.

Bouabdallah, S., Noth, A., and Siegwart, R. (2004). PID vs. LQ control techniques applied to an indoor micro quadrotor. In *Intelligent Robots and Systems*, pages 2451–2456.

Bouabdallah, S. and Siegwart, R. (2005). Backstepping and sliding-mode techniques applied to an indoor micro quadrotor. In *IEEE Conference on Robotics and Automation*, pages 2247–2252.

Bourquardez, O. (2008). *Commande d'engins volants par asservissement visuel*. PhD thesis, Université de Rennes 1.

Bristeau, P.-J., Martin, P., Salaun, E., and Petit, N. (2009). The role of propeller aerodynamics in the model of a quadrotor UAV. In *European Control Conference*, pages 683–688.

Brown, A. K. (1981). Interferometric attitude determination using the Global Positioning System. Master's thesis, Massachusetts Institute of Technology.

Brown, R. A. (1992). Instantaneous GPS attitude determination. In *IEEE Position Location and Navigation Symposium*, pages 562–573.

Castillo, P., Lozano, R., and Dzul, A. (2005). Stabilization of a mini rotorcraft with four rotors. *IEEE Control Systems Magazine*, pages 45–55.

Chen, D. (1994). *Development of a fast ambiguity search filtering (FASF) method for GPS carrier phase ambiguity resolution*. PhD thesis, University of Calgary.

Chen, D. and Lachapelle, G. (1995). A comparison of the FASF and least-square search algorithms for on-the-fly ambiguity resolution. *Navigation: Journal of The Institute of Navigation*, 42(2):371–390.

Choukroun, D. (2003). *Novel methods for attitude determination using vector observations*. PhD thesis, Israel Institute of Technology.

Civita, M. L., Papageorgiou, G., Messner, W. C., and Kanade, T. (2003). Design and flight testing of a gain-scheduled H_∞ loop shaping controller for wide-envelope flight of a robotic helicopter. In *IEEE American Control Conference*, pages 4195–4200.

Cohen, C. E. (1992). *Attitude determination using GPS*. PhD thesis, Stanford University.

Crassidis, J. L. and Markley, F. L. (1997). New algorithm for attitude determination using Global Positioning System signals. *AIAA Journal of Guidance, Control, and Dynamics*, 20(5):891–896.

Crassidis, J. L., Markley, F. L., and Cheng, Y. (2007). Survey of nonlinear attitude estimation methods. *AIAA Journal of Guidance, Control, and Dynamics*, 30(1):12–28.

Crassidis, J. L., Markley, F. L., and Lightsey, E. G. (1999). Global Positioning System integer ambiguity resolution without attitude knowledge. *AIAA Journal of Guidance, Control, and Dynamics*, 22(2):212–218.

Davenport, P. B. (1968). A vector approach to the algebra of rotations with applications. Technical Report TN D-4696, NASA.

Defara, L., Madani, T., and Benallegue, A. (2006). Dynamic modelling and experimental identification of four rotors helicopter parameters. In *IEEE International Conf. on Industrial Technology*, pages 1834–1839.

Ding, J., Shi, C., and Weintrit, A. (2007). An important waypoint on passage of navigation history: Zheng He's sailing to West Ocean. In *7th International Symposium on Navigation*, pages 403–411.

Doyle, J. C., Glover, K., and Francis, P. P. K. B. A. (1989). State-space solutions to standard H_2 and H_∞ control problems. *IEEE Transactions on Automatic Control*, 34(8):831–847.

Dzul, A., Hamel, T., and Lozano, R. (2002). Nonlinear control for a tandem rotor helicopter. In *IFAC World Congress*, pages 229–234.

El-Rabbany, A. (2002). *Introduction to GPS: The Global Positioning System*. Artech House INC.

Ellis, J. F. and Creswell, G. A. (1979). Interferometric attitude determination with the Global Positioning System. *AIAA Journal of Guidance, Control, and Dynamics*, 2(6):522–527.

Etkin, B. and Reid, L. D. (1996). *Dynamics of Flight: Stability and Control*. John Wiley and Sons, third edition.

Fabiani, P., Fuertes, V., Piquereau, A., Mampey, R., and Teichteil-Konigsbuch, F. (2007). Autonomous flight and navigation of VTOL UAVs: from autonomy demonstrations to out-of-sight flights. *Aerospace Science and Technology*, 11:183–193.

Farrell, J. L. (1964). Attitude determination by Kalman filtering: Volume I. Technical Report CR598, NASA.

Fleming, J., Jones, T., Gelhausen, P., and Enns, D. (2003). Improving control system effectiveness for ducted fan VTOL UAVs operating in crosswinds. In *Proc. of the 2nd AIAA "Unmanned Unlimited" System, Technologies and Operations-Aerospace*, number 2003–6514.

Fleming, J., Jones, T., Lusardi, J., Gelhausen, P., and Enns, D. (2004). Improved control of ducted fan VTOL UAVs in crosswind turbulence. In *the AHS 4th Decennial Specialist's Conference on Aeromechanics*.

Fossen, T. I. (1994). *Guidance and control of ocean vehicles*. Wiley.

Francis, B. A. and Zames, G. (1984). On H_∞-optimal sensitivity theory for SISO feedback systems. *IEEE Transactions on Automatic Control*, 29(1):9–16.

Frazzoli, E. (2001). *Robust hybrid control for autonomous vehicle motion planning.* PhD thesis, Massachusetts Institute of Technology.

Frazzoli, E., Dahleh, M. A., and Feron, E. (2000). Trajectory tracking control design for autonomous helicopters using a backstepping algorithm. In *IEEE American Control Conference*, pages 4102–4107.

Frazzoli, E., Dahleh, M. A., and Feron, E. (2002). Real-time motion planning for agile autonomous vehicles. *AIAA Journal of Guidance Control and Dynamics*, 25(1):116–129.

Garg, S. (1993). Robust integrated flight/propulsion control design for a STOVL aircraft using H-infinity control design techniques. *Automatica*, 29(1):129–145.

Graf, W., Fleming, J., and Gelhausen, P. (2005). Ducted fan aerodynamics in forward flight. In *Proc. of the AHS International Specialists' Meeting on Unmanned Rotorcraft.*

Grewal, M. S., Weill, L. R., and Andrews, A. P. (2001). *Global Positioning Systems, Inertial Navigation, and Integration.* John Wiley & Sons.

Guenard, N. (2007). *Optimisation et implémentation des lois de commande embarquées pour le téléopération intuitive de micro drones aériens "X4-flyer".* PhD thesis, Université de Nice-Sophia Antipolis.

Guenard, N., Hamel, T., and Mahony, R. (2008). A practical visual servo control for an unmanned aerial vehicle. *IEEE Transactions on Robotics*, 24(2):331–340.

Hamel, T. and Mahony, R. (2002). Visual servoing of an under-actuated dynamic rigidbody system: an image-based approach. *IEEE Transactions on Robotics*, 18(2):187–198.

Hamel, T. and Mahony, R. (2006). Attitude estimation on SO(3) based on direct inertial measurements. In *IEEE Conference on Robotics and Automation*, pages 2170–2175.

Hamel, T., Mahony, R., Lozano, R., and Ostrowski, J. (2002). Dynamic modelling and configuration stabilization for an X4-flyer. In *IFAC World Congress*, pages 200–212.

Hamilton, W. R. (1843). Letter from Sir William R. Hamilton to John T. Graves, Esq. on Quaternions.

Hamilton, W. R. (1844). On quaternions, or on the new system of imaginaries in algebra. *The London, Edinburgh and Dublin Philosophical Magazine and Journal of Science*, 25:489–495.

Han, S. and Rizos, C. (1996). Integrated method for instantaneous ambiguity resolution using new generation GPS receivers. In *IEEE Position Location and Navigation Symposium*, pages 254–259.

Hatch, R. R. (1990). Instantaneous ambiguity resolution. *Kinematic Systems in Geodesy, Surveying and Remote Sensing, International Association of Geodesy Symposia 107, Springer Verlag*, pages 299–308.

Hauser, J., Sastry, S., and Meyer, G. (1992). Nonlinear control design for slightly non-minimum phase systems: Application to V/STOL. *Automatica*, 28(4):665–679.

Herisse, H., Hamel, T., Mahony, R., and Russotto, F.-X. (2009). A nonlinear terrain-following controller for a VTOL Unmanned Aerial Vehicle using translational optical flow. In *IEEE Conference on Robotics and Automation*, pages 3251–3257.

Hill, C. D. and Euler, H.-J. (1996). An optimal ambiguity resolution technique for attitude determination. In *IEEE Position Location and Navigation Symposium*, pages 262–269.

Hirschberg, M. J. (2000). The American Helicopter: an overview of helicopter developments in America 1908–1999.

Hua, M.-D. (2006). Commande d'un minidrone à hélice carénée. Master's thesis, Université Paris-Sud XI.

Hua, M.-D. (2009). Attitude observers for accelerated rigid bodies based on GPS and INS measurements. In *IEEE Conference on Decision and Control*, pages 8071–8076.

Hua, M.-D. (2010). Attitude estimation for accelerated vehicles using GPS/INS measurements. *Control Engineering Practice*. doi:10.1016/j.conengprac.2010.01.016.

Hua, M.-D., Hamel, T., Morin, P., and Samson, C. (2008). Control of Thrust-Propelled Underactuated vehicles. Technical Report 6453, INRIA. Available at http://hal.inria.fr/inria-00258092/fr/.

Hua, M.-D., Hamel, T., Morin, P., and Samson, C. (2009a). Commande par retour d'état pour des engins volants de type VTOL: résultats et perspectives. In *7e Journées Nationales de la Recherche en Robotique (JNRR'09)*, pages 147–161.

Hua, M.-D., Hamel, T., Morin, P., and Samson, C. (2009b). A control approach for Thrust-Propelled Underactuated vehicles and its application to VTOL drones. *IEEE Transactions on Automatic Control*, 54(8):1837–1853.

Hua, M.-D., Hamel, T., Morin, P., and Samson, C. (2009c). Control of a class of Thrust-Propelled Underactuated vehicles and application to a VTOL drone. In *IEEE Conference on Robotics and Automation*, pages 972–978.

Hua, M.-D., Morin, P., and Samson, C. (2007). Balanced-Force-Control for Underactuated Thrust-Propelled vehicles. In *IEEE Conference on Decision and Control*, pages 6435–6441.

Huang, M., Hoffmann, G. M., Waslander, S. L., and Tomlin, C. J. (2009). Aerodynamics and control of autonomous quadrotor helicopters in aggressive maneuvering. In *IEEE Conference on Robotics and Automation*, pages 3277–3282.

Hwang, P. Y. C. (1990). Kinematic GPS: resolving integer ambiguities on the fly. In *IEEE Position Location and Navigation Symposium*, pages 579–586.

Isidori, A. (1995). *Nonlinear Control Systems*. Springer Verlag, third edition.

Isidori, A., Marconi, L., and Serrani, A. (2003). Robust nonlinear motion control of a helicopter. *IEEE Transactions on Automatic Control*, 48(3):413–426.

Jadbabaie, A., Yu, J., and Hauser, J. (1999). Receding horizon control of the Caltech Ducted Fan : A control Lyapunov function approach. In *IEEE Conference on Control Applications*, pages 51–56.

Johnson, E. N. and Kannan, S. K. (2005). Adaptive trajectory control for autonomous helicopters. *AIAA Journal of Guidance Control and Dynamics*, 28(3).

Johnson, E. N. and Turbe, M. A. (2005). Modeling, control, and flight testing of a small ducted fan aircraft. In *AIAA Guidance, Navigation, and Control Conference and Exhibit*.

Kadmiry, B. and Driankov, D. (2004). A fuzzy gain-scheduler for the attitude control of an unmanned helicopter. *IEEE Transactions on Fuzzy Systems*.

Khalil, H. K. (2002). *Nonlinear Systems*. Prentice Hall, third edition.

Kim, D. and Langley, R. B. (2000). GPS ambiguity resolution and validation: methodologies, trends and issues. In *7th GNSS Workshop - International Symposium on GPS/GNSS*.

Kim, H. J., Shim, D. H., and Sastry, S. (2002). Nonlinear model predictive tracking control for rotorcraft-based unmanned aerial vehicles. In *IEEE American Control Conference*, pages 3576–3581.

Ko, A., Ohanian, O. J., and Gelhausen, P. (2007). Ducted fan UAV modeling and simulation in preliminary design. In *AIAA Modeling and Simulation Technologies Conference and Exhibit*, number 2007–6375.

Koo, T. J., Ma, Y., and Sastry, S. S. (2001). Nonlinear control of a helicopter based unmanned aerial vehicle model. *IEEE Transactions on Control Systems Technology*.

Koo, T. J. and Sastry, S. (1998). Output tracking control design for a helicopter model based on approximate linearization. In *IEEE Conference on Decision and Control*, pages 3635–3640.

Kothare, M. V., Campo, P. J., Morari, M., and Nett, C. N. (1994). A unified framework for the study of anti-windup designs. *Automatica*, 30(12):1869–1883.

Kwakernaak, H. and Sivan, R. (1972). *Linear Optimal Control Systems*. John Wiley & Sons.

Lageman, C., Trumpf, J., and Mahony, R. (2010). Gradient-like observers for invariant dynamics on a Lie group. *IEEE Transactions on Automatic Control*, 55(2):367–377.

Le-Bras, F., Hamel, T., and Mahony, R. (2007). Visual servoring of a VTOL vehicle using virtual states. In *IEEE Conference on Decision and Control*, pages 6442–6447.

Le-Bras, F., Mahony, R., Hamel, T., and Binetti, P. (2006). Adaptive filtering and image based visual servo control of a ducted fan flying robot. In *IEEE Conference on Decision and Control*, pages 1751–1757.

Lee, D., Kim, H., and Sastry, S. (2009). Feedback linearization vs. adaptive sliding mode control for a quadrotor helicopter. *International Journal of Control, Automation, and Systems*, 7(3):419–428.

Lefferts, E., Markley, F., and Shuster, M. (1982). Kalman filtering for spacecraft attitude estimation. *AIAA Journal of Guidance, Control, Navigation*, 5:417–429.

Leonard, N. E. and Graver, J. G. (2001). Model-based feedback control of autonomous underwater gliders. *IEEE Journal of Oceanic Engineering*, 26(4):633–645.

Li, Y., Zhang, K., Roberts, C., and Murata, M. (2004). On-the-fly GPS-based attitude determination using single- and double-differenced carrier phase measurements. *GPS Solutions Journal, Springer*, 8(2):93–102.

Lightsey, E. G., Crassidis, J. L., and Markley, F. L. (1999). Fast integer ambiguity resolution for GPS attitude determination. In *AIAA Guidance, Navigation, and Control Conference and Exhibit*, volume 1, pages 115–123.

Lipera, L., Colbourne, J., Tischler, M., Mansur, M., Rotkowitz, M., and Patangui, P. (2001). The micro craft iSTAR micro-air vehicle: Control system design and testing. In *Annual Forum of the American Helicopter Society*, pages 1–11.

Lu, G. (1995). *Development of a GPS Multi-Antenna System for Attitude Determination*. PhD thesis, University of Calgary.

Luenberger, D. (1971). An introduction to observers. *IEEE Transactions on Automatic Control*, 16(6):596–602.

Luo, C.-C., Liu, R.-F., Yang, C.-D., and Chang, Y.-H. (2003). Helicopter H_∞ control design with robust flying quality. *Aerospace Science and Technology*, 7(2):159–169.

Ma, Y., Soatto, S., Kosecka, J., and Sastry, S. S. (2004). *An Invitation to 3-D Vision: From Image to Geometric Models*. Springer Verlag.

Mahony, R. and Hamel, T. (2001). Adaptive compensation of aerodynamic effects during takeoff and landing manoeuvres for a scale model autonomous helicopter. *European Journal of Control*, 0:1–15.

Mahony, R. and Hamel, T. (2004). Robust trajectory tracking for a scale model autonomous helicopter. *International Journal of Non-linear and Robust Control*, 14:1035–1059.

Mahony, R., Hamel, T., and Dzul, A. (1999). Hover control via lyapunov control for an autonomous model helicopter. In *IEEE Conference on Decision and Control*, pages 3490–3495.

Mahony, R., Hamel, T., and Pflimlin, J.-M. (2005). Complementary filter design on the special orthogonal group SO(3). In *IEEE Conference on Decision and Control*, pages 1477–1484.

Mahony, R., Hamel, T., and Pflimlin, J.-M. (2008). Nonlinear complementary filters on the special orthogonal group. *IEEE Transactions on Automatic Control*, 53(5):1203–1218.

Mahony, R., Hamel, T., Trumpf, J., and Lageman, C. (2009). Nonlinear attitude observers on SO(3) for complementary and compatible measurements: A theoretical study. In *IEEE Conference on Decision and Control*, pages 6407–6412.

Mammar, S. (1992). *Commande multivariable robuste par les approches LQG/LTR et H_∞ application à un hélicoptère*. PhD thesis, Université de Paris-Sud.

Mammar, S. and Duc, G. (1992). Loop shaping H_∞ design applied to the robust stabilization of an helicopter. In *IEEE Conference on Control Applications*, pages 806–811.

Marconi, L. and Isidori, A. (2000). Robust global stabilization of a class of uncertain feedforward nonlinear systems. *Systems & Control Letters*, 41:281–290.

Marconi, L., Isidori, A., and Serrani, A. (2002). Autonomous vertical landing on an oscillating platform: an internal-model based approach. *Automatica*, 38:21–32.

Marconi, L. and Naldi, R. (2006). Nonlinear robust control of a reduced-complexity ducted MAV for trajectory tracking. In *IEEE Conference on Decision and Control*, pages 1539–1544.

Marconi, L. and Naldi, R. (2007). Robust full degree-of-freedom tracking control of a helicopter. *Automatica*, 43:1909–1920.

Marconi, L. and Naldi, R. (2008). Aggressive control of helicopters in presence of parametric and dynamical uncertainties. *Mechatronics*, 18:381–389.

Markley, F. L. (2003). Attitude error representations for Kalman filtering. *AIAA Journal of Guidance, Control, and Dynamics*, 26(2):311–317.

Markley, F. L. and Mortari, D. (2000). Quaternion attitude estimation using vector observations. *The Journal of the Astronautical Sciences*, 48(2, 3):359–380.

Martin, P., Devasia, S., and Paden, B. (1994). A different look at output tracking: control of a VTOL aircraft. In *IEEE Conference on Decision and Control*, pages 2376–2381.

Martin, P. and Salaun, E. (2007). Invariant observers for attitude and heading estimation from low-cost inertial and magnetic sensors. In *IEEE Conference on Decision and Control*, pages 1039–1045.

Martin, P. and Salaun, E. (2008). An invariant observer for Earth-Velocity-Aided attitude heading reference systems. In *IFAC World Congress*, pages 9857–9864.

Martini, A. (2008). *Modélisation et Commande de vol d'un hélicoptère drone soumis à une rafale de vent (in French)*. PhD thesis, Université Paul Varlaine-Metz.

Mayer, A. (1960). Rotations and their algebra. *SIAM Journal on Control and Optimization*, 2(2):77–122.

McClure, C. L. (1960). *Theory of Inertial Guidance.* Prentice-Hall.

Mettler, B. (2002). *Identification Modeling and Characteristics of Miniature Rotorcraft.* Kluwer Academics Publisher.

Micaelli, A. and Samson, C. (1993). Trajectory tracking for unicycle-type and two-steering-wheels mobile robots. Technical Report 2097, INRIA. Available at http://www-sop.inria.fr/rapports/sophia/RR-2097.html.

Morin, P. and Samson, C. (2006). Control with transverse functions and a single generator of underactuated mechanical systems. In *IEEE Conference on Decision and Control*, pages 6110–6115.

Moutinho, A. and Azinheira, J. R. (2005). Stability and robustness analysis of the AURORA airship control system using dynamic inversion. In *IEEE Conference on Robotics and Automation*, pages 2265–2270.

Murray, R. M., Li, Z., and Sastry, S. S. (1994). *A mathematical introduction to robotic manipulation.* CRC Press.

Naldi, R. (2008). *Prototyping, Modeling and Control of a Class of VTOL Aerial Robots.* PhD thesis, University of Bologna.

Naldi, R., Marconi, L., and Sala, A. (2008). Modelling and control of a miniature ducted-fan in fast forward flight. In *IEEE American Control Conference*, pages 2552–2557.

Olfati-Saber, R. (2002). Global configuration stabilization for the VTOL aircraft with strong input coupling. *IEEE Transactions on Automatic Control*, 47:1949–1952.

Palais, B. and Palais, R. (2007). Euler's fixed point theorem: The axis of a rotation. *Journal of Fixed Point Theory and Applications*, 2:215–220.

Peddle, I. K., Jones, T., and Treurnicht, J. (2009). Practical near hover flight control of a ducted fan (SLADe). *IFAC Control Engineering Practice*, 17:48–58.

Pervan, B. S. and Parkinson, B. W. (1997). Cycle ambiguity estimation for aircraft precision landing using the Global Positioning System. *AIAA Journal of Guidance, Control, and Dynamics*, 20(4):681–689.

Pflimlin, J.-M. (2006). *Commande d'un minidrone à hélice carénée: de la stabilisation dans le vent à la navigation autonome (in French).* PhD thesis, Ecole Doctorale Systèmes de Toulouse.

Pflimlin, J.-M., Binetti, P., Trouchet, D., Souères, P., and Hamel, T. (2007a). Aerodynamic modeling and practical attitude stabilization of a ducted fan UAV. In *European Control Conference*, pages 4023–4029.

Pflimlin, J.-M., Hamel, T., Souères, P., and Mahony, R. (2006). A hierarchical control strategy for the autonomous navigation of a ducted fan flying robot. In *IEEE Conference on Robotics and Automation*, pages 2491–2496.

Pflimlin, J.-M., Hamel, T., Souères, P., and Metni, N. (2005). Nonlinear attitude and gyroscopes bias estimation for a VTOL UAV. In *IFAC World Congress*.

Pflimlin, J.-M., Souères, P., and Hamel, T. (2004). Hovering flight stabilization in wind gusts for ducted fan UAV. In *IEEE Conference on Decision and Control*, pages 3491–3496.

Pflimlin, J.-M., Souères, P., and Hamel, T. (2007b). Position control of a ducted fan VTOL UAV in crosswind. *International Journal of Control*, 80(5):666–683.

Pounds, P., Mahony, R., and Corke, P. (2006). Modelling and control of a quad-rotor robot. In *Australasian Conference on Robotics and Automation*.

Pounds, P., Mahony, R., and Corke, P. (2010). Modelling and control of a large quadrotor robot. *Control Engineering Practice*. doi:10.1016/j.conengprac.2010.02.008.

Pounds, P., Mahony, R., Hynes, P., and Roberts, J. (2002). Design of a four-rotor aerial robot. In *Australasian Conference on Robotics and Automation*, pages 145–150.

Prempain, E. and Postlethwaite, I. (2005). Static H_∞ loop shaping control of a fly-by-wire helicopter. *Automatica*, 41:1517–1528.

Prouty, R. W. (2002). *Helicopter Performance, Stability, and Control*. Krieger.

Radix, J. C. (1993). *Systèmes inertiels à composants liés "strap-down"*. Cépaduès.

Refsnes, J. E., Pettersen, K. Y., and Sørensen, A. J. (2006). Control of slender body underactuated AUVs with current estimation. In *IEEE Conference on Decision and Control*, pages 43–50.

Rifai, H., Marchand, N., and Poulin, G. (2008). Path tracking control of a flapping unmanned air vehicle (UAV). In *IFAC World Congress*.

Robinson, A. C. (1958). On the use of quaternions in simulations of rigid-body motion. Technical Report 58-17, Wright Air Development Center.

Ruffier, F. and Franceschini, N. (2004). Visually guided Micro-Aerial Vehicle: automatic take off, terrain following, landing and wind reaction. In *IEEE Conference on Robotics and Automation*, pages 2339–2346.

Ruffier, F., Serres, J., Portelli, G., and Franceschini, N. (2009). Boucles visuo-motrices biomimétiques pour le pilotage automatique de micro-aéronefs. In *7e Journées Nationales de la Recherche en Robotique (JNRR'09)*, pages 55–67.

Rynaski, E. G. (1966). Optimal helicopter station keeping. *IEEE Transactions on Automatic Control*, AC-11(3):346–355.

Saripalli, S., Montgomery, J. F., and Sukhatme, G. S. (2002). Vision based autonomous landing of an unmanned aerial vehicle. In *IEEE Conference on Robotics and Automation*, pages 2799–2804.

Sepulchre, R., Janković, M., and Kokotović, P. (1997). *Constructive Nonlinear Control*. Springer-Verlag.

Shamma, J. S. (1988). *Analysis and design of gain scheduled control systems.* PhD thesis, Massachusetts Institute of Technology.

Shamma, J. S. and Athans, M. (1992). Gain scheduling: potential hazards and possible remedies. *IEEE Control Systems Magazine*, pages 101–107.

Shuster, M. D. (1978). Approximate algorithms for fast optimal attitude computation. In *AIAA Guidance and Control Conference*, pages 88–95.

Shuster, M. D. (1989a). Maximum likelihood estimation of spacecraft attitude. *The Journal of the Astronautical Sciences*, 37(1):79–88.

Shuster, M. D. (1989b). A simple Kalman filter and smoother for spacecraft attitude. *The Journal of the Astronautical Sciences*, 37(1):89–106.

Shuster, M. D. (1990). Kalman filtering of spacecraft attitude and the QUEST model. *The Journal of the Astronautical Sciences*, 38(3):377–393.

Shuster, M. D. (1993). A survey of attitude representations. *The Journal of the Astronautical Sciences*, 41(4):439–517.

Shuster, M. D. (2006). The QUEST for better attitudes. *The Journal of the Astronautical Sciences*, 54(3,4):657–683.

Shuster, M. D. and Oh, S. D. (1981). Three-axis attitude determination from vector observations. *AIAA Journal of Guidance, Control, and Dynamics*, 4(1):70–77.

Stein, G. and Athans, M. (1987). The LQG/LTR procedure for multivariable feedback control design. *IEEE Transactions on Automatic Control*, 32(2):105–114.

Stevens, B. L. and Lewis, F. L. (1992). *Aircraft control and simulation.* John Wiley and Sons.

Stone, R. H. (2004). Control architecture for a tail-sitter unmanned air vehicle. In *5th Asian Control Conference*, pages 736–744.

Stuelpnagel, J. (1964). On the parametrization of the three-dimensional rotation group. *SIAM Journal on Control and Optimization*, 6(4):422–430.

Sutton, E. (1997). Optimal search space identification for instantaneous integer cycle ambiguity resolution. In *Proceedings of ION GPS-97*.

Sutton, E. (2002). Integer cycle ambiguity resolution under conditions of low satellite visibility. In *IEEE Position Location and Navigation Symposium*, pages 91–98.

Takahashi, M. D. (1993). Systhesis and evaluation of an H_2 control law for a hovering helicopter. *AIAA Journal of Guidance, Control, and Dynamics*, 16(3):579–584.

Tayebi, A. and McGilvray, S. (2006). Attitude stabilization of a VTOL quadrotor aircraft. *IEEE Transactions on Control Systems Technology*, 14(3):562–571.

Teel, A. R. (1992). Global stabilization and restricted tracking for multiple integrators with bounded controls. *Systems & Control Letters*, 18:165–171.

Teel, A. R., Kaiser, O. E., and Murray, R. M. (1997). Uniting local and global controllers for the Caltech ducted fan. In *IEEE American Control Conference*, pages 1539–1543.

Teunissen, P. J. G. (1994). A new method for fast carrier phase ambiguity estimation. In *IEEE Position Location and Navigation Symposium*, pages 562–573.

Teunissen, P. J. G. (1998). Success probability of integer GPS ambiguity rounding and bootstraping. *Journal of Geodesy*, 72:606–612.

Teunissen, P. J. G. (1999). An optimal property of the integer least-squares estimator. *Journal of Geodesy*, 73:587–593.

Teunissen, P. J. G. (2000). The success rate and precision of GPS ambiguities. *Journal of Geodesy*, 74:321–326.

Thienel, J. and Sanner, R. M. (2003). A coupled nonlinear spacecraft attitude controller and observer with an unknown constant gyro bias and gyro noise. *IEEE Transactions on Automatic Control*, 48(11):2011–2015.

Treichler, J. R. and Agee, B. G. (1983). A new approach to multipath correction of constant modulus signals. *IEEE Transactions on Acoustics, Speech and Signal Processing*, 31(2):459–472.

Trucco, E. and Verri, A. (1998). *Introductory Techniques for 3-D Computer Vision*. Prentice-Hall.

Tsui, J. B.-Y. (2005). *Fundamental of Global Positioning. Receivers. A Software Approach*. John Wiley & Sons, second edition.

Vasconcelos, J. F., Silvestre, C., and Oliveira, P. (2008). A nonlinear GPS/IMU based observer for rigid body attitude and position estimation. In *IEEE Conference on Decision and Control*, pages 1255–1260.

Vik, B. and Fossen, T. (2001). A nonlinear observer for GPS and INS integration. In *IEEE Conference on Decision and Control*, pages 2956–2961.

Vilchis, J. C. A. (2001). *Modélisation et commande d'hélicoptère*. PhD thesis, Institut National Polytechnique de Grenoble.

Vissière, D., Bristeau, P.-J., Martin, A. P., and Petit, N. (2008). Experimental autonomous flight of a small-scaled helicopter using accurate dynamics model and low-cost sensors. In *IFAC World Congress*, pages 14642–14650.

Vissière, D., Martin, P., and Petit, N. (2007). Using magnetic disturbances to improve IMU-based position estimation. In *European Control Conference*, pages 2853–2858.

Wahba, G. (1965). A least squares estimate of satellite attitude, Problem 65-1. *SIAM Review*, 7(3):409.

Wahba, G. (1966). A least squares estimate of satellite attitude. *SIAM Review*, 8(3):384–386.

Witkowski, A. (2006). On Young's inequality. *Journal of Inequalities in Pure and Applied Mathematics*, 7(5).

Xu, R. and Ozguner, U. (2008). Sliding mode control of a class of underactuated systems. *Automatica*, 44:233–241.

Zames, G. (1981). Feedback and optimal sensitivity: Model reference transformations, multiplicative seminorms, and approximate inverses. *IEEE Transactions on Automatic Control*, 26(2):301–320.

Zhao, H. W. and Bil, C. (2008). Aerodynamic design and analysis of a VTOL ducted-fan UAV. In *the 26th AIAA Applied Aerodynamics Conference*, number 2008–7516.

Abstract

The control of underactuated vehicles has received increasing interests in relation with various robotic applications. This thesis focuses more specifically on the general problem of automatic control of aerial vehicles, and in particular of Vertical Take-Off and Landing vehicles. The contributions of this work is twofold. Firstly, this work sets the foundations of a general control approach for a large family of thrust-propelled underactuated vehicles in order to stabilize reference trajectories either in thrust direction, velocity, or position. The basic modeling assumption is that the vehicle is propelled via a thrust force along a single body-fixed direction and that it has full torque actuation for attitude control. Motivated by robustness issues, a novel nonlinear integrator technique is proposed allowing to compensate for modeling errors and perform robustly against external perturbations. Secondly, we propose two novel attitude estimation algorithms, based on measurements provided by a GPS and an IMU embarked on the vehicle. The proposed methods make use of the measurement of the linear velocity to estimate the vehicle's acceleration, and improve significantly the precision of the estimated attitude, especially in the case of important accelerations.

Keywords: Feedback control, Attitude estimation, Underactuated vehicles, VTOL UAV, System modeling, Robustness, Nonlinear anti-windup integrator.

Résumé

Le contrôle automatique de véhicules sous-actionnés suscite depuis de nombreuses années un grand intérêt pour des applications diverses et variées. Cette thèse est consacrée au problème général du contrôle automatique de véhicules aériens, en particulier des véhicules à décollage et atterrissage vertical. Ce travail présente deux contributions théoriques. La première contribution concerne le développement d'une approche de commande générique pour une large classe de véhicules sous-actionnés. Cette approche exploite la structure d'actionnement commune à la plupart de véhicules conçus par l'homme, à savoir une seule commande en poussée dans une direction privilégiée du véhicule et un actionnement complet de la dynamique de rotation. La méthode de synthèse est conçue de façon incrémentale afin de traiter différents modes opérationnels: stabilisation de la direction de poussée, de la vitesse, ou de la position du véhicule. Une nouvelle technique d'intégrateur non-linéaire est proposée afin de garantir un comportement robuste vis-à-vis de perturbations extérieures ou d'erreurs de modèle. La seconde contribution concerne deux nouvelles méthodes d'estimation d'attitude du véhicule à partir de mesures fournies par une centrale inertielle et de mesures GPS. Les solutions proposées utilisent la mesure de vitesse linéaire pour estimer l'accélération du véhicule, et améliorent significativement la précision de l'attitude estimée, notamment en cas d'accélérations importantes du système.

Mos-clés: Commande par retour d'état, Estimation d'attitude, Véhicule sous-actionné, Véhicule à décollage et atterrissage vertical, Modélisation, Robustesse, Intégrateur anti-windup nonlinéaire.